Εθνικό Μετσόβιο Πολυτεχνείο
Σχολή Πολιτικών Μηχανικών
Τομέας Γεωτεχνικής

National Technical University of Athens
School of Civil Engineering
Geotechnical Department

Διπλωματική Εργασία

ΠΑΝΑΓΙΩΤΗ ΜΙΣΙΡΛΗ

Επιβλέποντες

Ν. Γερόλυμος Γ.Γκαζέτας

ΜΗ ΓΡΑΜΜΙΚΗ ΚΙΝΗΜΑΤΙΚΗ ΑΛΛΗΛΕΠΙΔΡΑΣΗ ΕΔΑΦΟΥΣ ΠΑΣΣΑΛΟΥ

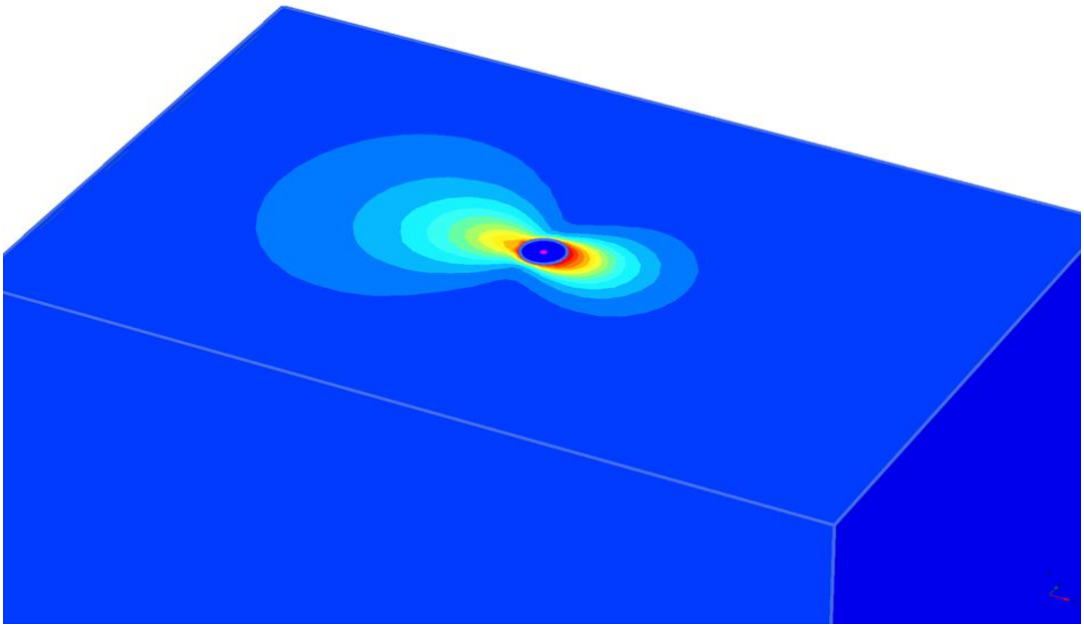

NON-LINEAR KINEMATIC SOIL PILE INTERACTION

Diploma Thesis

PANAGIOTIS MISIRLIS

Supervised by

N. Gerolymos G.Gazetas

Αθήνα Νοέμβριος 2018

Preface

This diploma thesis finalizes my studies in Civil Engineering, with specialization on Geotechnical Engineering at National Technical University of Athens.

Since this is a big achievement for me, I would like to thank all the people that have assisted me in this long and interesting journey.

First, I would like to express my deepest appreciation and gratitude to Professor G. Gazetas, for his valuable guidance throughout my studies. He was one of the biggest inspirations during my studies. He was the force that urged me to move forward and to always give it my best.

Furthermore, this thesis would not have been possible without the valuable assistance of Prof. Nikos Gerolymos. His constant support and guidance helped me grow as a person and as a scientist and his advice always helped me overcome many of the challenges I faced.

I would also like to express my gratitude to Maria Anthi, PHD candidate in NTUA for her help and assistance through the whole process.

Finally, I would like to thank my friends and family for always being there for me during the challenges I faced and for always cheering me up during these difficult yet rewarding period of my life.

Athens, Greece, 2/11/18

Contents

Abstract

Design of piles against kinematic loading is rarely applied in engineering practice. According to seismic codes, kinematic soil–pile interaction should be taken into account only when the pile is intersected by interfaces with large stiffness contrast of the consecutive soil layers. Although the last decade a considerable amount of studies has been devoted to this subject, only a few of them deal with soil nonlinearity, and, to the best of the author's knowledge, there is still no published paper that thoroughly investigates the role of group action on soil-pile kinematic interaction under intense nonlinear soil response conditions. In this paper, the results from a thorough finite element analysis with code PLAXIS are presented in which both the piles and the soil are modeled in 3D with volume elements. A suitable plasticity model is employed for treating the nonlinear soil behaviour in cyclic loading after appropriate calibration of its parameters to match published relationships of shear modulus and damping ratio curves. The influence of key-model parameters, such as: (a) strong motion intensity, (b) stiffness contrast ratio between the soil layers, (c) depth of the interface, (d) number of harmonic cycles, (e) resonance ratio etc., on the bending moment distribution along each pile, is investigated and critically discussed. The extraction closed-form expressions for the kinematic structural forces not only in the vicinity of the interface but at the head of the pile as well, is also attempted. Additionally, accelerograms from past earthquakes are used to test the validity of the derived equations.

1. Literature Review:

1.1 Introduction

In this specific chapter we are going to emphasize on theory behind the phenomenon of the kinematic loadings of piles. We are going to start with the fundamentals of the wave propagation theory in the field of soil-dynamics, the basic parameters of the waves like velocity and wave type and how these affect our field of study, meaning the kinematic loadings on piles. Following we will refer to the most important elements of piles as a type of foundation and the different types that exist.

Secondly comes the determination of the problem about the kinematic moments that occur in the pile from the kinematic loading. These moments are concentrated in the head of the pile (as we are only talking about fixed-head piles) or in the interface between the two-layered soil. This moment is a result from the difference between the motions of the soil and the pile, the difference in the Young Modulus between the two materials makes the pile "filter" most of the deformations that the surrounding soil tries to impose. The name kinematic moments prevailed in the literature so that these can be distinguished from the dynamic moments that are a result of the inertia forces of the superstructure. This phenomenon was first researched due to some failures of piles that didn't occur close to the head, where the inertia moments are maximized but in depths that inertia loading is insignificant (Kobe (1995)). After some years the phenomenon was also added in in the Greek Seismic Code- EAK (2000) as we all as the EC-8-Part 5 (2003) in both of which it is stated:

" Piles and piers shall be designed to resist the Kinematic forces arising from the deformation of the surrounding soil due to the passage of seismic waves"

Many different research papers have been published for this particular subject. Most of them are based on analytical solutions using elastic Beam Winkler Foundation models (Nikolaou&Gazetas (1997), Kavadas&Gazetas, Dezi et al , Mylonakis et al) and numerical ones using FEM. Most of the papers conclude in a closed form solution for the calculation of the bending moments. Despite the high number of papers on the subject none of them has taken into account the soil non-linearity, a simplification that may alternate strongly the results.

1.2 Earthquakes in Geotechnical Engineering

The study of geotechnical earthquake engineering requires an understanding of the various processes by which earthquakes occur and their effects on ground motion. Earthquakes have been for many years now in the center of the academic research in the field of Geotechnical Engineering as well as in Civil Engineering in general. This can be justified by the fact that the socio-economic consequences of such events can be

devastating, loses of human lives, economic breakdowns (look the 2011 japan eq). We are talking about a phenomenon that is complex and totally unpredictable and uncontrollable, so to be able to design resilient structures we must understand the basics about earthquakes and how they are created

1.2.1 The Origin

The whole surface of earth is composed of different plates (fig.1.2.1) with range of sizes (some big as continents and other smaller ones. The plates are moving constantly with an unpredictable way, due to the inner processes that occur bellow the rigid mantle of the earth. Hence using the theory of elasticity, collisions between the plates create relative deformations in the planes that separate one plate with the other (also known as faults). This elastic energy is being saved in the bedrock in the form of shear stress. When this cumulative shear stress reaches a point where it overpasses the shear strength of the rock then this energy can be released with two different ways. Either slowly, where the motion created isn't a seismic one or violently creating new faults or awaking older ones. Sudden movement of these faults is responsible for earthquakes. An earthquake is simply the vibrations caused by the blocks of rock on either side of a fault rubbing against each other as they move in opposite directions. The bigger the movement, the bigger the earthquake.

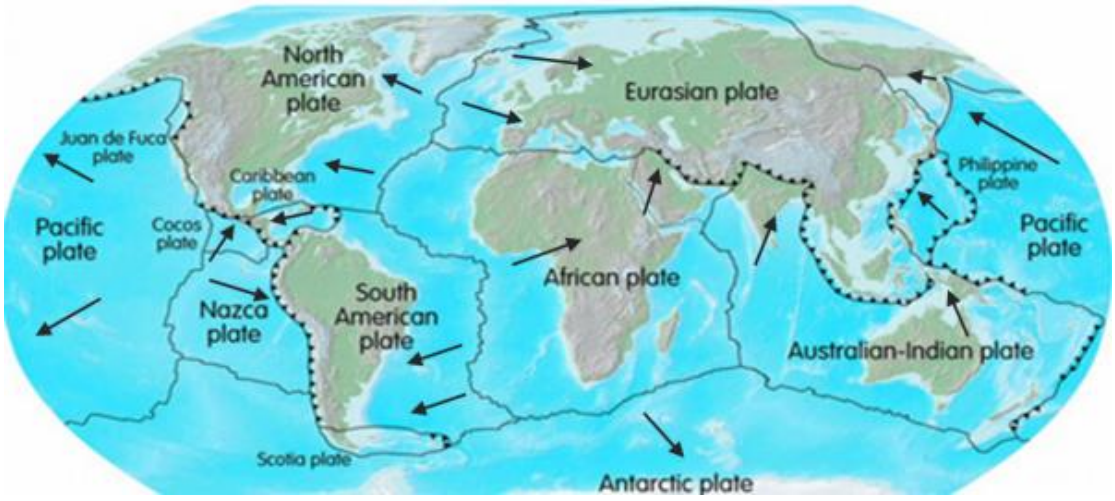

Fig. 1.2.1 Geographic Plates in which Earth's Crust is divided

1.2.2 Use of Wave Mechanics in Geodynamics

As it was mentioned above, the seismic energy that is being released in event of a shaking is transmitted in every direction in the form of waves. The propagation of those waves can be described with the use wave mechanics for solids. This simplification isn't far from the truth as we talk about the seismic waves, but in the

case of soil, a non-homogenous, non-linear, anisotropic material, the deviations for using elasticity theory can be significant. However, the use of elastic wave-mechanics is the core of the Geotechnical Seismic Mechanics not only for understanding the behavior of materials and structures under seismic motion but also for the seismic design of structures.

Seismic waves can be divided in two main categories: Waves that are transmitted through a material, body waves and waves that propagate only at the interface between two different media, surface waves.

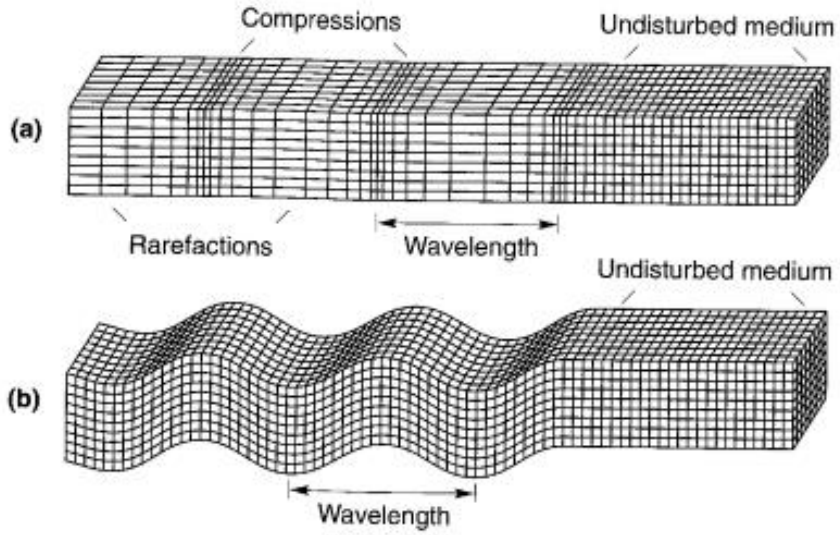

Fig. 1.2.2 Deformations produced by body waves: (a): P-waves , (b) : SV-waves (Kramer 1996)

Body waves are of two types P-waves and S-waves. P-waves also known as primary or compressional waves. As said in their name, compress the particles of the medium from which they pass, similar to the motion of sound waves. They are called primary, because they travel faster and are the first ones that can be recorded. They can travel through solids and fluids. The motion of a particle subjected to a P-wave is parallel to the direction of the velocity of the wave. Next, we have the S-waves also known as secondary or shear waves. They arrive after the P-waves , meaning that they travel slower. They can travel only through solids, because liquids have zero shear modulus (G). S-waves create shearing deformations as they travel through a material and the motion of a particle subjected to them is perpendicular of the direction of the wave velocity. This direction of particle movement can be further divide S-waves into the horizontal shear waves (SH-waves) if they travel horizontally and into the vertical shear waves (SV-waves) if they travel vertically. On the grounds that the speed of the body waves is directly connected with the stiffness of the materials they travel through, P-waves have higher velocities because soil as a material is much stiffer in compression. All of the above can be described numerically with the use of wave mechanics, starting from the simple problem of one-dimensional wave propagation in

a infinitely long rod. Consider such a rod with surface area A, Young modulus E, Poisson ratio and density ρ. If the angular deformations and rotations are impeded, then only the movements that are parallel to the direction of the rod are free. As a stress wave passes from the element shown in figure **(fig. 1.2.2)** the axial stress at the left of the element at the point x_0 is σ_{x_0} and on the right at the point $x=x_0+dx$ the axial stress is respectively, $\left(\sigma_{x_0} + \frac{\partial \sigma_x}{\partial x}\, dx\right)$. If we write down the dynamic equilibrium of this element we will get:

$$\left(\sigma_{x_0} + \frac{\partial \sigma_x}{\partial x}\, dx\right) A - \sigma_{x_0}\, A = \rho\, A\, dx \frac{\partial^2 u}{\partial t^2} \qquad (1.2.1)$$

Where u is the movement at the x-direction. The former equation can be simplified into:

$$\frac{\partial \sigma_x}{\partial x} = \rho\, \frac{\partial^2 u}{\partial t^2} \qquad (1.2.2)$$

which is the differential equation of motion for the infinite rod. But we also know that $\sigma x = M\, \varepsilon x$, where $M = \left[\frac{1-\nu}{(1+\nu)(1-2\nu)}\right] E$ and $\varepsilon_x = \frac{\partial u}{\partial x}$. These substitutions can further simplify the equation (1.2.2) into the same form as the one-dimensional longitudinal wave equation for a constrained rod:

$$\frac{\partial^2 u}{\partial^2 t} = \frac{M}{\rho}\, \frac{\partial^2 u}{\partial x^2} \qquad (1.2.3)$$

Where the term $\frac{M}{\rho}$ is equal to the wave propagation velocity squared (Vp^2) so:

$$Vp = \sqrt{\frac{M}{\rho}} \qquad (1.2.4)$$

It is important to notice in the last equation that the value of the propagation velocity doesn't depend on the motion, but only on the properties of the rod material (stiffness, density, Poisson ratio etc.). The wave propagation velocity is the velocity at which the body wave travels through a medium and has nothing to do with the particle velocity that describes the movement of every individual mass that constitutes the rod. This particle velocity is equal to:

$$\dot{u} = \frac{\partial u}{\partial t} = \varepsilon_x \frac{\partial x}{\partial t} = \frac{\sigma_x}{M} V_p \frac{\partial t}{\partial t} = \frac{\sigma_x}{M} V_p = \frac{\sigma_x}{\rho\, {V_p}^2} V_p \Rightarrow \dot{u} = \frac{\sigma_x}{\rho\, V_p} \qquad (1.2.5)$$

Eq. 1.2.5 shows that $\dot{u}$ is proportional to the axial stress of the rod

Using the same methodology, we can acquire the differential equation for a rod subjected to torsional moment T. In a random cross-section equally from before we will have:

$$\left(T_{x_0} + \frac{\partial T}{\partial x}\, dx\right) - T_{x_0} = \rho\, J\, dx \frac{\partial^2 \theta}{\partial t^2} \qquad (1.2.6)$$

Next if we simplify the Eq. 1.2.6 the equation of motion is produced:

$$\frac{\partial T}{\partial x} = \rho\, J \frac{\partial^2 \theta}{\partial t^2} \qquad (1.2.7)$$

Where J is the polar moment of inertia of the rod about its axis. Considering that

$T = G\, J\, \frac{\partial \theta}{\partial x}$ and substituting in the Eq. 1.2.7:

$$\frac{\partial^2 \theta}{\partial^2 t} = \frac{G}{\rho} \frac{\partial^2 \theta}{\partial x^2} = V_s^2 \frac{\partial^2 \theta}{\partial x^2} \qquad (1.2.8)$$

In which $V_s = \sqrt{\frac{G}{\rho}}$ is the propagation velocity of torsional wave. We can discern that also in this case the velocity is independent of the amplitude of the motion.
It is worth noting that, the afore mentioned have to do with the propagation of waves in an infinite linear rod. However, the result can be extended in the case of a 3-D space, with very complex mathematical formulas, but with the same logic. By solving the dynamic equilibrium for the cases of compression and shear waves we will have the following velocities:

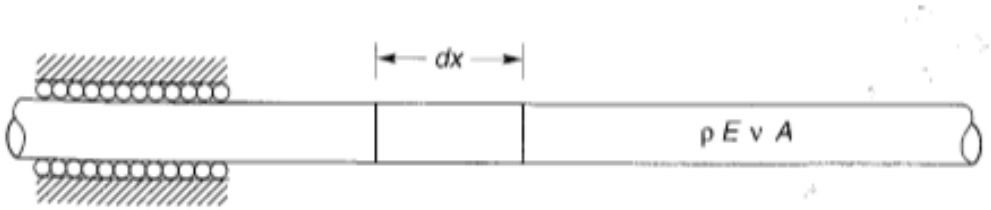

Fig. 1.2.3 Constrained, infinite rod for one dimensional wave propagation. Constrained against radial straining schematically represented by rollers (Kramer 1996)

Surface Waves are created with the interaction of P- and S-waves at the interfaces of the different soil layers and mostly the earth surface. The S-waves follow the earths curvature moving “trapped” at the surface of the earths mantle. Which means that in a surface wave the energy dissipation is far less, due to the 2-D transmission (surface) instead of the body waves that are having a 3-D movement. This effect lets the surface waves travel in further distances maintaining high amplitudes. For this reason, the surface waves are the most dangerous ones. The two most important types of surface waves are Rayleigh waves (1885), that are generated from the interaction of P- and SV- waves and Love waves that are created from the interaction of P- and SH- waves. Rayleigh waves are born close to the surface of the homogenous elastic half-space and their amplitude is decreasing exponentially with the distance. Rayleigh waves are responsible for the biggest part of the earthquake vibrations and their amplitude can be much larger than the one of the other waves. Love waves(1927) on the other hand can only be found in cases where there is soil layer with high velocity beneath

another with a much smaller one. Their nothing but SH-wave trapped in a soil layer. Love waves velocity is much lower than the P- and S- waves but higher than the Rayleigh ones.

1.3 Damping

Damping is a general term which can be divided in many subcategories depending on the type and source that creates it.

In a homogenous linear elastic soil the waves travel to infinity without any alterations in their amplitude (if the scatter effects are not taking into account). But this type of behavior cannot occur though in real materials. The amplitude of waves in real materials attenuate with distance. This attenuation can be accrued to two sources, one depending on the material, in which the wave is travelling and the other the geometry of the problem of wave propagation (Kramer,1996)

1.3.1 Material Damping

Material Damping is divided into two components hysteric damping and viscous damping.

A. Hysteretic Damping:

Hysteretic damping is the result of friction between the grains of dry soils. The energy dissipated over a cycle of deformation has been found to be independent of frequency over a wide range of frequencies, and proportional to the square of the amplitude of vibration. This behavior forms the basis of the so-called material damping or hysteric damping model; the resulting stress-strain curve forms a tilted ellipse with average slope equal to Young's modulus as shown in Figure 1.3.1.

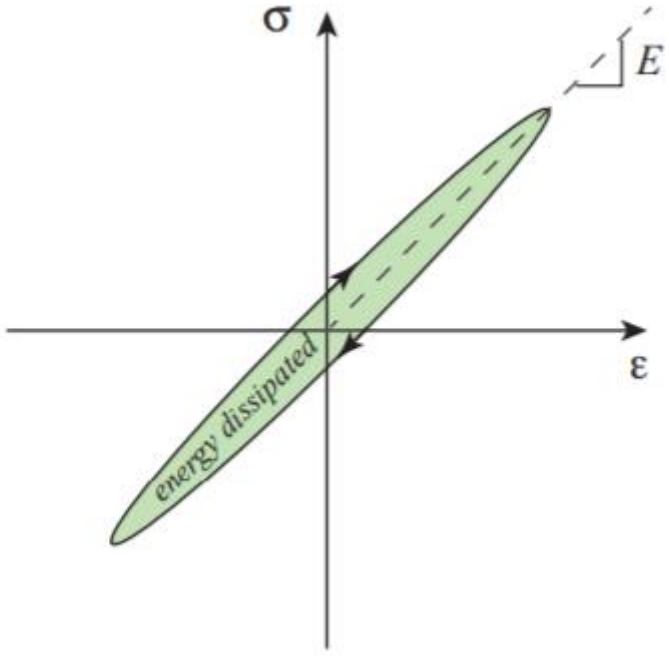

Fig. 1.3.1 Stress-Strain curve of Hysteric Dumping Model

The energy dissipated over a cycle is given by

$$Wh = \alpha h X^2 \qquad (1.3.1)$$

Hence,

$$C_{eq} = C_h = \frac{\alpha_h}{\pi \omega} \qquad (1.3.2)$$

B. Viscous Damping:

For saturated permeable soils heat is being produced from the movement of the fluid inside the pores of the soil's frame. This approach confronts soils as truly viscous, depending from frequency and forms a comparison between the dynamic damping and creeping effects. (Abbiss 1986). For the purpose of viscoelastic wave propagation three models can be used for simulation Kelvin-Voigt model, Maxwell model and linear solid model. The first one is the most used one because of its accuracy. With the Kelvin-Voigt model a counterpart viscosity is being used, $\eta = 2G\xi / \omega$ with a constant shear modulus. With this method soil damping can be considered independent from frequency.

1.3.2 Radiation Damping (Geometric Damping)

Other than material damping there is also another which is purely based on geometry. It is called radiation or geometric damping. This reduction on the amplitude of the wave is of purely geometric origin, a result due to the spreading of constant elastic energy over a greater volume of material. For problems where the source of the radiation is finite (foundation vibrations) radiation damping can be extremely important. In this case the radiation damping plays a predominant role in the total damping of the system.

- **Foundations**: Every time a foundation moves against the soil, stress waves originate at the contact surface and propagate outward in the form of body and surface waves. These waves carry away some of the energy transmitted by the foundation on to the soil, a phenomenon reminiscent of the absorption of energy by a viscous damper (hence the name) (Gazetas,1983).

1.3.3 Rayleigh Damping

One of the most used ways of analyzing non-linearities, geometric or the ones that have to do with the material, is dynamic analysis with Rayleigh damping. The high popularity of this method is deriving from the its simplicity. Similar to a viscous damping model it leads to the interpretation of damping in the mass and stiffness matrixes in a linear form. However, we are still talking about an artificial way of damping meaning that its not based in physics. Rayleigh damping (Rayleigh, 1954) is a special case of which. Rayleigh damping known as proportional damping or classical damping model expresses damping as a linear combination of the mass and stiffness matrices, that is, damping matrix for a system:

$$[C] = a\,[\boldsymbol{M}] + \beta\,[\boldsymbol{K}] \qquad (1.3.3)$$

where α and β: damping coefficients and real scalars

[C]: Damping Matrix

[M]: Mass Matrix

[K]: Stiffness Matrix

Coefficient α is responsible for the effect of the mass in the damping of the system. When this increases we have higher damping in low frequencies. Coefficient β determine the effect of stiffness in the damping of the system and respectively when it increases the damping on the higher frequencies increases. The damping ratio for the nth mode of such a system is

$$\xi_n = \frac{a}{2}\,\frac{1}{\omega_n} + \frac{\beta}{2}\omega_n \qquad (1.3.4)$$

We can understand from eq. 1.3.4 that α and β can be calculated d from specified damping ratios ξ_i and ξ_j for two different frequencies ω_i and ω_j.

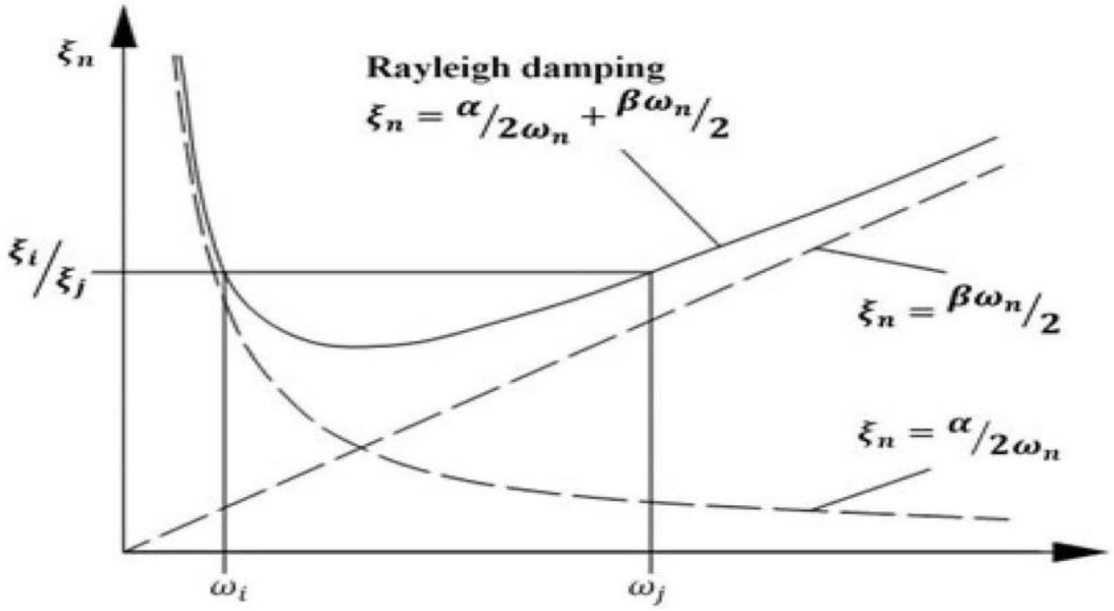

Fig. 1.3.2 Rayleigh damping is presented with both of its two components: mass proportional damping (α), stiffness proportional damping (β)

1.4 Pile foundations

Pile are one of the most common method of deep foundations. Figure (1.4.1) shows the different foundation types that are generally used in structural systems. Surface or embedded foundations have small $\frac{L}{D}$ ratios, where piles have really high slenderness ratios. In the middle of the two others we have the caisson foundations, slenderness and embedment wise. For a more realistic distinction of the foundation types, the compressibility of the soil as well as the structure should be considered.

Piles can be made from wood, steel or concrete. They are principally used to transfer the loads from a superstructure, through weak, compressible strata or water onto stronger, more compact, less compressible and stiffer soil or rock at depth, increasing the effective size of a foundation and resisting horizontal loads (Tomlinson & Woodward, 2007). Most common structures are really large buildings, bridges , wind-turbines and cases where the soil conditions under the superstructure are not suitable for construction. They have the form of cylinder with diameter d, that can vary from 0,3- 1,5 m. Their length L is the most crucial parameter for the load transfer to stiffer soils, which means that the $\frac{L}{D}$ should be high enough to satisfy that function $(\frac{L}{D} > 8)$. However piles aren't only used for transferring loads, but also for settlements prevention, increase lateral load capacity and more.

Piles can be further divided by their installation method to driven and cast in place piles. Driven piles are piles of pre-cast concrete that are then forced into the ground. On the other hand, cast in place piles have a bit more complicated installation sequence. The soil is bored is out of the ground, then reaming is performed and lastly the concrete is poured in the hole. There is also another way, where reaming and concrete pouring are done simultaneously and the pile in that case have a different name called as, CFA piles.

The bearing capacity of a pile in a compression load is the sum two components, shear resistance of the shaft Q_s and base resistance Q_b. Those two numbers are affected by the type of pile and surrounding soil as we as the installation technique. Depending on the way the mechanism that is created in order for the pile to withstand a compression force we can divide them into end bearing and floating (friction) piles (Fig. 1.4.2). The end bearing piles are mostly based on transferring the superstructure load through their toe ($Q_b>>Q_s$), base resistance is predominant. Contrariwise floating (or friction) piles are the ones that shaft-frictional component is predominant, most of the pile capacity is developed by shear in the sides ($Q_s>>Q_b$). It is worth noting though that the displacement for a pile to reach its bearing capacity is different for the shaft resistance (≈0.5% d) and for base resistance(≈5-10% d).

The driving of bearing piles to support structures is one of the earliest examples of the art and science of a civil engineer. The first recorded use of piles is from the Neolithic Era, in Switzerland close to 12000 years ago. The citizens there used tree logs that forced in the soft seabed of lakes, on which they built tall houses so that can be safe from the wild animals. In mediaeval times, piles of oak and alder were used in the foundations of the great monasteries constructed in the fenlands of East Anglia. In China, timber piling was used by the bridge builders of the Han Dynasty (200 BC to AD 200). Other than that Venice citizen build their city on top of wood piles in the delta of the river Po, so that they could defend against the invasion of the enemies. In the end the construction and design of piles obtained academic base with the establishment of Soil-Mechanics by their “father”, Terzaghi at 1925.

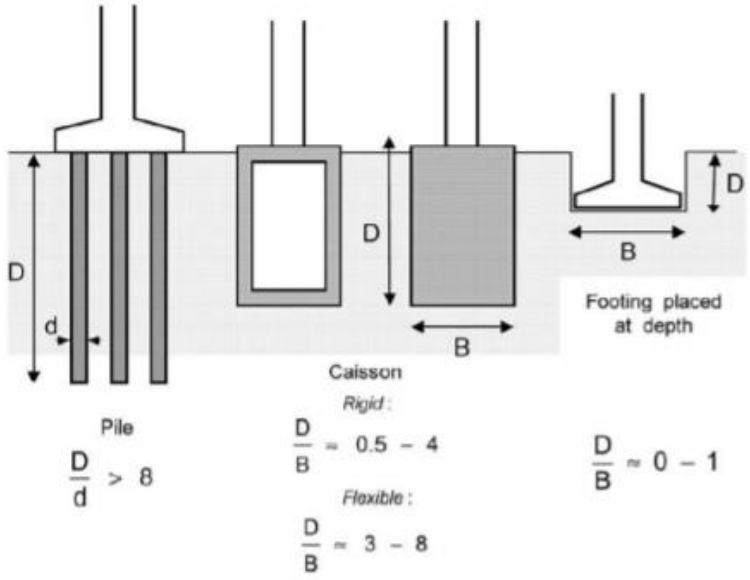

Fig. 1.4.1 Different foundation types that are used in structural systems (Gerolymos Gazetas 2006)

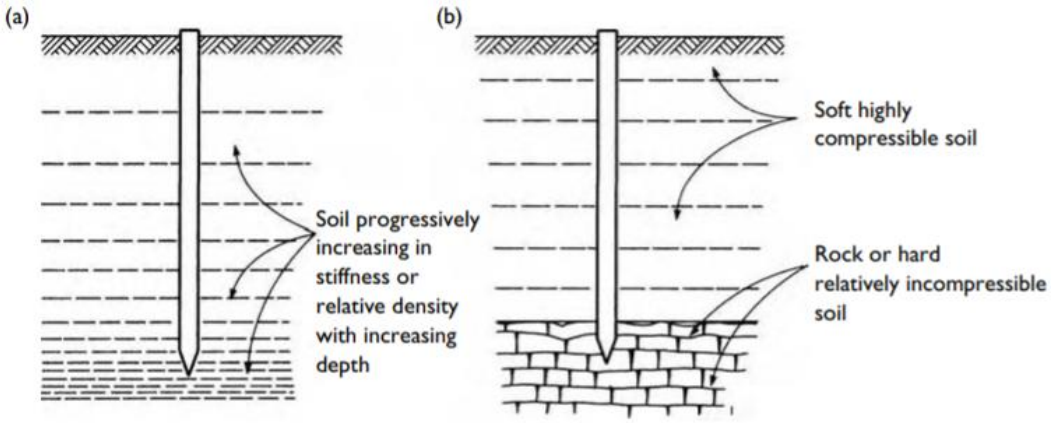

Fig. 1.4.2 Types of Bearing piles (a)->floating (b)-> end bearing(Tomlinson & Woodward, 2007)

1.5 Inertial and Kinematic Loading on Piles

It is noted in EC-8 that piles should be designed in order to withstand the two following types of loading:

- Inertial forces from the super-structure
- Kinematic loadings due to vibratory deformations of the surrounding soil induced by the passage of seismic waves through the soil

While the seismic waves propagate through the soil there is a difference observed between the motion of the pile and the soil surrounding it. This difference between them is a result of many factors like, the soil layering, pile-soil stiffness contrast (E_p/E_s), the predominant soil frequency, excitation frequency and lastly the kinematic boundary conditions of the pile at the head and the toe. As curvatures are imposed to the pile body by the vibrating soil, bending and shearing will develop even in the absence of a superstructure. The associated pile bending moments are, thereby, referred to as ‘‘kinematic’’, to be distinguished from those generated by loads acting at the pile head due to the dynamic response of the superstructure (so-called ‘‘inertial’’ moments). Kinematic and inertial bending moments constitute complementary aspects of a unique phenomenon known as soil–pile–structure interaction (SPSI) (Mylonakis,Sica)

Supports for the third scenario comes from the fact that damages have often been observed in piles after earthquakes at depths, that are too deep, meaning that it is not the result of inertial loadings and secondly at soils where there was no sign of liquefaction. This type of damage after many field observations and analytical solutions (Nikolaou & Gazetas, Mylonakis) has been associated with the presence of strong discontinuities in the soil layering (High contrast between Soil stiffnesses). The reason behind those bending strains that are created is the large curvatures that are imposed at the interface, as the top part and the bottom part are deformed differently, due to the stiffness contrast. The soil shear strain on the interface is discontinuous because of the different shear moduli between the consecutive layers which makes the soil curvature in that given point not finite (curvature is the derivative of strain).

The kinematic loading creates bending moments other than the interface, also in the head. Which means that at the head except from the inertial bending moments from the superstructure there is also a kinematic component. As far as inertial bending moments, their maximum occurs at the head (in the case of fixed head of course) but in the case of kinematic moments it's not that simple. The maximum can occur either at the head or the interface, depending on the stiffness contrast between the soil layers as we will see later on.

1.5.1 Different types of analysis for Kinematic loadings

The response of the pile by the passage of vertical S-waves in a multi-layer soil profile can be analyzed either Finite Element Models (Kausel & Roesset,1976) or with Beam-on-Dynamic-Winkler-Foundation model.

1.5.1.1 Finite Element Analysis

The soil close to the pile can be simulated with the use of volume elements whereas the boundaries of the model play the role of free-field boundaries using specific boundary multilayer profile or even a parabolic (using HS small) or a linear profile. But the soil profile can't change in x or y direction, given the fact that we have free boundary conditions in both. After the calculation of the stiffness of the surrounding soil it is possible to calculate the forces that are imposed to the pile and secondly the piles motion mechanism. This formula is being followed by the FEM analysis programs like ABAQUS, PLAXIS or ADINA.

1.5.1.2 Beam on Dynamic Winkler Model Foundation analysis (BDWF)

The soil pile interaction is simulated with a set of springs and dashpots continuously distributed along the pile. Where the parameters of the springs k=k(ω) (stiffness) and c=c(ω) (damping) are dependent on the frequency of the input motion. These parameters can be estimated after model calibration with use of a FEM program (i.e. PLAXIS). They are affected by the soil stiffness and by the soil damping (propagation and hysteric). This approach has been used extensively to estimate the dynamic impedance of piles in relation to inertial interaction analyses. The springs and dashpots connect the pile with the free-field soil with any available method. This type of analysis can also consider non-linearities with the use of non-linear springs. The equations that can describe the kinematic soil-pile interaction are the following:

$$\frac{\partial^2 U_{ff}}{\partial z^2} + \left(\frac{\omega}{V_s}\right)^2 U_{ff} = 0 \qquad (1.5.1)$$

$$E_p I_p \frac{\partial^4 u}{\partial z^4} - \rho_p A_p \omega^2 u + (k_x + i\,\omega c_x)(u - U_{ff}) = 0 \qquad (1.5.2)$$

1.5.2 Literature review for Kinematic Loadings

In the literature there many different equations for the simplified approximated calculation of the max kinematic Moment that is developed on the pile in the depth of the interface between two different soil layers. Some of them are based on semi-analytical solutions that are trying to simulate the specific phenomenon and others are based on experimental data

and Finite Element analyses (Closed form equation through data processing). However all of these solutions are for a specific geometry and soil parameters, because even for small changes in one of the above parameters (geometrical or material ones) can give totally different Moments.

1.5.2.1 Analytical Estimation of Kinematic Moments (Nikolaou & Gazetas 1997)

Nikolaou and Gazetas paper focused on improving the understanding of the importance of kinematic loadings on the seismic performance of piles. The geometric characteristics of the analysis that they performed can be seen in figure 1.5.1. New analytical results for piles in homogenous and layered soil deposits were developed by implementing BDWF model. A closed form solution has also been developed for computing approximately the maximum steady-state bending moment at the interface between two layers. This expression is based on the estimation of a 'characteristic' shear stress τ_{inter}, which is proportional to the actual shear stress that is likely to develop at the interface, as a function of the free-field acceleration at the soil surface, α_{sur}. Therefore, we have:

$$\tau_{inter} \approx a_{sur}\rho_1 H_1 \quad (1.5.3)$$

Where, ρ_1: density of the upper soil layer

H_1: height of the upper soil layer

a_{sur}: free-field acceleration at the soil surface

And the kinematic bending moment at the interface is:

$$M_{max} = 0.042\,\tau_{inter}\,d^3\left(\frac{L}{d}\right)^{0.3}\left(\frac{E_p}{E_{s1}}\right)^{0.65}\left(\frac{V_{s1}}{V_{s2}}\right)^{-0.5} \quad (1.5.4)$$

Where, d: pile diameter

L: pile length

E_p: piles elastic modulus

E_{s1}: upper soil layer elastic modulus

$V_{s1.2}$: shear velocity for the upper and lower soil

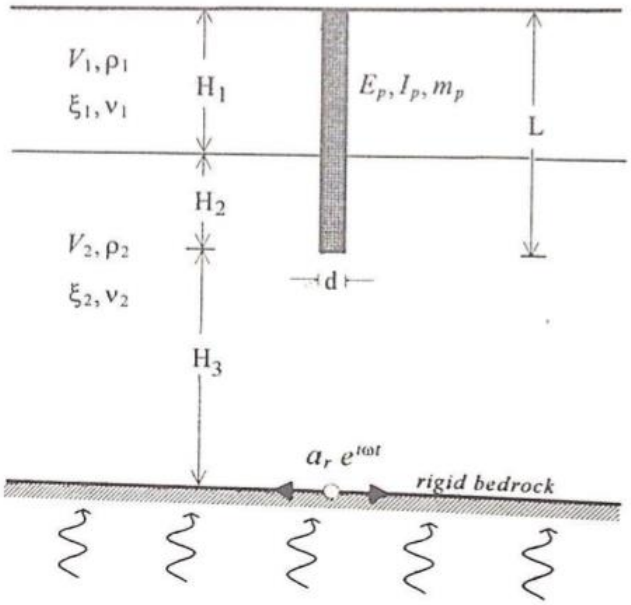

Fig. 1.5.1. The system used in the parametric study: a single pile embedded in a two-layer profile on rigid bedrock, excited by harmonic SH seismic waves

The same authors proposed another expression for maximum bending moment at the interface, which is based on the maximum deformation that is developed at the horizontal cross section of the pile is:

$$\varepsilon_M = \frac{M}{E_p I_p}\frac{d}{2} = \frac{M}{I_p\left(\frac{\pi d^4}{64}\right)}\frac{d}{2} \cong \frac{10M}{E_p d^3} \tag{1.5.5}$$

Using this equation the maximum bending moment is:

$$Mmax = \frac{2.7}{10^7} E_p d^3 \left(\frac{a_r}{g}\right)\left(\frac{L}{d}\right)^{1.3}\left(\frac{E_p}{E_{S1}}\right)^{0.7}\left(\frac{V_{S1}}{V_{S2}}\right)^{-0.3}\left(\frac{H_1}{L}\right)^{-1.25} \tag{1.5.6}$$

Both of the above expressions were based on BDWF analyses (fig. 1.5.2) and represent only the case of a two layered profile. It is also worth mentioning that these equations have to do with constant accelerations, meaning they were conducted with constant harmonic motions at the base of the model. In the case of accelerograms (real or synthetic ones) was almost thee same, in a smaller scale.

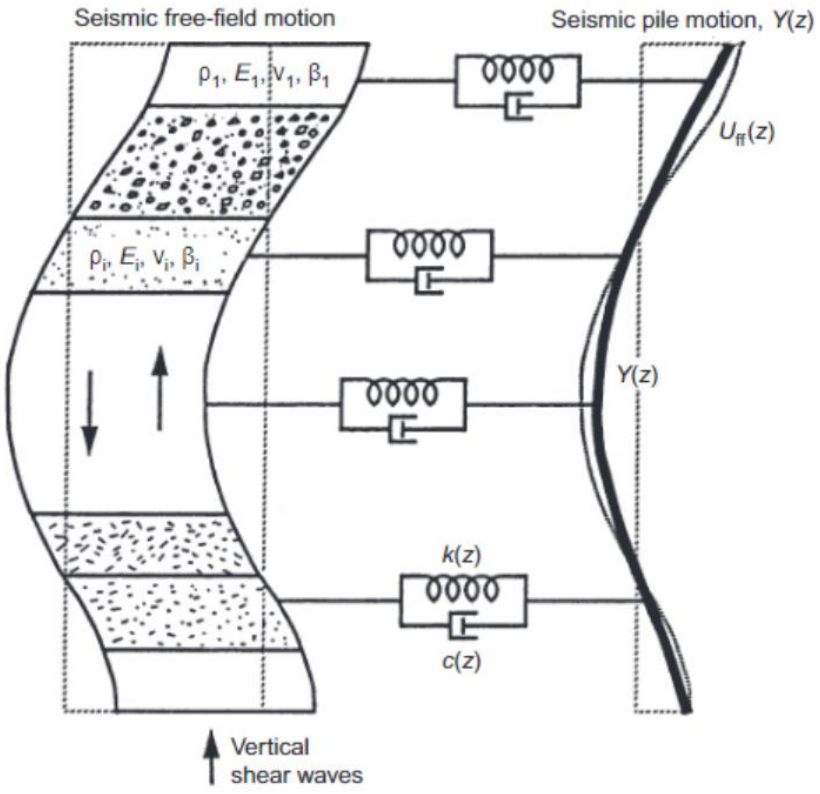

Fig. 1.5.2 The beam on dynamic Winkler foundation (BDWF) model for a pile in a multi-layer soil profile used in the Nikolaou & Gazetas paper (2001). The pile is excited by vertically propagating S waves.

However harmonic steady state results can only rarely be used directly in design. This is because only a hypothetical harmonic excitation with very large number of cycles would produce a response with amplitude equal to the steady state value. A more transient excitation like an earthquake, would tend to produce smaller response. The authors tried to correlate steady-state and transient peak response with a comprehensive numerical parameter study in a form like the following:

$$maxM(t) = \eta\, maxM(\omega) \qquad (1.5.7)$$

in which M(t): is the moment that is developed from a real accelerogram motion and

M(ω): is the moment that is developed in the case of steady state motion where $f_{inp}=f_{s1}$

η: reduction factor

The η reduction factor depends from the following:

- The duration of the accelerogram in the case of cycles of motion (meaning the cycles of the predominant frequency of the accelerogram) (N_{cycles})
- The ratio of $\frac{T_p}{T_s}$ where T_p is the predominant period of the earthquake and Ts is the 1st resonance period of the soil profile

- The ratio of $\frac{maxM(T)}{M(T)}$, that is directly linked with the damping of the system soil and pile

Conclusively we have the analogy:

$$\eta = \eta\left(Ncycles, \frac{T_p}{T_s}, \xi_{eff}\right) \quad (1.5.8)$$

The calculation of the parameters N_{cycles} and T_p is conducted with the help of over 80 analysis that were conducted with the use of different accelerograms. At figure 1.5.3 (the one with the graphs of η) one can see the proposed diagram for the reduction factor *η*. One can see two different lines the lower one is for the case that the T_{inp} is far off the T_{s1} (meaning not close to resonance) the other one is the opposite. The reduction factor η is designed to frequency on the time field while the damping ratio is set to ξ_{eff}=10%.

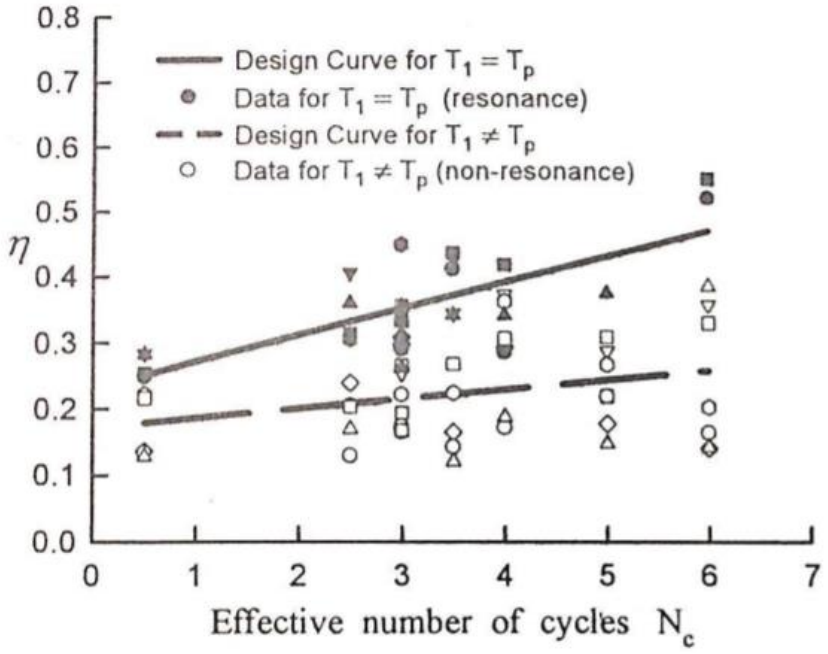

Fig. 1.5.3 The design curves that were proposed by Nikolaou & Gazetas for the frequency to time reduction factor η as a function of the number of "effective" excitation cycles and resonance conditions.

However observing the graph one can notice that if the number of cycles increases and as the period of loading gets closer to the predominant period of the soil then we have an increase in the *η*, meaning that the reduction is getting smaller in comparison to the harmonic motion. It is also clear that the increase in cycles in the case of the lower line in the graph (Tinp/Ts not close to 1) has almost no effect on the factor *η*. For this reason, for the construction of the graph there were used seismic data with predominant periods close to the resonance period of the soil as well as outside of the resonance field.

Case Study:

The authors in order to validate the proposed formula they did a case study about a 12 storey building located in Japan. Its foundation is a pile group of 20 piles. Comprehensive instrumentation of this building was conducted, were accelerometers at the free field as well as the bottom of the foundation was installed and also at two of the piles pile strains were installed at 6 different depths. So having all the above data it was possible to simulate a seismic loading that was measured by the instruments with the use of the BDWF model and see the deviations between the two of them (notice that the BDWF model doesn't take into account the interaction phenomena of the pile group). Several interesting trends are worthy to note. Firstly the strains measured between the corner and the center pile are almost identical meaning that the kinematic phenomena are minor (which has also been shown by many authors Makris & Gazetas(1993), Dobry & Gazetas (1988). Secondly the computed peak values (inteface) tend to overestimate the Bending Moments by as much as 50%. While modelling errors are possible, this may also imply that the gauges might not be located at exactly the interface or that maybe the measured V_s difference between the soil layers is less. Nevertheless, the agreement between the predicted and recorded time histories is quite satisfactory.

Picture of the piles at the Kobe earthquake 1995 in Japan. One of the first observations of failures at depths that didn't coincide with the dynamic loadings and introduced the kinematic loadings to the world.

1.5.2.2 Transient Kinematic Pile Bending in two-layer soil (Sica, Mylonakis, Simmoneli 2011)

This article is focused in the case of flexible piles (piles greater than the so called active length) embedded in two layer stratum with interface placed deep beneath the surface. Mylonakis developed a simple formulation for predicting kinematic bending moment at a layer interface under low- frequency excitation (ω->0). The kinematic bending moment may be derived from a strain transmissibility parameter ε_p/γ_1, which is simply the ratio between peak pile bending strain ε_p, and free-field soil shear strain at the interface γ_1. The corresponding analytical solution is

$$\left(\frac{\varepsilon_p}{\gamma_1}\right)_{\omega\to 0} = \frac{1}{2c^4}(c^2 - c + 1)\left(\frac{h_1}{d}\right)^{-1}\left\{\left[3\left(\frac{k_1}{E_p}\right)^{\frac{1}{4}}\left(\frac{h_1}{d}\right) - 1\right]c(c-1) - 1\right\} \quad (1.5.9)$$

Where $c = \left(\frac{G_2}{G_1}\right)^{0.25}$ is the layer stiffness contrast

H_1/d the embedment ratio

K_1 the Winkler spring modulus associated with the spring layers

As it was mentioned above this equation doesn't take into account the transient dynamic nature of the phenomenon, we are talking about static conditions. So Mylonakis in order to take into account the frequency parameter introduced a correction function *Φ* of the form:

$$\Phi_1 = \frac{M(t)_{max}}{M_{resonance}} \quad (1.5.10)$$

, which accounts for the effect of frequency on kinematic pile bending. Considering this the kinematic moments takes the following form:

$$M(t)_{max} = 2\frac{E_p I}{d}\left(\frac{\varepsilon_p}{\gamma_1}\right)_{static}\Phi_1 \quad (1.5.11)$$

Where $(\varepsilon_p/\gamma_1)_{\omega=0}$ is provided by Eq. (1.5.9) and Φ_1 by (1.5.10), $(\gamma_1)_{static}$ can be obtained through the following equation:

$$(\gamma_1)_{static} = \frac{a\, h_1}{V_{s1}^2} \quad (1.5.12)$$

Where $a=a_s=a_r$ is a uniform psedostatic seismic acceleration in the profile. This approach is attractive specifically for engineers as it does not require a free-field site responses analysis. Though the biggest disadvantage is that parameter Φ_1 is sensitive to variations of $(finp/f_1)$, which is often unknown with sufficient accuracy in practice. Another important thing to notice in this article is the figure 1.5.4. One can see that the M_{dyn} is at the most area of the graph lower than the static one (the one with ω=0). This can be justified easily, if someone takes a look at the parameters of the analysis that were conducted. All the accelerograms that were used are so high (4-8 *Hz*) , where the first resonance period of the soil studied is at (f_1=1.6 *Hz*). An enlarged version of figure 1.5.4 is figure 1.5.5, where one can better understand the ϕ_1 factor as well as the reduction factor, *η,* proposed by the Nikolaou&Gazetas:

$$\eta = \frac{M(t)_{max}}{M_{resonance}} \quad (1.5.13)$$

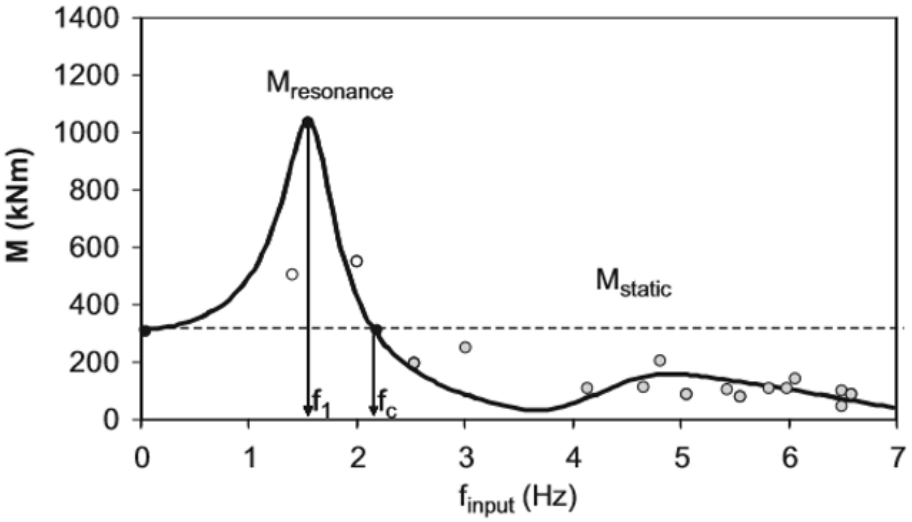

Fig 1.5.4 Comparison of the static moment to the dynamic moment in the frequency domain. At values close to the predominant period of the soil the Mdynamic becomes maximum due to resonance effects

Also the authors derived expressions for the Φ_1 and η parameters with the use of numerical regression BDWF analysis. The regression relations are the following:

$$\eta = 0.68 \left(\frac{f_{input}}{f_1}\right)^{-1.5} \quad (1.5.14)$$

$$\Phi_1 = 1.94 \left(\frac{f_{input}}{f_1}\right)^{-1.3} \quad (1.5.15)$$

Which are valid for long piles and f_{input}/f_1 ratios greater than approximately 1.5. Those two equations can be used to quantify the effect of transient nature of input motion on kinematic response of piles. Naturally, both parameters tend to drop with increasing f_{input}/f_1 that is for conditions far from resonance. For $f_{input}/f_1 \approx 1$ the result exhibit significant dispersion. In that frequency range, response is known to depend on number of excitation cycles an affect which is not captured

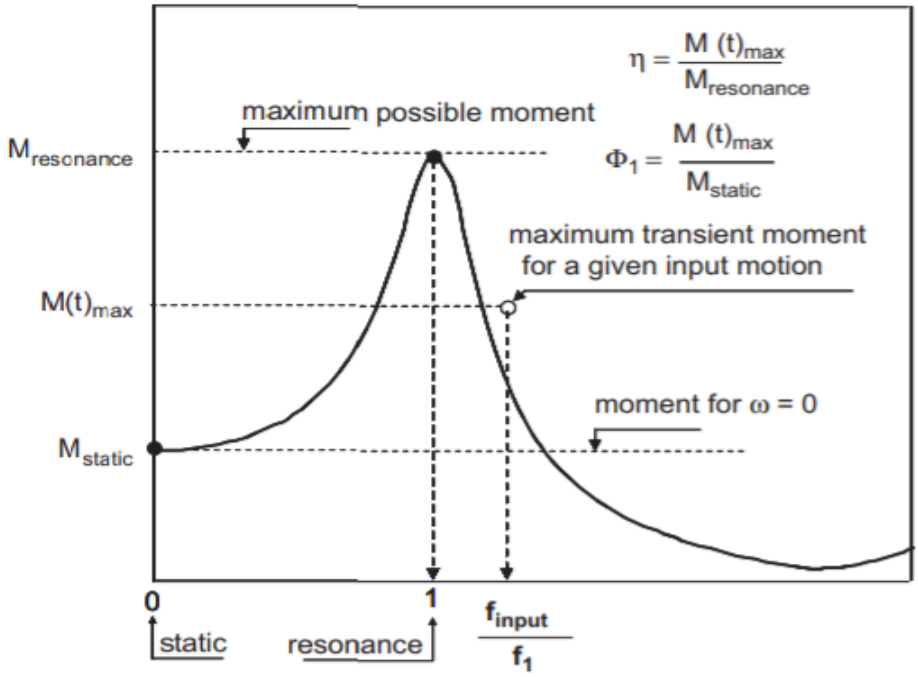

Fig. 1.5.5 The Φ_1 and η factor from the Sica,Mylonakis paper 2011.

1.5.2.3 Insight on kinematic bending of flexible piles in layered (Di Laora, Mandolini, Mylonakis 2012)

In this paper the equation for the kinematic moments is the following:

$$M(t)_{max} = \frac{2E_p I}{d}\left(\frac{\varepsilon_p}{\gamma_1}\right)_{st}(\gamma_1)_{dyn}\,\Phi_2 \qquad (1.5.16)$$

This equation looks a lot like the one from the last paper (Mylonakis 2011), the only differences are that in this case it's a dynamic approach, meaning that $(\gamma_1)_{\omega=0}$ is now $(\gamma_1)_{dyn.}$ The ratio $\left(\frac{\varepsilon_p}{\gamma_1}\right)_{st}$ can be computed with the use of this expression:

$$\varepsilon_p = \chi\gamma_1\left[-\frac{1}{2}\left(\frac{h_1}{d}\right)^{-1} + \left(\frac{E_p}{E_1}\right)^{-0.25}(c-1)^{0.5}\right] \qquad (1.5.17)$$

This equation tries to take into consideration the sign of the Kinematic Moment at the interface and broaden the area where this equation is valid. To overcome this limitation, FE data in terms of absolute pile bending strain, which encompasses site response, is presented in Fig. 1.5.6 corresponding to uniform peak acceleration for all signals with reference to a deep interface. Evidently, the correlation is quite satisfactory, especially at large strain amplitudes resulting from resonance and/or strong stiffness contrasts. The first term inside the brackets pertains to site response and the second to the stiffening effect due to the presence of the second layer (interface action); w is a regression coefficient. Note that for G2/G1=c=1 the latter term disappears and only the negative contribution, due to the first layer, remains. Conversely, for (h1/d)->oo the first term vanishes and only the positive contribution remains.

The associated coefficient w was found to be close to unity (about 0.93) and, thereby, is of minor importance from a practical viewpoint.

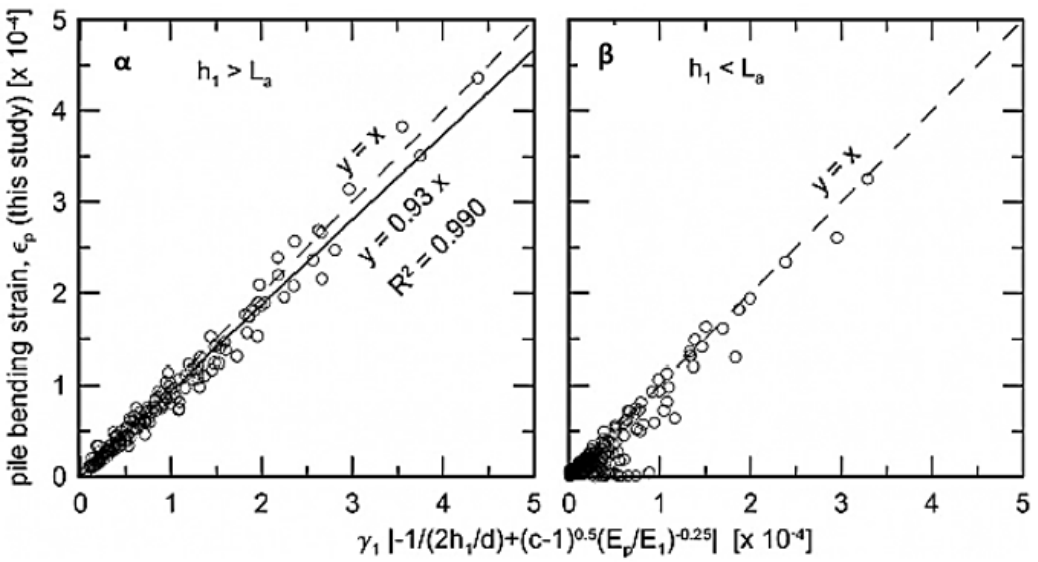

Fig. 1.5.6 Comparison between absolute pile bending strain from finite element results and the regression formula proposed by Mylonakis et al 2012, for a)deep and b)shallow interfaces.

After analyzing the data with the use of linear regression, it was found that Φ_2 is usually between 1-1.5. From figure we can see that Φ_2 exhibits a weak dependence on frequency.

Alternatively, peak transient bending moment may be estimated on the basis of surface acceleration, as, thereby avoiding a site response analysis. In this case:

$$M_{max} = \frac{2E_p I_p}{d}\left(\frac{\varepsilon_p}{\gamma_1}\right)_{st}\frac{a_s \rho_1 h_1}{G_1}\,\Phi_{1,s} \qquad (1.5.18)$$

Factor $\Phi_{1,s}$ generally attains values below unity (Fig.1.5.7). The term $\frac{a_s \rho_1 h_1}{G_1}$ on the right side defines an interface shear strain evaluated for a stress reduction factor rd¼1 [18], thereby being an upper bound to the true shear strain in that elevation, s a conservative selection for $\Phi_{1,s}$ would be 1.

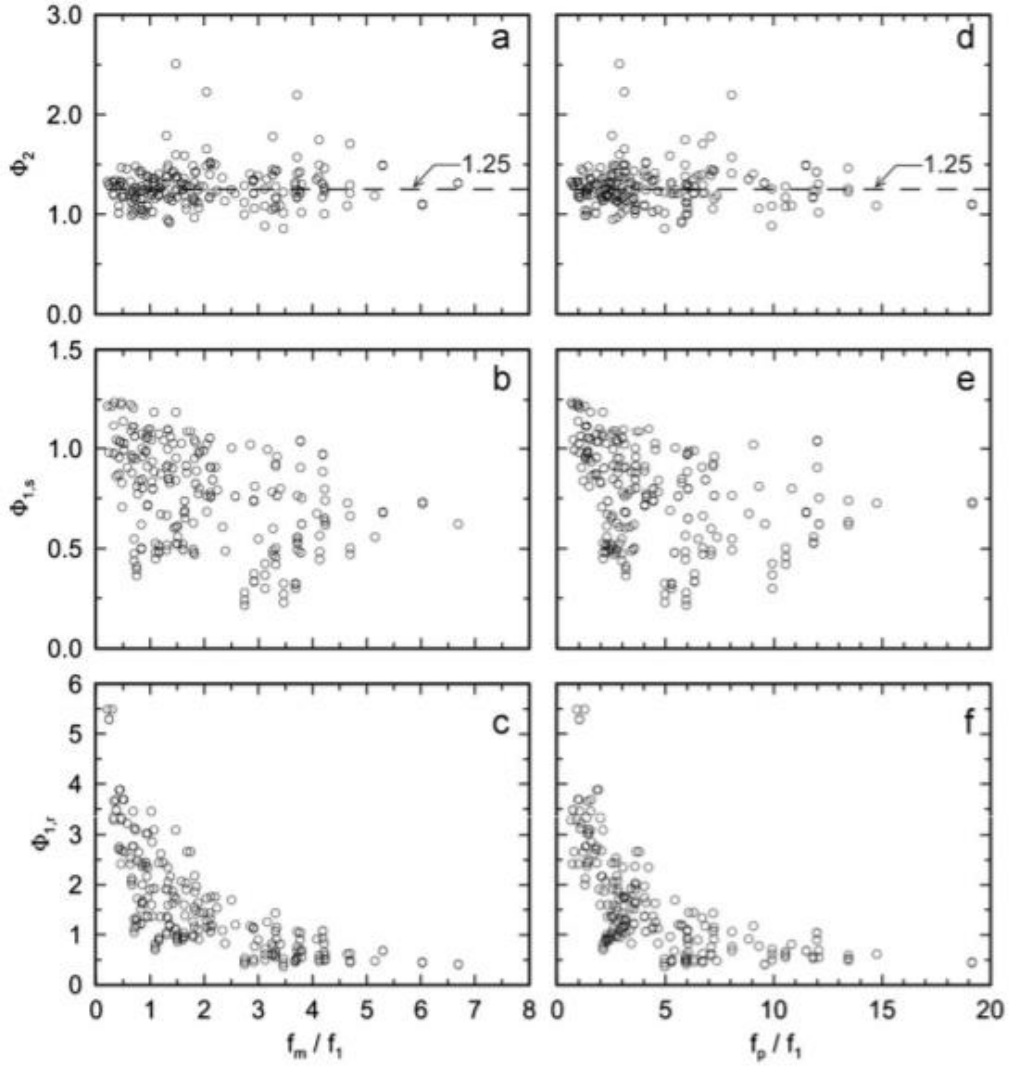

Fig. 1.5.7 Dynamic factors against dimensionless frequencies f_m/f_1 (a),(b),(c) and f_p/f_1 (d),(e),(f). Results are relative to cases coresponding to deep interface (Mylonakis et al 2012)

As a third alternative, Mmax can be correlated to rock acceleration, ar, through the analogous expression:

$$M_{max} = \frac{2E_p I_p}{d}\left(\frac{\varepsilon_p}{\gamma_1}\right)_{st}\frac{a_r \rho_1 h_1}{G_1}\Phi_{1,r} \qquad (1.5.19)$$

where $\Phi_{1,r}$ is an pertinent factor (Fig.1.5.7). Compared to the previous parameter $\Phi_{1,r}$ exhibits a stronger dependence on frequency which can be attributed to site response. Naturally, the ratio between $\Phi_{1,r}$ and $\Phi_{1,s}$ can be interpreted as a ‘‘site factor’’ in the context of seismic Codes for perfectly rigid bedrock conditions. Fig. 1.5.7, e, f present corresponding results based on the predominant frequency fp obtained from the peak value of the 5%-damped acceleration response spectrum. The observed trends are analogous to those based on the mean frequency fm. Accordingly, knowledge of an ‘‘exact’’ excitation frequency is deemed inessential for interpreting the results.

On the basis of the above results, new regression analyses were carried out for computing the transient pile bending moments at the soil layer interface. Three alternative procedures were outlined to solve the problem in the realm of routine engineering calculations. Specifically: a) The approach based on Φ_1 is perhaps the most attractive for engineering purposes, as it does not require a free-field site response analysis. A disadvantage is that parameter Φ_1 is sensitive to variations of (f_{input}/f_1) ratio, which is often not known with sufficient accuracy in practice. b) The approach based on Φ_2 is also attractive as dynamic effects due to frequency content of the input motion are incorporated into parameter $(\gamma_1)_{dyn}$, whereas Φ_2 is a constant. A potential disadvantage is that a free-field site response analysis is required to establish the value of $(\gamma_1)_{dyn}$. c) The approach based on Z requires knowledge of $M_{resonance}$, which can be realized by means of Eq. (1.5.19). As in the case of parameter Φ_1, η is sensitive to variations of frequency ratio (f_{input}/f_1).

1.5.2.4 Kinematic Bending Moments in Pile Foundations (Dezi, Carbonari , Leoni 2009)

In this paper a numerical procedure is specialized and validated to analyze the seismic behavior of single piles embedded in layered soil. A finite element model is used for the piles and Winkler-type medium for the soil. Both the piles and soil are considered to have linear behavior. The soil-pile interaction is performed in the frequency domain and the excitation motion is obtained by means of a 1-D propagation analysis. A comprehensive parametric analysis is carried out by considering piles with fixed-head and by varying the main parameters governing the dynamic response of piles. The influence of soil properties, the bedrock location, the stiffness transition between layers, the diameter and the bedrock embedment of piles are discussed. Finally, on the basis of the parametric analysis that was carried out, new design formulas are proposed for predicting the kinematic bending moment in end-bearing piles, valid both for the cross-sections at the head and the interface.

The kinematic bending moment expression proposed is the following:

$$M(V_s, D, h, PGA) \cong \frac{PGA}{0.25\,g}\, M_{400}(D,h)\exp[f(D,h)(V_s - 400)] \qquad (1.5.20)$$

Where the PGA/0.25g accounts for the different seismic motion intensities owing to the problem linearity. Formulas for evaluating bending moments $M_{400}(D,h)$ and the function $f(D,h)$, defining the dependency of the exponential regression on D and h, are calibrated with a nonlinear least square procedure by fitting the data obtained in the parametric analysis.

With reference to the maximum bending moment at the **interface** between bedrock and deposit, the following polynomial approximations hold:

$$M_{400}(D,h) = (77.7\,D^3 + 409D^2 - 192D + 24.5)(-0.0009\,h^2 + 0.068\,h - 0.2) \quad (1.5.21)$$

$$f(D.h) = (0.000124h - 0.01106)(-0.05D + 0.864) \qquad (1.5.22)$$

On the other hand, with reference to the maximum bending moment at the pile head , the following expressions are obtained:

$$M_{400}(D,h) = (85D^3 - 85.75D^2 + 30.93D - 3.37)(0.000133h^2 - 0.00042h + 1.091) \quad (1.5.23)$$

$$f(D,h) = (0.00067h - 0.0113)(-0.07D + 1.002) \quad (1.5.24)$$

The above equation permits predicting straightforward the bending moments at the critical sections of an end-bearing pile embeedded in a generic homogenous soii by knowing the *PGA* association to the soil class A as defined in EC-8, the velocity of the shear wave of the deposit, the pile diameter and the bedorck depth. It is worth noticing that this expression accounts both for the local site response and the soil-pile kinematic interaction.

1.5.2.5 Kinematic Bending Moments in Square Pile Groups (Dezi, Poulos 2016)

This paper deals with kinematic bending moments resulting from the soil deformations during seismic events and presents simplified formulas for the assessment of the maximum kinematic bending moments in piles within square pile groups, starting from the knowledge of bending moments on a fixed-head single pile. Formulas refer to both the pile head and the pile cross section at the interface between different soil layers with high-impedance contrast. Correlation factors between bending moments arising in the single pile and the group were obtained by fitting results of an extensive parametric investigation in which different square pile groups and different soil profiles were investigated. In particular, for each soil profile of the parametric investigation the procedure proposed by Dezi et al. (2009) was used to perform the analyses, considering different square pile groups and the fixed-head single pile. Kinematic bending moments obtained from the single-pile analyses were used to normalize moments for the groups, thus quantifying the group effect for the specific soil profile.

An empirical formula for calculating the bending moments for piles in square groups, both at the head and at the interface separating soil layers was proposed,which was derived as follows:

$$M_{max}^{G} = M^{S} a(n, \frac{s}{d}) \quad (1.5.25)$$

where M_{max}^{G} is the maximum bending moments arising in the piles of the group at the head or at the interface separating soil layers; M^{S} is the relevant single pile bending moment *a* is the group factor depending on the number of piles and spacing; and *n* is the number of piles constituting the square group. M^{S}has to be determined from a dynamic analysis or by means of simplified methods available in the literature. The following expressions were proposed for the group factor *a*:

$$a\left(n, \frac{s}{d}\right) = a\left(\frac{s}{d}\right) \log n + b\left(\frac{s}{d}\right) \quad (1.5.26)$$

In which coefficients *a* and *b* assume different expressions depending on the considered pile cross section. For the pile head

$$a\left(\frac{s}{d}\right) = 0.16\left(\frac{s}{d}\right)^{-0.28} \quad (1.5.27)$$

$$b\left(\frac{s}{d}\right) = 0.58\left(\frac{s}{d}\right)^{0.23} \quad (1.5.28)$$

Whereas for the interface separating soil layers

$$a\left(\frac{s}{d}\right) = -0.12\left(\frac{s}{d}\right)^{-0.3} \quad (1.5.29)$$

$$b\left(\frac{s}{d}\right) = 0.88\left(\frac{s}{d}\right)^{0.04} \quad (1.5.30)$$

1.5.3 General Conclusion for Kinematic Loadings on Piles

Here are presented some general conclussions that can be derived from the papers that were listed above.

Considering the Nikolaou&Gazetas(1997) considering differences between free and fixed-head piles:

- The kinematic Bending strain in a free-hesd pile in homogenous soil increases with depth, reaching its maximum at approximately the mid-length of the pile. In contrast, for a fixed-head pile, bending strain is decreasing with depth, having its maximum at the head.
- For a two-layered profile the bending strain diagram exhibits a pronounced peak close to (but not exactly at) the interface between the two layers. This is in agreement with the foregoing discussion about the concentration of kinematic moments in the variety of layer interfaces.
- The bending strain diagrams of free-head and fixed head piles converge with depth and become practically identical beyond a certain distance from the surface. This depth concides with the so-called 'active pile length', beyond which a head-loaded pile behaves as in infinitely long beam.

And some general conclussions about the parameters that affect the kinematic moments:

- For a given excitation frequency, the kinematic bending strain depends mainly on : the stiffness contrast (V_1/V_2) between any two consecutive soil layers in the deposit; the boundary conditions at the pile head or cap; the proximity of the excitation period, T_1, of the soil deposit; and the relative depth, h_1/L_a, measured from the top of the pile down to the interface of the layers with the sharpest stifness contrast, normalised with the respect to the active length, L_a, of the pile.
- The bending strains are largest either at the pile head or at the vicinity of the interface of soil layers with the sharpest stifness contrasts. The strains at the interface for free-head and fixed-head piles are identical, except when the pile is 'short' or 'rigid'. (i.e. when $h_1<L_a$).
- In most cases, the maximum harmonic bending strain occurs at the fundamental natural period of the soil deposit. The pile strain transfer functions display a very rapid reduction when moving away from resonance. The variation of kinematic bending strain with frequency follows, more or less, the amplification of the free-field acceleration: a_s/a_r. This shows the great influence of the first mode of vibration on the magnitude of bending strain, and contraditcs some earlier statements in the literature that higher modes would produce larger kinematic

bending. Indeed while higher frequencies tend to generate wavy shapes of deflection (and this having the potential for inducing large curvatures at the interface), the actual curvature is also affected by overall drift between the top and the bottom of the pile. This drift usually becomes maximum at the first naturam modem and thereby produces the largerst bending at the first resonance.

- Pile curvatures are in most cases not equal to soil cuvatures (as assumed in some design methods). Their values depend on the characteristics of the soil and the pile, the excitation frequency and the depth from the soil surface.

Conclusions from Mylonakis, Di Laora, Mandolini (2013):

- Kinematic Moments at the pile head were found to increase in proportion of the fourth power of pile diameter, d whereas corresponding inertial moments increase in proportion to the second or third power. This suggests that kinematic moments will tend to dominate seismic demand with increasing pile diameter. Moreover, because the moment capacity of a pile is proportional to d^3, there always exists a maximum diameter beyond which a pile cannot sustain kinematic action at the head. Conversely, inertial loading imposes a minimum required diameter.
- Contrary to kinematic moments at the pile head, kinematic moments at a layer interface increase in proportion to d^3, the same as the dependence on pile diameter of yield resistance M_y. Accordingly, a variation in diameter does not improve or reduce safety in that elevation and, thus, the value of interface moment cannot control pile size in design.
- As the interface depth increases there is a moment that is transmitted from the interface to the head. The basis of the interpretation is that the increased stiffness of the second layer acts as a partial fixity, which tends to reduce pile rotation at the interface, thus generating a positive contribution to bending moment in that location. A certain percentage of this moment is transmitted to the pile top, as a function of thickness of the surface layer and stiffness mismatch between pile and soil. This interaction may be investigated by means of a simple Winkler beam, which is loaded at one end by a bending moment (representing the action of the interface) and is fixed against rotation at the other end (representing the boundary condition at the pile head). The length of the beam stands for the thickness of the surface layer. Figure(1.5.8) depicts the moment reaction at the pile head, as a function of the applied interface moment and the dimensionless beam length. The positive bending contribution generated at the interface is transmitted as a positive fraction to the pile head, thus reducing the absolute value of the bending moment. On the contrary, for larger depths (h_1) the positive additional moment at the interface is transmitted to the pile head as a negative contribution, thus increasing the overall bending moment
- Time domain results have shown that we have three different response regions are distinguishable depending on the depth of the upper soil layer (h_1).

- $H_1<H_{c1}$, then there is reduction of the moment at the head, because the moment is transmitted from the interface with a negative sign
- $H_1>H_{c2}$, then there is the case where the interface is far too deep so there is no interaction at the piles head.
- $H_{c2}<H_1<H_{c1}$, then there is an increase of the moment at the head because the moment is transmitted from the interface with a positive sign.

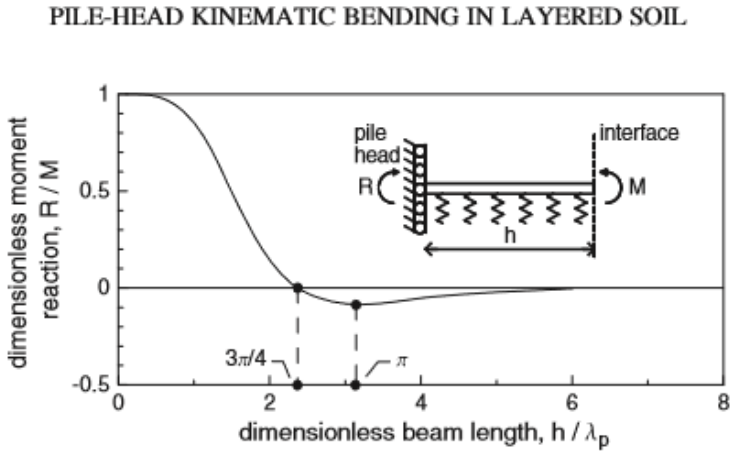

Fig. 1.5.8 End reaction ,R, of a Winkler beam fixed against rotation at one end and loaded at the other end by a concentrated bending moment M.

Conclusions from Dezi et al. (2009):

- As V_{s1} increases the moments at the interface as well as the head are decreased. This can be explained if someone thinks about the cause of the kinematic moments, which is the difference in motion between the pile and the surrounding soil. This difference is decreasing as the soil's stiffness increases (V_{s1} increase means G_{s1} increase), because firstly the ratio E_p/E_{s1} is getting smaller and secondly the soil develops smaller displacements meaning that u_{ff}-u_{pile} decreases.
- As the depth of the bedrock increases there is a transfer of moment from the head to the interface (as before mentioned by Mylonakis (2013)).
- The peak values of bending moment in the pile, at the interface between the deposit and the bedrock, increase with the pile diameter and the thickness of the surface soil layer as well as with the stiffness contrast between layers.
- For small values of the surface soil layer thickness, the maximum bending moment arises at the pile head instead of the layer interface.

- A reduction of the bending moment is obtained considering soil profiles with transition layers instead of sharp change of properties. Bending moment peaks become considerably smoother and wider.

A common simplification of all the above articles is that we are talking about a single pile, while there are no expressions for the case of pile groups. A case like this is really difficult to simulate or solve analytically due to the complex mechanisms of pile groups in a two layered soil under dynamic loading. Also the geometry of the problem is a crucial factor for the motion of the group as well as the parameters of the materials. We try to take look at this problem in some of the next chapters with the use for 3D FEM linear and non-linear analyses.

1.6 Group Effects in Kinematic Loadings

In the most cases of deep soil foundations not a single pile is used, but a group of piles (only maybe in wind turbines someone uses mono piles). The action of a pile group isn't only used for bearing the loads of the superstructure but also to enhance the soil surrounding the piles. But practice and many papers proves that when a pile is a member of a pile group its efficiency decreases. This efficiency is being affected by the number of piles in the group as well as the distance between them, which means that the bearing capacity of the pile group isn't equal with the bearing capacity of one pile multiplied by the pile number($P_{u,group} \neq n \sum P_u$). This means that increasing the pile's number in the group isn't always the best solution to overcome a capacity problem. So with the term efficiency that is used frequently in the case of pile groups, is equal to mean critical load for each pile at the case of fracture of the pile group, divided by the critical load for a singe pile. Also the settlement of a pile group differ strongly from the settlement of a single pile , where group mean load in each pile of the group is equal to then one imposed to the single pile. Similar observations have been made also for the case of lateral loads.

For the correct design of a pile group the mechanism behind the interaction between the piles as well as the group and the surrounding soil must be analyzed. In the case of the pile to pile interaction there is a lot of research with the use of analytical solutions (Makris & Gazetas 1993) as well as micro scale experiments. Data from real scale experiments are limited , due to the huge cost of each one of them. Generally, the design of a pile group must include the following inspections:

- Distribution of the loads to each individual pile of the group and finding which pile is the most strained.
- The bearing capacity of the soil that is affected by the pile group
- And last that the settlements of the group are not greater than the opposed limit.

The behavior of a pile group is affected strongly by the type and the quality of the surrounding soil, the construction type of the piles and the boundary conditions of them. One of the goals of this thesis is to research the case of the group effects using linear and non-linear constitutive models for the soil in the case of kinematic loadings.

2. Finite Elements and Constitutive Models

2.1 Introduction

Among the several methods that are aiming to solve soil mechanics problems are methods that are trying to satisfy all the theoretical requirements using realistic simulations of soils behavior. Because of the complexity and the nonlinear behavior of the soil, these methods are numerical. Usually approaches based in the Finite Element Method Analysis are the most commonly used in the geotechnical engineering.

In this chapter a brief description of the Finite Element Method is presented, which is followed by a presentation of the main operation principles of PLAXIS Software which was used for the numerical analysis of the present essay.

In the following chapters a clarification of some technical and scientific terms will be presented, which are determining for the correct use of the Software as well as for the realistic simulation of the particular problem under investigation.

2.2 Solving Methods

The main subject of the Soil Mechanics is the study of the strength and the deformation of one ideally simplify material that represents the real soil with the best accuracy possible, under loading conditions and conditions according to the limits that are defined by the type and the data of every problem. (Valalas, 1981)

The methods which are used for the solving of Soil Mechanics problems are divided in three groups (Valalas, 1981).

- The analytical methods
- The Numerical methods
- The Empirical methods

The calculating procedure used in the first two type of methods is almost the same and is divided in two main parts. In the first part is made an attempt to understand and analyze the physical problem and then to create a mathematical model that most accurately represent this problem. The second part consists of the solution of the mathematical problem which usually has the form of one or more differential equations with determined independent variables which are usually one or more of the dimensions X, Ψ, Z or the time t.

The difference between the two Methods is that while Analytical Methods use the analytical methodology to solve the mathematical problems, the Numerical Methods use some numerical technic. Up to now, the analytical method has solved only problems that the physical problem can be analyzed in a small number of differential equations.

The third type of methods are based in the observation and the systematic study of a big number of cases that lead through statistics to the assessment of an empirical formula. There

are many completed empirical calculation methods, like i.e. calculation of Foundations or calculation of thrusting e.t.c. Many famous scientists claim that the empirical methods give

implement. Nevertheless, it should be mentioned that these methods could be applied only for cases that are equivalent with the ones that the empirical formulas have been based on.

The rapid development of the computers in recent years has given a significant boost to numerical methods for solving Engineering problems. For this reason, engineers that were studying Soil Mechanics began to re-examine the old known problems from the beginning and accept assumptions near the complex reality, taking into account characteristic properties such as heterogeneity, non-linearity of the material medium, complex initial stress conditions, random geometry, discontinuities, variability with space and time properties, and various other factors. At the same time, thanks to the great capabilities of PCs, they have been able to densify the network used so that the accuracy of the calculations to be totally satisfactory.

There are various numerical methods that have been successfully used. Of all these methods, the Finite Element method and the Finite Difference method have been used more. The basic principle of most numerical methods is the principle of discretization. In simple words, discretization is the work with which the problem you are studying in an important area is appropriately divided into small elements. Where appropriate, discretization may be in different forms. For example, we can say that in the Finite Element method, the area you are studying temporarily breaks down in small dimensional geometric elements while in fact it is continuous.

In the following chapters a brief description of the Finite Element Method is presented.

2.3 General Information for the Finite Element Method

The Finite Element Method (FEM), is a numerical method for solving problems of engineering and mathematical physics. The term FEM was introduced for the first time by Clough in 1960, during the study of the dynamic situation of a dam that he has divided in triangle elements.

The FEM Analysis is a very useful and accurate approach for solving geotechnical problems. Of course should be mentioned that the use of this Method to solve geotechnical problems has as requirement an in depth knowledge regarding the Finite Elements Method and the Soil Mechanics. Also the user of the Method should have a very good understanding of the limitations of the software that is used for the finite elements analysis.

The FEM is a numerical method that tries to physically approach a problem by dividing the physical space in individual distinguishable finite elements, for which equations are produced that have accurate solution.

In general this approximate method, which is based in the energy theorems, offers great potential and gives solutions for cases that other methods fail. The basic characteristic of this method is the need to determine a compatible field through functions defined throughout the material, which meet certain boundaries conditions. With this approach, if we consider for example the problem of the displacement of a material, the initial problem of the determination of the field of displacements at each point of the material is transformed in

the problem of determining a finite number of unknown coefficients. In this way an approximate solution to the original problem arises.

When the boundary of the material is simple, the construction of the functions that satisfy the conditions at the boundaries is a relatively simple matter but when the boundary of the material becomes complex, the fulfillment of the boundary conditions becomes almost impossible. This difficulty is overcome with the use of the Finite Element method. According to this method the material is divided into a number of designated areas, called elements. The functions used through these elements are simple and usually polynomial form.

The implementation of the FEM (Method of Finite Elements) to problems of elasticity (or generally deformation of materials) in two or three dimensions includes the following stages (Desai, 1979):

- Division of the field, which is examined in appropriate elements. The division of fields with irregular geometry is approximated with small straight lines sections.
- Selecting appropriate functions for the distribution of unknown variables in each element
- Determining the Functions linking the open deformation with the strain - displacement and the functions that connect the tension with stress-strain to connect the cause (tension, force) with the result (displacement) that is the unknown value.
- Construct the fundamental equations for each element (element equations).
- Aggregate by node of the element equations for definition of the final system and introduction of boundary conditions.
- Calculating the intensive state of each element as a function of the displacements at the nodes of the element.
- Calculation of the secondary values resulting from the solution (i.e. open deformations, tensions, etc.).
- Evaluation of the results.

The above steps are general and exist in the majority of problems faced by the FEM.

To solve a problem we have to construct a geometry in a software environment and then integration of this geometry into the finite element software. There are software programs for solving geotechnical problems with the use of finite element, like PLAXIS, which by themselves construct the geometry and then the solution.

The type of finite element to be used is determined by the needs of the analysis which is selected. An important step is also the definition of the problem to be solved, for example if it is chosen to solve the model in static stress, it should at this stage provide the data on the forces and supports. Finally, the discretization of the geometry of the construction follows.

The physical and mechanical qualities of the materials and the imposition of border conditions should then be defined. The properties to be defined in each case vary and depend on the nature of the analysis. The properties commonly used are the elastic modulus and the Poisson ratio. The definition of the boundary conditions also depends both on the nature of the analysis and on the characteristics of the finite elements, which determine the degrees of freedom.

The solving method chosen will depend on the requirements of the problem. Regarding the way to resolve, a quick resolution or certain repetitive resolutions can be used, which latter give more accurate results.

The results of the resolution may be presented in many different ways. For example, the results may be presented graphically in the form of diagrams or tables. In addition, the results may be presented on the nodes or on the elements. Specialized Software, like PLAXIS, offer a big variety of ways to present the results.

Because the mechanics of the deformations are described by differential equations with some producers, we can solve them with the help of finite elements. Differential equations for the problems of mechanics of deformable materials arise from a number of other equations such as correlations between displacement - reduced deformations, equations of symmetry of deformations and equilibrium equations in space. Like in every problem expressed by differential equations, and in the case of finite elements there are also boundary conditions such as natural boundary conditions (loads, etc.) and basic boundary conditions or conditions of Dirichlet and Newman (supports, etc.). Taking into account that, with the finite element method, we end up with a system of algebraic equations that their plurality is identified with the plurality of degrees of freedom of the problem, it is obvious that these can be solved only with the help of computers and hence the development of the method in line with the development of computer technology. The development of PCs with the increasing capacity to manage large volumes of data but also by increasing the speed of execution of numerical calculations in combination with the finite element method made it possible to resolve complex engineering problems which were considered unapproachable some years ago, so while earlier problems were solved in two dimensions, now with the use of PCs they can be solved as they are in nature, in three dimensions.

The use of finite elements for the solving of geotechnical problems began in 1966 when Clough and Woodward used this method to define motions and shifts in embankments, while Reyes and Deer described its application in underground rock excavation analysis. The method was initially used for materials that are linear elastic. An important extension of the method especially for soil mechanics was the application of the method to non-linear materials, such as soil. Many research papers and practical applications have taken place since its implementation until today. Today we have specialized software, such as PLAXIS, which solves purely geotechnical problems with the finite element method. The ability of the finite element method to accurately reflect ground conditions, is basically based on the ability of the structural model to represent the behavior of the actual soil and the correctness of the imposed boundary conditions.

Analyzing the system in its elements, individual behavior is more easily understood, and then the ability to synthesize and view the entire system allows the study of its total behavior (Valalas, 1981). The user should only define the appropriate geometry, construction process, soil parameters and boundary conditions. Components may need to be turned on and off during the numerical simulation to describe the field conditions. May be taking into consideration retaining structures consisting of several walls made up of components and due to the soil mass simulated in the analysis, the complex interaction between the sloping slopes or anchors and the ground can be taken into account. The influence of time on the

development of the distribution of water pressures can also be simulated by including a combined configuration.

During the implementation of the method no supposed mechanism of failure or method of behavior of the problem is required, as this arises from the kind of analysis. The analysis allows for the full history of the value limits problem and even a simple analysis can provide information on all design requirements. Potentially the method can solve completely three-dimensional problems and not depend on the limitations of the other methods.

2.3.1 Steps to resolve Finite Element Method

2.3.1.1 Discretization

The finite element method may be understood in the following example. Lets consider a body in which we want to find the distribution of an unknown variable, such as the displacement, then the body should be divided into a set of smaller geometric forms (Figure 2.3.1), ie elements. These elements are interconnected at specific points, the nodes. This process of dividing the medium into smaller elements or segments is called discretization (Agioutantis, 2002).

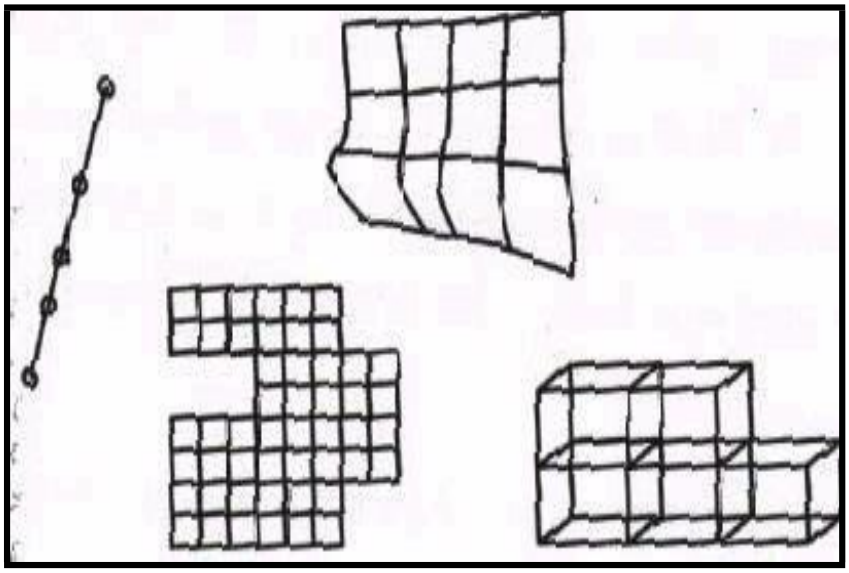

Fig. 2.3.1 Body division in elements (Agioutantis, 2002).

Discretization is one of the most necessary elements for the implementation of FEM. During discretization, there is a division of the medium into elements with the help of virtual lines or surfaces.

These elements consist of nodes that are connected with straight or curved segments. The picks of the elements define the nodes of the grid or the mesh of the discretization of the problem. On each node essentially correspond the physical quantities describing the cause and effect.

Typical element styles are one-dimensional or linear, triangular and rectangular, or quadrilateral in two dimensions, and pyramidal and prismatic (three-dimensional). The simplest forms of elements are those in which the number of the element node is equal to

the number of sides, such as triangular and tri-nodes figures, quadrilateral and quadro-nodes (levels) data, pyramidal and tetrakomvika (solids) components, etc. There, but also cases where there are more nodes describing an element, such as triangular and hexadecimal elements, quadrilateral and octal (flat) elements, etc. (Agioutantis, 2002).

For linear functions in 2D and 3D, the most common elements are illustrated in the figure 2.3.2 below. The linear basis functions, as defined in a triangular mesh that forms triangular linear elements, are depicted in this figure and this figure above. The basis functions are expressed as functions of the positions of the nodes (x and y in 2D and x, y, and z in 3D).

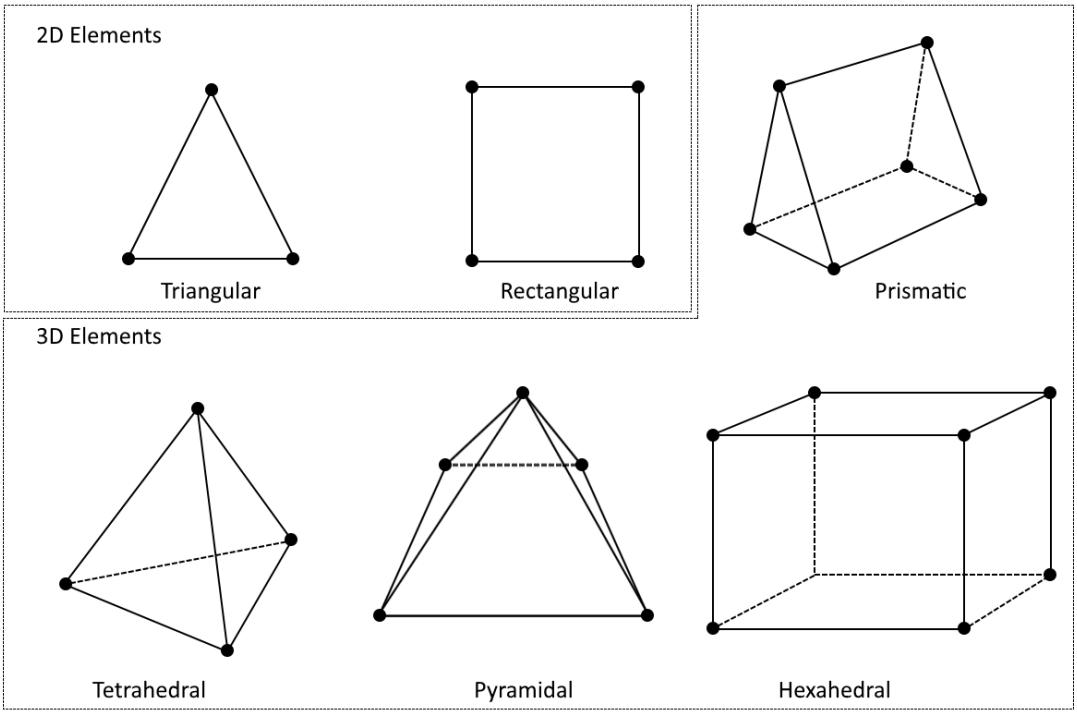

Fig. 2.3.2 Samples of 2D and 3D elements

In 2D, rectangular elements are often applied to structural mechanics analyses. Their 3D analogy is known as the hexahedral elements, and they are commonly applied to structural mechanics and boundary layer meshing as well. In the transition from hexahedral boundary layer elements to tetrahedral elements, pyramidal elements are usually placed on top of the boundary layer elements.

The number of degrees of freedom of an element is the set of unknown variables that correspond to each element. Also, the element is characterized by how its behavior and, by extension its properties, is linked with the sizes corresponding to their nodes. Thus, a linear element, which essentially represents a rod with the appropriate properties (with or without mass) depending on the problem being considered, may have two or more nodes and 1, 2, 3 or more degrees of freedom in each node depending on the type of the problem.

Flat elements may represent surfaces in two- or three-dimensional problems. In the usual cases of engineering problems, each node has two or three degrees of freedom that correspond to the vector components of the node shift. If the nodes transfer torques, then the degrees of freedom per node can increase by one in one dimension and by ,three in three

dimensions. In geotechnical applications, it is common to use triangular or quadrangular (flat) elements, which depict parts of a material whose the third dimension is unitary (where such simplified assumption is possible) (Agioutantis, 2002).

For the successful simulation of the behavior of a body with the FEM it is necessary to properly divide the body (field) into individual parts. This process includes the following parameters (Agioutantis, 2002):

- Selection of the geometry of the element
- Selection of the number of nodes of the element and by extension the degrees of freedom of each element
- Selection of the form functions of each element
- Selection of the density of the grid

Common practice for selecting the dimensions and the form of the elements is the use of smaller elements where large variations of the calculated variables are expected.

For example, when we have two-dimensional analysis triangular or quadrilateral elements with three and four nodes are the most common. It is possible, depending on the requirements of the problem, to increase the degrees of freedom of an element by adding more nodes, such as the use of a quadrilateral element with eight nodes.

The division of the field is such that the size of the elements is small at those points where high precision is required in the calculations, or where a sharp change in the desired size is expected, while the size of the elements is larger in the remaining areas of the field.

The selection of functions that express the distribution of the unknown variables (e.g., shifts) to each element as a function of the values of the variables in the nodes is directly related to the desired precision in the calculations but also with the time for resolving the problem. These functions are called shape functions (Agioutantis, 2002).

2.3.1.2 Shape Functions

The finite element method works by considering a known distribution across each element for the unknown variables. The equations that define the approximate distribution of variables are called shape function functions and they can be formulated in any mathematical form. In practice, however, the polynomial form is used. This choice is quite popular because of the ease of mathematical handling. This format is quite simple to differentiate and to integrate. In addition, the accuracy of the analysis can be improved by increasing the grade of the polynomial equations.

It is obvious that the higher grade the polynomials are, the analysis is closer to the real solution However, by increasing the grade of polynomial, the number of calculations to be made to analyze the model is increased also. For example, the element analysis described by second-grade polynomial requires three times the computing time than a linearly defined element need. This is the reason, that often it is preferable to use a denser grid of elements of a lower grade than a thinner grid of higher grade elements (Fagan 1992).

In the general case, the displacement at each point of an element is expressed as a function of the generalized coordinates (ie coordinates of the nodes and values in the nodes). For an element with two nodes the offset is expressed as follows:

$u=a1+a2y$ (2.3.1.1)

where a1 and a2 contain the displacements, as well as the coordinates of nodes 1,2.

If in the above relation the vectors u are replaced with the individual components, it gives:

$u_1=a_1+a_1y_1$ (2.3.1.2)

$u_2=a_1+a_2y_2$ (2.3.1.3)

Finally, we have

$\{q\}=[A]\{a\}$ (2.3.1.4)

where {q} is the vector of unknown displacements, [A] is the array with the coordinates of the element and {a} the unknown coefficients. Resolving we get:

$u= \sum u_iN_i$ (2.3.1.5)

Regarding to two-dimensional elements, the actions taken to connect cause-effect are summarized below, while for three-dimensional elements the actions are similar:

The displacement at each point of an element is expressed as a function of displacements at the nodes {ui} from the relationship:

$u = N_1u_1 + N_2u_2 + N_3u_3 + N_4u_4$ (2.3.1.6)

The constitutive equations of behavior represented by relationships of the form:

$\sigma_{ij}= f(\varepsilon_{ij})$ (2.3.1.7)

which can be written in the form of tables as follows:

$\{\sigma\}=[E]\{\varepsilon\}$ (2.3.1.8)

where table [E] represents a generalized record of the elastic properties of the material. The dynamic energy of each element arises as a sum of the internal energy as well as the work of the external forces that affect the element according to the relation:

Dynamic Energy = Internal Energy – External Forces Work

The External Forces belong to three categories:

• Field Forces (eg gravitational)

• Tensions (eg hydrostatic)

• Point forces

The relationship that connects the force {F} that each node receives and the displacement {q} is:

$$\{F\} = [K] \{Q\} \quad (2.3.1.9)$$

The dimension of the vector {F} for each element depends on the number of nodes of the element and on the degree of freedom of each node. For two-dimensional quadrilaterals, there is a total of eight degrees of freedom.

The physical significance of the register [K] may be given schematically as a square of nodes connected by virtual springs, where the coefficients of the register, Kij are equivalent constants of virtual springs that connect the nodes (degrees of freedom) of the element to each other. (Agioutantis, 2002).

It is obvious that the solution of the above equation over the vector of displacements will give the values of the unknown variables. However, in order to do this, the boundary conditions applied to the solid must be defined and then the inversion of the rigidity record to be made, which is a very difficult process, because a large number of equations are required to describe the large number of nodes. In recent years with the development of computers and the creation of specific mathematical models, it has been possible to solve these equations within a satisfactory timeframe.

By solving the equation and finding the unknown displacements for each node it is easy to calculate the deformations and stresses throughout the solid (Kalogirou, 2003).

2.3.1.3 Boundary Conditions

After creating and correlating the constitutive equations of the elements to form the system equations of the model and to fully describe the problem, the integration of the boundary conditions applied to the body must also be made. The integration of boundary conditions is necessary because the system of equations cannot be solved because the rigidity record cannot be reversed. Failure to reverse the rigidity record means uncontrolled movement in the form of a rigid body, and for this reason restrictive forces such as boundary conditions must be applied in order to keep the model in equilibrium (Kalogirou, 2003).

There are three types of boundary conditions (Agiouantis, 2002):

- Determining the requested parameter (displacement). These conditions are called geometric and are also known as Dirichlet conditions.
- Determining the change of the requested parameter (derivative of the displacement). These conditions are called natural border conditions and are known as the Neumann conditions.
- Determining both of the above parameters or mixed conditions. These are known as the mixed boundary conditions. In a mixed boundary value problem, the solution is required to satisfy a Dirichlet or a Neumann boundary condition in a mutually exclusive way on disjoint parts of the boundary.

2.3.1.4 Material behavior models

The choice of the appropriate behavioral model of the material as well as the selection of the values of the constants of this model is one of the most important factors for the successful simulation of the behavior of natural materials.

The simplest model that can be used is the linear elastic model. This model is not considered the most suitable for describing the behavior of rocks and soil materials in one or more dimensions. The material is considered to be deformed linearly and isotropically, as given by the following relation (Agioutantis, 2002):

$$\sigma_{ij} = \frac{E}{1+\nu} * \left[\varepsilon_{ij} + \frac{\nu}{1-2\nu} * \varepsilon_{kk} * \delta_{ij}\right] \quad (2.3.1.10)$$

where:

σ_{ij} : the stress tensor indicating the intense condition in the body[MPa],

E : the modulus of elasticity of the material [MPa]

v: the Poisson ratio of the material

ε_{ij} : the tensor of strain

δ_{ij} : the unit tensor (Kronecker delta).

For the case of deformation in one dimension, it is: $\sigma = E\varepsilon$ where:

σ: the stress applied to the material [MPa],

E = its modulus of elasticity [MPa],

In addition, other constitutive behavioral models, such as non-isotropic (orthotropic or anisotropic) elastic behavior models, as well as non-elastic behavior models can be easily used. Also, as the division of the field creates continuous but distinct parts of the body, it is possible to define different models of material at different points of the body (Agioutantis, 2002).

2.3.2 Deformation Theory

This chapter is about the basic equations for the static deformation of a soil body are formulated within the framework of continuum mechanics. A restriction is made in the sense that deformations are considered to be small. This enables a formulation with reference to the original undeformed geometry.

2.3.2.1 Basic Equations of Continuum Deformation

The static equilibrium for a continuum media can be formulated as:

$$\underline{L}^T \underline{\sigma} + \underline{b} = \underline{0} \quad (2.3.2.1)$$

Equation (2.3.1) relates the derivatives of the six stress components, assembled in vector $\underline{\sigma}$, to the three components of the body forces, assembled in vector $\underline{b}$. $\underline{L}^T$ is defined as:

$$\underline{L}^T = \begin{bmatrix} \frac{\partial}{\partial_x} & 0 & 0 & \frac{\partial}{\partial_y} & 0 & \frac{\partial}{\partial_z} \\ 0 & \frac{\partial}{\partial_y} & 0 & \frac{\partial}{\partial_x} & \frac{\partial}{\partial_z} & 0 \\ 0 & 0 & \frac{\partial}{\partial_z} & 0 & \frac{\partial}{\partial_y} & \frac{\partial}{\partial_x} \end{bmatrix} \quad (2.3.2.2)$$

Furthermore, the kinematic relation can be formulated as:

$$\underline{\varepsilon} = \underline{L}\,\underline{u} \qquad (2.3.2.3)$$

Equation 2.3.2.3 expresses the six strain components, assembled in vector $\underline{\varepsilon}$, as the spatial derivatives of the three displacement components, assembled in vector $\underline{u}$, using the previously defined differential operator $\underline{L}$. The link between Eqs. (2.3.2.1) and (2.3.2.2) is formed by a constitutive relation representing the material behavior. The general relation for constitutive models is:

$$\dot{\underline{\sigma}} = \underline{M}\,\dot{\underline{\varepsilon}} \qquad (2.3.2.4)$$

Combining Eqs. (2.3.2.1), (2.3.2.3) and (2.3.2.4) would lead to a second-order partial differential equation in the displacements $\underline{u}$.

However, instead of a direct combination, the equilibrium equation is reformulated in a weak form according to Galerkin's variation principle:

$$\int \delta\, \underline{u}^T (\underline{L}^T \sigma + \underline{b})\, dV = 0 \qquad (2.3.2.5)$$

In this formulation $\delta\underline{u}$ represents a kinematically admissible variation of displacements.

Applying Green's theorem for partial integration to the first term in Eq. (2.5) leads to:

$$\int \delta\, \varepsilon^T \sigma\, dV = \int \delta\, \underline{u}^T\, \underline{b}\, dV + \int \delta\, \underline{u}^T\, t\, dS \qquad (2.3.2.6)$$

This introduces a boundary integral in which the boundary traction appears. The three components of the boundary traction are assembled in the vector $\underline{t}$. Eq. (2.3.2.6) is referred to as the virtual work equation.

The development of the stress state $\underline{\sigma}$ can be regarded as an incremental process:

$$\sigma^i = \sigma^{i-1} + \Delta\sigma \qquad \Delta\sigma = \int \dot{\sigma}\, dt \qquad (2.3.2.7)$$

In this relation $\underline{\sigma}^i$ represents the actual state of stress which is unknown and $\underline{\sigma}^{i-1}$ represents the previous state of stress which is known. The stress increment $\Delta\underline{\sigma}$ is the stress rate integrated over a small time increment.

If Eq. (2.3.2.6) is considered for the actual state i, the unknown stresses $\underline{\sigma}^i$ can be eliminated using Eq. (2.3.2.7):

$$\int \delta\, \varepsilon^T \boldsymbol{\Delta}\sigma\, dV = \int \delta\, \underline{u}^T\, \underline{b}^j\, dV + \int \delta\, \underline{u}^T\, t^j\, dS - \int \delta\, \varepsilon^T\, \sigma^{j-1}\, dV \qquad (2.3.2.8)$$

It should be noted that all quantities appearing in Eqs. (2.3.2.1) till (2.3.2.8) are functions of the position in the three-dimensional space.

2.3.2.2 Finite Element Discretisation

According to the finite element method a continuum is divided into a number of (volume) elements. Each element consists of a number of nodes. Each node has a number of degrees

of freedom that correspond to discrete values of the unknowns in the boundary value problem to be solved. In the present case of deformation theory, the degrees of freedom correspond to the displacement components. Within an element the displacement field $\underline{u}$ is obtained from the discrete nodal values in a vector $\underline{v}$ using interpolation functions assembled in matrix $\underline{N}$:

$$\underline{U} = \underline{N}\,\underline{v} \tag{2.3.2.9}$$

The interpolation functions in matrix $\underline{\mathbf{N}}$ are often denoted as shape functions. Substitution of Eq. (2.3.2.9) in the kinematic relation (Eq. 2.3.2.3) gives:

$$\underline{\varepsilon} = \underline{L}\,\underline{N}\,\underline{v} = \underline{B}\,\underline{v} \tag{2.3.2.10}$$

In this relation $\underline{B}$ is the strain interpolation matrix, which contains the spatial derivatives of the interpolation functions. Eqs. (2.3.2.9) and (2.3.2.10) can be used in variational, incremental and rate form as well.

Eq. (2.3.2.8) can now be reformulated in discretised form as:

$$\int (\underline{\underline{B}}\,\delta\underline{\nu})^T \Delta\underline{\sigma}\, dV = \int (\underline{\underline{N}}\,\delta\underline{\nu})^T \underline{b}^i\, dV + \int (\underline{\underline{N}}\,\delta\underline{\nu})^T \underline{t}^i\, dS - \int (\underline{\underline{B}}\delta\underline{\nu})^T \underline{\sigma}^{i-1}\, dV \tag{2.3.2.11}$$

The discrete displacements can be placed outside the integral

$$\delta\underline{\nu}^T \int \underline{\underline{B}}^T \Delta\underline{\sigma}\, dV = \delta\underline{\nu}^T \int \underline{\underline{N}}^T \underline{b}^i\, dV + \delta\underline{\nu}^T \int \underline{\underline{N}}^T \underline{t}^i\, dS - \delta\underline{\nu}^T \int \underline{\underline{B}}^T \underline{\sigma}^{i-1}\, dV \tag{2.3.2.12}$$

Provided that Eq. (2.3.2.12) holds for any kinematically admissible displacement variation $\delta\,\underline{v}^T$, the equation can be written as:

$$\int \underline{\underline{B}}^T \Delta\underline{\sigma}\, dV = \int \underline{\underline{N}}^T \underline{b}^i\, dV + \int \underline{\underline{N}}^T \underline{t}^i\, dS - \int \underline{\underline{B}}^T \underline{\sigma}^{i-1}\, dV \tag{2.3.2.13}$$

The above equation is the elaborated equilibrium condition in discretised form. The first term on the right-hand side together with the second term represent the current external force vector and the last term represents the internal reaction vector from the previous be balanced by a stress increment $\Delta\,\underline{\sigma}$.

The relation between stress increments and strain increments is usually non-linear. As a result, strain increments can generally not be calculated directly, and global iterative procedures are required to satisfy the equilibrium condition (Eq. 2.3.2.13) for all material points. Global iterative procedures are described later in Section 2.3.2.4, but the attention is first focused on the (local) integration of stresses.

2.4 PLAXIS Finite Element Method Software

2.4.1 Introduction

PLAXIS is a finite element program, developed for the analysis of deformation, stability and groundwater flow in geotechnical engineering. It is a part of the PLAXIS product range, a suite of finite element programs that is used worldwide for geotechnical engineering and design.

The development of PLAXIS began in 1987 at Delft University of Technology as an initiative of the Dutch Ministry of Public Works and Water Management (Rijkswaterstaat).

The initial purpose was to develop an easy-to-use 2D finite element code for the analysis of river embankments on the soft soils of the lowlands of Holland. In subsequent years, PLAXIS was extended to cover most other areas of geotechnical engineering. Because of continuously growing activities, the PLAXIS company (Plaxis bv) was formed in 1993.

In 1998, the first PLAXIS 2D for Windows was released. In the meantime, a calculation kernel for 3D finite element calculations was developed which resulted in the release of the 3D Tunnel program in 2001. 3D Foundation was the second three-dimensional PLAXIS program, and was developed in cooperation with Netherlands Organisation for Applied Scientific Research. The 3D Foundation program was released in 2004. However, in neither 3D Tunnel nor 3D Foundation it was possible to define arbitrary 3D geometries, because of their geometrical limitations. So in 2010 the first PLAXIS 3D program was released, which is a full three-dimensional finite element program which combines an easy-to-use interface with full 3D modelling facilities.

The main problem of the most finite element codes is that they are very complicated for an engineer who is not familiar with computer programming. This problem gets more complicated when 3D geometry has to be considered. Quite often engineers consider non-linear finite element computations cumbersome and time-consuming. The PLAXIS research and development team has addressed this issue by designing robust and theoretically sound computational procedures, which are encapsulated in a logical and easy-to-use shell. The main advantage of PLAXIS 3D program is that it can be used by geotechnical engineers who are not necessarily numerical specialists. It is a practical tool for geotechnical applications that provide finite element computations in an easy and not complicated way. As a result, many practical engineers world-wide have adopted this product and use it for engineering purposes. Furthermore, PLAXIS 3D is used more and more lately by researchers in universities all over the world in the field of geo-mechanics and numerical methods. Important conclusions have been made by researchers using the PLAXIS code.

This user-friendly interface hides however some risks especially when the program is used by engineers who have not much experience to filter and judge the out coming results. These risks refer not only to PLAXIS but also to all finite element codes that are available. Above all, the simulation of reality by a computer program remains an approximation which implicitly involves some inevitable numerical and modelling errors. Moreover, the accuracy at which reality is approximated depends highly on the expertise of the user regarding the modelling of the problem, the understanding of the soil models and their limitations, the selection of model parameters, and the ability to judge the reliability of the computational results. In

conclusion, proper attention should always be paid and the results should be compared, even crudely, with other solutions, simplified or not the mechanical behaviour of soils may be modelled at various degrees of accuracy. Hooke's law of linear, isotroplc elasticity, for example, may be thought of as the simplest available stress-strain relationship. As It involves only two. input parameters, ί.e. Young's modulus, E, and Poisson's ratio, v, it is generally too crude to capture essential features of soίl and rock behavlour. For modeling massive structural elements and bedrock layers, however, lίnear elasticity tends to be appropriate. There is a big number of different Models in use some of which are presented in the following chapter.

2.4.2 Models used in Simulation

A. Linear Elastic model (LE)

The Linear Elastic model is based on Hooke's law of isotropic elasticity. I! involves two basic elastic parameters, i.e. Young ‘s modulus E and Poisson's ratio v. Although the Linear Elastic model is not suitable to model soil, it may be used to model stiff volumes in the soil, like concrete walls, or intact rock formations.

B. Hardening Soil model (HS)

The Hardening Soil model is an advanced model for the simulation of soil behaviour. As for the Mohr-Coulomb model, limiting states of stress are described by means of the friction angle, ϕ, the cohesion, C, and the dilatancy angle, ψ. However, soil stiffness is described much more accurately by using three different input stiffnesses: the triaxial loading stiffness, E50, the triaxial unloading stiffness, Eur, and the oedometer loading stiffness, Eoed. As average values for various soil types, Eur ~ 3E50 and Eoed ~ E50 are suggested as default settings, but both very soft and very stiff soils tend to give other ratios of Eoed/E50, which can be entered by the user.

The Hardening Soil model, in contrast to the Mohr-Coulomb model, also accounts for stress dependency of stiffness moduli. This means that all stiffnesses increase with pressure. Hence, all three input stiffnesses relate to a reference stress, usually taken as 100 kPa (1 bar).

Besides the model parameters mentioned above, initial soil conditions, such as pre-consolidation, play an essential role in most soil deformation problems. This can be taken into account in the initial stress generation. Even though the hs small wasn’t used in the analyses its referred here for better understanding the HSsmall.

C. Hardening Soil model with small-strain stiffness (HSsmall)

The Hardening Soil model with small-strain stiffness (HSsmall) is a modified model of the above that takes into account the increased stiffness of soils at small strains. At small strain levels the majority of soils exhibit a higher stiffness than at high strain levels. This stiffness varies non-linearly with strain. This behaviour is described in the HSsmall model using one extra strain-history parameter and two additional material parameters, such as G_0^{ref}, which is the shear modulus for small-strains, and $\gamma_{0.7}$, meaning the strain level at which the shear modulus has reduced to about 70% of the small-strain shear modulus. The advanced features of the HSsmall model are most apparent in working load conditions. The HS-small model gives more close to reality displacements than the HS model. When used in dynamic applications, the Hardening Soil model with small-strain stiffness also introduces hysteretic material damping.

Two of the above Models have been used for this thesis. The linear elastic Model was used for the Pile Element and the HS Small Model for the Soil. A brief description of the HS Small Model is presented in the following chapter.

2.5 The Hardening Soil Model with Small-Strain Stiffness (HSSMALL)

The original Hardening Soil model assumes elastic material behavior during unloading and reloading. However, the strain range in which soils can be considered truly elastic is very small. With increasing strain amplitude, soil stiffness decays nonlinearly. Plotting soil stiffness against log(strain) yields characteristic S-shaped stiffness reduction curves. Figure 2.5.1 gives an example of such a stiffness reduction curve. It outlines also the characteristic shear strains that can be measured near geotechnical structures and the applicable strain ranges of laboratory tests. It turns out that at the minimum strain which can be reliably measured in classical laboratory tests, i.e. triaxial tests and oedometer tests without special instrumentation, soil stiffness is often decreased to less than half its initial value.

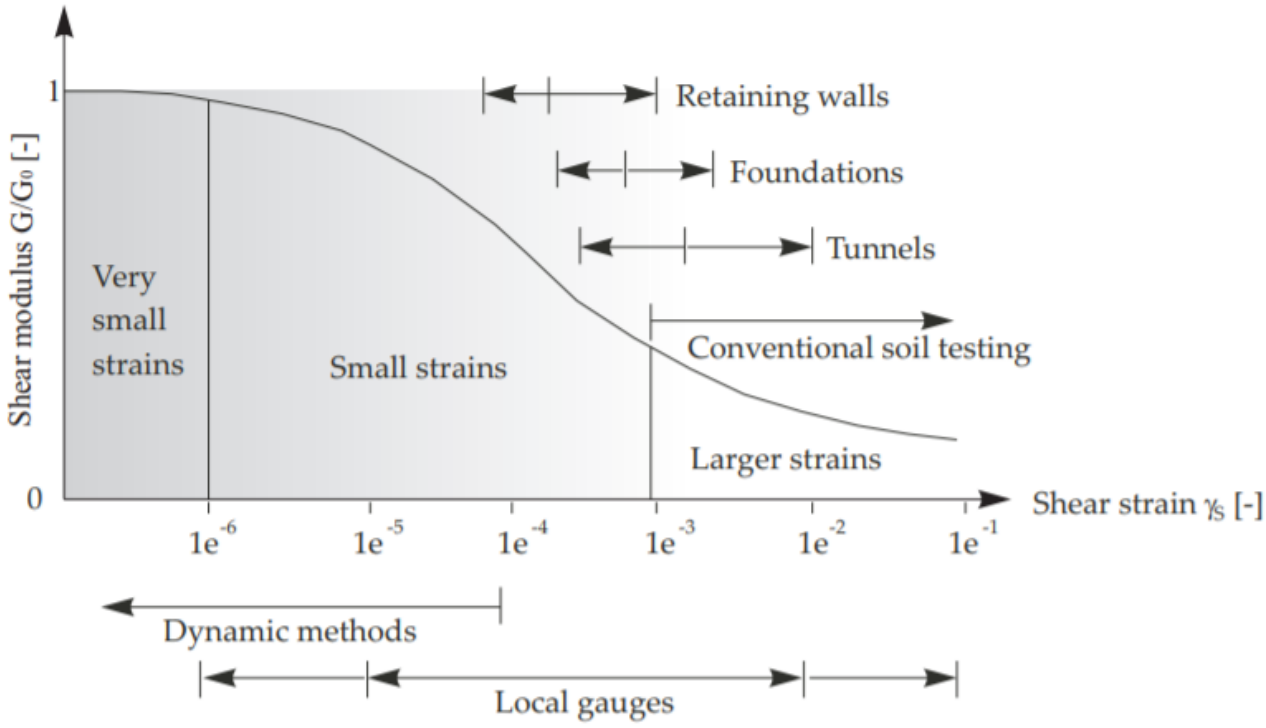

Figure 2.5.1 Characteristic stiffness-strain behavior of soil with typical strain ranges for laboratory tests and structures (after Atkinson & Sallfors (1991))

The soil stiffness that should be used in the analysis of geotechnical structures is not the one that relates to the strain range at the end of construction according to Figure 2.5.1. Instead, very small-strain soil stiffness and its non-linear dependency on strain amplitude should be properly taken into account. In addition to all features of the Hardening Soil model, the Hardening Soil model with small-strain stiffness offers the possibility to do so.

The Hardening Soil model with small-strain stiffness implemented in PLAXIS uses almost entirely the same parameters with the Hardening Soil model. Actually, only two additional parameters are needed to describe the variation of stiffness with strain:

- the initial or very small-strain shear modulus G_o (meaning the maximum shear modulus)
- the shear strain level $\gamma_{0.7}$ at which the secant shear modulus G_s is reduced to about 70% of the initial shear modulus , G_o

2.5.1. Describing Small-Strain Stiffness with a Simple Hyperbolic Law

In soil dynamics, small-strain stiffness has been a well-known phenomenon for a long time. In static analysis, the findings from soil dynamics have long been considered not to be applicable.

Seeming differences between static and dynamic soil stiffness have been attributed to the nature of loading rather than to the magnitude of applied strain which is generally small in dynamic conditions (earthquakes excluded). As inertia forces and strain rate have only little influence on the initial soil stiffness, dynamic soil stiffness and small-strain stiffness can in fact be considered as synonyms.

Probably the most frequently used model in soil dynamics is the Hardin-Drnevich relationship. From test data, sufficient agreement is found that the stress-strain curve for small strains can be adequately described by a simple hyperbolic law. The following analogy to the hyperbolic law for larger strains by Kondner (1963) was proposed by Hardin & Drnevich (1972):

$$\frac{G_S}{G0} = \frac{1}{1+\left|\frac{\gamma}{\gamma_r}\right|} \qquad (2.5.1)$$

Where the threshold shear strain γ_r is quantified as:

$$\gamma_r = \frac{\tau_{max}}{G_0} \qquad (2.5.2)$$

with τ_{max} being the shear stress at failure. Essentially, the above two Eqs. (2.5.1) and (2.5.2) relate large (failure) strains to small-strain properties which often work well.

More straightforward and less prone to error is the use of a smaller threshold shear strain. Santos & Correia (2001), for example suggest to use the shear strain $\gamma_r = \gamma_{0.7}$ at which the secant shear modulus Gs is reduced to about 70% of its initial value. Eq. (2.5.1) can then be rewritten as:

$$\frac{G_S}{G0} = \frac{1}{1+a\left|\frac{\gamma}{\gamma_{0.7}}\right|} \quad where\ a = 0.385 \qquad (2.5.3)$$

In fact, using a = 0.385 and $\gamma = \gamma_{0,7}$ gives $G_S/ G_o = 0.722$. Hence, the formulation "about 70%" should be interpreted more accurately as 72.2%.

Figure 2.5.2 shows the fit of the modified Hardin-Drnevich relationship (Eq. 2.5.3) to normalized test data

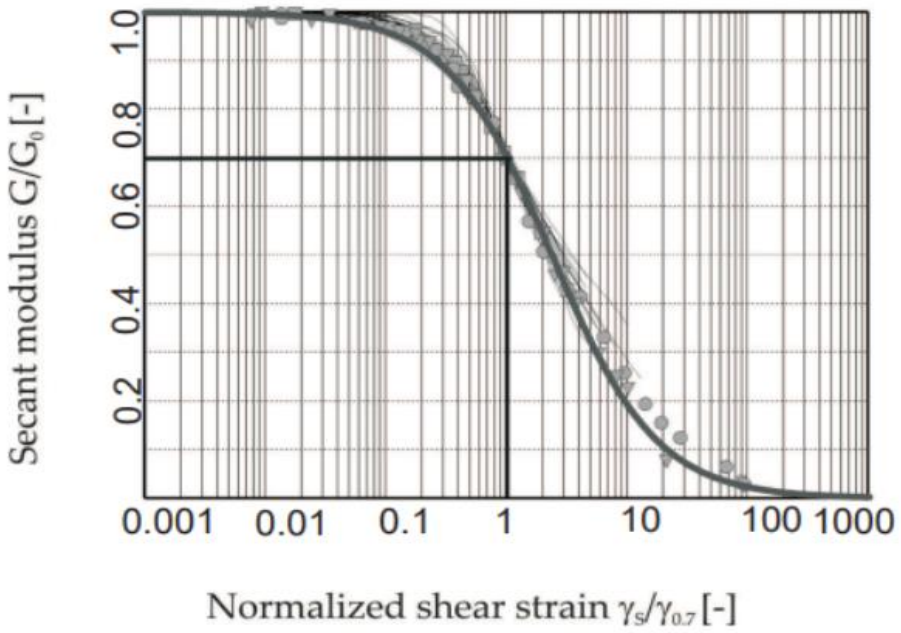

.

Figure 2.5.2 Results from the Hardin-Drnevich relationship compared to test data by Santos& Correia (2001)

2.5.2 Virgin (Initial) Loading vs. Unloading/ Reloading

Masing (1926) described the hysteretic behavior of materials in unloading and reloading cycles in the form of the following rules:

- The shear modulus in unloading is equal to the initial tangent modulus for the initial loading curve.
- The shape of the unloading and reloading curves is equal to the initial loading curve, but twice its size. In terms of the above introduced threshold shear strain $\gamma_{0,7}$:

$$\gamma_{0.7-reloading} = 2\ \gamma_{0.7-virgin\ loading}$$

(2.5.11)

The HS small model adopts Masing's rule. However, instead of doubling the threshold shear strain, hardening plasticity accounts for more rapidly decaying small-strain stiffness during virgin loading. Figures 2.5.4 and 2.5.5 illustrate Masing's rule and the secant stiffness reduction in virgin loading and unloading / reloading.

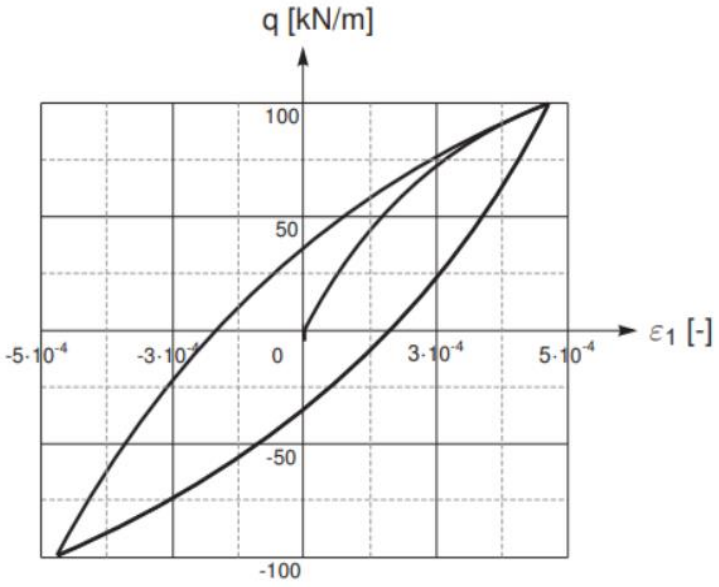

Figure 2.5.3 Hysteretic material behavior

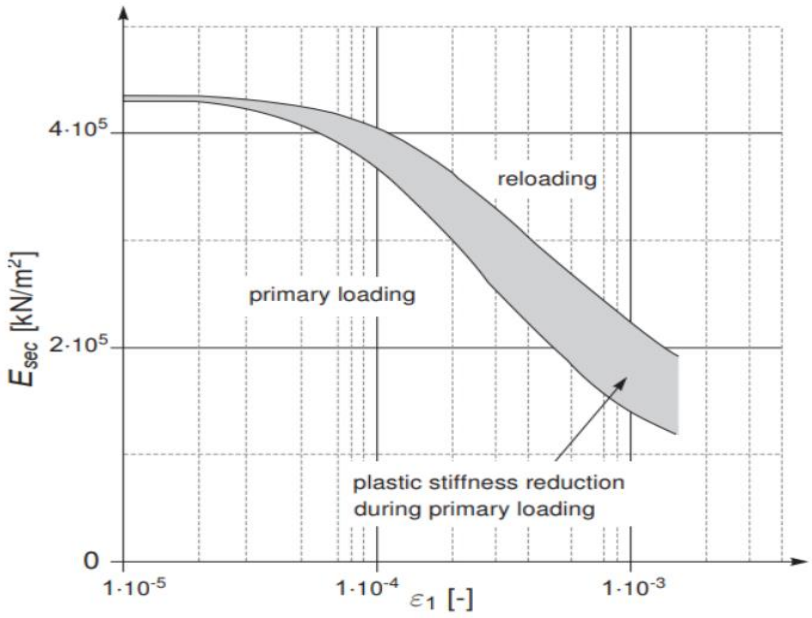

Figure 2.5.4 Stiffness reduction in initial or primary loading and in unloading/reloading

2.5.3 Model Parameters

Compared to the standard Hardening Soil model, the Hardening Soil model with small-strain stiffness requires two additional stiffness parameters as input: G_0^{ref} and $\gamma_{0.7}$.

All other parameters, including the alternative stiffness parameters, remain the same as in the standard Hardening Soil model. G_0^{ref} defines the shear modulus at very small strains e.g. $\varepsilon < 10^{-6}$ at a reference minor principal stress of $-\sigma'_3 = p^{ref}$.

Poisson's ratio v_{ur} is assumed a constant, as everywhere in PLAXIS, so that the shear modulus can also be calculated from the very small strain Young's modulus as $G_0^{ref} = E_0^{ref}/(2(1 + \nu_{ur}))$.The threshold shear strain $\gamma_{0.7}$ is the shear strain at which the secant shear modulus G_s^{ref} is decayed to 0.722 G_0^{ref} .The threshold shear strain $\gamma_{0.7}$ is to be supplied for virgin loading. in summary, the input stiffness parameters of the Hardening Soil model with small-strain stiffness can be seen in figure 2.5.7 and are the ones below:

m : Power for stress-level dependency of stiffness [-]

E_{50}^{ref} : Secant stiffness in standard drained triaxial test [kN/m2]

E_{oed}^{ref} : Tangent stiffness for primary oedometer loading [kN/m2]

E_{ur}^{ref} : unloading / reloading stiffness from drained triaxial test [kN/m2]

v_{ur} : Poisson's ratio for unloading-reloading [-]

G_0^{ref} : reference shear modulus at very small strains (ε < 10-6) [kN/m2

$\gamma_{0.7}$: threshold shear strain at which $G_s = 0.722\ G_0$ [-]

Figure 2.5.6 illustrates the model's stiffness parameters in a drained triaxial test: E_{50}, E_{ur} and $E_o = 2G_o\ (1 + v_{ur})$' For the order of strains at which E_{ur} and G_o are defined and determined, one may refer to e.g. Figure 2.5.1 and Figure 2.5.3.

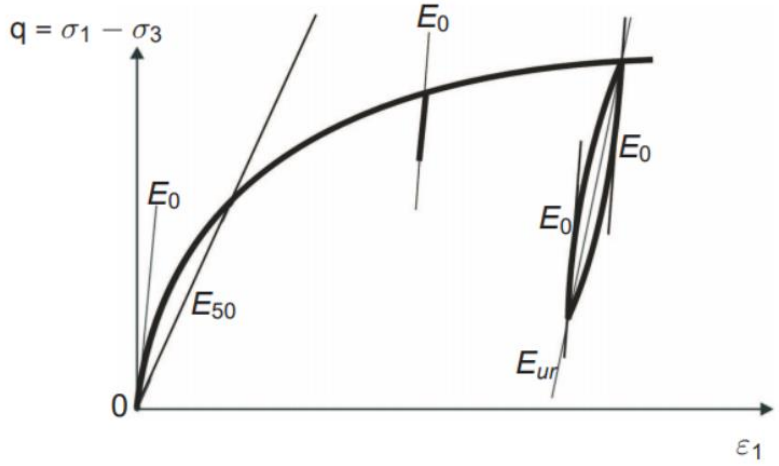

Figure 2.5.5 Stiffness parameters E_{50}, E_{ur}, and $E_o = 2G_o(1 + v_{ur})$ of the Hardening Soil model with small-strain stiffness in a triaxial test

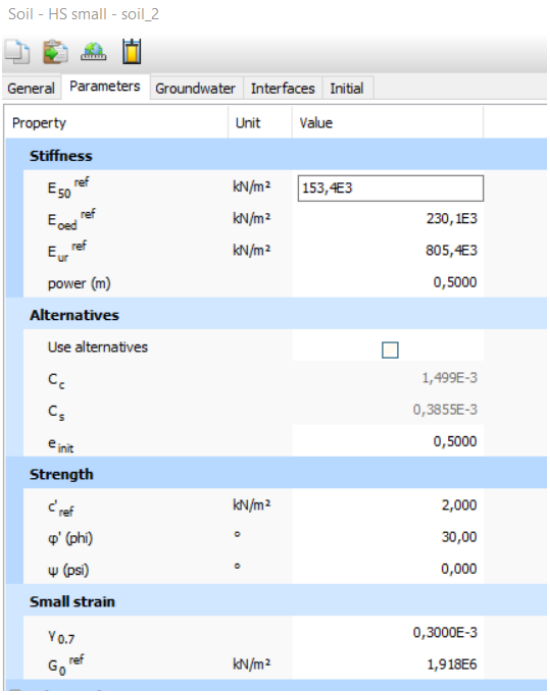

Figure 2.5.6 Parameters of the HS-small constitutive model from the PLAXIS software

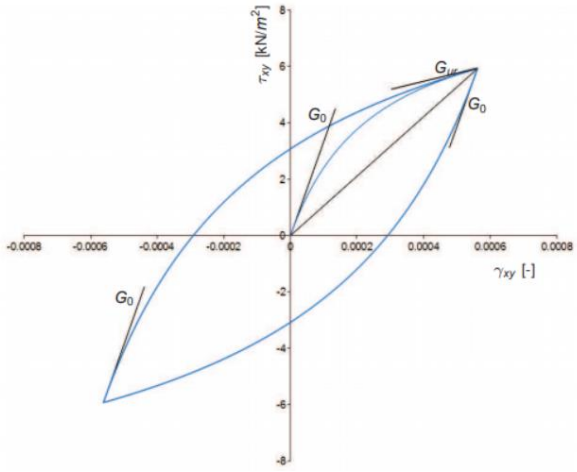

Figure 2.5.7 Stiffness parameters in cyclic shear test

A first estimation of the HSsmall parameters for quartz sand based on the relative density (RD) is given in Brinkgreve, Engin & Engin (2010).

2.5.4 On the Parameters G_0 and $\gamma_{0.7}$

A number of factors influence the smaII-strain parameters G_0 and $\gamma_{0.7}$. Most importantly they are influenced by the material's actual state of stress and void ratio e. In the HSsmaII model, the stress dependency of the shear modulus G_0 is taken into account with the power law:

$$G_0 = G_0^{ref} \left(\frac{c\ cos\varphi - \sigma_3' sin\varphi}{c\ cos\varphi + p^{ref} sin\varphi} \right)^m \quad (2.5.12)$$

which resembles the ones used for the other stiffness parameters. The threshold shear strain $\gamma_{0.7}$ is taken independently of the mean stress.

Assuming that within a HSsmaII (or HS) computation void ratio changes are rather small, the material parameters are not updated for changes in the void ratio. This means that densification of the soil isn't taken into account. Knowledge of a material's initial void ratio can nevertheless be very helpful in deriving its small-strain shear stiffness G_0. Many correlations are offered in the literature (Benz, 2006). A good estimation for many soils is for example the relation given by Hardin & Black (1969):

$$G_0^{ref} = 33 \frac{(2.97-e)^2}{1+e}\ [MPa]\ \ for\ p^{ref} = 100\ [kPa] \quad (2.5.13)$$

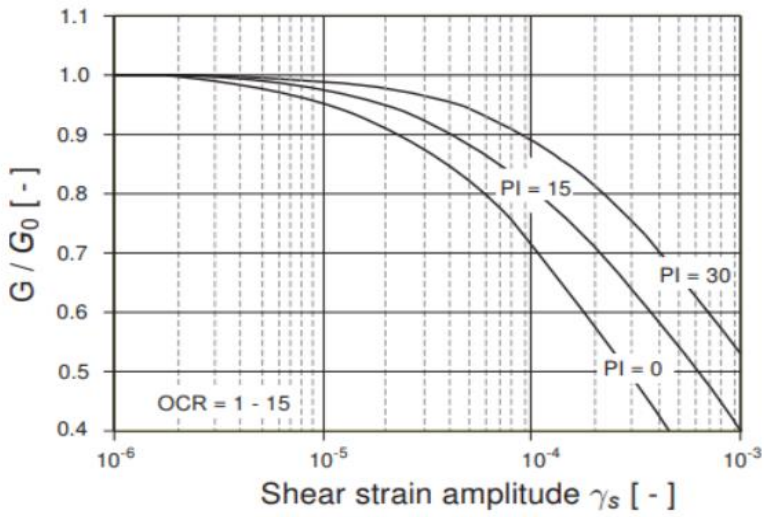

Figure 2.5.10 Influence of plasticity index (PI) on stiffness reduction after Vucetic & Dobry (1991)

Applying the Mohr-Coulomb failure criterion in Eqs. (2.5.2) and (2.5.3) yields:

$$\gamma_{0.7} = \left(\frac{1}{9G_0} \right) [2c'(1 + cos(2\varphi')) - \sigma_1'(1 + K_0) sin(2\varphi')] \quad (2.5.14)$$

where K_0 is the earth pressure coefficient at rest and σ_1' is the effective vertical stress (pressure negative),

3. Calibration Methodology

In order to fit the constitutive model that was used for the soil (HS-small) with the shear and damping curves that exist in the literature (with the Ishihara equations) many parameters are selected for calibration.

Shear modulus is expressed as function of the mean effective stress (σ_m) and the relative soil density (D_r), as it was first proposed by Seed and Idriss, 1970. The Souliotis and Gerolymos, 2015 curve fitting expression will be used for the initial shear strength (G_{max}):

$$G_{max} = 1592\, p_a\, D_{r0}^{0.6464} \left(\frac{p}{p_a}\right)^{0.5}$$

(3.1)

The calibration is then based on matching the already established experimental G:γ and ξ:γ curves from Ishihara to the ones that are calculated using soil experimental tests in the PLAXIS FEM code. As it was mentioned also in the last chapter there are many parameters of the HS-small strains model that must be calibrated, which are:

E_{50}^{ref} E_{oed}^{ref} E_{ur}^{ref} $\gamma_{0.7}$

The only known parameter that is taken for granted is the G_{max} which is calculated using the above equation for the case of a sand with D_{r0}=30% and σ_m=100 kPa. E_{50}/E_{oid} is assumed equal to 1.5, given the fact that the PLAXIS doesn't allow values of this ratio greater than 2 and lower than 1. This means that the final parameters that need to be calibrated are:

a. $\frac{E_{ur}}{E_{oid}}$
b. $\frac{G_{max}}{E_{50}}$
c. $\gamma_{0.7}$

For these three parameters we assume the following range of values:

$$2 \leq \frac{E_{ur}}{E_{oid}} \leq 5$$

$$8 \leq \frac{G_{max}}{E_{50}} \leq 17$$

$$10^{-4} \leq \gamma_{0.7} \leq 6\ 10^{-4}$$

For each parameter we consider three values that are contained in the proposed fields, the upper and lower boundary as well as the mean of them. As a result there are three parameters with three values for each one of them; that makes a total of twenty-seven soil elements tests. With the use of the Haltonset function in Matlab the number of tests to be examined was reduced to 16. Haltonset, allows the user to reduce the number of cases needed to be examined without substantially reducing the accuracy of the results. (decreasing the homogeneity of the sampling sequence). The user sets the number of parameters that he has and then calls for the number of the wanted cases (in this case 16). Then the function gives

back numbers for each parameter from 0 to 1. So in our case the results from the function were the following:

Scenario	Parameter 1	Parameter 2	Parameter 3
1	0.15	0.41	0.03
2	0.65	0.74	0.23
3	0.40	0.19	0.43
4	0.90	0.52	0.63
5	0.09	0.86	0.83
6	1	0.30	0.07
7	0.34	0.63	0.27
8	0.84	0.97	0.47
9	0.21	0.02	0.67
10	0.71	0.35	0.87
11	0.46	0.68	0.11
12	0.96	0.13	0.31
13	0.05	0.46	0.51
14	0.55	0.79	0.71
15	0.30	0.24	0.91
16	0.80	0.57	0.15

Table 3.1: List of parameter combinations generated by Haltonset function

Knowing the values of each parameter we can use them to interpret the above,

Eur/Eoid	**0 - 0.33**	**0.33 - 0.67**	**0.67 - 1**
	2.00	**3.50**	**5**
Gmax/E50	**0 - 0.33**	**0.33 - 0.67**	**0.67 - 1**
	8.00	**12.50**	**17**
g0.7	**0 - 0.33**	**0.33 - 0.67**	**0.67 - 1**
	10^-4	**3*10^-4**	**6*10^-4**

Table 3.2: Adaptation of the parameters used to the Haltonset function results

And derive the values for the parameters for each scenario. The examined scenarios are the following:

Scenario	Eur/Eoid	Gmax/E50	g0.7
1	2	12.5	0.0001
2	3.5	17	0.0001
3	3.5	8	0.0003
4	5	12.5	0.0003
5	2	17	0.0006
6	5	8	0.0001
7	3.5	12.5	0.0001
8	5	17	0.0003
9	2	8	0.0006
10	5	12.5	0.0006
11	3.5	12.5	0.0001
12	5	8	0.0001
13	2	12.5	0.0006
14	3.5	12.5	0.0003
15	2	8	0.0006
16	5	12.5	0.0001

Table 3.3 : List of the parameters values selected for each scenario.

The purpose of the soil element tests that were conducted was to forge the G-γ and ξ-γ curves for each of these cases and see the deviations between them and the Ishihara ones. To create each curve five different shear deformations were used (0.001%,0.01%,0.1%,1%,10%) for each scenario. From the 16 scenarios only the 5 ones with the smaller deviations were kept, to which extra soil element tests were conducted for different mean stresses σ_m=50 , 200 . The formed soil-element curves in comparison with the Ishihara ones are presented below as well as the τ-γ graphs.

To find the best fitting scenario to the Ishihara curves the rRMSE method is used (minimizing the relative root mean squared error).

$$rRMSE(M) = \sqrt{\frac{1}{n}\sum_{i=1}^{n}\left(\frac{M_i - M_{T,i}}{M_{T,i}}\right)^2}$$

The results from this error minimization are the following:

σ=50	***Error***		
Scenario	*G/Gmax*	*ξ*	*Total*
3	0,322626	0,798925	1,121551
4	0,324544	0,816943	1,141487
8	0,32506	0,811764	1,136824
10	0,329147	0,896058	1,225204
14	0,350703	0,786297	1,137

Table 3.4: Errors for the 5 final scenarios for σ=50 kPa between the soil element tests and the ishibash curves.

σ=100 kPA	***Error***		
Scenario	*G/Gmax*	*ξ*	*Total*
3	0,304278	0,729221	1,033498
4	0,306298	0,731657	1,037955
8	0,305712	0,720591	1,026303
10	0,309278	0,821488	1,130766
14	0,305427	0,717131	1,022558

Table 3.5: Errors for the 5 final scenarios for σ=100 kPa between the soil element test and Ishibashi curves

σ=200	***Error***		
Scenario	*G/Gmax*	*ξ*	*Total*
3	0,341522	0,715548	1,05707
4	0,34558	0,731274	1,076854
8	0,347782	0,716547	1,064329
10	0,328977	0,815949	1,144926
14	0,345279	0,70392	1,049201

Table 3.6: Errors for the 5 final scenarios for σ=200 kPa between the soil element test and Ishibashi curves

Scenario	**3**	**4**	**5**	**8**	**10**	**14**
Total Error	3,21212	3,256295	3,256295	3,227456	3,500896	3,208759

Table 3.7: Total Errors for each scenario, the case 14 is the one with the lowest accumulative erros.

As we can see from the final table 3.7 the best fitting curve from the ones selected is the scenario 14. In the following pages are presented the diagrams from the soil element tests as well as the G-γ and ξ-γ curves for each scenario . We can see that PLAXIS in each case overestimated the damping ratio for high values of shear deformations γ. (A problem that is common in the commercial finite element suites)

14. σ=100 kPa

0.001 %

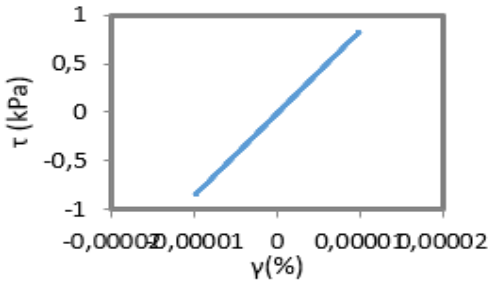

0.01 %

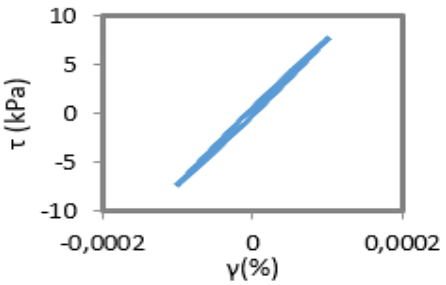

0.1 %

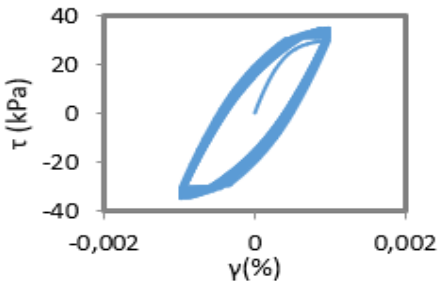

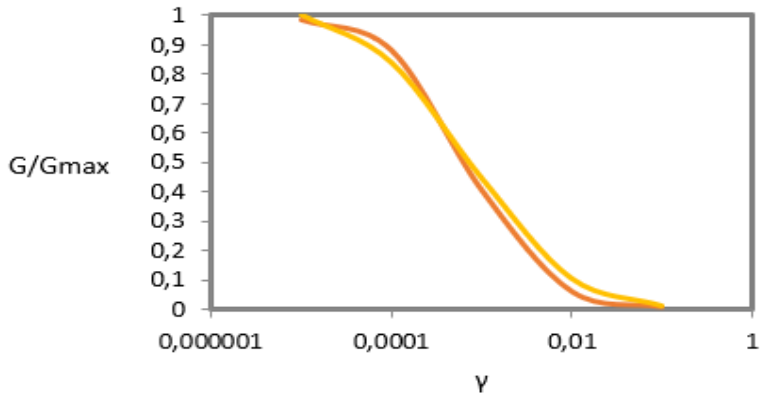

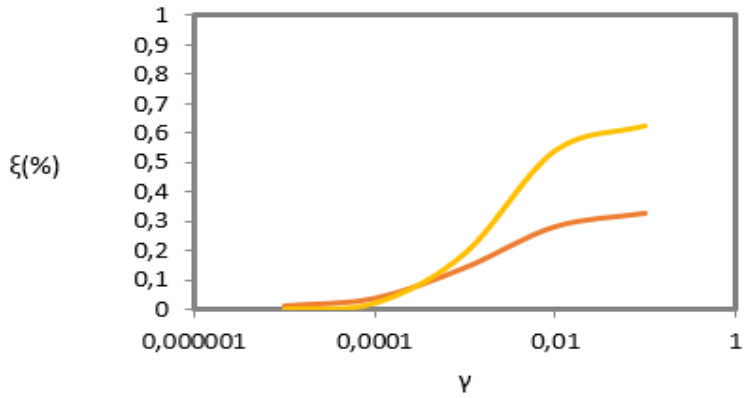

1 %

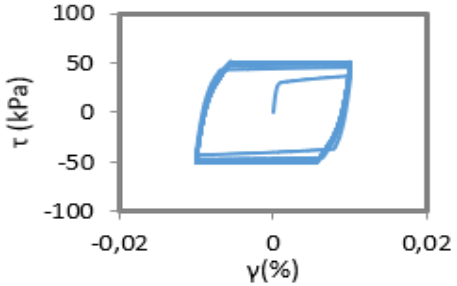

10 %

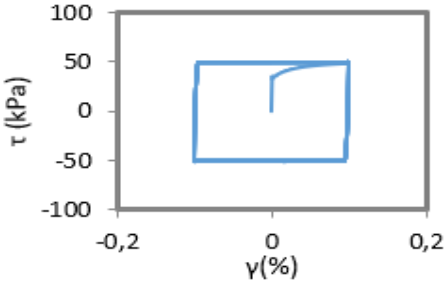

ε_{vol} (0.1%)

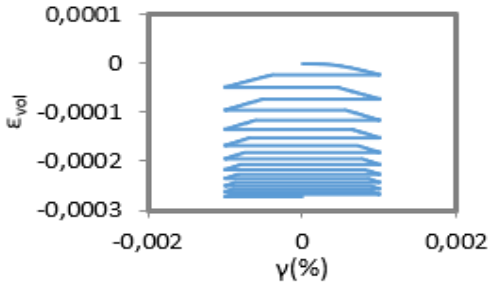

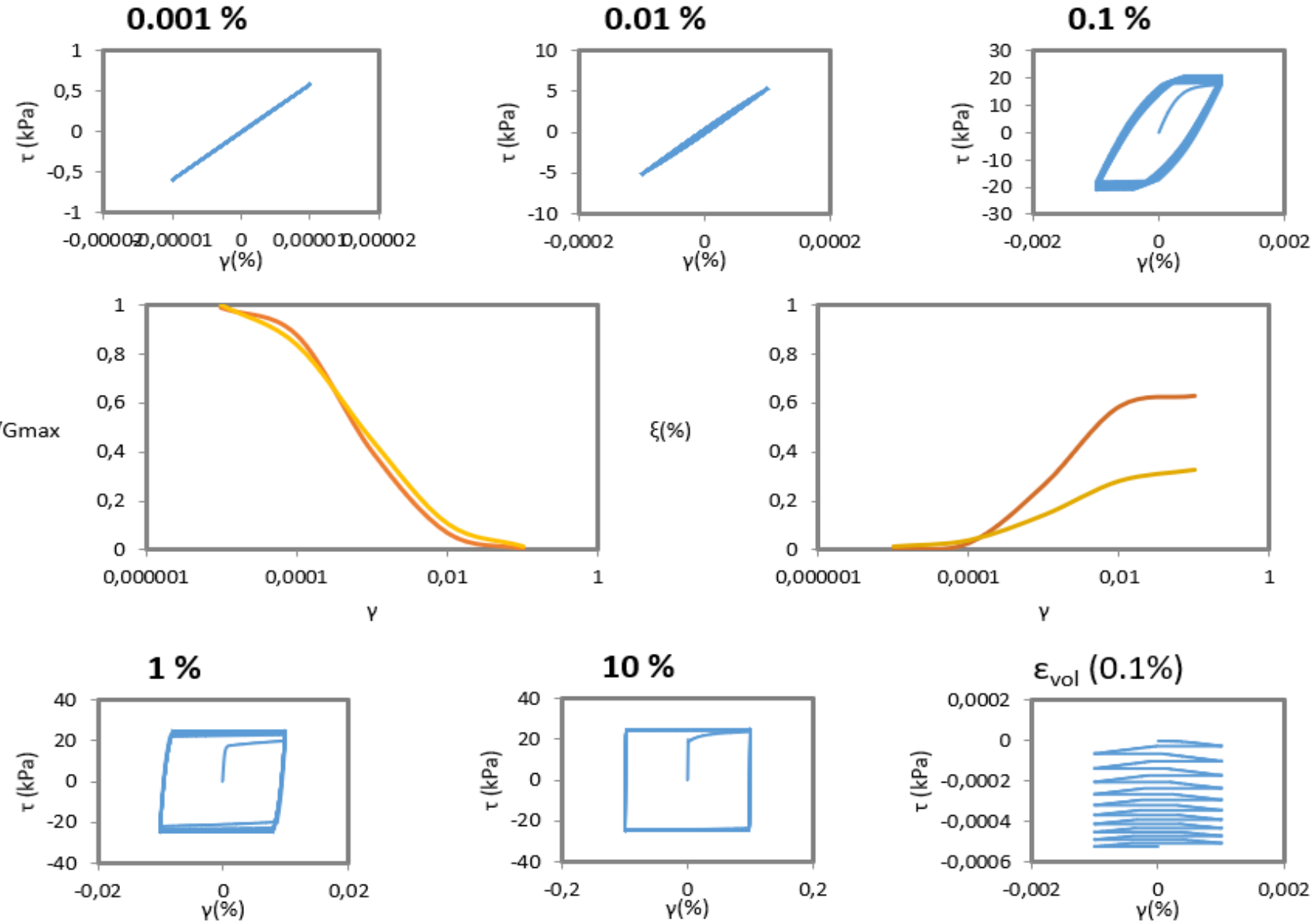

14. σ=50 kPa

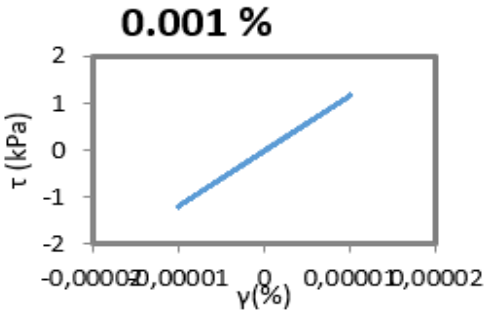
0.001 %
τ (kPa)
γ(%)

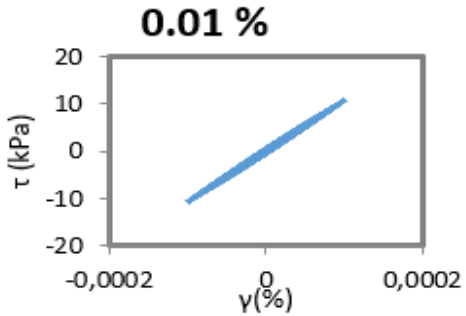
0.01 %
τ (kPa)
γ(%)

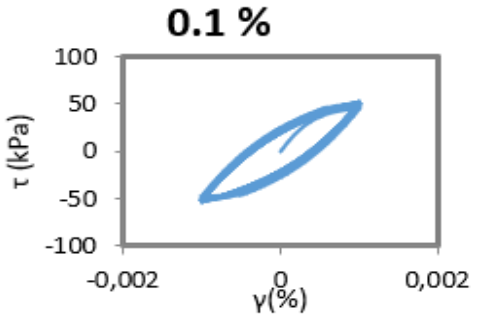
0.1 %
τ (kPa)
γ(%)

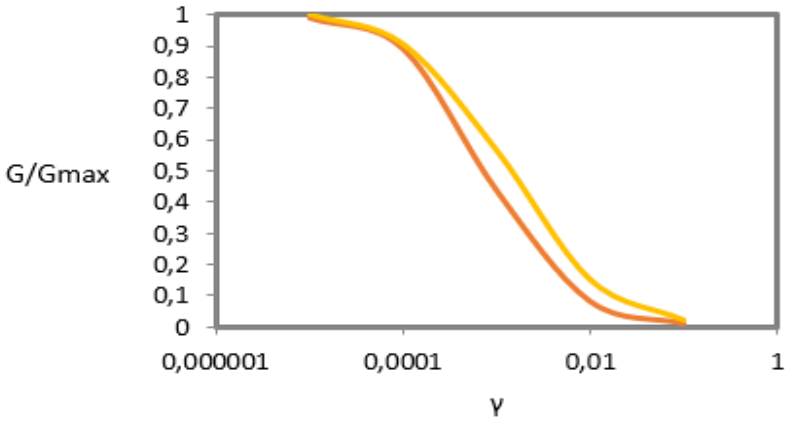
G/Gmax
γ

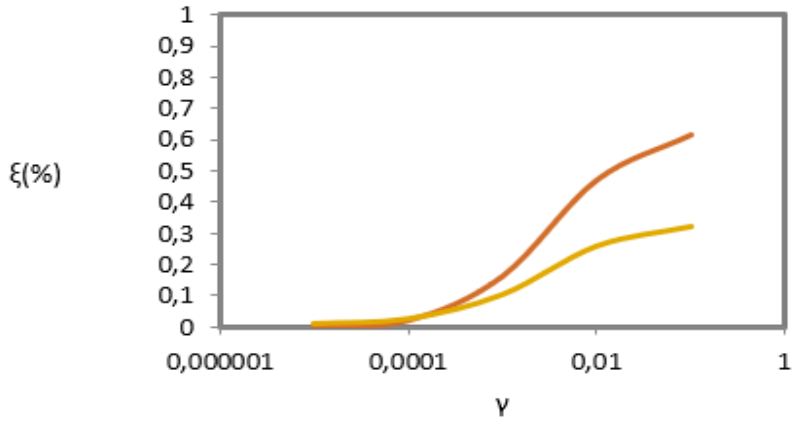
ξ(%)
γ

14. σ=200 kPa

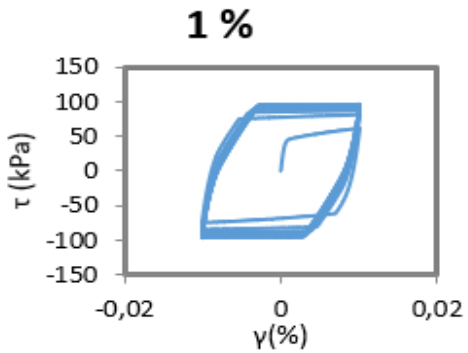
1 %
τ (kPa)
γ(%)

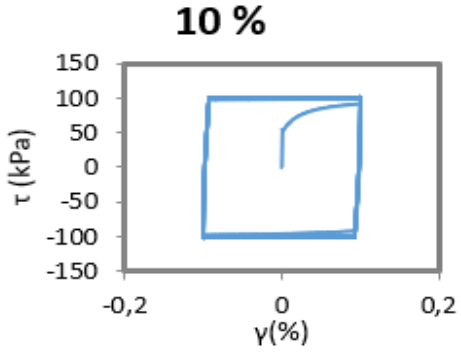
10 %
τ (kPa)
γ(%)

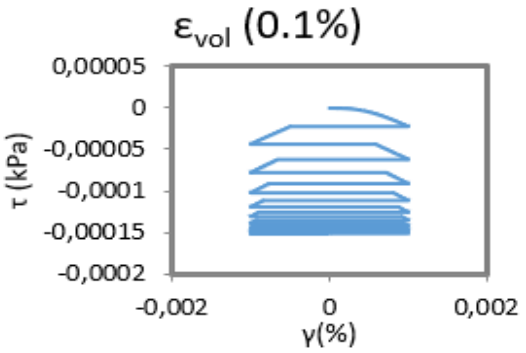
εvol (0.1%)
τ (kPa)
γ(%)

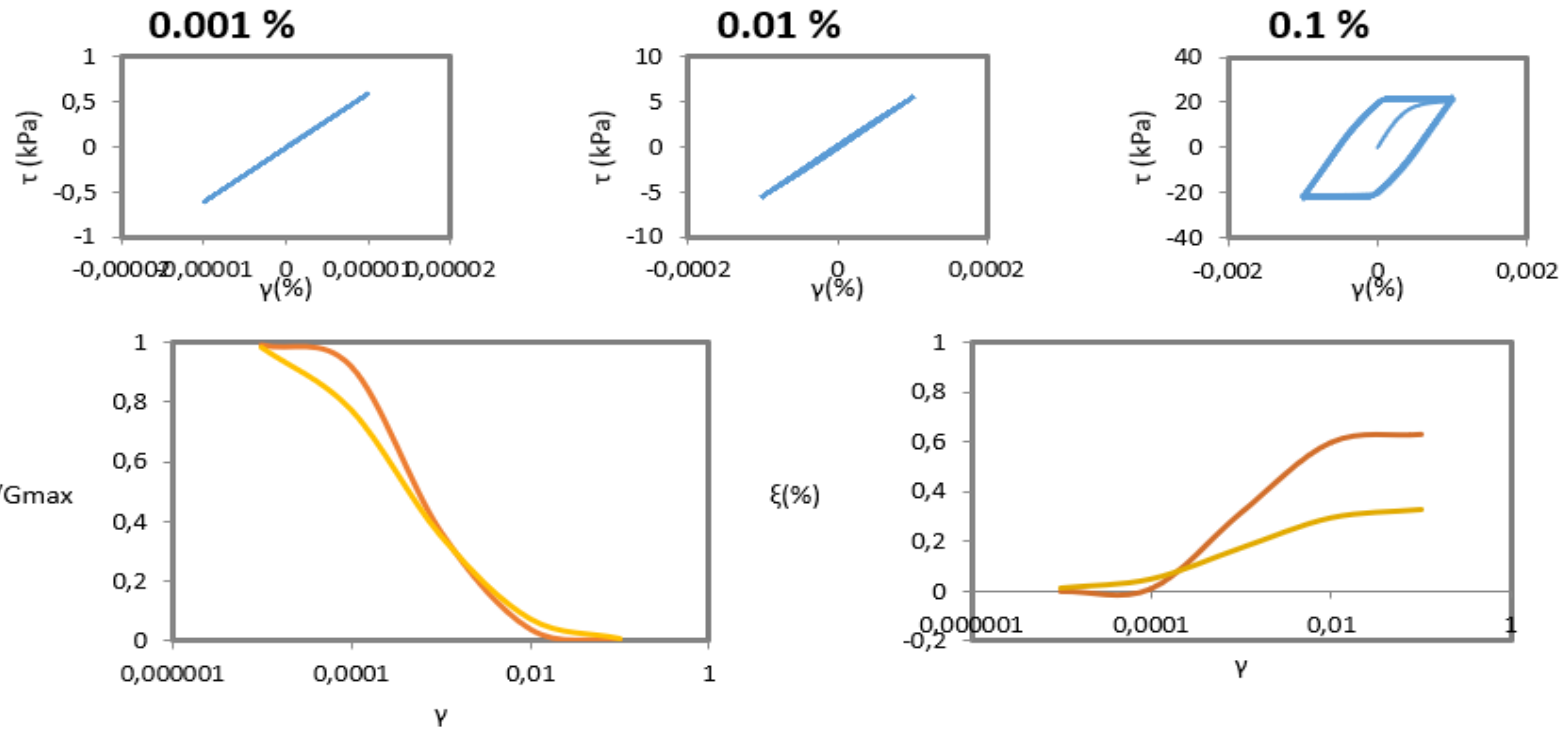

10. σ=50 kPa

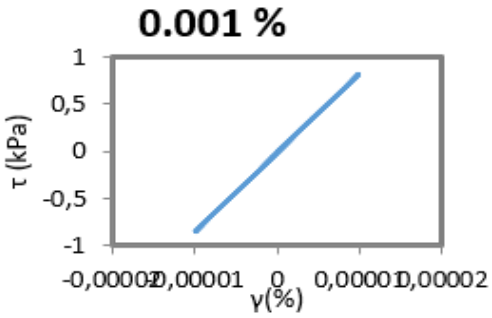
0.001 %
τ (kPa)
γ(%)

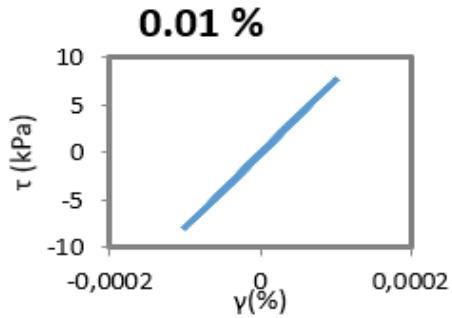
0.01 %
τ (kPa)
γ(%)

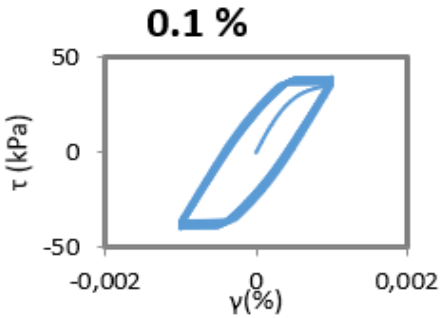
0.1 %
τ (kPa)
γ(%)

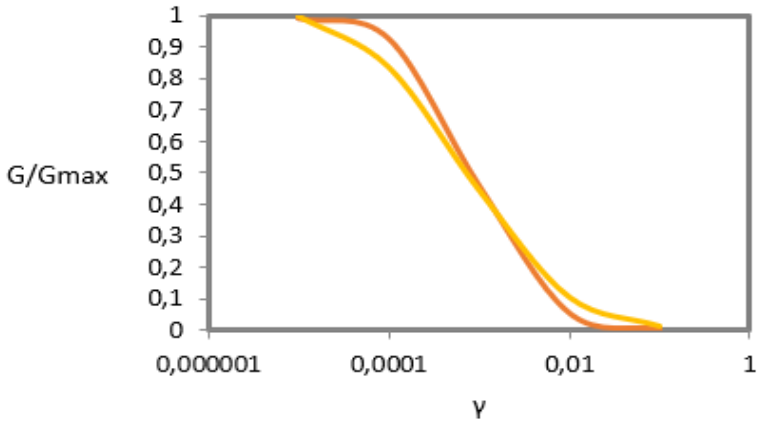
G/Gmax
γ

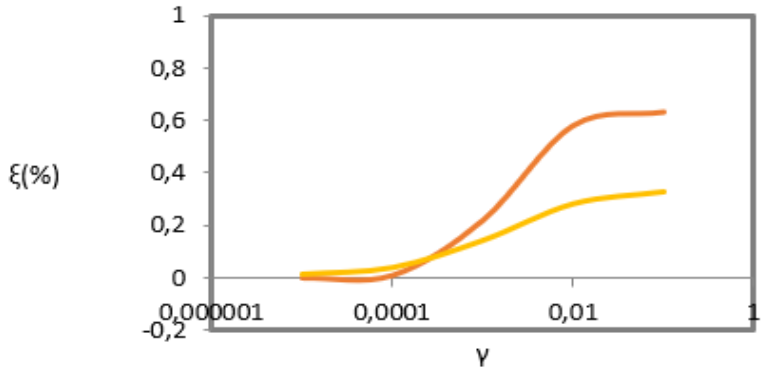
ξ(%)
γ

10. σ=100 kPa

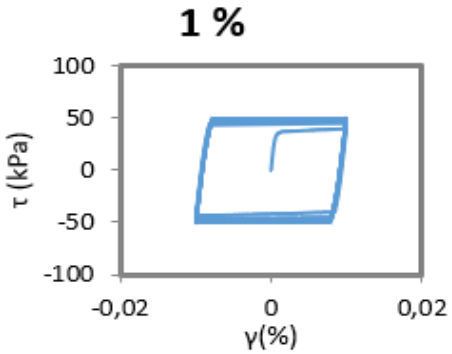
1 %
τ (kPa)
γ(%)

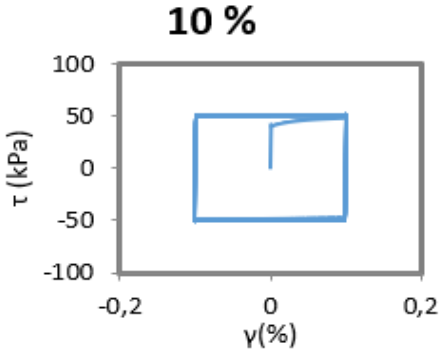
10 %
τ (kPa)
γ(%)

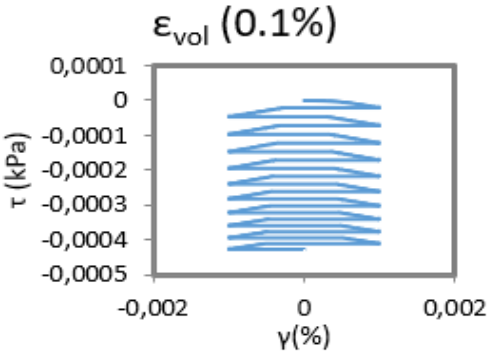
εvol (0.1%)
τ (kPa)
γ(%)

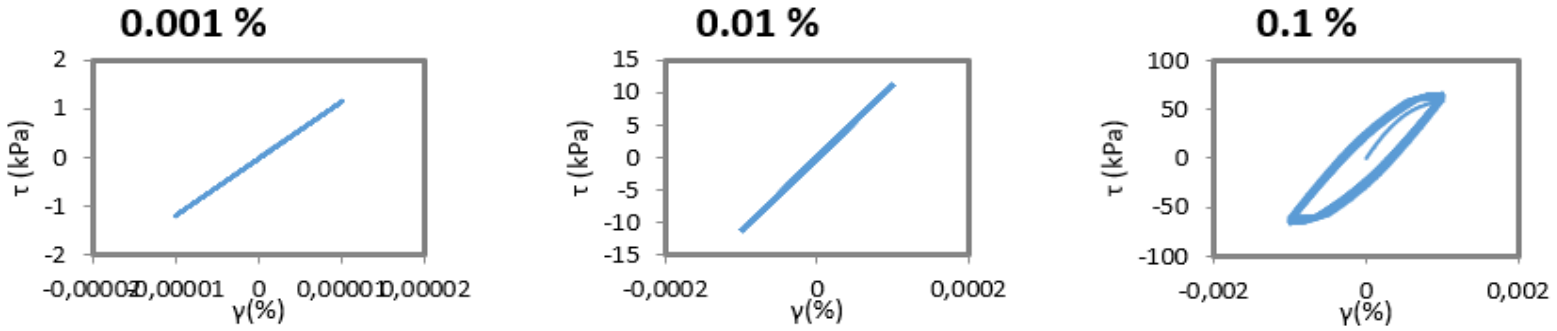

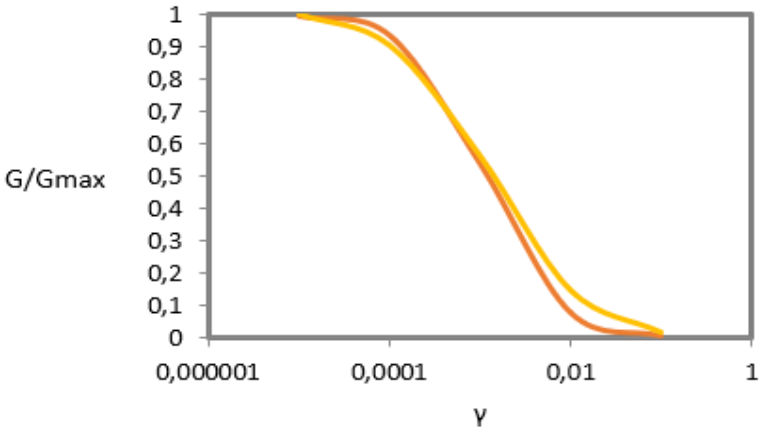

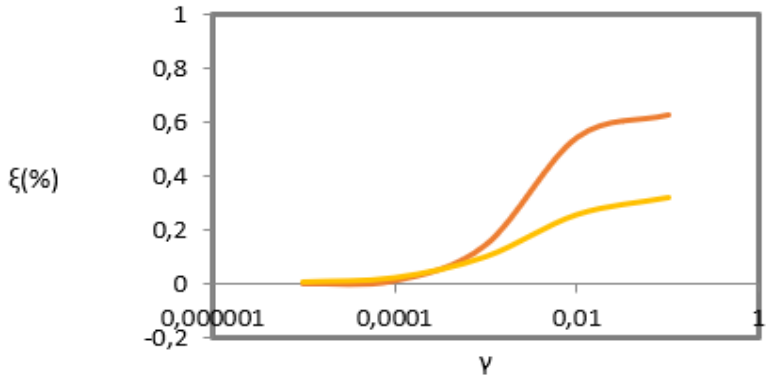

10. σ=200 kPa

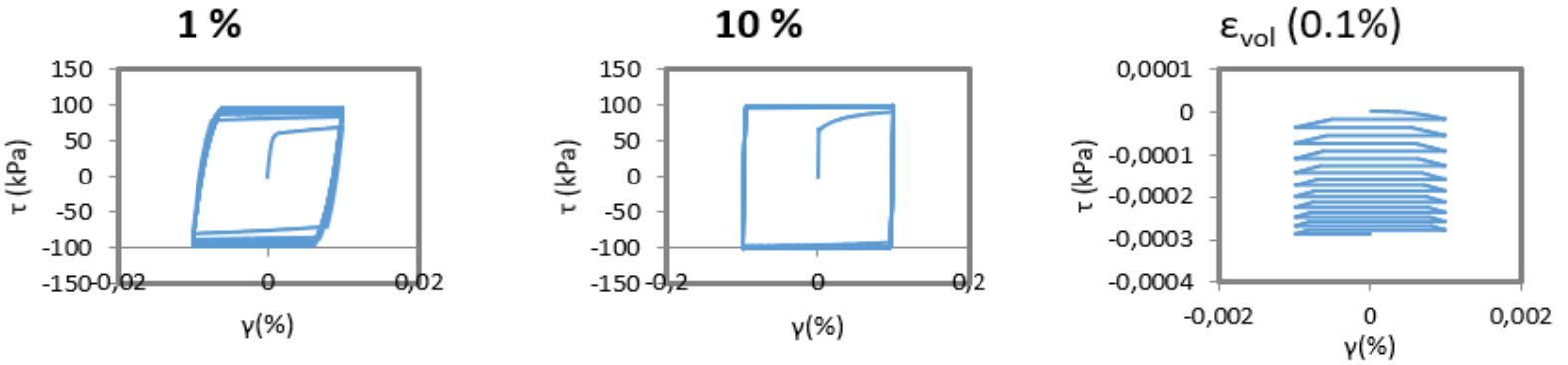

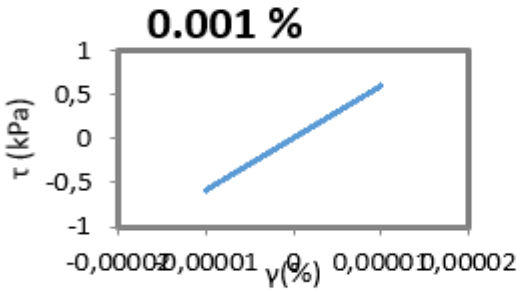
0.001 %
τ (kPa)
γ(%)

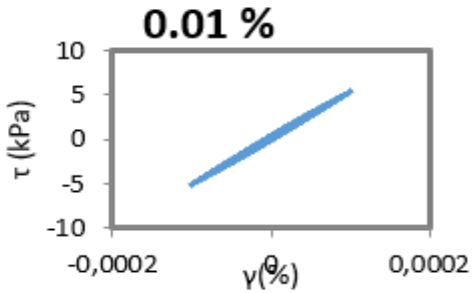
0.01 %
τ (kPa)
γ(%)

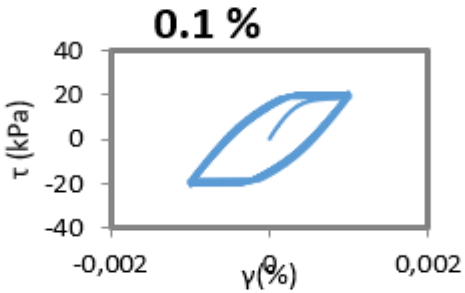
0.1 %
τ (kPa)
γ(%)

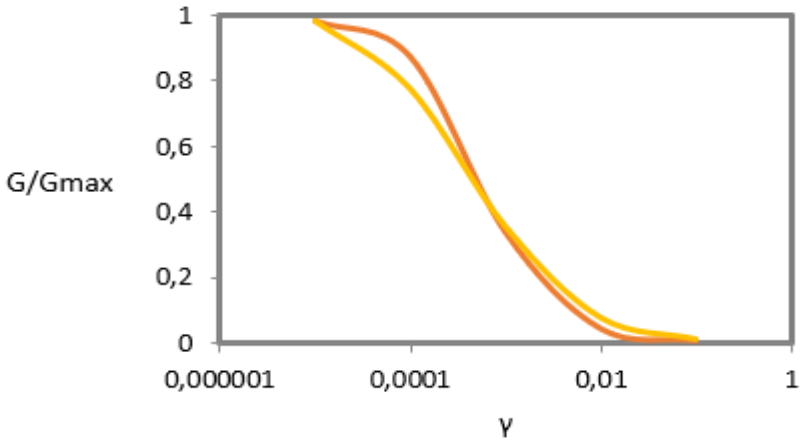
G/Gmax
γ

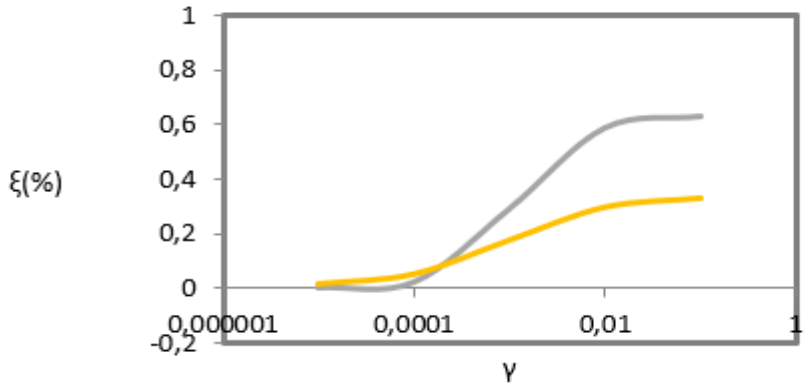
ξ(%)
γ

8. σ=50 kPa

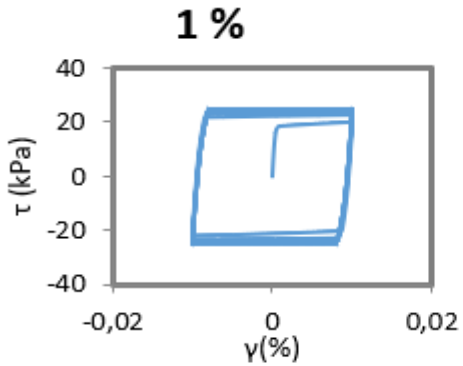
1 %
τ (kPa)
γ(%)

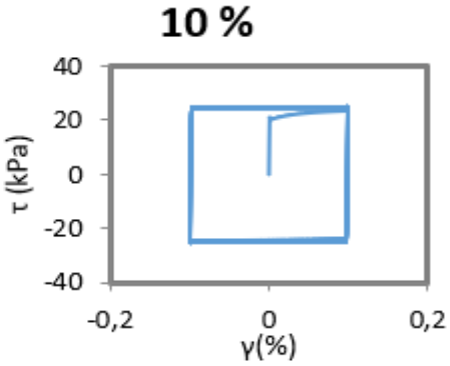
10 %
τ (kPa)
γ(%)

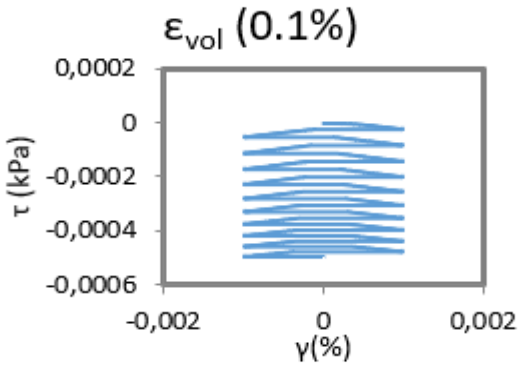
εvol (0.1%)
τ (kPa)
γ(%)

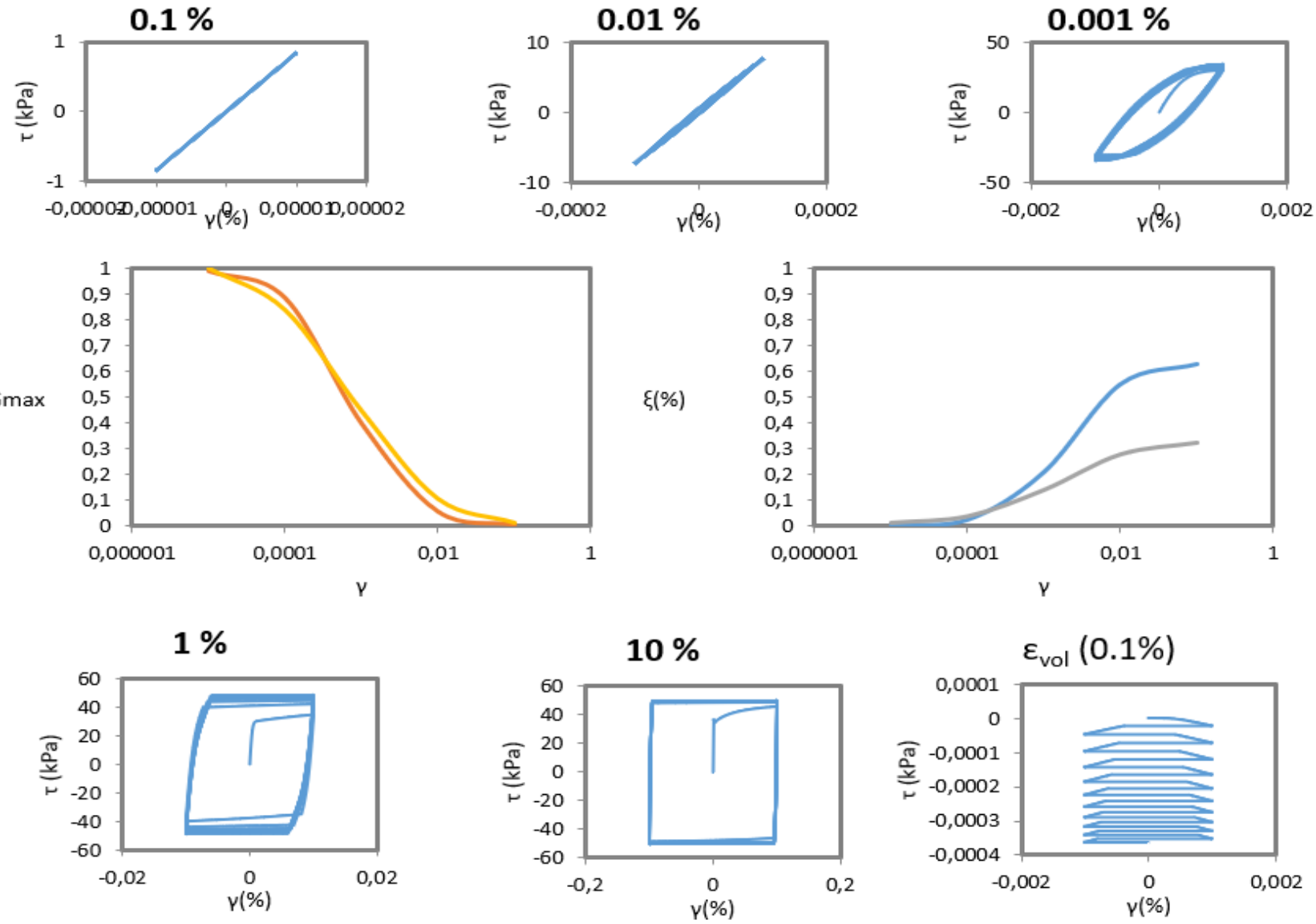

8. σ=100 kPa

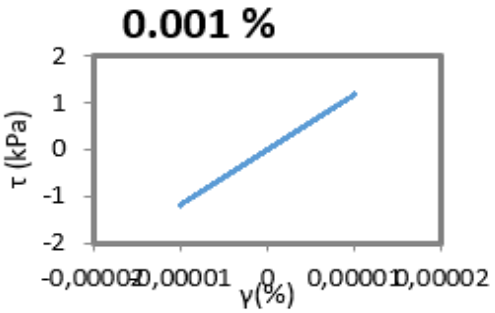
0.001 %
τ (kPa)
γ(%)

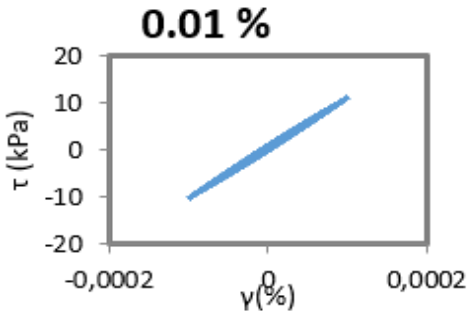
0.01 %
τ (kPa)
γ(%)

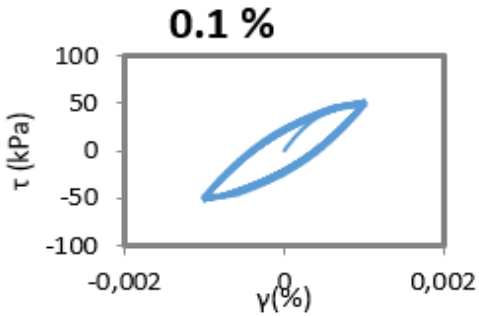
0.1 %
τ (kPa)
γ(%)

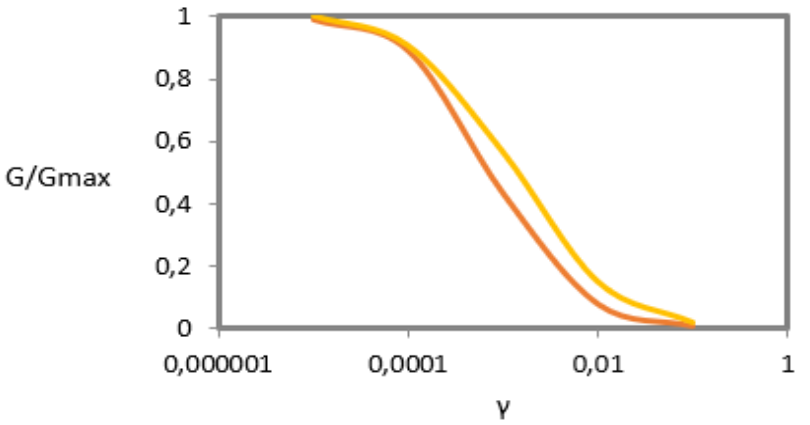
G/Gmax
γ

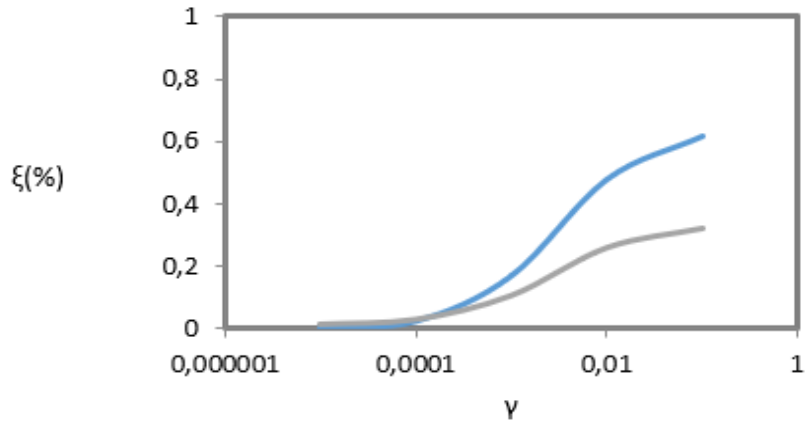
ξ(%)
γ

8. σ=200 kPa

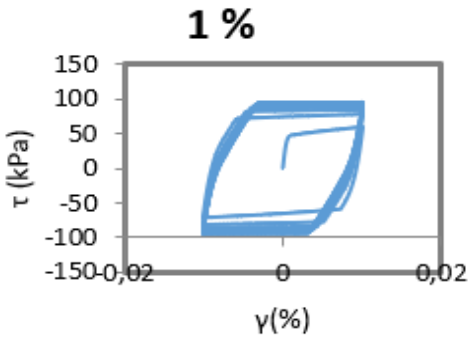
1 %
τ (kPa)
γ(%)

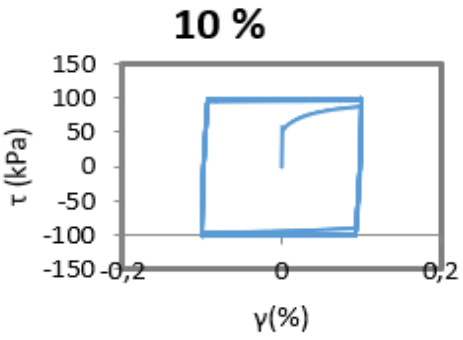
10 %
τ (kPa)
γ(%)

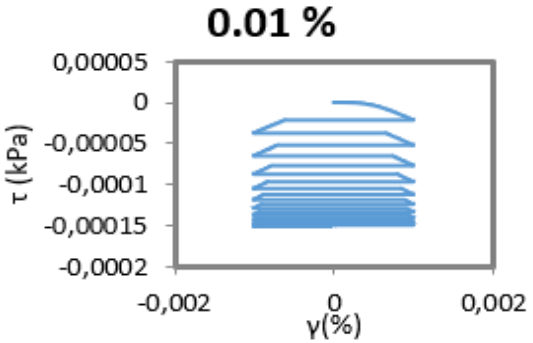
0.01 %
τ (kPa)
γ(%)

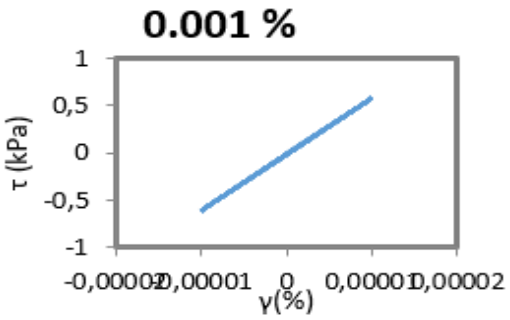
0.001 %
τ (kPa)
γ(%)

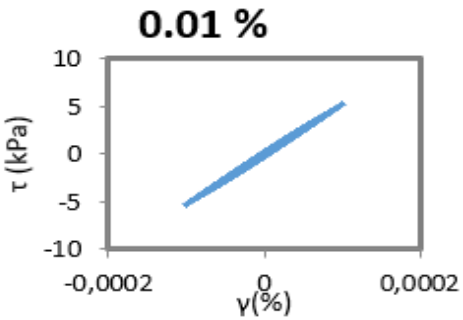
0.01 %
τ (kPa)
γ(%)

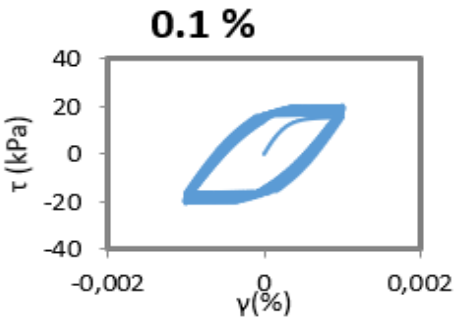
0.1 %
τ (kPa)
γ(%)

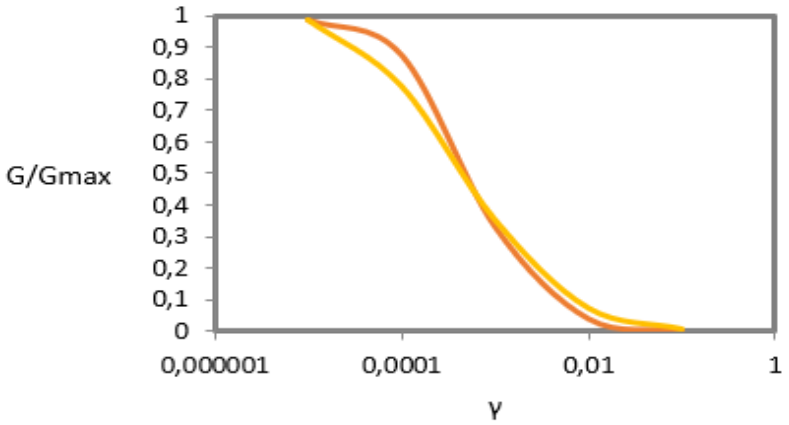
G/Gmax
γ

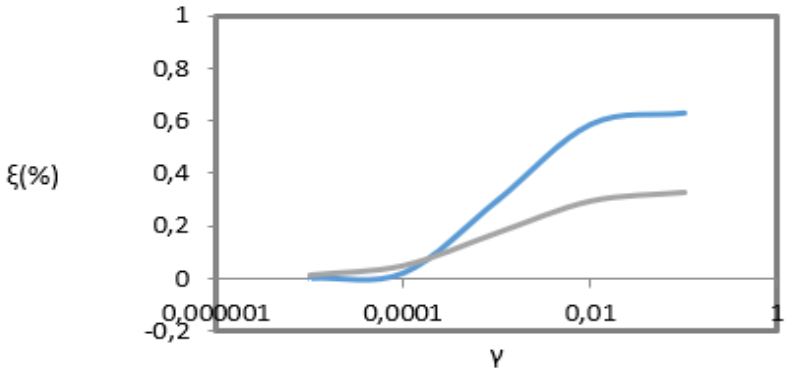
ξ(%)
γ

4. σ=50 kPa

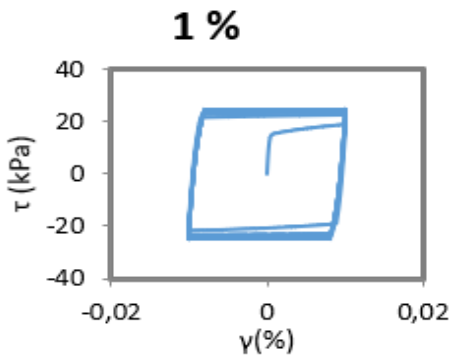
1 %
τ (kPa)
γ(%)

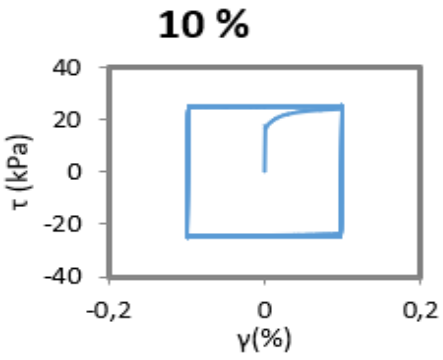
10 %
τ (kPa)
γ(%)

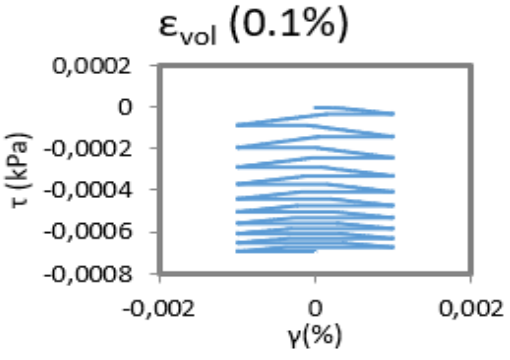
εvol (0.1%)
τ (kPa)
γ(%)

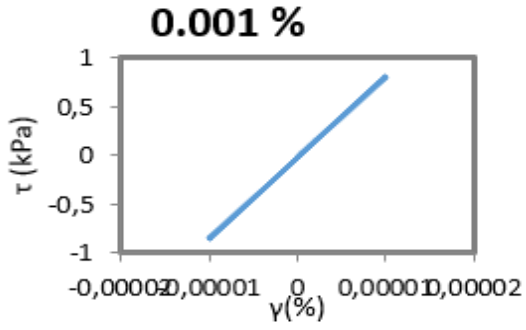
0.001 %
τ (kPa)
γ(%)

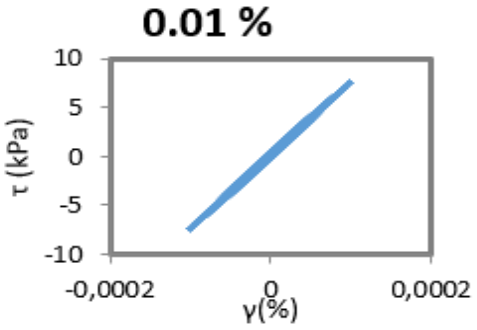
0.01 %
τ (kPa)
γ(%)

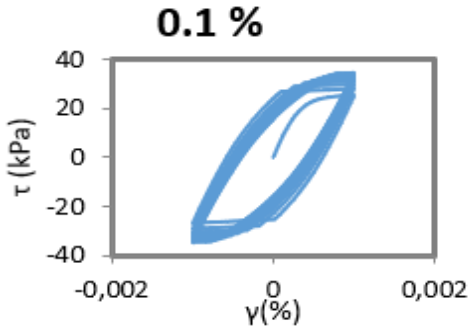
0.1 %
τ (kPa)
γ(%)

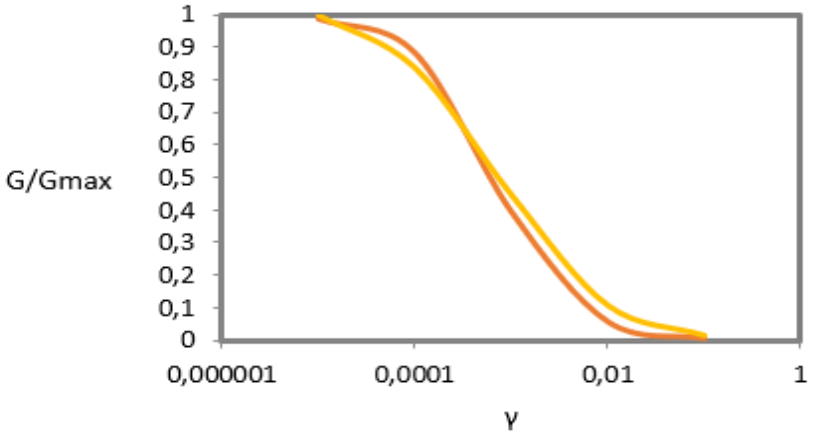
G/Gmax
γ

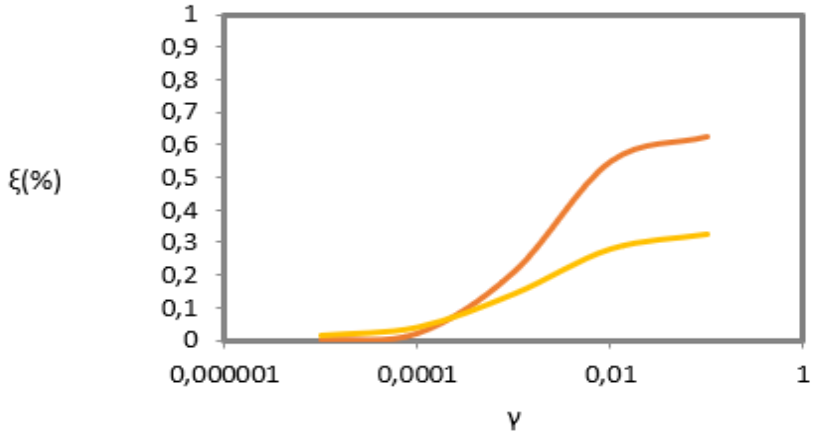
ξ(%)
γ

4. σ=100 kPa

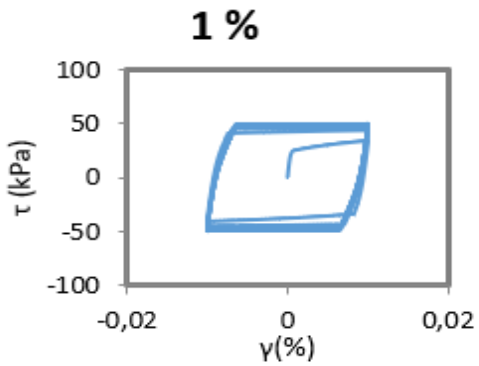
1 %
τ (kPa)
γ(%)

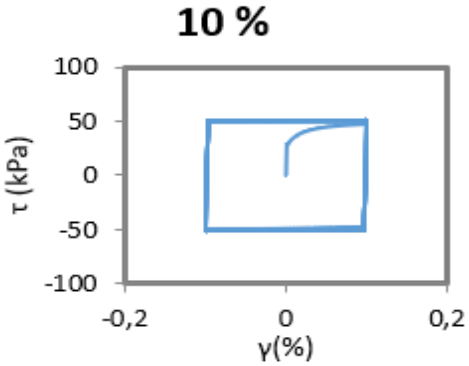
10 %
τ (kPa)
γ(%)

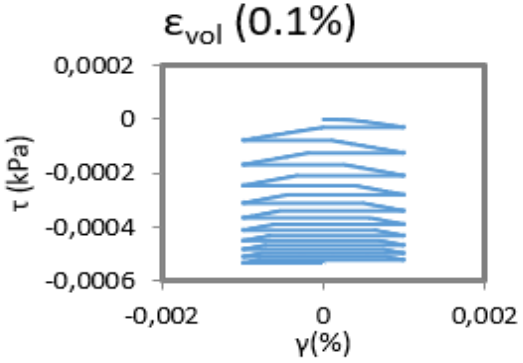
εvol (0.1%)
τ (kPa)
γ(%)

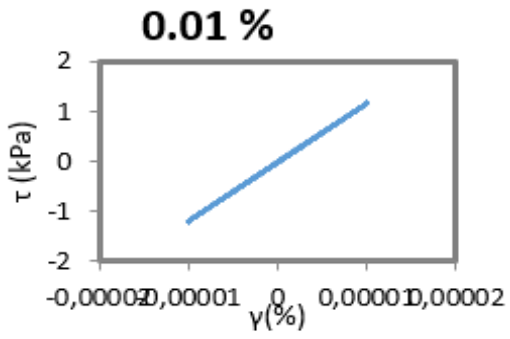
0.01 %
τ (kPa)
γ(%)

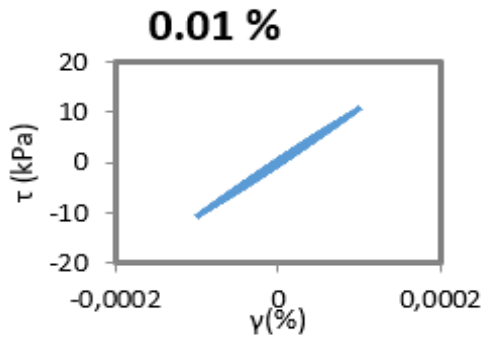
0.01 %
τ (kPa)
γ(%)

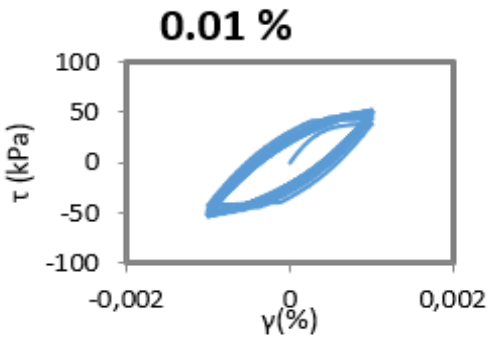
0.01 %
τ (kPa)
γ(%)

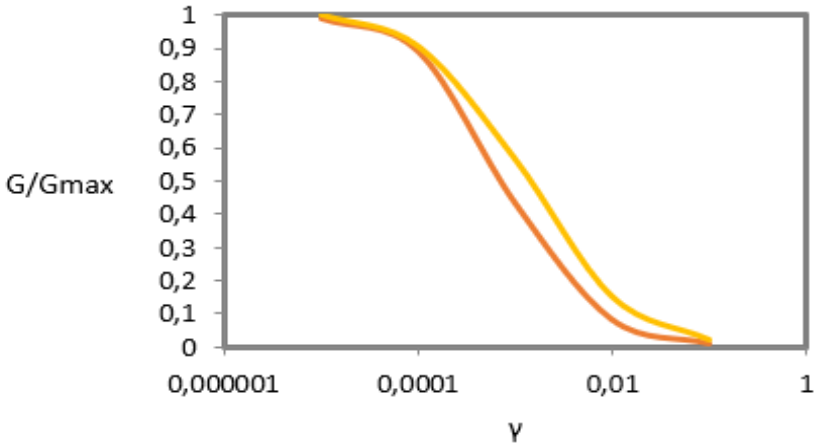
G/Gmax
γ

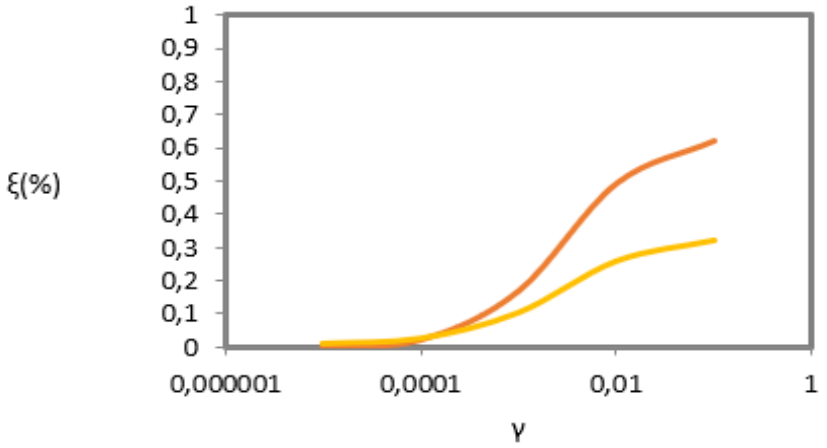
ξ(%)
γ

4. σ=200 kPa

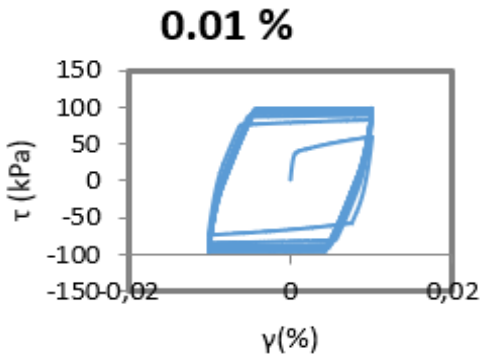
0.01 %
τ (kPa)
γ(%)

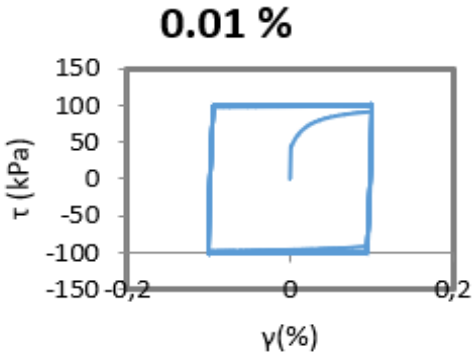
0.01 %
τ (kPa)
γ(%)

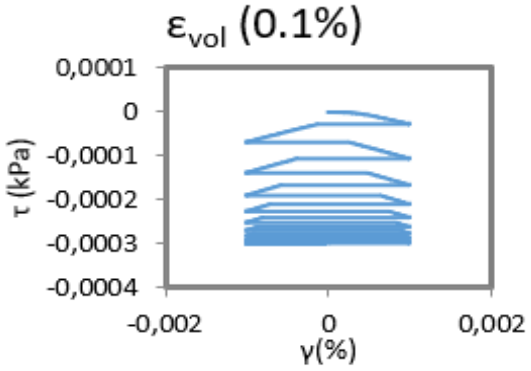
εvol (0.1%)
τ (kPa)
γ(%)

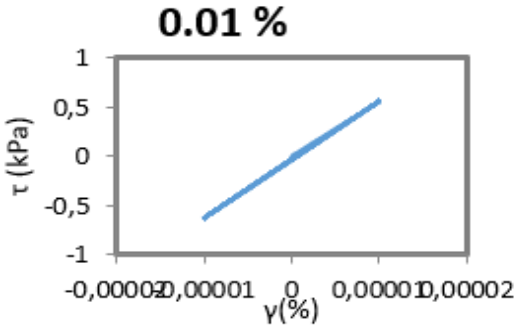
0.01 %
τ (kPa)
γ(%)

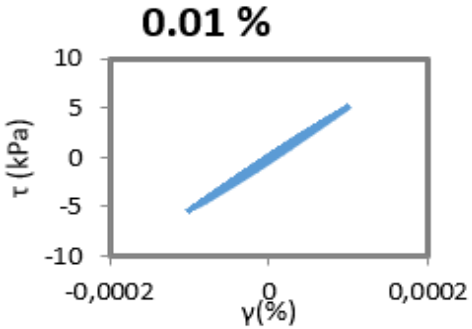
0.01 %
τ (kPa)
γ(%)

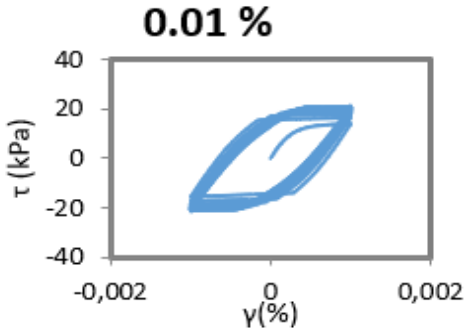
0.01 %
τ (kPa)
γ(%)

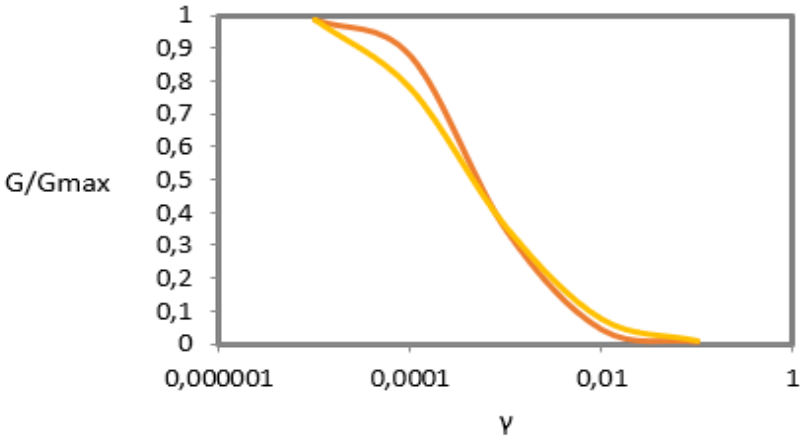
G/Gmax
γ

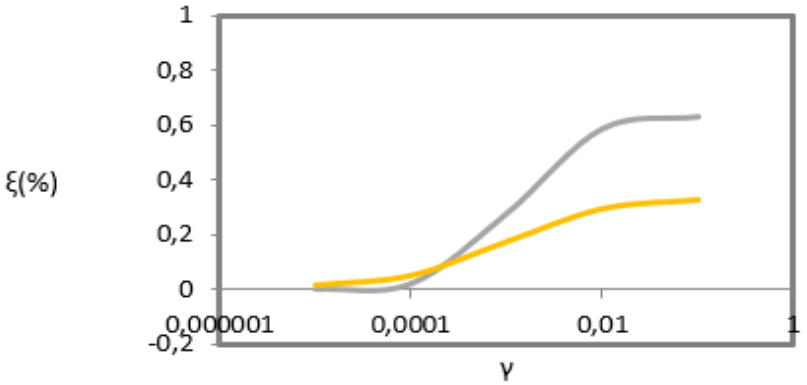
ξ(%)
γ

3. σ=50 kPa

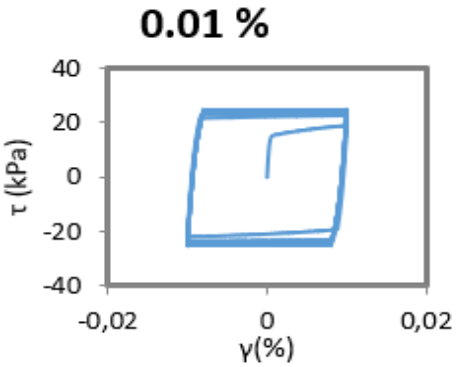
0.01 %
τ (kPa)
γ(%)

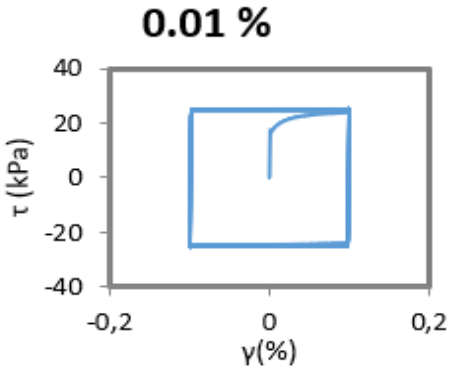
0.01 %
τ (kPa)
γ(%)

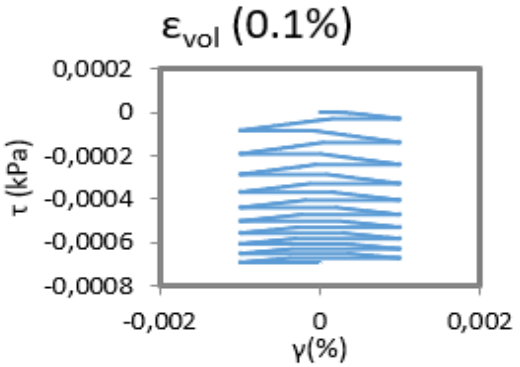
εvol (0.1%)
τ (kPa)
γ(%)

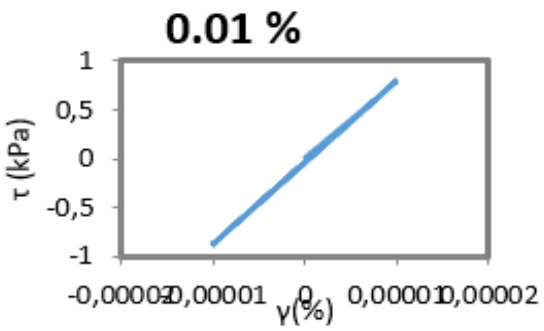
0.01 %
τ (kPa)
γ(%)

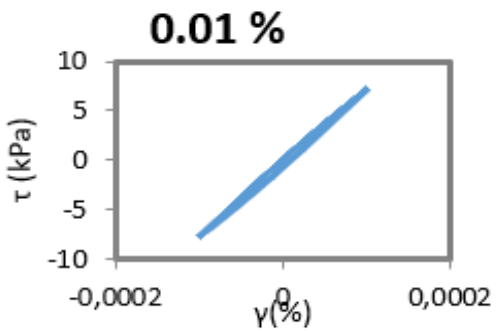
0.01 %
τ (kPa)
γ(%)

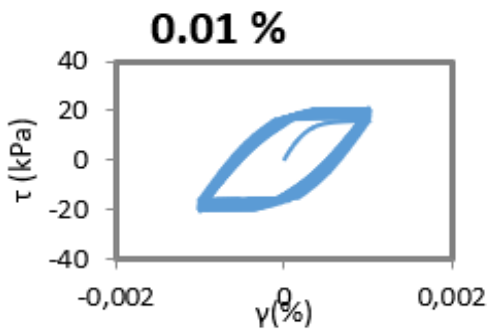
0.01 %
τ (kPa)
γ(%)

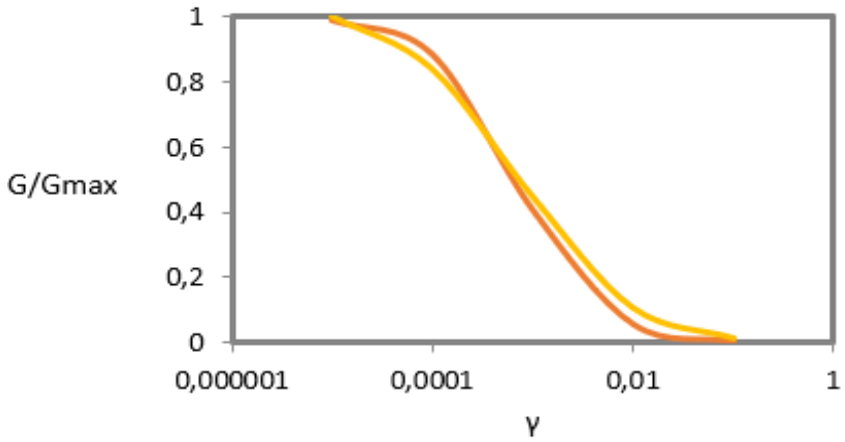
G/Gmax
γ

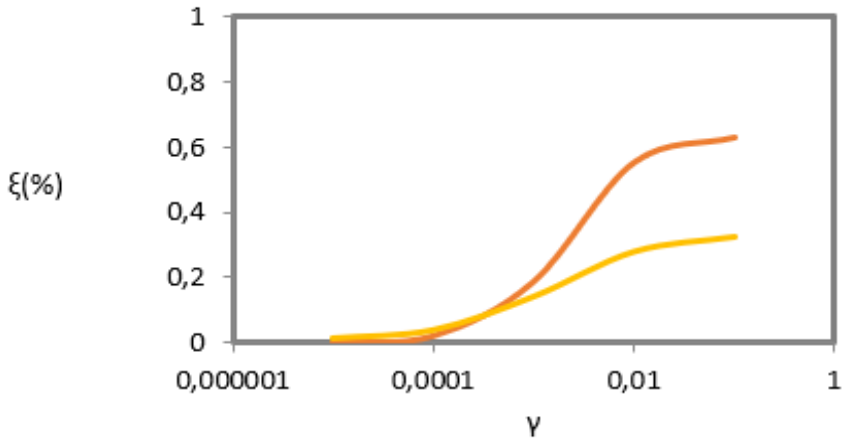
ξ(%)
γ

3. σ=100 kPa

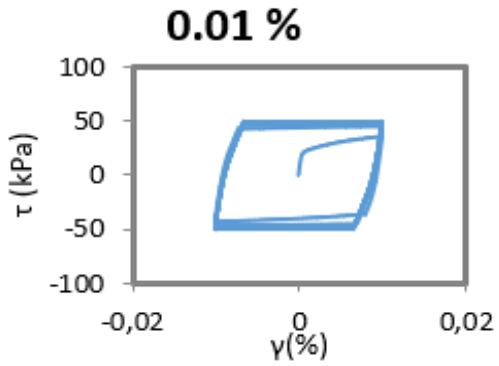
0.01 %
τ (kPa)
γ(%)

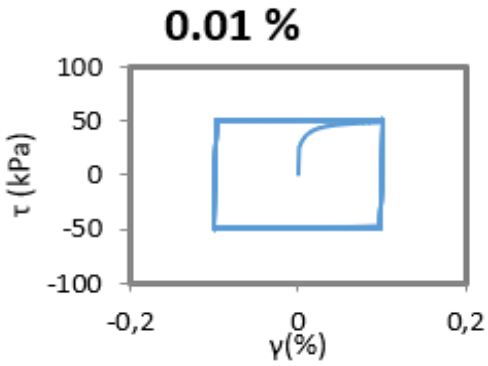
0.01 %
τ (kPa)
γ(%)

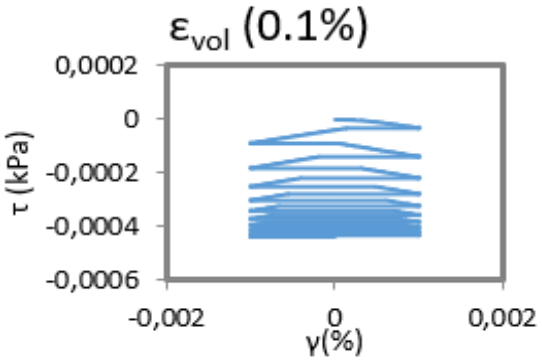
εvol (0.1%)
τ (kPa)
γ(%)

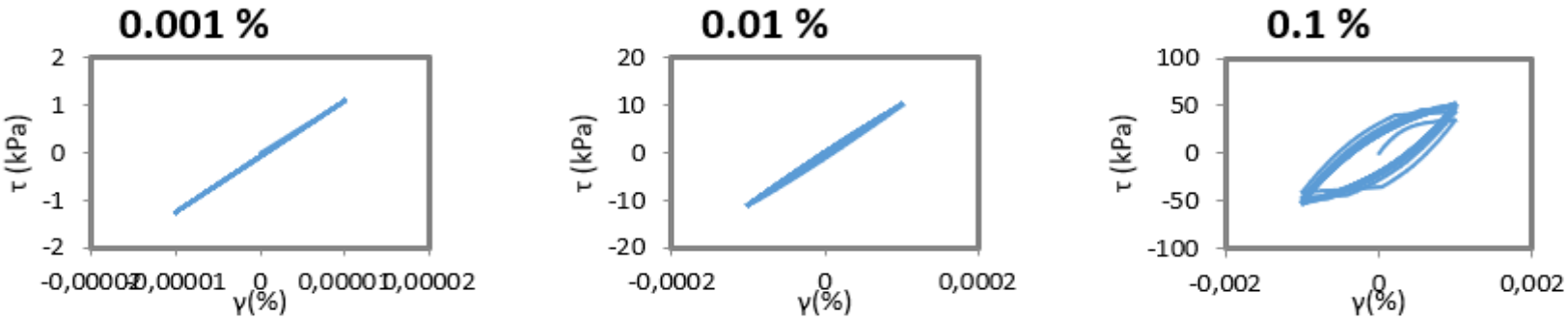
0.001 %
τ (kPa)
γ(%)
0.01 %
τ (kPa)
γ(%)
0.1 %
τ (kPa)
γ(%)

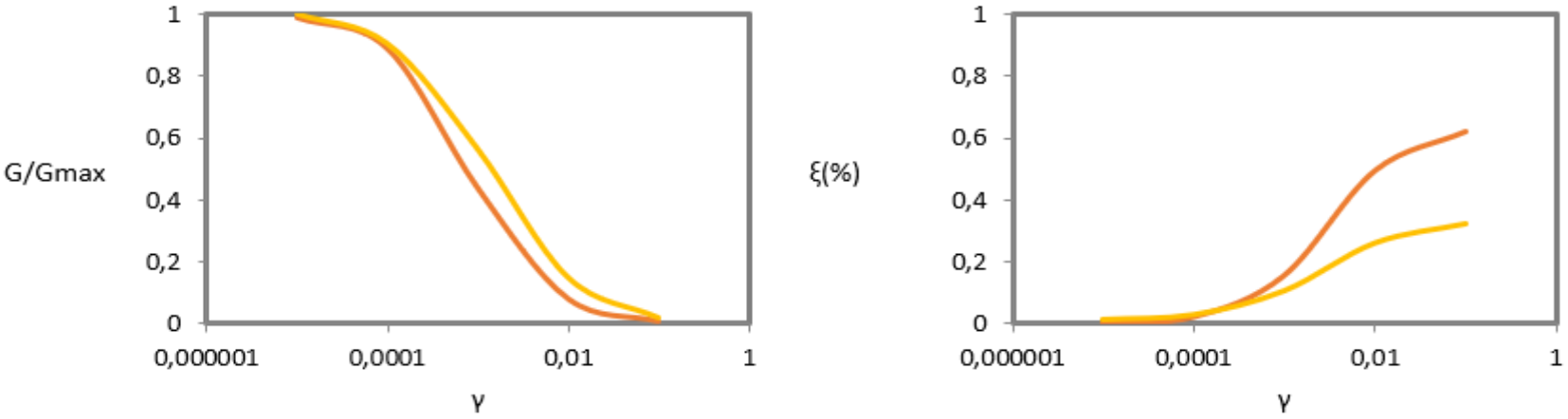
G/Gmax
γ
ξ(%)
γ

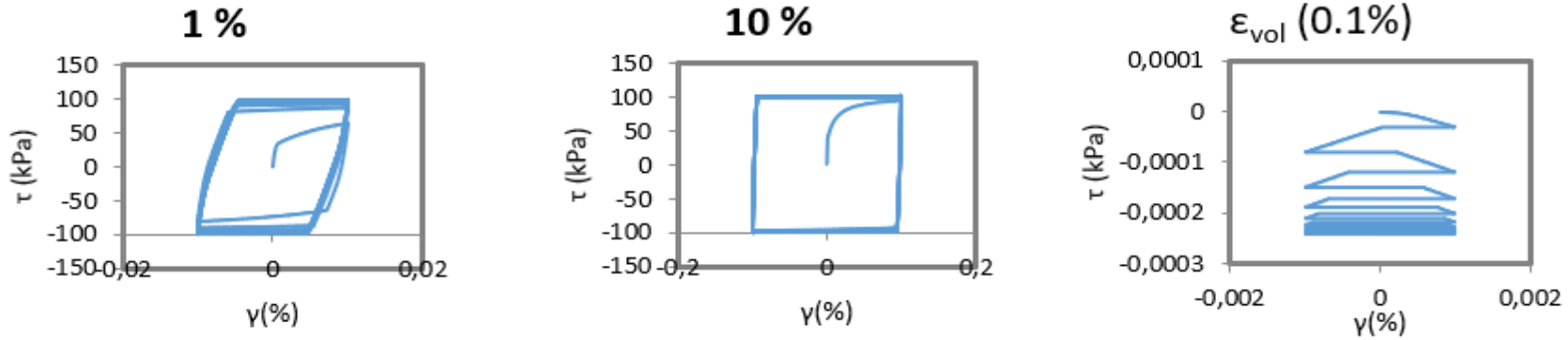
1 %
τ (kPa)
γ(%)
10 %
τ (kPa)
γ(%)
εvol (0.1%)
τ (kPa)
γ(%)

3. σ=200 kPa

4. Definition of the problem

The problem under investigation consists of a flexible cylindrical fixed-head pile embedded in a two-layer subsoil over a rigid bedrock. The pile is modelled as a solid elastic cylinder and in the soil non-linearities are considered. Seismic excitation is presented in the problem by vertically propagated shear waves specified as a horizontal motion in the bedrock. First of all, the parameters of the problem must be identified. Looking at Figure (4.1) one can identify the geometric parameters of the problem:

1. Length of the pile (L)
2. Diameter of the pile (d)
3. Height from the soil surface till the end of the model, bedrock (H)
4. Height of the upper layer of the soil (h_1)

Secondly, the material parameters:

1. Shear velocity of each layer (Vs_1) , (Vs_2)
2. Hysteric damping coefficient of each layer (ξ_1) , (ξ_2)
3. Specific weight of each layer (γ_1) , (γ_2)
4. Poison ratio for each soil layer (ν_1) , (ν_2)
5. Elastic Modulus of the pile (E_p)
6. Specific weight of the pile (γ_p)
7. Poisson ratio of the pile (ν_p)
8. Cohesion of the soil (c)
9. Friction angle of the soil

Finally, the excitation properties of the problem:

1. Number of cycles (N)
2. Predominant period of the excitation (T_{inp})
3. Rock acceleration amplitude (a_{rock})

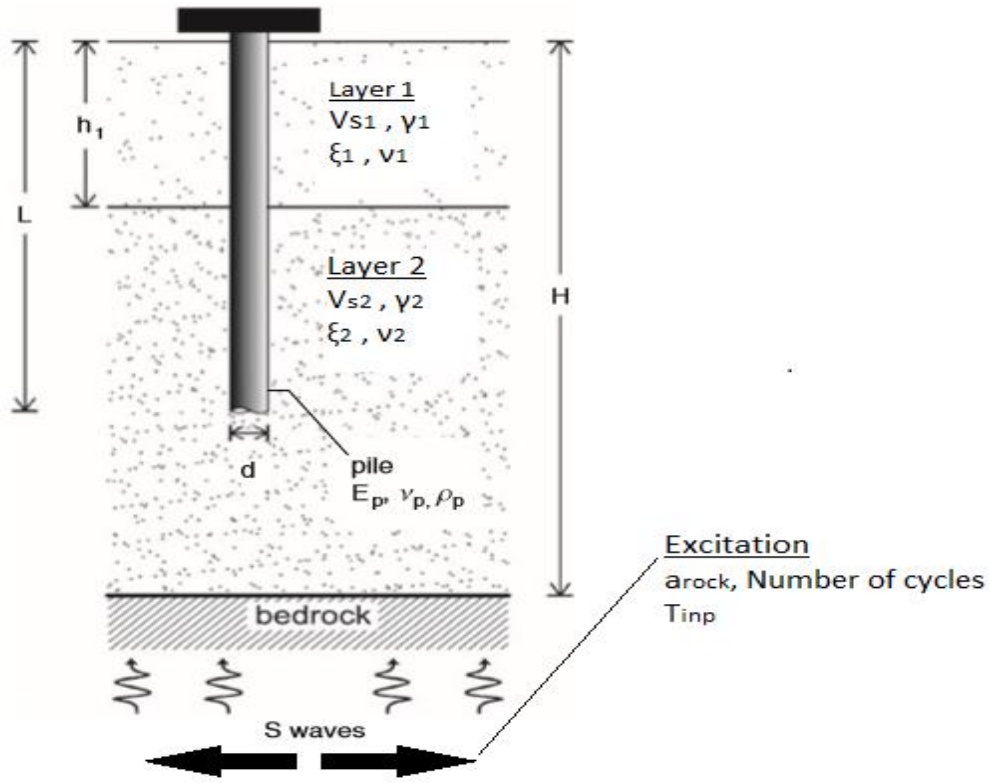

Figure 4.1 Geometry and main parameters of the defined problem

Response to harmonic earthquake excitation of the pile is governed by those 18 independent variables. Not all these parameters are going to be researched in this study. For the them, values will be selected that are commonly used in practice and the literature. Those are:

Cohesion (C): 2 kPa

Friction angle of the soil (ϕ): 30°

Damping Coefficients (ξ_1), (ξ_2): 5%

Specific weight for the second layer (γ_2):23 kN/m^3

Poisson ratio for the soil (ν_1), (ν_2): 0.3

Pile's Elastic modulus (E_p): 30 MPa

Pile's Poisson ratio (ν_p): 0.2

Pile's specific weight (γ_P): 25 kN/m^3

These assumptions reduced the variables to 10. So, in terms of bending moments the function is the following:

$$M = f(\gamma_1 , h_1 , d , a_{sur} , L, E_p , V_{s1} , V_{s2} , T_{inp} , N)$$

Using dimensional analysis, the Buckingham theorem specified that 8 independent dimensionless ratios are eligible to describe fully the pile response:

$$\frac{M}{\gamma_1 \, h_1 d^3} = f\left(\frac{a_{sur}}{g}, \frac{L}{d} , \frac{E_p}{E_{s1}} , \frac{V_{s2}}{V_{s1}} , \frac{h_1}{L} , \frac{T_{inp}}{T_{soil}} , N\right)$$

The $\frac{a_{sur}}{g}$ represents the intensity of the excitation, a parameter that strongly the affects the results in the case of non-linear soil, due to the link between the soil properties and the deformations (in comparison with the linear case where the amplitude of the excitation is like a multiplication factor in the moments).

Second one, $\frac{L}{d}$, is the slenderness ratio of the pile. To understand the influence of this parameter an extreme case will be presented. A very short and hence rigid pile, meaning a mall slenderness ratio, doesn't follow the soil displacement curvatures closely, which means that normalized bending moments are much smaller than in more flexible piles. Also in absolute terms M increases approximately in proportion to pile length and to d^3.

Where, the $\frac{E_p}{E_{s1}}$ variable represents the relative stiffness of the pile to the surrounding soil, a ratio that plays an important role in the motion of the pile. And as we saw in the first chapter the result of the deviation in the relative motion of the pile to the surrounding soil is the reason for the bending moments, which means that if the relative stiffness of the pile increases, the relative curvature and the moments of the pile will also increase.

The $\frac{V_{s2}}{V_{s1}}$ refers to shear velocity ratio between the two layers. As many researches have already shown (chapter 1) the moments at the interface of the soil layers and in some cases at the head of the pile are affected significantly by the stiffness contrast (same as shear velocity contrast) between the two layers. This is a result of the discontinuity of the displacements of the soil surrounding the pile (Gazetas & Kavadas 1993) creating large curvatures at the interface.

Next one is $\frac{h_1}{L}$, which describes the interface location in comparison with the pile length. This is a parameter of great importance for the kinematic bending moments, because the increased stiffness of the second layer acts as a partial fixity for the pile, which tends to reduce pile rotation at the interface thus generating a positive contribution bending moment in that location. A certain percentage (which is dependent on the height of the upper layer h_1) of that moment is transmitted to the head (Chapter 1, Mylonakis et al. 2013).

The "resonance ratio" $\frac{T_{inp}}{T_{soil}}$, defines the difference between the excitation period that is imposed in the problem to the predominant period of the subsoil (hence the resonance). As we know from the theory the function A-T , where A is the amplification factor and T the

period, at regions close to the eigen periods of the soil we have enormous amplification (Chapter 1), this means that the amplitude of the motion at the pile can be tremendously altered by the resonance ratio.

Last the number of cycles N, as it was also shown by Nikolaou & Gazetas (1997) plays a huge impact in the bending moments of the pile. Especially in the case that is examined in this study, where the non-linearity of the soil accumulates for each cycle of excitation and phenomena like “plastic shakedown” occur at the pile-soil system.

Now that the Moment equation is formed, comes the value estimation for each of the variables.

Specific weight of the upper layer (γ_1): 13, 17, 20, 23 kN/m^3

Length of the pile (L): 15 ,20, 30 m

Diameter of the pile (d): 0.6, 1, 1.5 m

Height of the upper soil layer (h_1): 1/3 L , 1/2 L , 2/3 L

Shear wave velocity of the second layer (V_{s2}): 400, 600, 800 m/s

Shear velocities ratio (V_{s2}/V_{s1}): 1.5, 2, 3, 5

Number of cycles (N): 3, 6, 11, 15

“Resonance Ratio” (T_{inp}/T_{s1}): 0.75, 1, 1.33 , 1.5

Excitation acceleration magnitude (a_{rock}): 0.1, 0.25, 0.4, 0.6 g

With the above values the sum of all the possible scenarios is more than 1000 different cases. Again with using the Haltonset function the number of cases was reduced to 60. The different cases that will be studied in the study are presented below (Table 4.1)

	γ1	*A_{rock}*	*d*	*L*	*H_1*	*V_{s2}*	*V_{s1}*	*N*	*T_{inp}/T_{s1}*
1	13	0,1	0,6	15	5	800	400	6	1
2	20	0,1	1,5	20	6,667	800	533,328	6	1
3	17	0,25	0,6	20	10	800	533,328	6	1
4	23	0,4	1	30	15	800	533,328	6	1
5	13	0,6	1,5	30	15	400	80	11	1
6	20	0,1	0,6	15	7,5	400	80	11	1,333333
7	17	0,25	1	15	10	400	80	11	1,333333
8	23	0,25	1,51,5	15	10	400	133,32	11	1,333333
9	13	0,4	0,6	20	13,33	600	199,98	11	1,333333
10	20	0,6	1	20	13,33	600	199,98	11	1,5
11	17	0,1	1,5	30	10	600	300	15	1,5
12	23	0,25	0,6	30	10	600	300	15	1,5
13	13	0,4	1	15	5	600	300	15	1,5
14	20	0,4	1,5	15	7,5	800	400	15	1,5

15	17	0,6	0,6	15	7,5	800	533,328	15	0,75
16	23	0,1	1	20	10	800	533,328	3	0,75
17	13	0,25	1,5	20	10	800	533,328	3	0,75
18	20	0,4	0,6	30	20	400	80	3	0,75
19	17	0,6	1	30	20	400	80	3	0,75
20	23	0,6	1,5	15	10	400	80	3	1
21	13	0,1	0,6	15	10	400	133,32	3	1
22	20	0,25	1	20	6,667	600	199,98	6	1
23	17	0,4	1,5	20	6,667	600	199,98	6	1
24	23	0,6	0,6	20	6,667	600	300	6	1
25	13	0,6	1	30	10	600	300	6	1,333333
26	20	0,1	1,5	30	15	800	400	6	1,333333
27	17	0,1	0,6	15	7,5	800	400	6	1,333333
28	23	0,25	1	15	7,5	800	533,328	11	1,333333
29	13	0,4	1,5	20	10	800	533,328	11	1,5
30	20	0,6	0,6	20	13,33	800	533,328	11	1,5
31	17	0,1	1	20	13,33	400	80	11	1,5
32	23	0,1	1,5	30	20	400	80	11	1,5
33	13	0,25	0,6	30	10	400	80	11	1,5
34	20	0,4	1	15	5	400	133,32	15	0,75
35	17	0,6	1,5	15	5	600	199,98	15	0,75
36	23	0,1	0,6	20	6,667	600	199,98	15	0,75
37	13	0,25	1	20	10	600	300	15	0,75
38	20	0,25	1,5	30	15	600	300	15	0,75
39	17	0,4	0,6	30	15	800	400	3	1
40	23	0,6	1	30	15	800	533,328	3	1
41	13	0,1	1,5	15	10	800	533,328	3	1
42	20	0,25	0,6	15	10	800	533,328	3	1
43	17	0,4	1	20	13,33	800	533,328	3	1
44	23	0,4	1,5	20	6,667	400	80	3	1,333333
45	13	0,6	0,6	30	10	400	80	6	1,333333
46	20	0,1	1	30	10	400	80	6	1,333333
47	17	0,25	1,5	30	10	400	133,32	6	1,333333
48	23	0,4	0,6	15	7,5	600	199,98	6	1,5
49	13	0,6	1	15	7,5	600	199,98	6	1,5
50	20	0,6	1,5	15	7,5	600	300	6	1,5
51	17	0,1	0,6	20	10	600	300	11	1,5
52	23	0,1	1	20	13,33	800	400	11	1,5
53	13	0,25	1,5	30	20	800	533,328	11	0,75
54	20	0,4	0,6	30	20	800	533,328	11	0,75
55	17	0,6	1	15	5	800	533,328	11	0,75
56	23	0,1	1,5	15	5	800	533,328	15	0,75
57	13	0,1	0,6	15	5	400	80	15	0,75
58	20	0,25	1	20	6,667	400	80	15	1
59	17	0,4	1,5	20	10	400	80	15	1
60	23	0,6	0,6	30	15	400	133,32	15	1

Table 4.1: The analyses that were generated with the use of the Haltonset function and are going to be performed in the next chapters.

An important step for the analysis is the estimation of the soil's predominant period, but there is no analytical solution for the case of two layered non-linear subsoil. Due to the non-linear behavior of the soil the G-z distribution would have looked something like the Figure 4.2. This is a "double" parabolic distribution with a leap at the interface depth equal to the ratio of the shear velocities (V_{s2}/V_{s1}). The incapability of simulating the amplification function with the use of mathematical formulas for a soil with parabolic distribution, led to the division of the layers in multiple sublayers with a constant shear modulus (G_i) for each one of them, a case that can be treated with the use of mathematics.

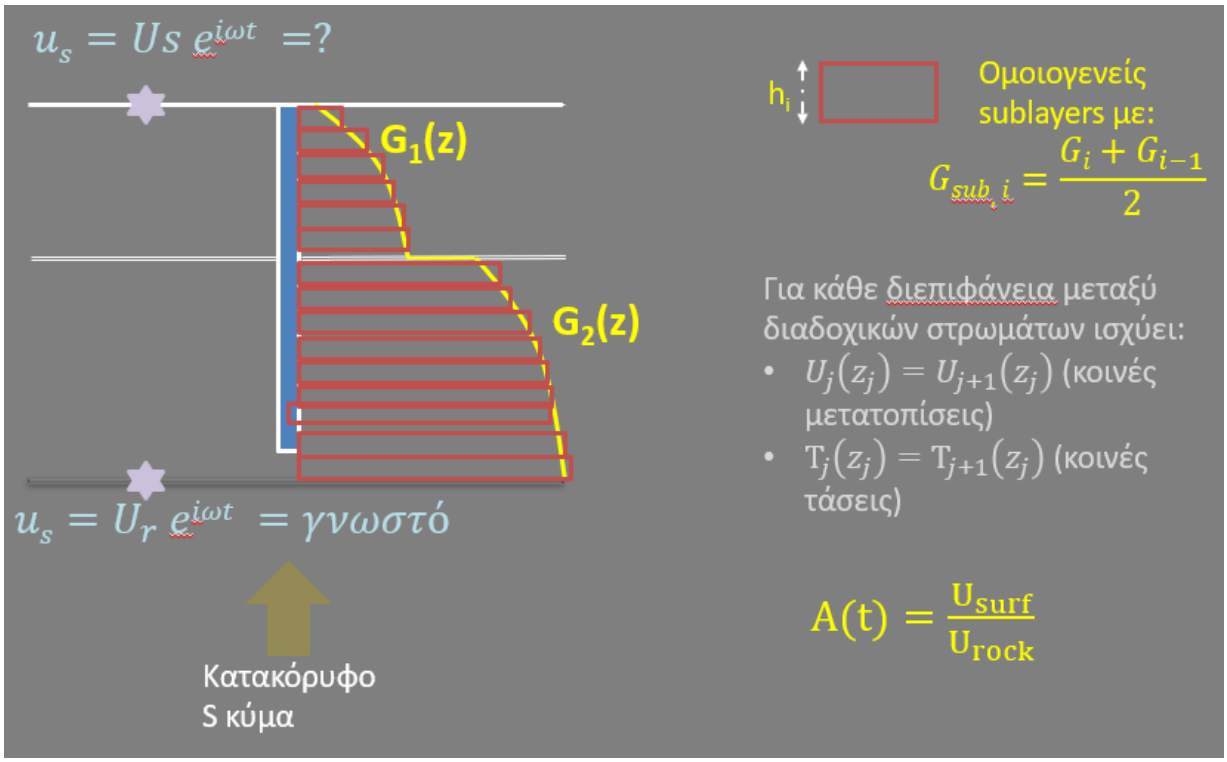

Figure 4.2: Distribution of G with depth for the problem to be tested. The red parallelograms are the sublayers created in order to evaluate the amplification factor.

4.1 Response of multilayer stratum in vertical shear waves SV

Looking at figure (4.1) we can identify the main parameters of the problem. As in the case scenario that is tested here the excitation at the bedrock is known (harmonic excitation with known amplitude and frequency) and the deformations at the soil surface is the desideratum.

For each layer:

$$u = U\,e^{i\omega t}, \qquad U = B'e^{-ikz} + B''e^{ikz}\ [Displacements]$$

$$\tau = T\,e^{i\omega t}, \quad T = -ikG\left(B'e^{-ikz} - B''e^{ikz}\right)\ [Stresses]$$

Or in matrix form:

$$\begin{bmatrix} U \\ T \end{bmatrix} = \begin{bmatrix} e^{-ikz} & e^{ikz} \\ -ikGe^{-ikz} & ikGe^{ikz} \end{bmatrix} \begin{bmatrix} B' \\ B'' \end{bmatrix}$$

2x1 deformations/ stresses vector	2x2 matrix	*2x1 vector for the unknown amplitudes*
$\Sigma(z)$	$\Delta(z)$	B

For a random soil interface z=z$_j$: $U_j(z_j) = U_{j+1}(z_j)$

$$T_j(z_j) = T_{j+1}(z_j)$$

$$\Sigma_j(z_j) = \Sigma_{j+1}(z_j)$$

$$\boldsymbol{\Delta}_j(z_j)\,\boldsymbol{B}_j = \boldsymbol{\Delta}_{j+1}(z_j)\,\boldsymbol{B}_{j+1} \qquad \boldsymbol{B}_{j+1} = \boldsymbol{\Delta}_{j+1}^{-1}(z_j)\,\boldsymbol{\Delta}_j(z_j)\boldsymbol{B}_j$$

$$\nabla_j \rightarrow (2 \times 2)$$

Using inductively the last equation from the n_{th} soil layer till the 1_{st} one:

$$\boldsymbol{B} = \nabla_{n-1}\boldsymbol{B}_{n-1} = \nabla_{n-1}\nabla_{n-2}\boldsymbol{B}_{n-2} = \cdots = (\nabla_{n-1}\nabla_{n-2}\cdots\nabla_1)\boldsymbol{B_1}$$

$$\prod_{n-1}^{1}(\nabla_j) \rightarrow (2 \times 2)$$

And for the bottom of the soil layer n:

$$\begin{bmatrix} U_r \\ T_r \end{bmatrix} = \boldsymbol{\Delta}_n(Z_n) \prod_{n-1}^{1}(\nabla_j)\ \boldsymbol{\Delta}_1^{-1}(0) \begin{bmatrix} U_s \\ T_s \end{bmatrix}$$

$$\begin{bmatrix} U_r \\ T_r \end{bmatrix} = \boldsymbol{F} \begin{bmatrix} U_s \\ 0 \end{bmatrix} = \begin{bmatrix} F_{11} & F_{12} \\ F_{21} & F_{22} \end{bmatrix} \begin{bmatrix} U_s \\ 0 \end{bmatrix}$$

Which means that $U_r = F_{11}\, U_s \rightarrow U_s = F_{11}^{-1}\, U_r$ ⇒ $A = F_{11}^{-1}$

Therefore, to calculate the soil amplification factor, the F_{11}^{-1} is needed. A Mathcad routine was created using the above formulas and the parameter values used in our case study. More precisely the (G_i) of each sublayer is equal to:

$$G_j := Gmaxref_j \cdot (1 + 2 \cdot i \cdot \xi_j) \cdot \left(\frac{c \cdot \cos\left(\varphi \cdot \frac{\pi}{180}\right) + \gamma_j \cdot K0 \cdot z_j \cdot \sin\left(\varphi \cdot \frac{\pi}{180}\right)}{c \cdot \cos\left(\varphi \cdot \frac{\pi}{180}\right) + pa \cdot \sin\left(\varphi \cdot \frac{\pi}{180}\right)} \right)^m$$

Where the character j indicates the sublayer that is examined, $Gmaxref_j$ is equal to the Gmax of the particular soil layer, ξ_j and γ_j equal to the damping and specific weight of the corresponding layer. Also, ϕ=30°, K_0=0.5, c=2 kPa, m=0.5 and pa=100 kPa. As it was expected the G of each sublayer is depth depended. With this estimation procedure and with the use of MATHCAD a routine was created with the intention of creating the graph of the amplification function with frequency *A-f* . The first peak of this function, as we know from theory is the predominant period of the subsoil (T_{s1}). So using trace in Mathcad we can find the value of the first eigen period. (Figure 4.2). This period will then be multiplied with "Resonance Ratio" and the result of this will be the input of the harmonic excitation in the model.

To better understand the steps of the analysis, an example will be given.

We have the case scenario number ten (table 4.1). First of all we must calculate the $Gmax_{ref}$ for each of the two soil layers. $Gmax_{ref}$ is calculated with the use of the following formulas:

$$V_s = \sqrt{\frac{G_s}{\rho}} \rightarrow G_s = V_s^2 * \rho$$

$$G_{ref\ 1} = \frac{G_{s1}}{\left(\frac{2\ \cos\varphi + K_0\ \gamma_1\ H_1 * \sin\varphi}{2\cos\varphi + p_\alpha \sin\varphi}\right)^{0.5}}$$

Where H_1 =13,33 , γ_1= 20 , G_{s1}=92000 kPa meaning that G_{ref1}=74742,27 kPa meaning that for the second layer:

$$G_{ref2} = G_{ref1}\left(\frac{\rho_2\ V_{s2}^2}{\rho_1\ V_{s1}^2}\right)$$

With ρ_2=2,3 , V_{s2}=600 m/s the Greference for the second layer is, G_{ref2}=672680 kPa. All of the parameters are then transferred to the MATHCAD routine for the discretization. For a more accurate representation of the parabolic distribution each layer was further divided to 1000 layers (a sublayer for each centimeter). The results of the analysis can be shown in Figure 4.2 One can easily identify the first frequency for the soil, the first peak of the A-f equation.

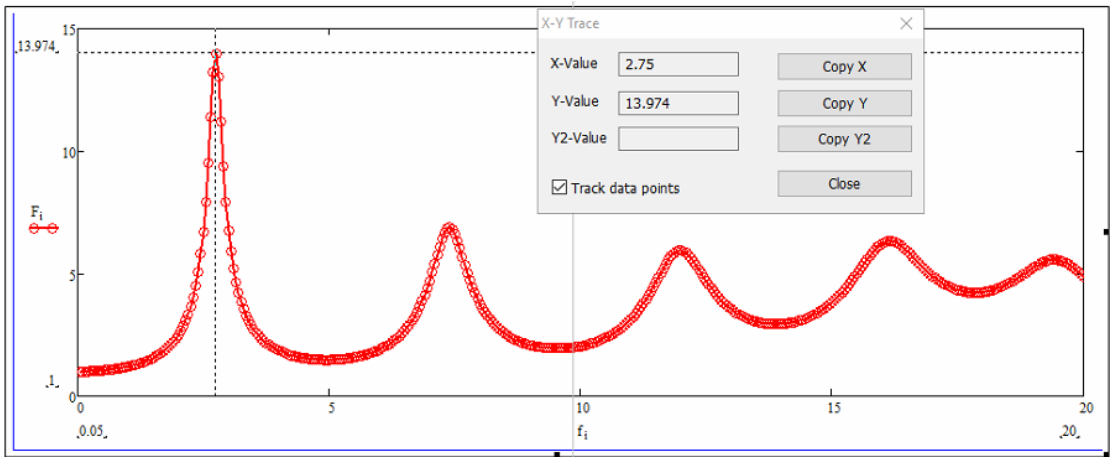

Figure 4.3 A graph produced with the code written in Mathcad. The amplification factor to the frequency. The first pick shown is the predominant period for the subsoil.

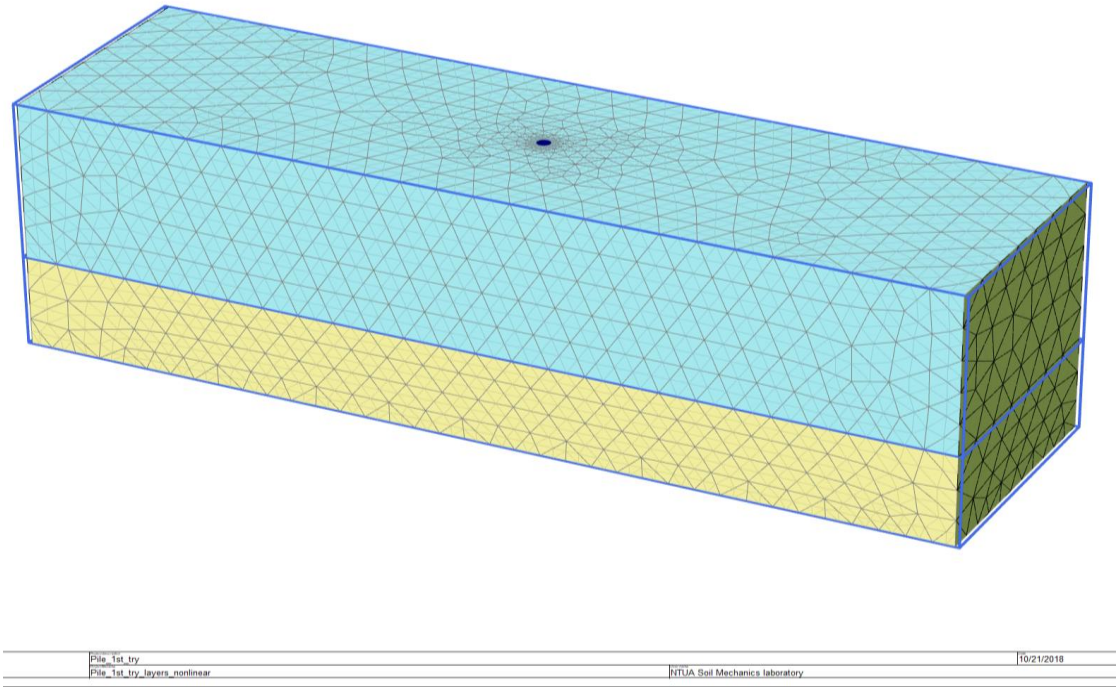

Figure 4.4: Case number 10, analysis that was used for the example.

It should be pointed out, that in the case of a multilayered soil the amplification factor can reach values higher than the value of the homogenous amplification factor at the first eigen period for ξ=5% , which is 12.9 (in this example the amplification factor is 14).

Arock-Asurface:

In the moment equation that lists all the variables, there is a variable that has to do with the acceleration at the soil surface in the free field (a_{sure}) but the excitation is at bedrock. In order to overcome this problem soil column analyses were conducted (with no pile) for each different case and the accelerations were monitored at the surface, giving us the a_{sur}.

Figure 4.3 Soil-column model that was used for the estimation of the free field acceleration at the surface of the soil (a_{sur}).

5.Numerical Modeling and sensitivity analyses

In this thesis 3D finite element analyses were conducted for simulating the problem. For the simulations the PLAXIS-3D code was used (2017 edition) which was presented in chapter 2.

5.1 Basic Geometry

On figure 5.4.2 one can see the basic geometry of the model that was used in this thesis. A pile of circular diameter is placed in the middle of the model with the head of the pile being at the top of it. The height between the end of the model and the toe of the pile will be discussed later on in chapter 5.4.3 . The excitation is simulated with the use of a prescribed displacement at the bottom of the model. This will be in most cases a harmonic excitation with prescribed amplitude and frequency. In chapter 8, the input motion at the base of the model is represented by acceleration time histories from past earthquakes. In Figure 5.4.3 is shown one of the model used (As the values for the diameter and the length of the pile are not constant the one shown is one of them. Generally, 9 models were created with different pile's length and diameter).

5.2 Pile simulation

The pile was simulated with use of linear elastic soil elements. The values of the pile's parameters were introduced in the last chapter and are the following:

Young modulus: E_p=30 GPa

Diameter: D= 0.6, 1, 1.5 m

Length: L= 15, 20 , 30 m

Unit weight: γ=25 kN/m^3

Poisson's ratio: ν=0.2

For the problem that is examined here, the kinematic bending moments of the pile must be reviewed throughout the time-history of the motion. Therefore, in the center of the pile an inclinometer was placed, which is a linear beam element that develops similar behavior with that of the pile. This way, the motion of the pile is recorded in a continuous way throughout it's length (instead of discrete elements). The values for the inclinometer's parameters are:

Young modulus: $E_{inc}=E_p/1000$=30 MPa

Cross section Area: $A_{inc}=A_{pile}= \pi D^2$ (depending on each case) (m^3)

Moment of Inertia: $I_{inc}= \pi D^4/64$ (m^4)

Unit weight: γ=1 KN/m^3

The moments from the inclinometer that will be derived for each saved step of the analysis for the whole length of the pile must be multiplied with 1000, equal to the ratio between the Pile- Inclinometer Elastic Modulus.

Next step is the placement of a plate at the head of the pile to overcome any Bernoulli Phenomena at the simulation. The plate gives the pile stiffness, but has no weight (almost zero unit weight). The plate's parameter values are:

Plates width: d= 10 m

Unit Weight: γ=0,01 KN/m^3

Poisson's ratio: v=0,2

Elastic Modulus: E_{plt}=30 GPa

5.3 Boundary Conditions

Different boundary conditions are used for the deformations part and the dynamic part of the analysis. Since the analysis is in 3D we have 6 different boundary conditions deformationwise and dynamicwise $X_{min,max}$ $Y_{min,max}$ $Z_{min,max}$. For the deformations at the x direction the boundaries are free, because the excitation is place on the x direction whereas for the dynamic part there are free field boundaries (representing that the soil continues over the proposed boundaries) to overcome any wave reflections. Moreover for the y coordinates for the deformations both ends are normally fixed , we don't want the model to deform vertically to the excitation but for the dynamics there are no boundaries at the y direction (we can't put viscous boundaries because they will affect the movement of the model at the x direction). Last, at the z direction for the top of the model (z_{max}) the deformations must be free in order for the soil to deform nature-like, while the bottom of the model (z_{min}) the boundary condition must be fixed.

Coordinate	Deformations	Dynamics
X_{min}	free	free field
X_{max}	free	free field
Y_{min}	normally fixed	none
Y_{max}	normally fixed	none
Z_{min}	normally fixed	none
z_{max}	free	none

Table 5.1 : Boundary conditions for the deformation's part and the dynamic part for all 6 boundaries.

5.4 Sensitivity Analyses

In this Chapter follow sensitivity analyses which have to do with the size of the finite elements, the meshing of the model as also with the dimensions of the numerical model.

5.4.1 Discretization of the Mesh

For a dynamic analysis, the discretization of the mesh plays a huge impact on deriving realistic results, especially for cases with complex geometry. A very coarse discretization fails to understand the small changes in the stresses and strains at some parts of the model, especially at the points where concentration of stress appears. From the other hand, a fine mesh leads to enormously large calculation times. Therefore, a solution must be found, so that the accuracy of the results is good enough but with a logical calculation time. In order to obtain the density of the mesh that will be used for the dynamic analyses later on, a sensitivity analysis is performed for the maximum size of the element. Thus, there are implemented different densities of the mesh for one of the cases from the ones that were performed in chapter 7 , number 41. For these analyses the boundaries of the problem are set at L=70m for the x direction and B=20m for the y direction.

From the analyses that were conducted the envelope of the bending moments was the criterion for any deviations. Below is a table 5.2 with the results from the analyses that were conducted:

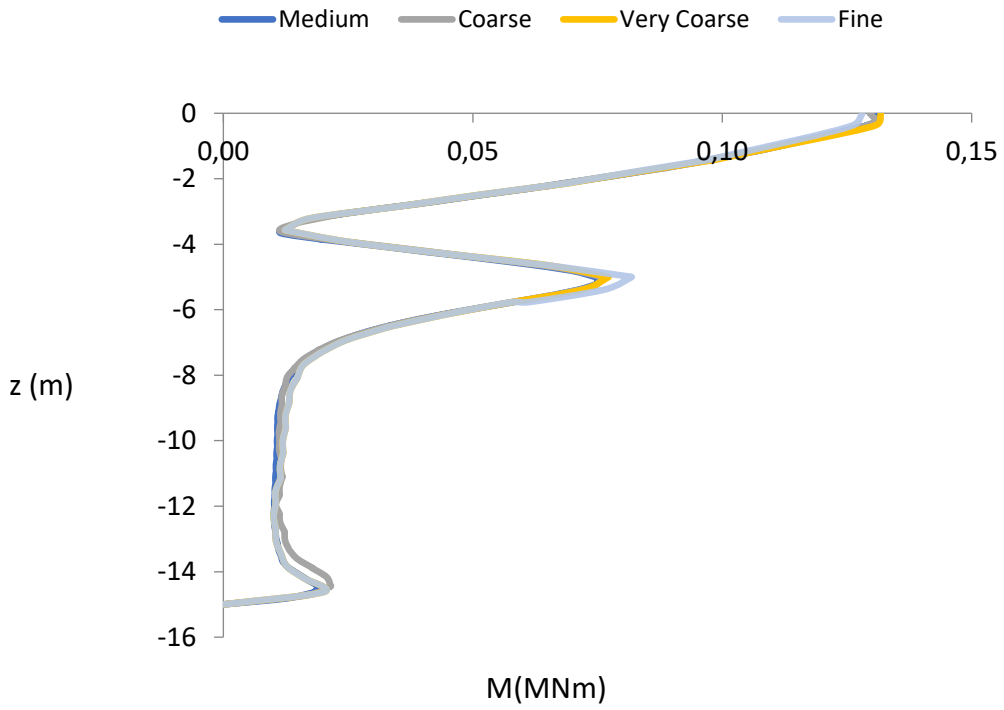

Figure 5.4.1: Sensitivity analyses for the discretization of the pile.

Discretization	Number of Elements	Deviations (%)	
		Head	Interface
Very coarse	6825	2,88	8,84
Coarse	13011	1,23	7,08
Medium	47847	1,20	5,66
Fine	118543	0,00	0,00

Table 5.2: Deviations for the four different cases of discretization

We see that the deviations are insignificant for the discretization, with a maximum error for the very coarse case to be less than 9%. The one selected is the medium case which can be seen in figure 5.4.2.

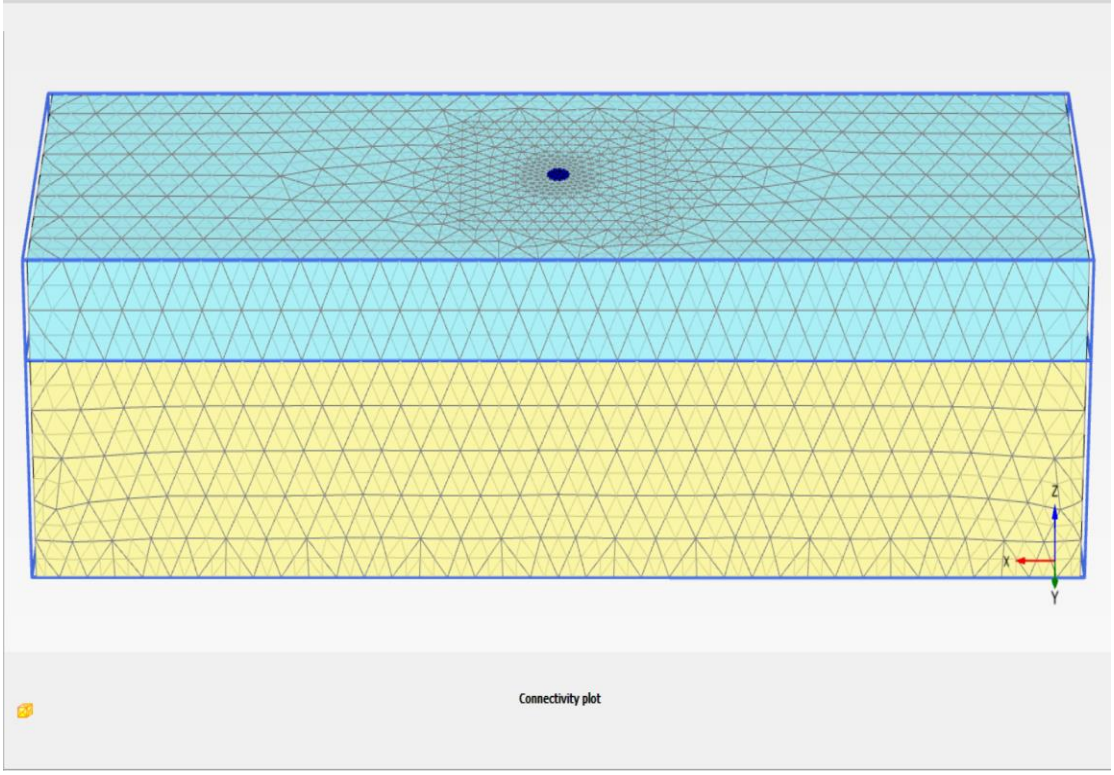

Figure 5.4.2 The model discretization that was used for the analyses later on.

5.4.2 Dimensions of the Model

At this part of the study, the retrofitting of the dimensions of the model are researched. The dimensions must be those, that can reduce the calculation time of the problem without affecting the results of the analyses. At the figure (5.4.3) the length (L) and the width of the model (B) can be identified.

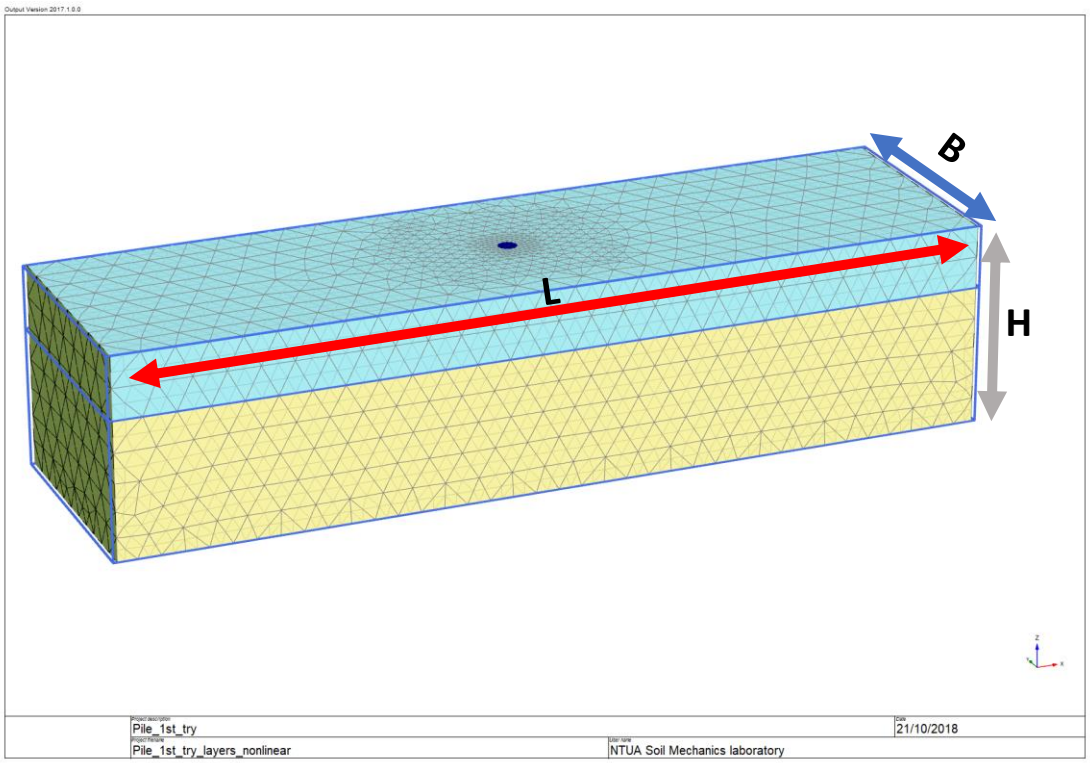

Figure 5.4.3 The dimensions of the problem LxBxH

Taking into account that the dynamic models that have to do with shear waves are affected highly by the reflected waves that propagate and reflect at the boundaries of the model, it's a must to keep the point of interest area of the model as much as it is possible unaffected by the reflection of the waves. Generally, the dimensions of dynamic problems are selected much greater than the corresponding static ones. To determine the best dimensions for the kinematic problem, different cases of LxB. The purpose of this sensitivity analyses is to establish dimensions, beyond which the soil is simulated as a semi-infinite medium.

The dynamic analyses were conducted for the case 35 (Table 4.1) a harmonic excitation with the highest case amplitude equal to 0.6, number of cycles 15 frequency equal to 11 Hz. The case with the highest amplitude of the excitation as well as the highest number of cycles was selected for being the most critical one for reflection phenomena at the boundaries. The criterion that was selected was the maximum bending moments at the interface and at the head. The envelope of bending moments can be seen in the next figure (fig. 5.4.4).

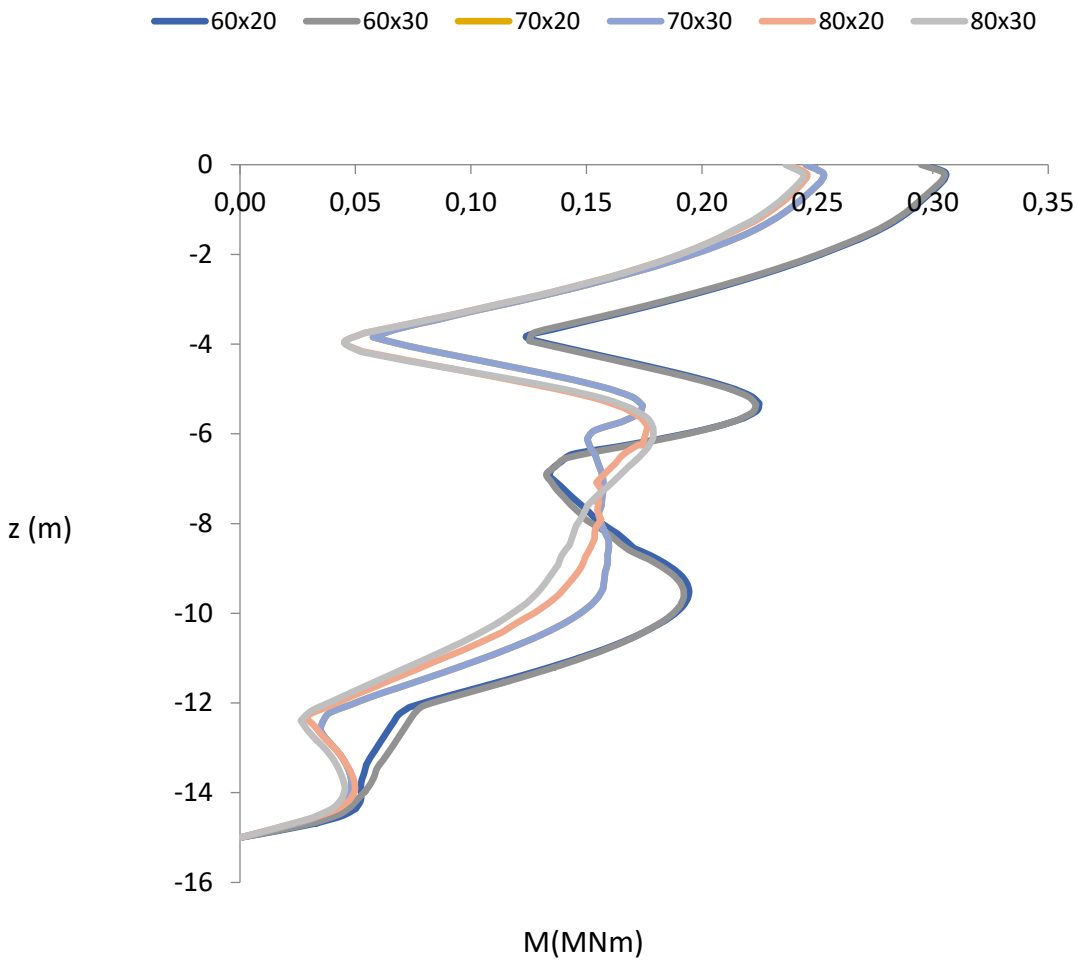

Fig. 5.4.4 Envelopes of bending moments for different model dimensions

Dimensions		Moment Deviations(%)	
B	L	Head	Interface
20	60	-25,10	-25,66
30	60	-24,59	-24,91
20	70	-4,01	2,95
30	70	-3,53	2,55
20	80	-0,61	1,35
30	80	0,00	0,00

Table 5.3 Results from the sensitivity analyses for the dimensions of the model

5.4.3 Sensitivity analysis for the toe of the pile

A sensitivity analysis was conducted for the influence of the pile to toe—to—bedrock distance on the response of the pile (fig. 5.4.2). In the case where the pile was hinged at the bottom of the model the bending moments had huge discrepancies with the normal bending moments in cases of kinematic bending moments, huge curvatures were amassed at the toe of the pile affecting strongly the Bending moments at the head and the interface. Thus, the analyses that were carried out were with different heights between the pile's toe and the end of the model. The criterion was the difference between the bending moments at the interface and the head for each case. But because the Height of the soil changes for every different analysis, that means that the amplification factor as well as the predominant period of the soil changes. That's why the moments for every case were normalized, using the ratio between the amplification factor of the hinged case (A_{hing}) to the amplification factor of the examined case (A_{exam}). Below is a table with the bending moments deviations at the head and the interface:

Case	**Amplification factor**	**DEVIATIONS**	
		Head	Interface
Hinged	12,7	0,00	0,00
5 D	13,7	-19,00	-0,95
2 D	13,15	-21,82	-9,40
1 D	12,7	-23,28	-17,20
0,5 D	12,7	-24,21	-17,72

Table 5.4 Results for the different heights between the end of the model and the toe of the pile.

In order to have a common ground with the equations used in the literature the case of 1D is selected being close to the problem that was researched by the previous authors,

6. Validation- Comparison with existing methods

In order to test the validity of the FEM model for the case of kinematic bending moments, some analyses were conducted. First nonlinear dynamic analyses to test the constitutive model that is going to be used and also some linear analyses in order to check for the deviations with the proposed formulas in literature (Chapter 1).

6.1 Nonlinear dynamic analyses

The purpose of the nonlinear analyses is to test the Force-deformation (F-d) loops of the HS-small model. To do that a pushover was conducted on the pile applying a point load at the surface, to find the maximum load that the pile can withstand. The results of the Pushover can be seen on the graph below (fig. 6.1):

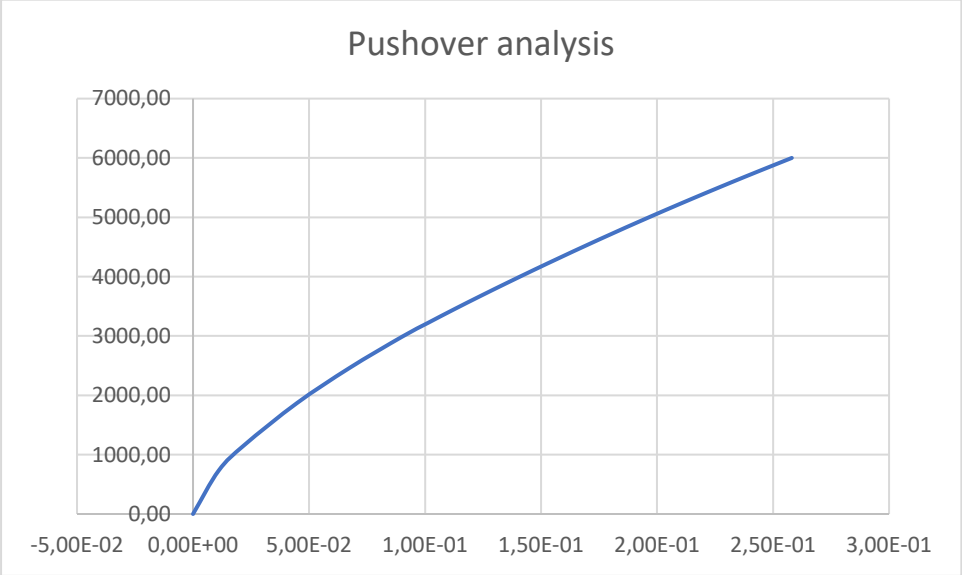

Fig 6.1 Results of the pushover conducted on the pile

For the sake of finding the maximum load of the pile, the deformations of the pile are going to be used. The maximum lateral deformation as known from practice is close to 10 cm. By using that value on the pushover that was conducted, the maximum force on the pile is 3000 kN.

Now that the bearing capacity of the pile for lateral loads is known, we continue with the two dynamic analyses. A dynamic point load was applied at the top of the pile with a harmonic excitation $F = F_{max} * \sin(\omega_j t)$. The only thing that changed in the two analyses was the ω, where in the first one the input period of the load was $0.75*T_{s1}$, meaning the predominant period of the subsoil and in the second $T_{inp}=2*T_{s1}$. Those two different periods were selected to see if the constitutive model (HS small) can understand the cut-off frequency. Just a reminder, cut-off frequency is the frequency lower than which no radiation damping occurs (or vice versa). Thus, what we expect to see is in the first analysis a much higher damping ratio than the second analysis. Though some problems arise such as, the calculation of the damping

ratio for each case. Two different methodologies are going to presented one “direct” calculation of the damping and one “indirect”.

Direct Calculation:

To quantify the damping that is occurred due to the cycling loading a damping ratio is defined by the ratio of the energy that dissipates to the maximum elastic energy that is stored in the system as the figure 6.2 below shows.

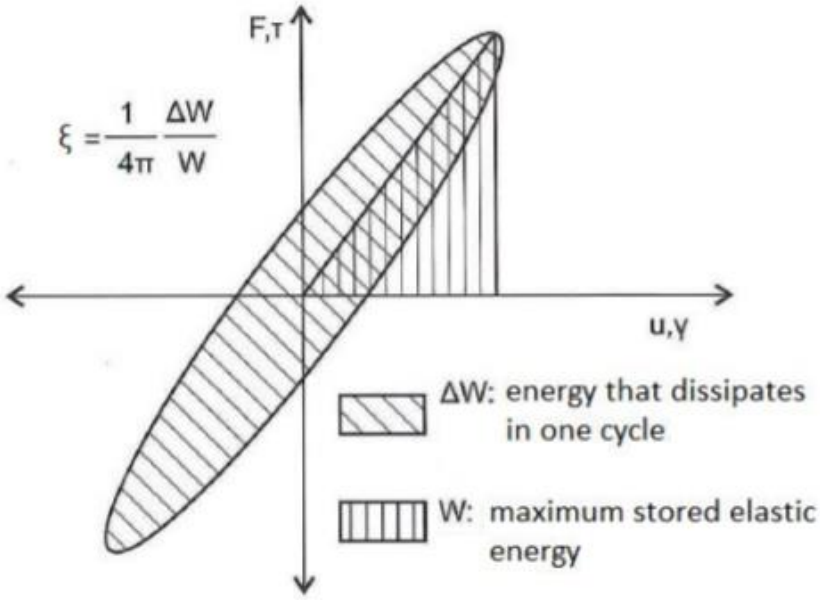

Fig. 6.2 Types of energy and direct way for computing the damping coefficient ξ.

The areas of the loop (ΔW) will be computed with the column method, for one of the last cycles of the excitation, for the purpose of reaching steady state in the problem. While the maximum stored elastic energy will be computed according to the following formula $W = \frac{1}{2} P_{max} d_{max}$ for the same cycle. The damping ratio is going to be calculated with the use of the formula seen in the above figure (6.2) ($\xi = \frac{1}{4\pi} \frac{\Delta W}{W}$)

Indirect calculation:

The second methodology is based on the impedance of the pile in the lateral direction. As we know the dynamic impedance of a pile can be expressed in the following form:

$$\left[\acute{K}\right] = K + i\ \omega\ C$$

Which means that the damping (C) can be expressed as,

$$C = \sqrt{\frac{\left[\acute{K}\right]^2 - K^2}{\omega^2}}$$

Now considering computing the impedance and the stiffness, the P-d diagram is used. For the case of the impedance, $\left[\acute{K}\right]$,the value is computed by dividing the maximum force of the cycle

to the corresponding deformation (meaning the tangent stiffness for the maximum force). Whereas the stiffness K , is equal to the tangent modulus for the maximum deformation (dmax), over the corresponding force for that deformation.

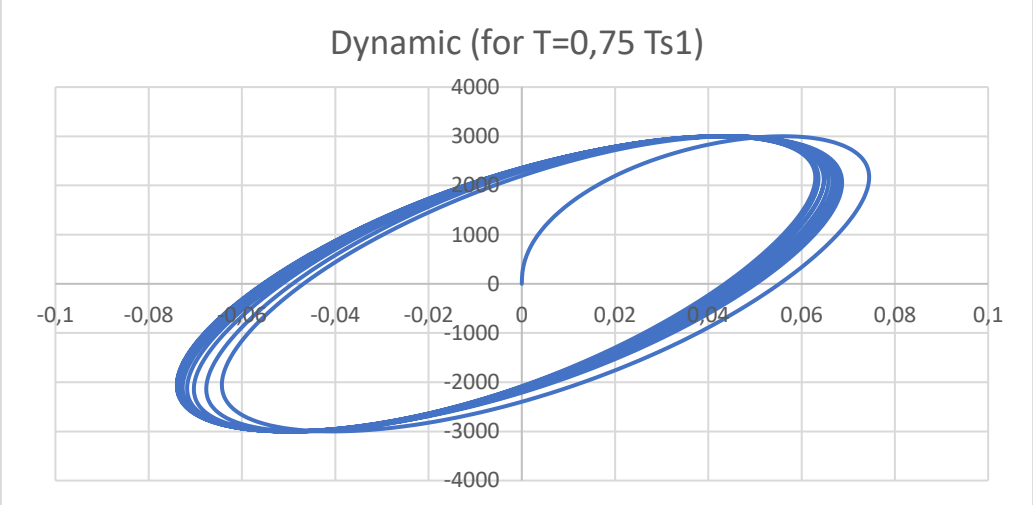

Fig. 6.3 Hysteric loop for the Case that the resonance ratio is 0.75

Direct calculation:

C	**ξ**		
4633,540731	**0,580104226**		
In-direct calcualtion:			
[K]	K	**C**	**ξ**
43693,56248	29359,09674	**4401,929068**	**0,5511072**

Table 6.1 Damping results for the first case , in terms of C and ξ.

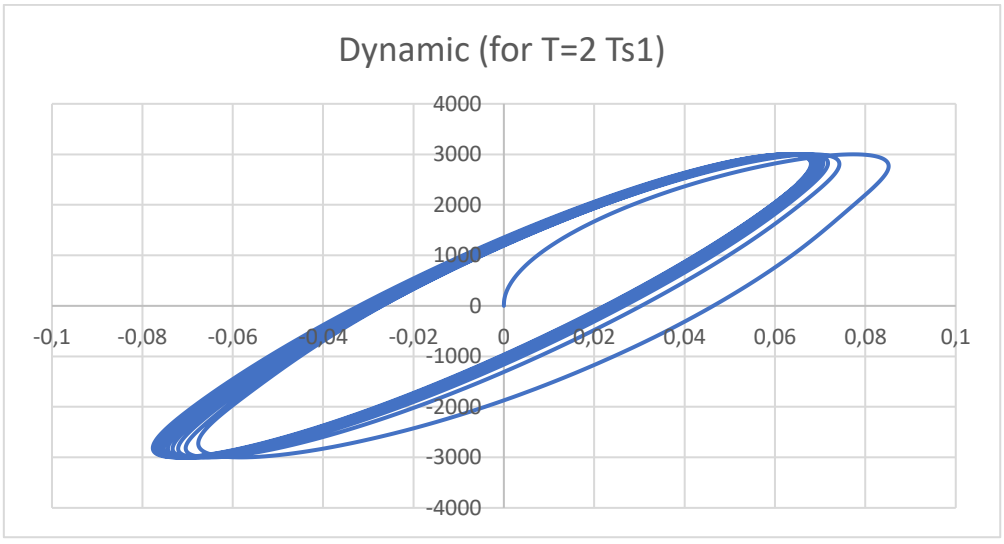

Fig. 6.4 Hysteric loop for the Case that the resonance ratio is

Direct calculation			
C	**ξ**		
6248,187448	**0,213577315**		
In-direct calcualtion:			
[K]	K	**C**	**ξ**
44057,39666	41358,16992	**5370,266205**	**0,183567963**

Table 6.2 T Damping results for the second case , in terms of C and ξ.

As it was expected the damping ratio in the first case is much higher than the one in the second case, which means that the constitutive model takes into account the cut-off frequency and the radiation damping correctly.

6.2 Linear- Dynamic analyses

To validate the finite element model that was created, a number of linear analyses were conducted and then the results were compared with expressions from the literature that were presented in chapter 1.

The geometric features of the model that was tested can be seen in Figure (4.1). A pile of twenty-meter length with diameter of one meter and Pile's Young modulus equal to 30 GPa. The cases that were carried out in terms of soil-properties are the following:

	L/d	**H_1/L**	**V_2/V_1**	**E_p/E_{s1}**
1	20	0,67	2	5000
2	20	0,33	8	5000
3	20	0,67	8	5000

Table 6.3: The soil-properties of the cases examined

The results of the analyses are presented below compared with the values from analytical solutions from the literature.

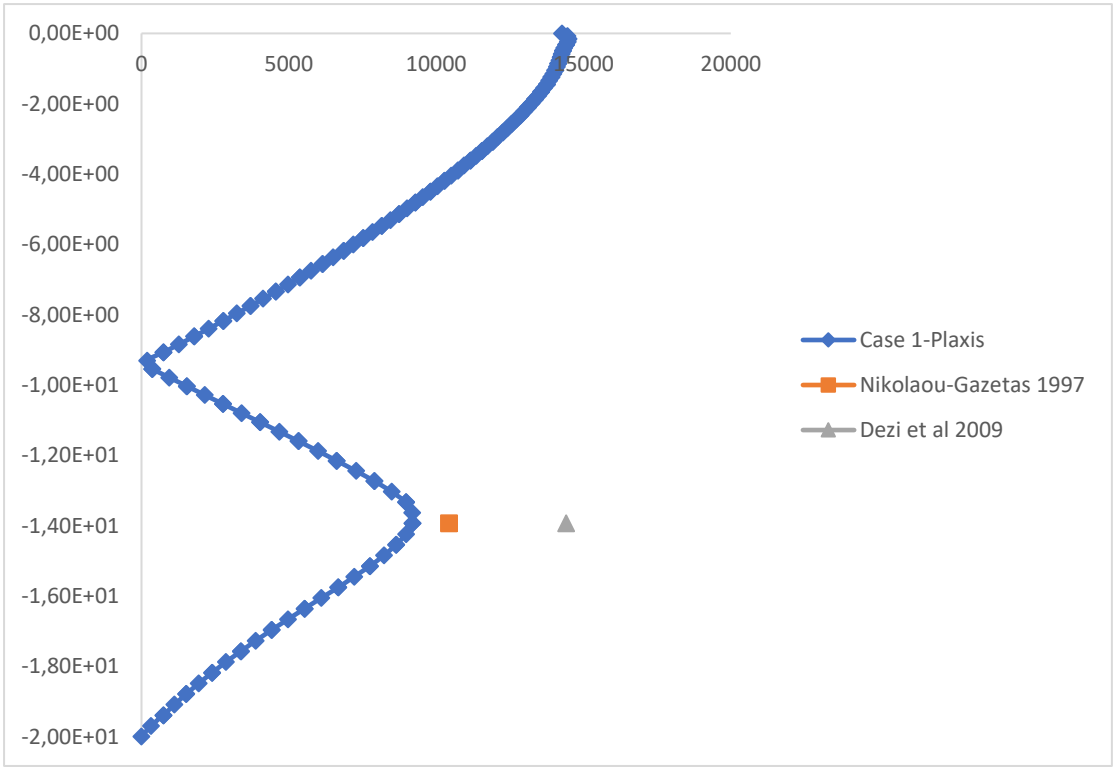

Fig. 6.5: Results of the analysis of case 1 compared with analytical solutions

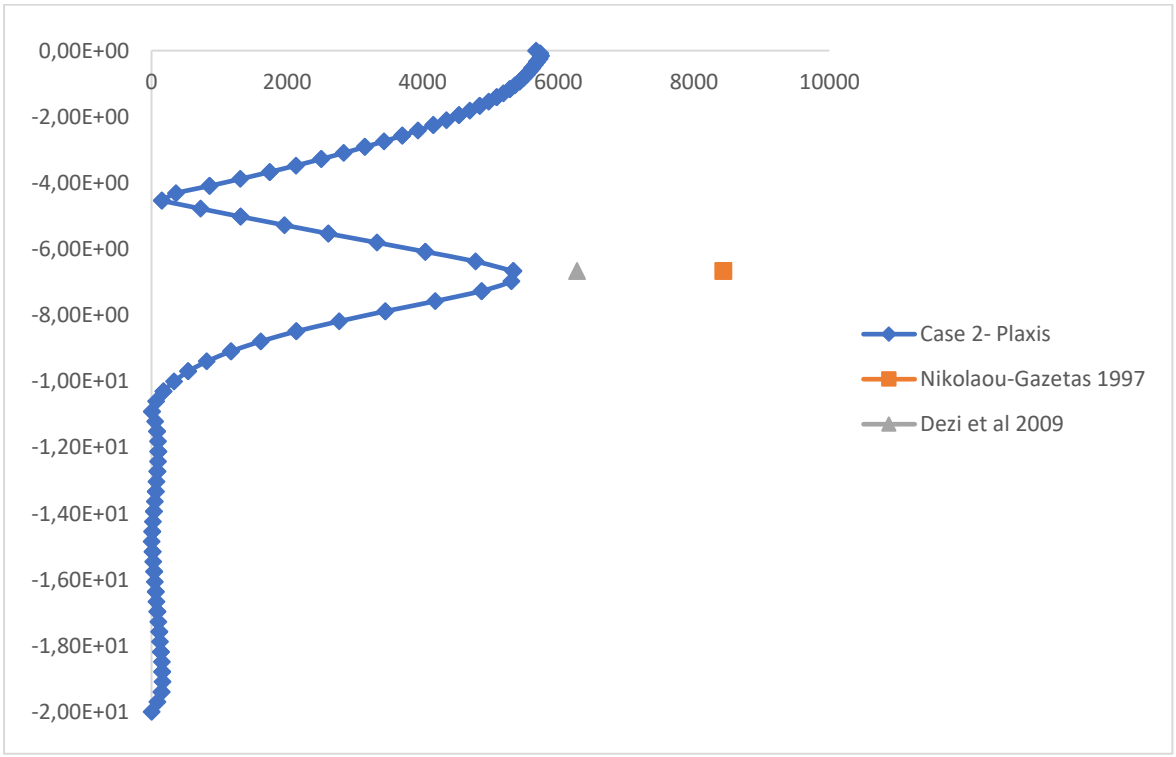

Fig 6.6: Results of the analysis of case 2 compared with analytical solutions

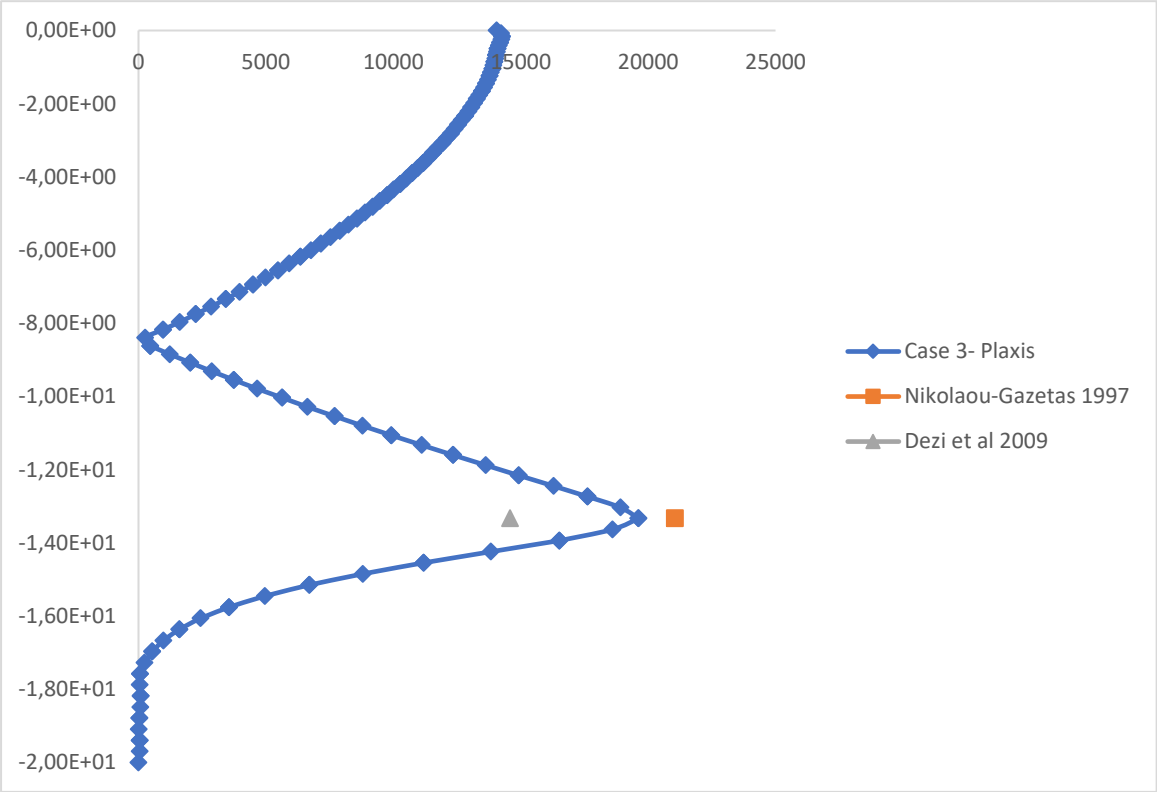

Fig. 6.7: Results of the analysis of case 3 compared with analytical solutions

The discrepancies between the results and the analytical expressions are the following:

Case	Deviations (%)	
	Nikolaou-Gazetas	Dezi et al
1	36,15	11,84
2	36,72	15
3	7,28	-21,60

Table 6.4: Deviations between results of the simulation model and analytical expressions

The mean error between the expressions and the results is 14% meaning that the simulation model that was created is valid for the subject that is researched.

7. Non-Linear analyses with sinusoidal motion

7.1 Introduction

In this chapter the motion of the pile in the case of harmonic excitation at the base of the model is tested accounting as well soil-nonlinearities. The scope is to research how the non-linearity of the soil affects the bending of the pile in the terms of bending moments. These conditions represent the real problem more accurately, than assuming linear-elastic soil, especially in the cases of dynamic loadings where the strains are significantly big. As it was addressed in chapter 5, 60 non-linear analyses were conducted, generated with the use of the Haltonset function (see chapter 2). The purpose of these analyses is to firstly understand the mechanisms that govern the case of kinematic loadings in non-linear soil and the differences with the linear case and secondly to derive a closed-form expression that can be used easily in practice, giving an accurate estimation of the bending moments in the critical points of the pile (head and interface).

Numerical Model

The geometry of the numerical model that is used is the same with the one used in the sensitivity analyses in chapter 4. The dimensions of the model are 70x20 (Length x width) and the depth of the model is a parameter of the problem, meaning it depends on the scenario. On the boundaries of the model dampers were used to neglect wave reflection phenomena.

7.2 Cyclic lateral response of piles

To be able to understand the physics behind kinematic loading on piles, the cyclic lateral pile response is used, which has been meticulously researched by many. One of the first thorough studies on the lateral response of cyclically loaded piles was carried out by Poulos (1982). According to this study, there are two phenomena that may contribute to the increased deflection of lateral loaded piles with increasing number of cycles:

1) Structural “Shakedown” of the pile-soil system. This phenomenon occurs on every pile embedded in elastoplastic soil mass whose properties remain unaltered. When the accumulated permanent deformations stabilize “shakedown” will occur, otherwise, Incremental collapse will result.
2) Soil stiffness decay, degradation

Generally, during cyclic loading its observed that both deflection and moment increase with increasing number of cycles and load magnitude, the ultimate lateral load capacity decreases with increasing number of cycles and load magnitude, the location of the plastic hinge moved deeper when the pile is subjected to fully cyclic loading, due to soil stiffness degradation and effects of soil degradation are more severe for stiff than for soft soils.

Another detailed study is the one of Giannakos, Gerolymos, Gazetas 2012. In this paper the

authors tried to investigate the parameters that affect the shakedown effect in the case of pile comparing it with three centrifuge experiments. The follow observations are worthy of note:

- The maximum bending moments increase with the number of cycles and shifts to greater depths, following the progressive extension of soil yielding. The plastic shakedown effect is reflected by the gradually developing fan shaped stress bulb, the frontal part of which represents the mobilized soil mass that is in a passive state and expands with increasing cycles of loading while the trailing part corresponds to the mobilized soil zone that is in an active state and shrink with increasing number of cycles. The larger the bulb of the passive stresses the greater the soil reaction that resist the applied load when finally, the pile reaches a steady state equilibrium of constant plastic strain (plastic shakedown).

- Soil material densification played a minor role in the pile's motion. Comparing the centrifuge test's results and the FEM results the discrepancies are insignificant, even though the constitutive model that was used didn't consider soil densification.

- Upon unloading and for zero lateral force the bending moments and shear forces are not zero. Instead they retain large values comparable to those for the maximum applied load, meaning there is a moment due to residual deformations in the regions of the pile with vast deformations. Notice that in the case of a linear soil all the aforementioned quantities would vanish to zero, as soil elasticity would act as a restoring force for the pile.

- Conclusively, the system densification is the reallocation of reaction forces along the pile for each cycle due to expansion of the bulb of the passive forces. On each cycle a bigger volume of soil is energized, due to soil hardening, enlarging the bulb until an equilibrium state is reached. (steady-state)

7.3 Dynamic analyses

The cases that were examined for this study are shown in the following table. How the table was obtained has been seen in chapter 5.

	$\gamma 1$	A_{rock}	d	L	H_1	V_{s2}	V_{s1}	N	T_{inp}/T_{s1}
1	13	0,1	0,6	15	5	800	400	6	1
2	20	0,1	1,5	20	6,667	800	533,328	6	1
3	17	0,25	0,6	20	10	800	533,328	6	1
4	23	0,4	1	30	15	800	533,328	6	1
5	13	0,6	1,5	30	15	400	80	11	1
6	20	0,1	0,6	15	7,5	400	80	11	1,333333

7	17	0,25	1	15	10	400	80	11	1,333333
8	23	0,25	1,51,5	15	10	400	133,32	11	1,333333
9	13	0,4	0,6	20	13,33	600	199,98	11	1,333333
10	20	0,6	1	20	13,33	600	199,98	11	1,5
11	17	0,1	1,5	30	10	600	300	15	1,5
12	23	0,25	0,6	30	10	600	300	15	1,5
13	13	0,4	1	15	5	600	300	15	1,5
14	20	0,4	1,5	15	7,5	800	400	15	1,5
15	17	0,6	0,6	15	7,5	800	533,328	15	0,75
16	23	0,1	1	20	10	800	533,328	3	0,75
17	13	0,25	1,5	20	10	800	533,328	3	0,75
18	20	0,4	0,6	30	20	400	80	3	0,75
19	17	0,6	1	30	20	400	80	3	0,75
20	23	0,6	1,5	15	10	400	80	3	1
21	13	0,1	0,6	15	10	400	133,32	3	1
22	20	0,25	1	20	6,667	600	199,98	6	1
23	17	0,4	1,5	20	6,667	600	199,98	6	1
24	23	0,6	0,6	20	6,667	600	300	6	1
25	13	0,6	1	30	10	600	300	6	1,333333
26	20	0,1	1,5	30	15	800	400	6	1,333333
27	17	0,1	0,6	15	7,5	800	400	6	1,333333
28	23	0,25	1	15	7,5	800	533,328	11	1,333333
29	13	0,4	1,5	20	10	800	533,328	11	1,5
30	20	0,6	0,6	20	13,33	800	533,328	11	1,5
31	17	0,1	1	20	13,33	400	80	11	1,5
32	23	0,1	1,5	30	20	400	80	11	1,5
33	13	0,25	0,6	30	10	400	80	11	1,5
34	20	0,4	1	15	5	400	133,32	15	0,75
35	17	0,6	1,5	15	5	600	199,98	15	0,75
36	23	0,1	0,6	20	6,667	600	199,98	15	0,75
37	13	0,25	1	20	10	600	300	15	0,75
38	20	0,25	1,5	30	15	600	300	15	0,75
39	17	0,4	0,6	30	15	800	400	3	1
40	23	0,6	1	30	15	800	533,328	3	1
41	13	0,1	1,5	15	10	800	533,328	3	1
42	20	0,25	0,6	15	10	800	533,328	3	1
43	17	0,4	1	20	13,33	800	533,328	3	1
44	23	0,4	1,5	20	6,667	400	80	3	1,333333

45	13	0,6	0,6	30	10	400	80	6	1,333333
46	20	0,1	1	30	10	400	80	6	1,333333
47	17	0,25	1,5	30	10	400	133,32	6	1,333333
48	23	0,4	0,6	15	7,5	600	199,98	6	1,5
49	13	0,6	1	15	7,5	600	199,98	6	1,5
50	20	0,6	1,5	15	7,5	600	300	6	1,5
51	17	0,1	0,6	20	10	600	300	11	1,5
52	23	0,1	1	20	13,33	800	400	11	1,5
53	13	0,25	1,5	30	20	800	533,328	11	0,75
54	20	0,4	0,6	30	20	800	533,328	11	0,75
55	17	0,6	1	15	5	800	533,328	11	0,75
56	23	0,1	1,5	15	5	800	533,328	15	0,75
57	13	0,1	0,6	15	5	400	80	15	0,75
58	20	0,25	1	20	6,667	400	80	15	1
59	17	0,4	1,5	20	10	400	80	15	1
60	23	0,6	0,6	30	15	400	133,32	15	1

Table 7.1: Contains all the analyses that were performed with all their characteristics.

7.3.1 Comparison of elastic with non-linear analyses

For some of the non-linear analyses also elastic were performed in order to see the effect of non-linearity in the case of kinematic loadings. The linear elastic analyses were performed using the same model but with excitations amplitude small enough to sustain elastic behavior for the whole simulation model. Afterwards the results were multiplied by a factor so that the accelerations at the surface of the soil are equal in linear and non-linear. With this alteration the resonance and the soil amplification effects are neglected. This is done so that the results focus in only the non-linear behavior of the soil and how it affects the problem that is studied.

The cases that were studied are going to be presented further down. For each case there will be presented the envelope of bending moments, the Bending Moment time diagrams for the head and the interface as well as the bending moments at the step that the maximum bending moment is reached.

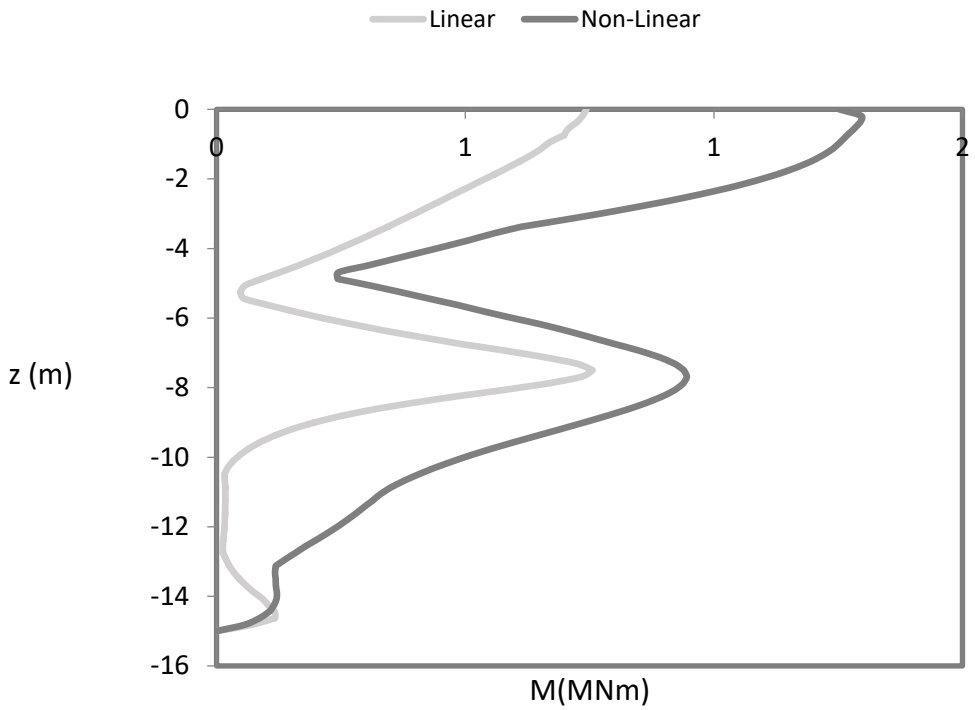

Figure 7.1: Envelope of bending moments for the case 14 for linear and non-linear analyses, dark grey non-linear and grey linear.

Comments: The big differences that appear between the two analyses are a result of the "normalization process" that was performed in order to exclude the soil amplification phenomena and take into account only the soil non-linearities. The 0.4 g at the base is the result of the high deviations. Other than that we can see from figure 7.2-3 the differences in the physics behind the shown bending moments. In the linear case no permanent displacements occur, meaning that the residual part is zero in comparison with the non-linear where we see residual moments for both the head and the interface. Furthermore, the plastic shakedown occurs at the 9^{th} cycle, after that steady state response can be observed.

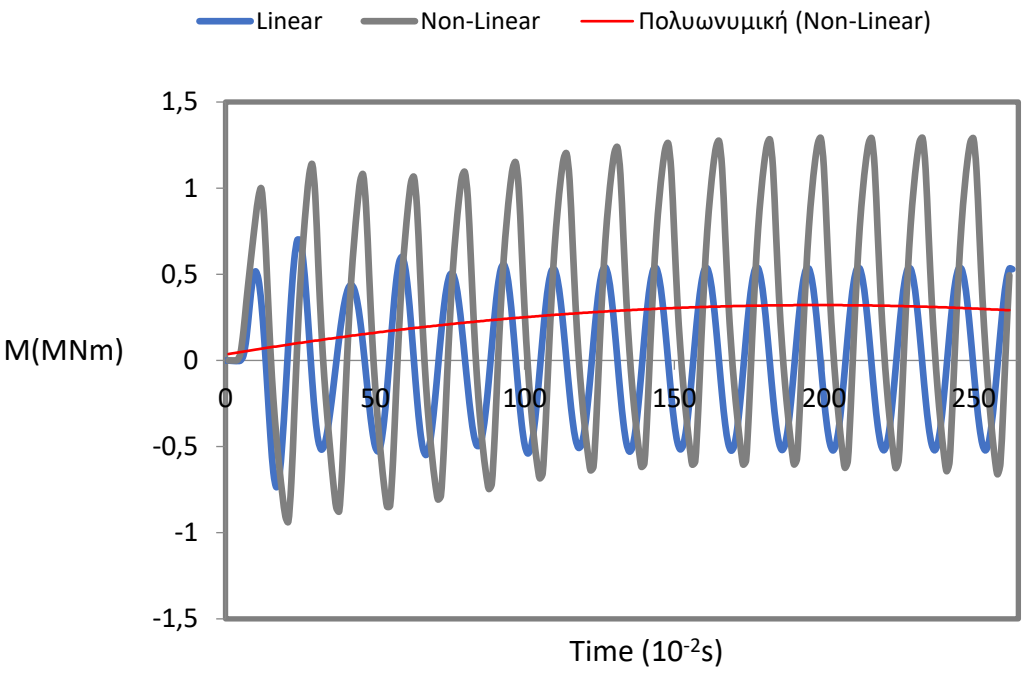

Figure 7.2: Moment – Time graph for the head of the pile in the case 14.

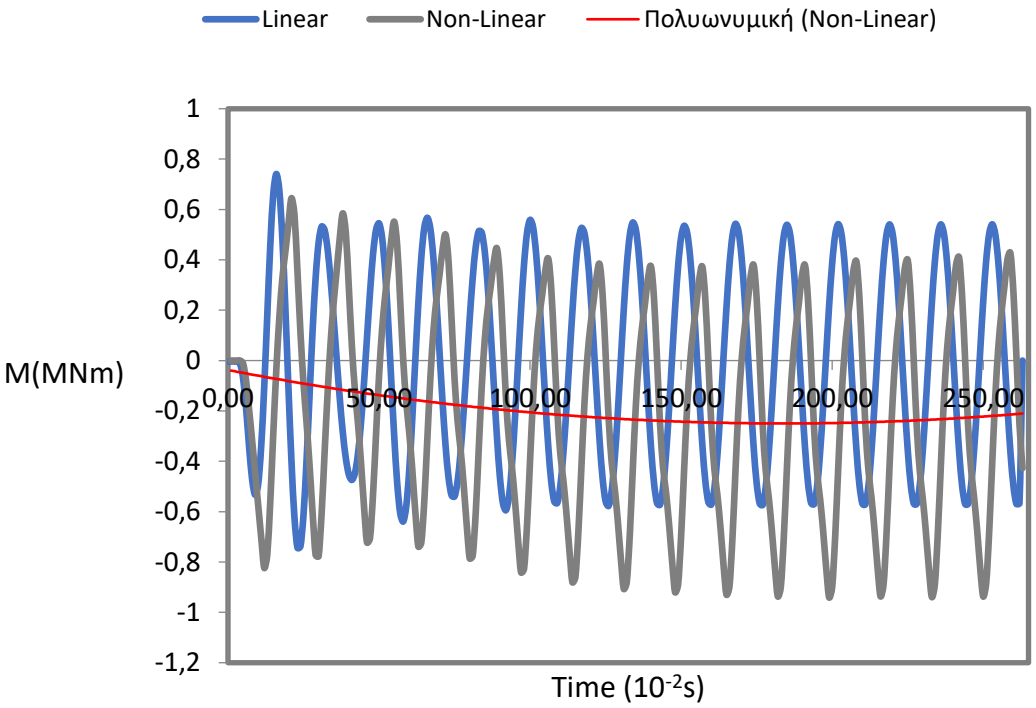

Figure 7.3: Moment – Time graph for the interface of the pile in the case 14.

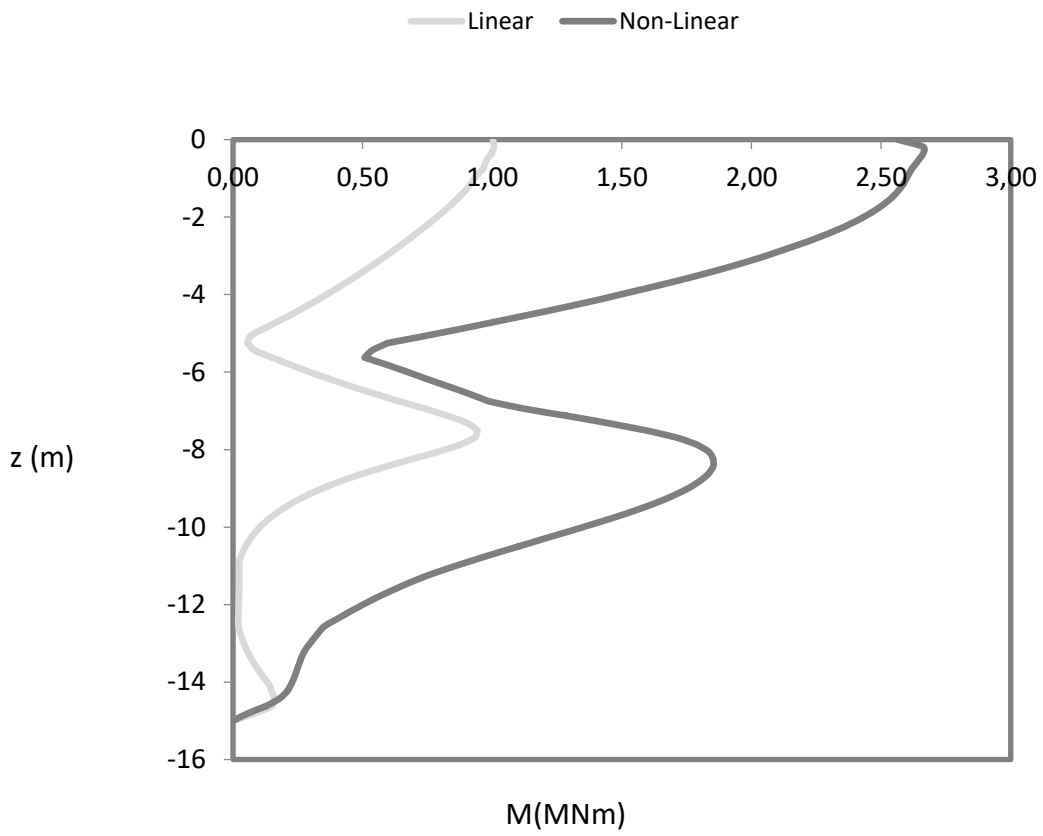

Figure 7.4: Envelope of bending moments for the case 50 for linear and non-linear analyses, dark grey non-linear and grey linear.

Comments: Again huge differences between the linear and the non-linear analyses even bigger than the analysis above. This is the result from the much higher acceleration, in this case at 0.6 g. Also in figure 7.4 we can observe that the maximum interface bending moment is at 8.5 m depth for the non-linear case in comparison with the actual depth of the interface being at 7.5 m. The soil hardening that occurs around the pile at that depth forces the plastic hinge to greater depths but also it widens the interface. No residual moments were observed at the interface or the head even though the excitation was powerful, the shear velocities for the layers were also pretty high at 300 and 600 m/s meaning the soil layers were strong enough to withstand the imposed deformations without having significant permanent displacements.

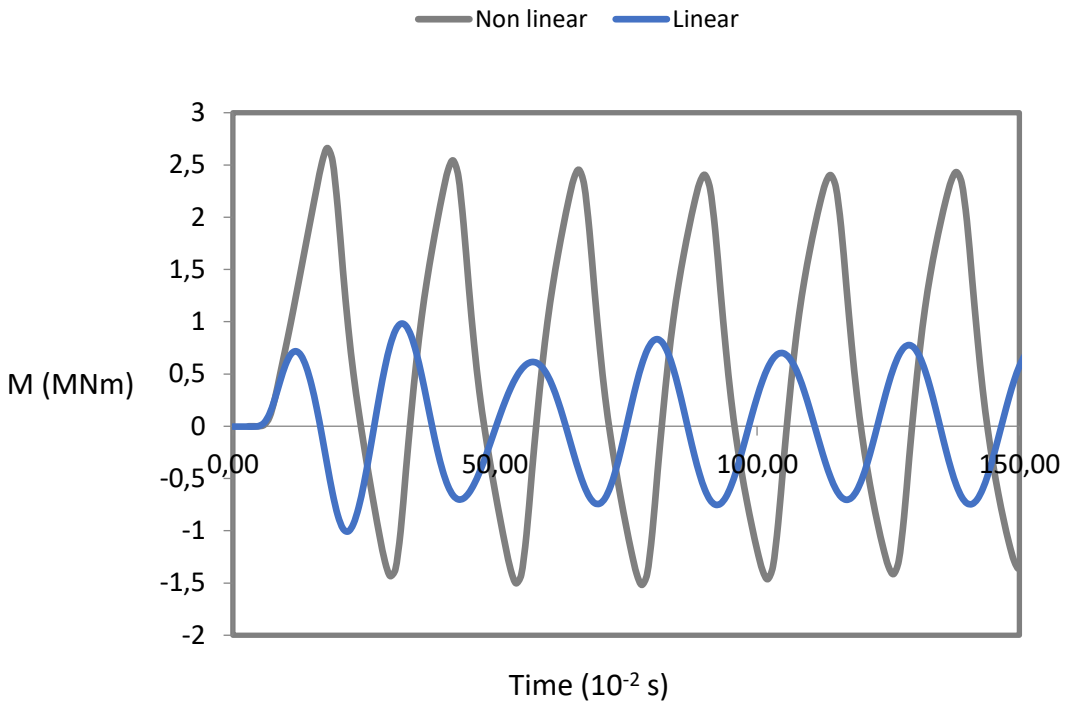

Figure 7.5: Moment – Time step graph for the head in case 50.

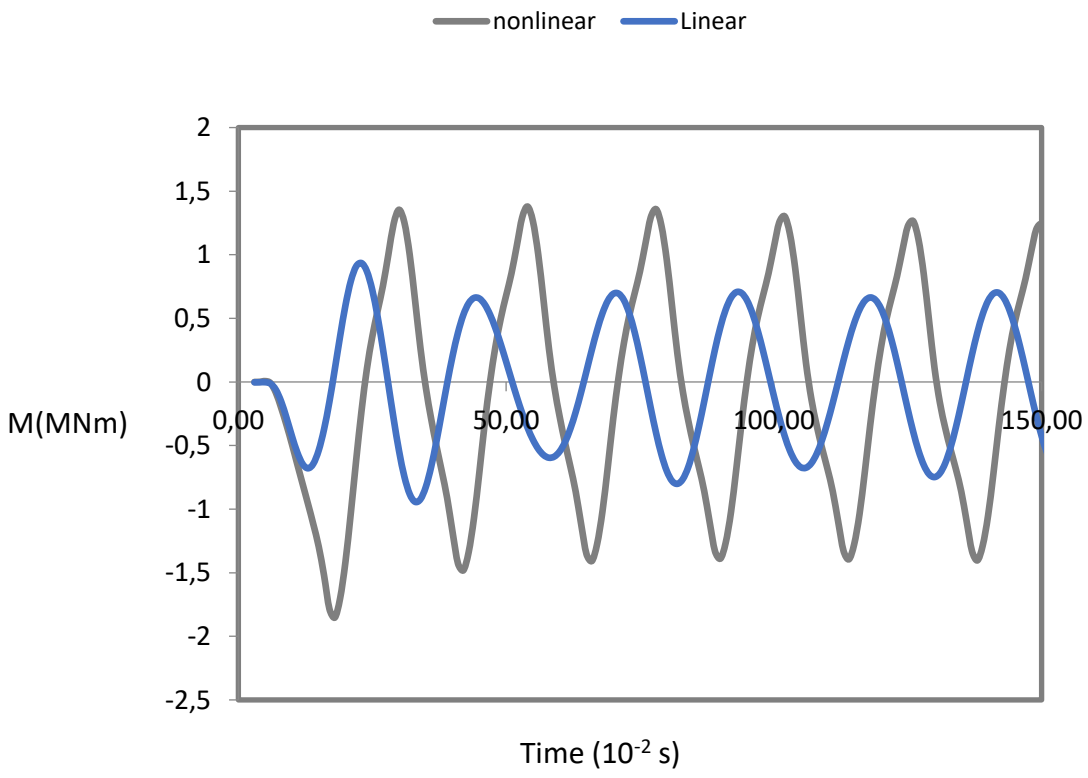

Figure 7.6: Moment - Time graph for the head in case 50.

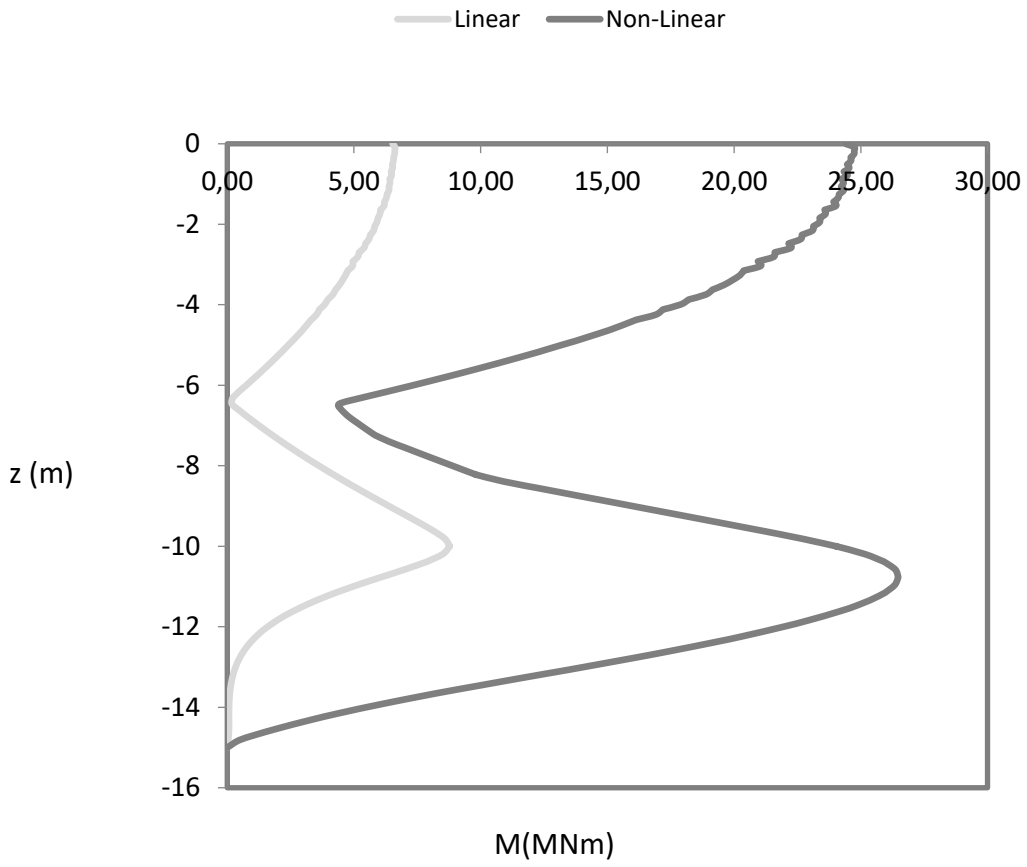

Figure 7.7: Envelope of bending moments for the case 20 for linear and non-linear analyses, dark grey non-linear and grey linear.

Comments: In this analysis the excitation amplitude is also 0.6 g, thus the significant changes between the two. In comparison with the previous case there are three differences: a) bigger shear velocity ratio,5 instead of 2, b) lower shear velocities for both layers V_{s1}=80 m/s and V_{s2}=400 m/s, and c) Lower interface depth, 10m instead of 7.5m . Due to the a) the moment at the interface is greater than the one at the head in this case. The b) difference is responsible for the residual moments that are observed; softer soil can't withstand the deformations without becoming plastic, meaning permanent displacements and therefore residual moments. The deeper interface enhances the displacements, because now a longer part of the pile is embedded in the "softer" soil.

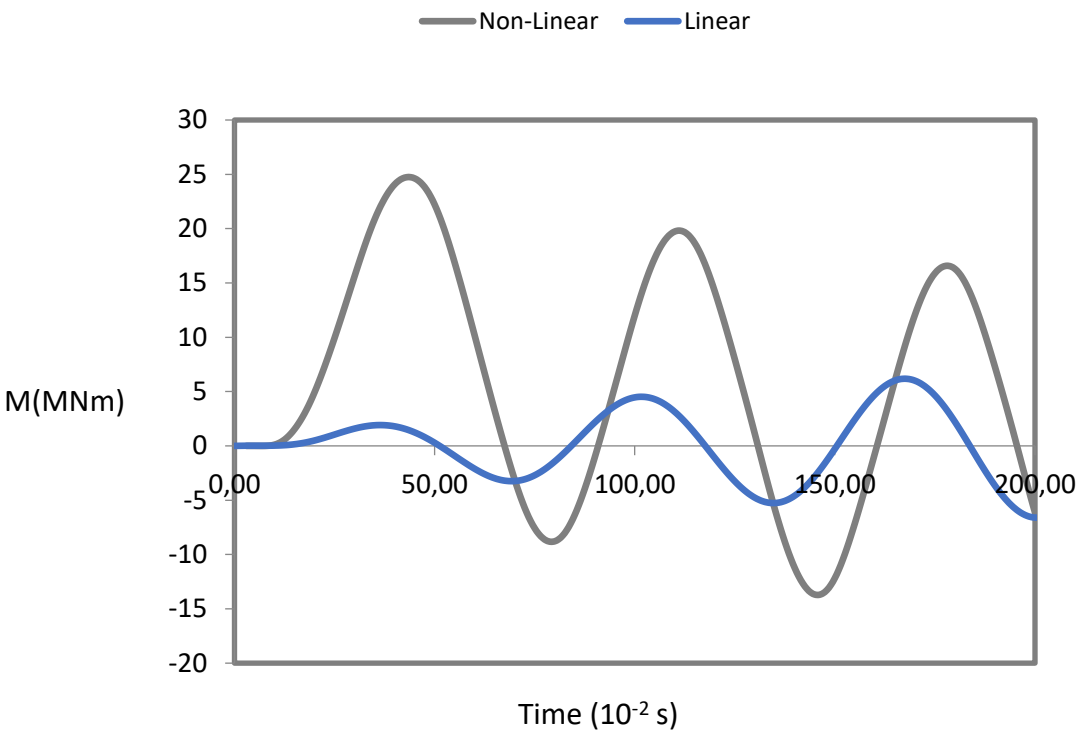

Figure 7.8: Moment - Time graph for the head in the case 20.

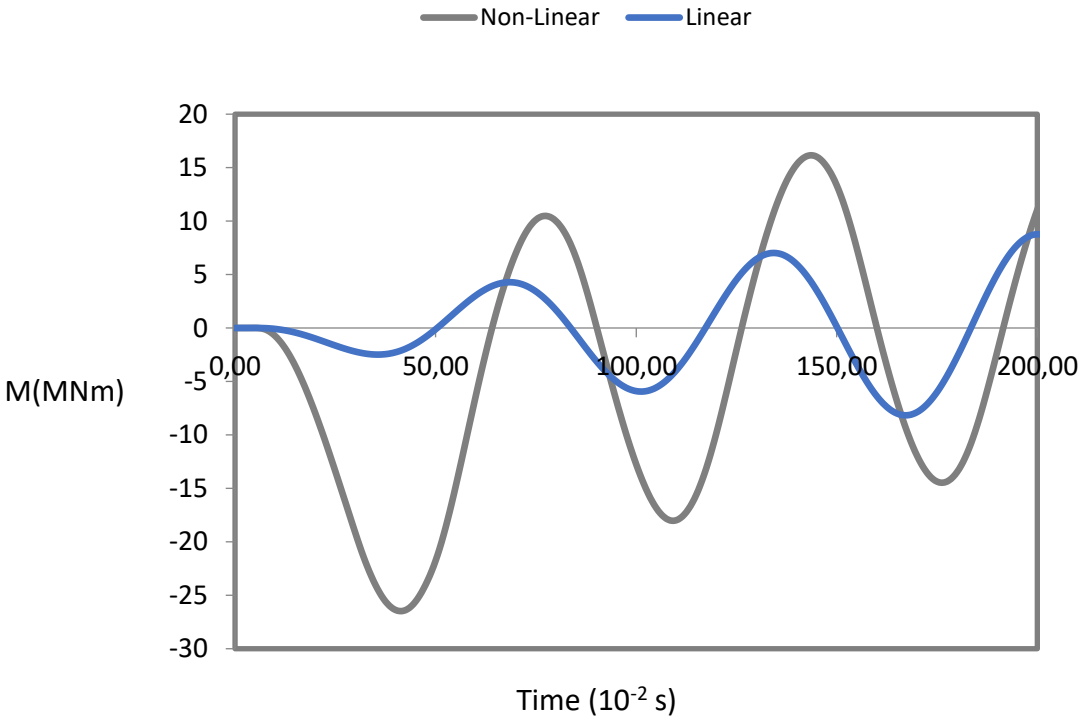

Figure 7.9: Moment - Time graph for the interface in the case 20.

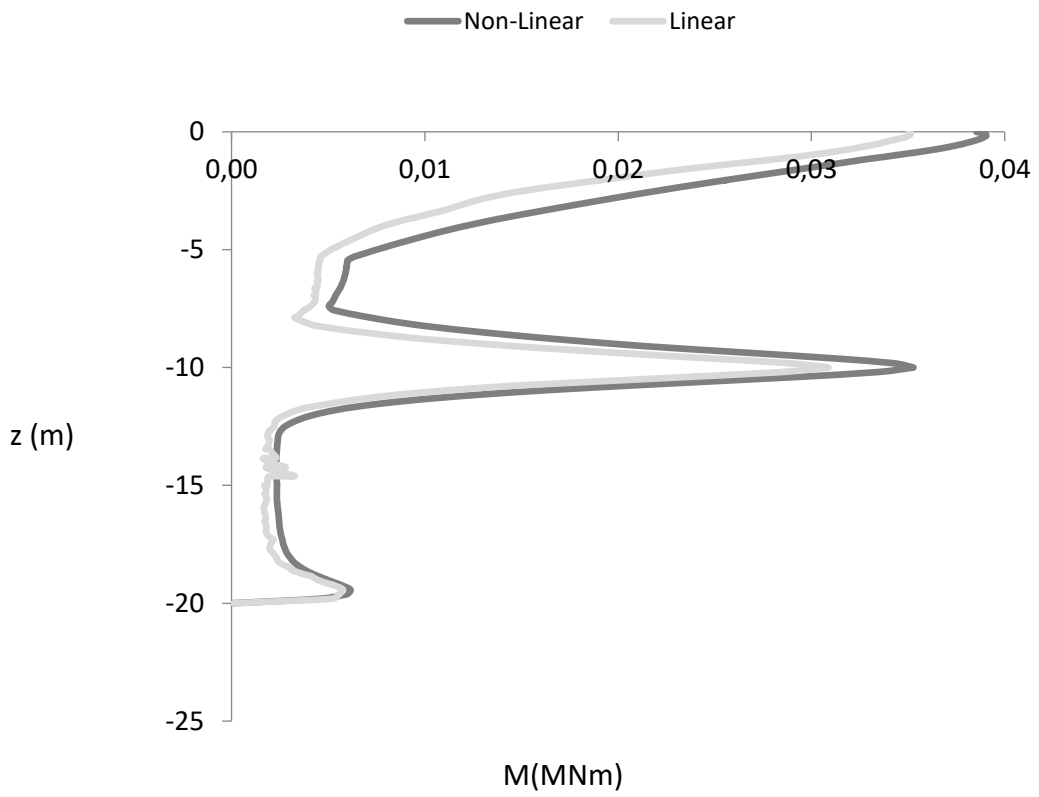

Figure 7.10: Envelope of bending moments for the case 16 for linear and non-linear analyses, dark grey non-linear and grey linear.

Comments: We see that the two analyses are almost identical. This is happening due to the extremely small amplitude of the excitation (0.1 g) which limits soil nonlinearity. for the non-linear case, thus the non-linear effects are not put in action. Also the moment-Time graphs are identical with the linear ones and no signs of residual moments appear.

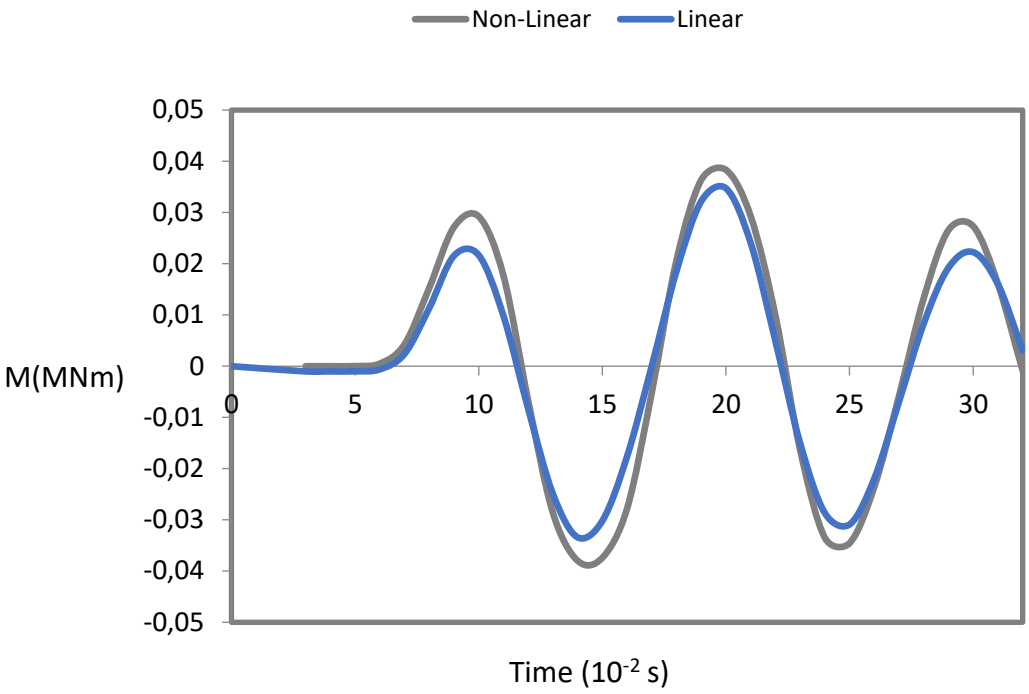

Figure 7.11: Moment - Time graph for the head in the case 16.

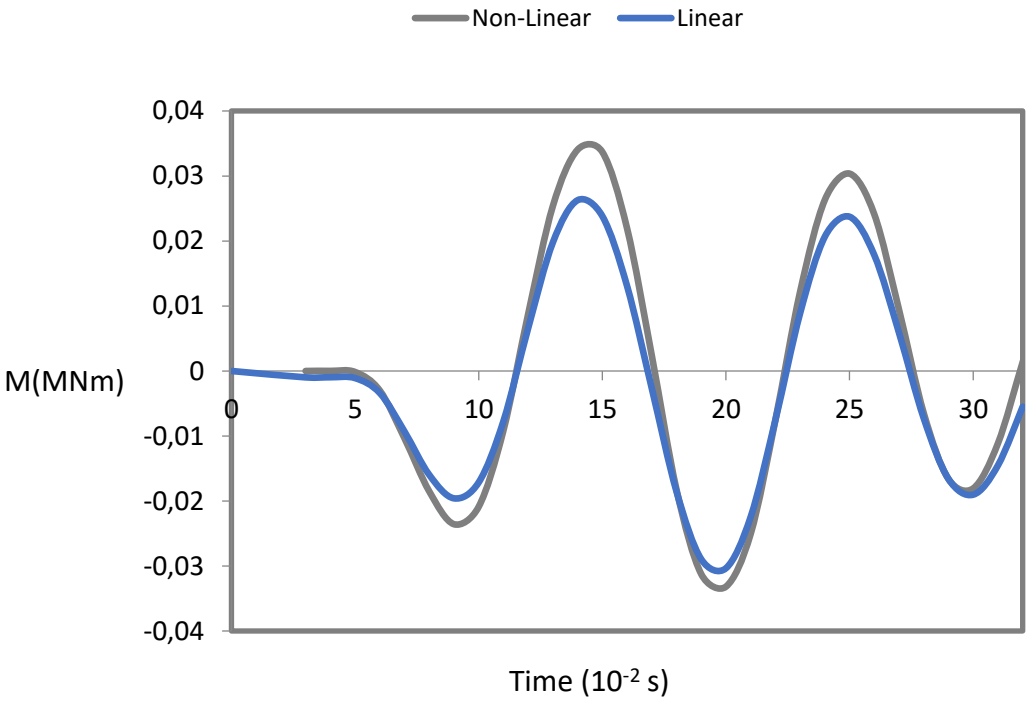

Figure 7.12: Moment- Time graph for the interface in the case 16.

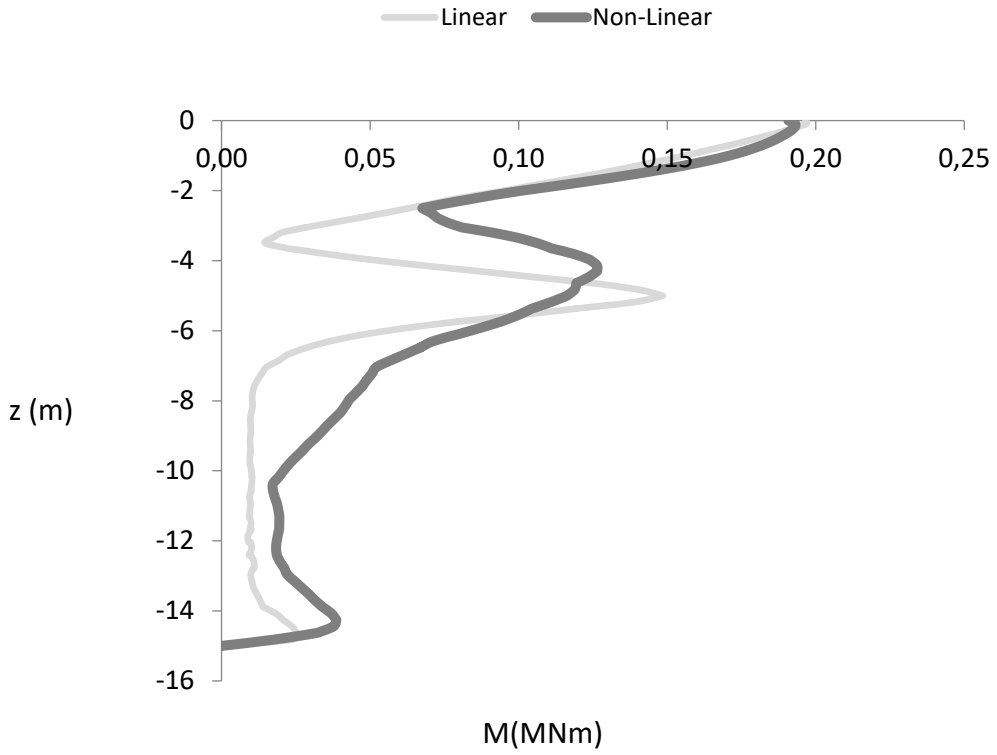

Figure 7.13: : Envelope of bending moments for the case 55 for linear and non-linear analyses, dark grey non-linear and grey linear.

Comments: This case doesn't follow the pattern from the previous ones. It's a strong excitation case with a_{rock}=0.6 g, but with high shear velocities for both layers (V_{s1}=533.33 and V_{s2}=800 m/s). We can see that the linear with the non-linear case are the same for the part of the head of the pile but in the interface the linear reaches higher bending moments. This difference with the above mentioned is that that T_{inp}/T_{s1} is equal with 1,33 meaning that resonance isn't reached for the linear case, thus the amplification phenomena are neglected. Furthermore the interface get wider for the non-linear case and also the M_{int} is smaller.

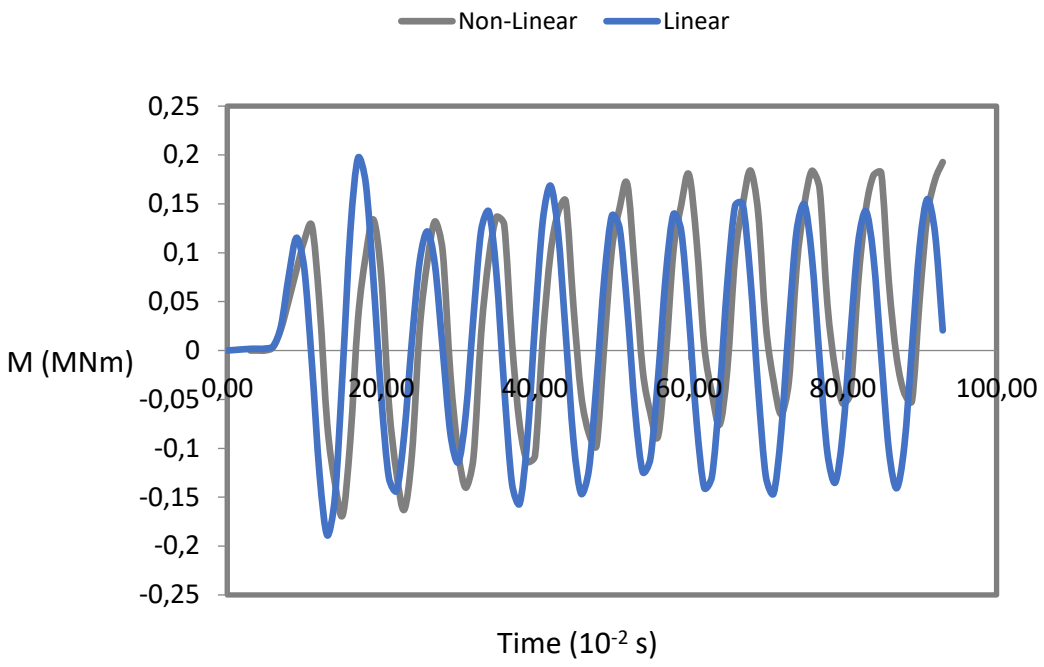

Figure 7.14: Moment- Time graph for the head in the case 55.

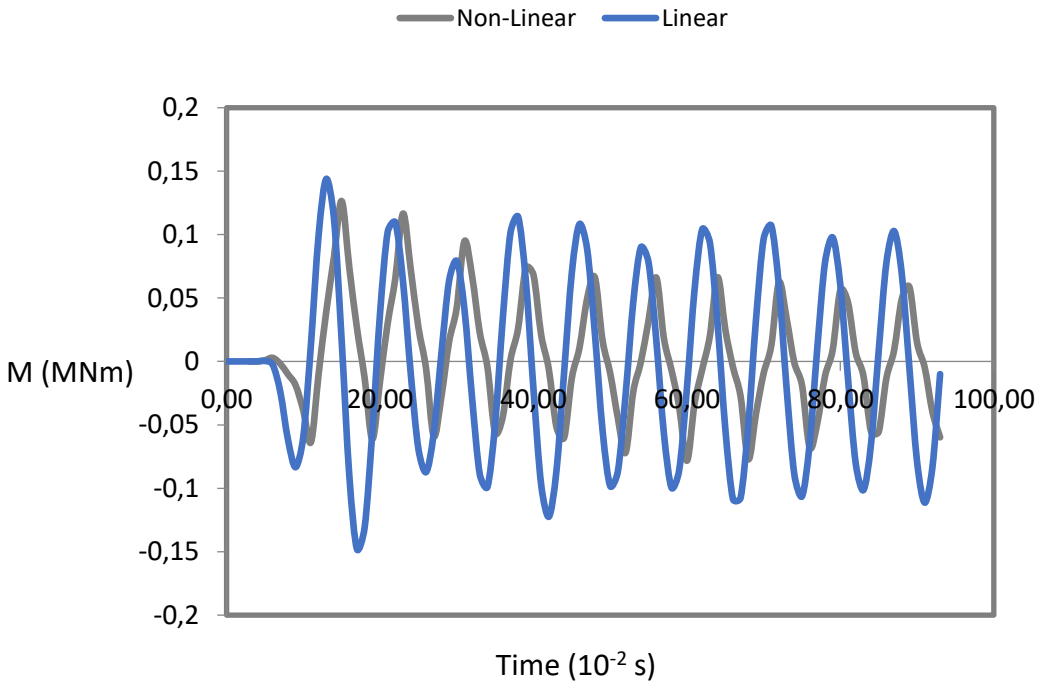

Figure 7.15: Moment- Time graph for the interface in the case 55.

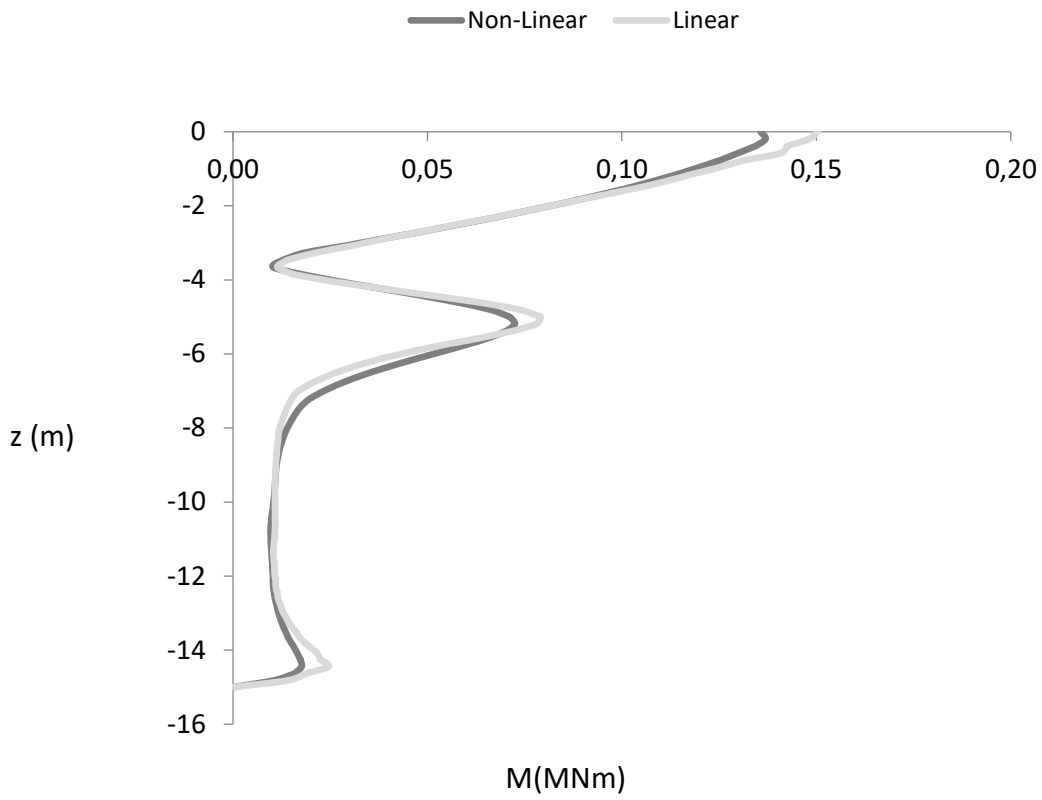

Figure 7.16: : Envelope of bending moments for the case 56 for linear and non-linear analyses, dark grey non-linear and grey linear.

Comments: linear and non-linear are the same here, excitation 0.1 g for the non-linear case, and so the differences are insignificant. This can be seen also in figure 7.17-18 where, the moment-time diagrams are identical.

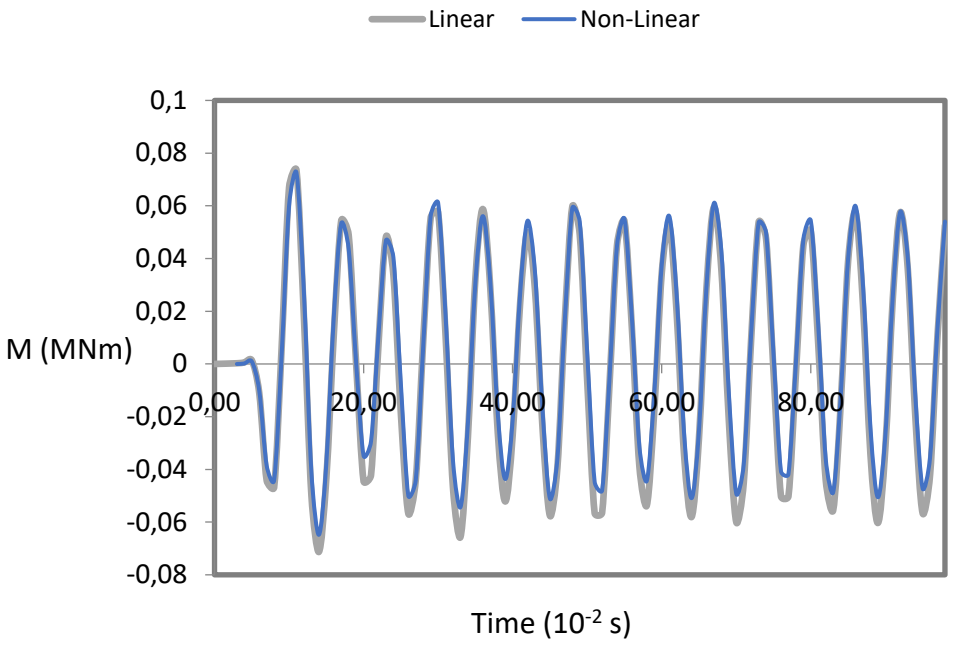

Figure 7.17: Moment – Time graph for the head in the case 56.

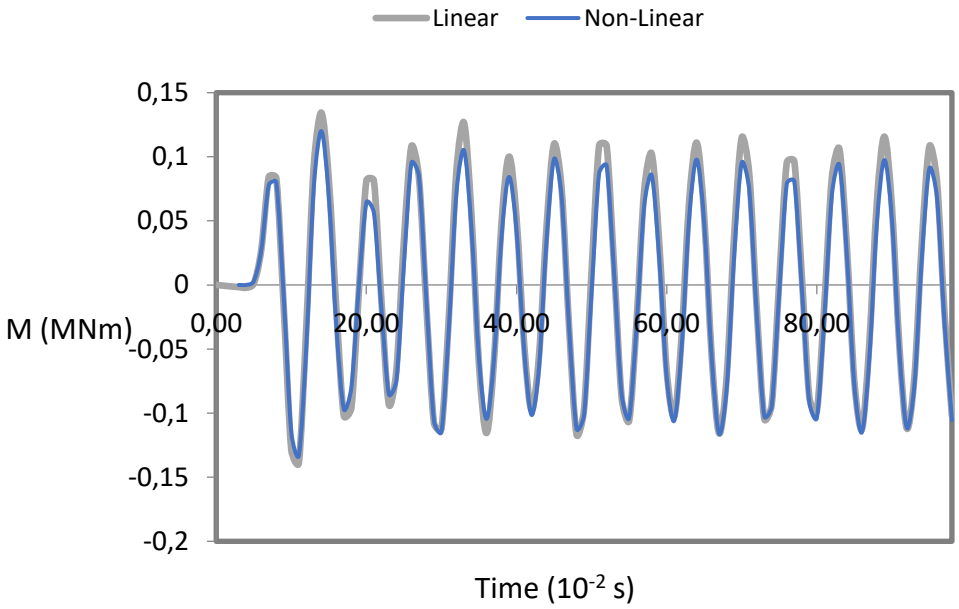

Figure 7.18: Moment – Time graph for the interface case 56.

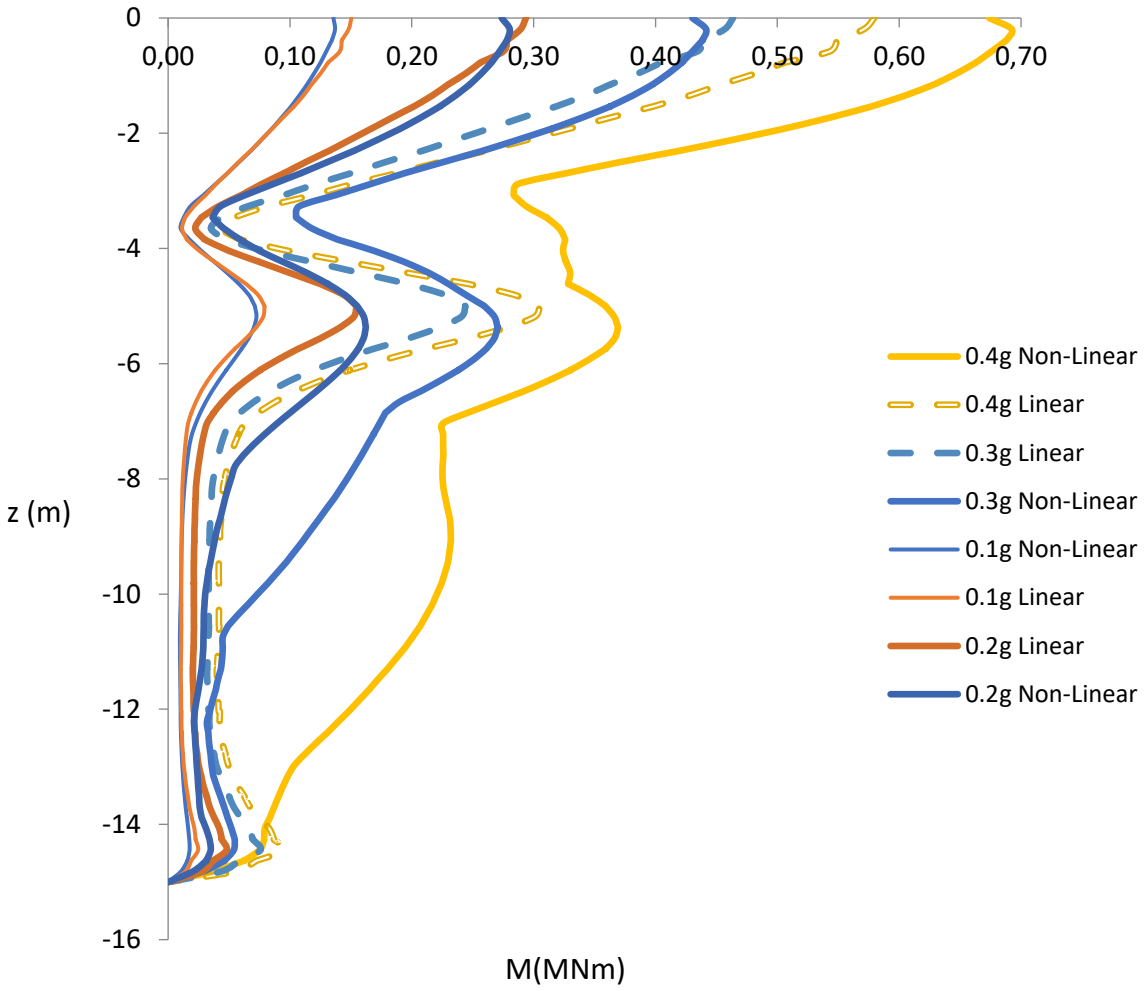

Figure 7.18: : Envelopes of bending moments for the case 56 for linear and non-linear analyses for excitations from 0.1-0.4g. Effect of the amplitude of the excitation to the non-linear behavior of the problem and comparison with the corresponding linear analyses.

Conclusions from the above analyses:

- First, from the last figure 7.18 it is observed that as the amplitude of the excitation increases, the differences between the linear and the non-linear analysis results increase. This can be explained easily if someone thinks about the two main parameters that govern the problem, the relative stiffness ratio (E_p/E_{s1}) and the shear velocity ratio between the two layers. As the amplitude of the excitation increases, both the deformation of the soil and soil yielding increase as well. This accumulation of deformations has as an effect to decrease the soil shear modulus G (G-γ curves) meaning that the E_{s1} in the first parameter will increase also. As the E_p/E_{s1} increases the inflicted bending moments increase, lower relative stiffness ratio means the pile will come stiffer and so more resistant to the deformations inflicted by the surrounding soil. This will be represented as an increase in the bending moments. Now in the same concept with decreasing of E_{s1} also the shear velocity of the upper layer decreases as a square root of that decreases meaning that the shear velocity ratio also increases. This increase means that the moment at the interface will also increase.

- Secondly as the amplitude of the excitation increases the critical area around the interface depth for the bending moments becomes wider. That is a result of the plastic shakedown mechanism. The soil around the pile at the interface depth softens, meaning that for each cycle a bigger volume of soil is needed to counter the forces from the pile to the soil. It is important to notice that, the forces that pile inflicts to the soil is the same but the soil around the pile has lost a part of its strength, meaning that the soil volume energized from the passive forces must be larger.

- Thirdly looking at the resonance ratio (T_{inp}/T_{s1}) for the case of non-linear soil, resonance doesn't exist. The amplification factors in all of the analyses, in which the soil behaved plastic of course, was around 1-2 regardless if the input motion was close to the predominant period of the soil. As it was referred at the start of this semi-chapter the liner analyses were multiplied by a factor so that the acceleration at the surface on the non-linear case is equal to the linear one. That's why in the case 20 (figure 7.7) the deviations between the moments on the two analyses are so high.

- Fourthly, after the excitation due to the plastic behavior of the soil there are permanent deformations on it in the critical regions, meaning the head and the interface. Which means that there are residual moments "left" on the pile even after the end of the dynamic motion. These residual moments can be seen in the figures 7.2 , 7.23 and many more cases. This residual part is a function of the intensity if we

compare the 0.1-0.2-0.3-0.4 g figures (7.18-7.23) as well as number of cycles and soil characteristics.

- Fifth, looking at the Moment-Time graphs we should focus on the following: In order the pile to reach steady-state response a number of cycles is needed. The number of cycles is linked to the excitation amplitude. For example at figure 7.21 the polynomial equation that represents the residual moment becomes constant for N>10 , whereas at figure 7.23 12 cycles are needed to reach steady state.

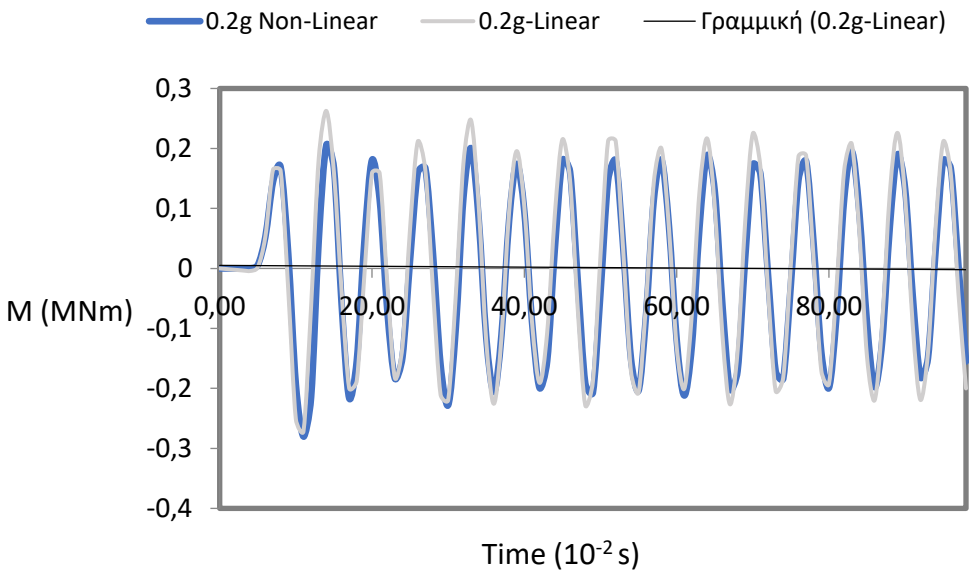

Figure 7.19: Moment - Time graph for the head for case 56 -0.2g.

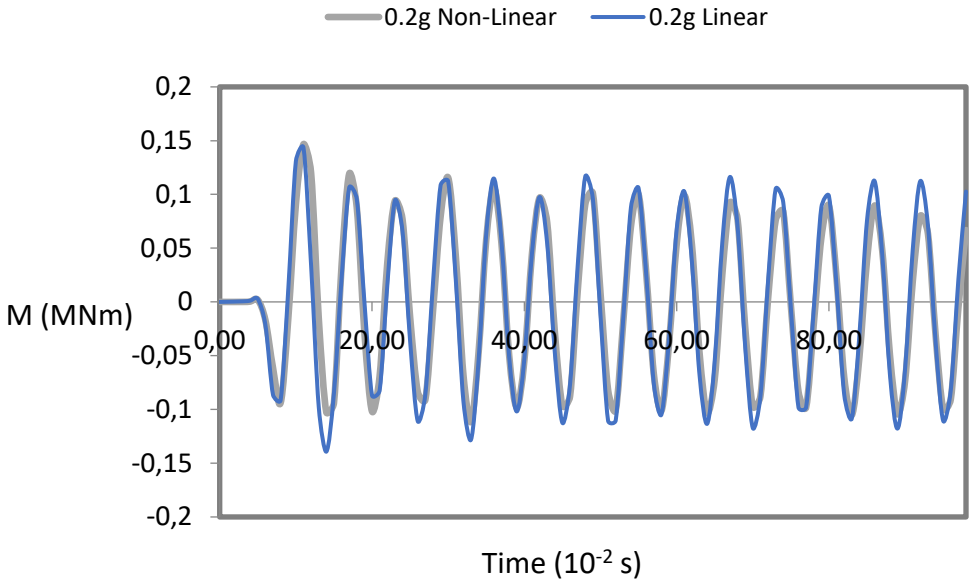

Figure 7.20: Moment - Time graph for the interface for case 56-0.2g.

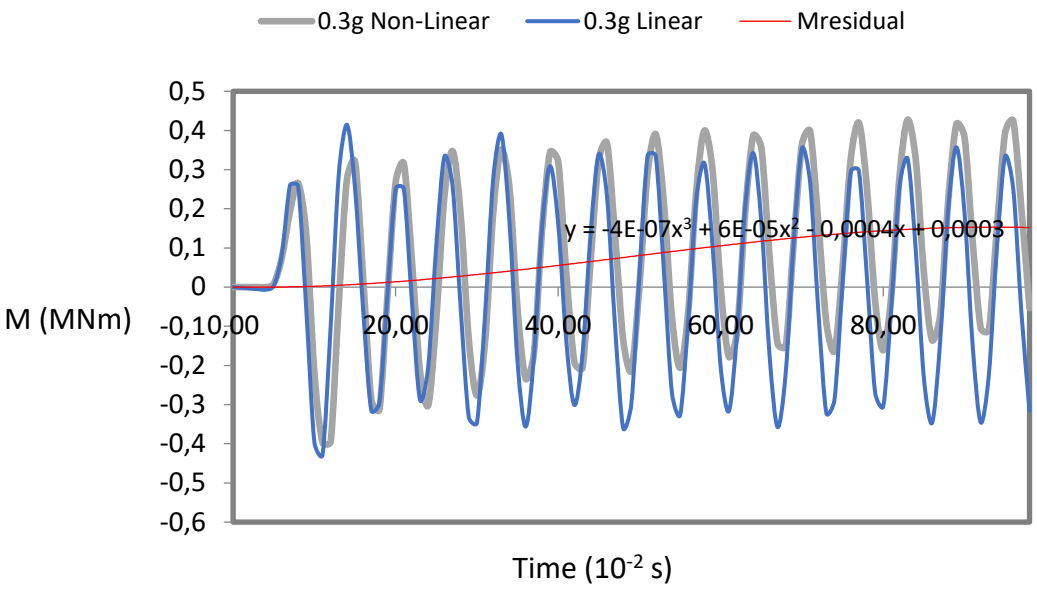

Figure 7.21: Moment - Time graph for the head for case 56-0.3g

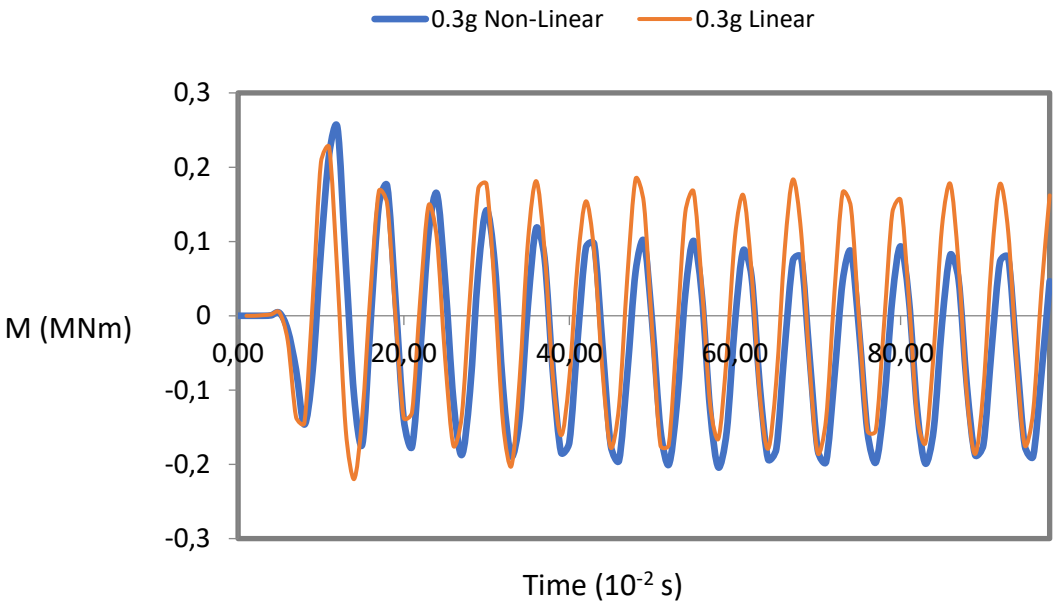

Figure 7.22: Moment –Time graph for the interface for case 56-0.3g.

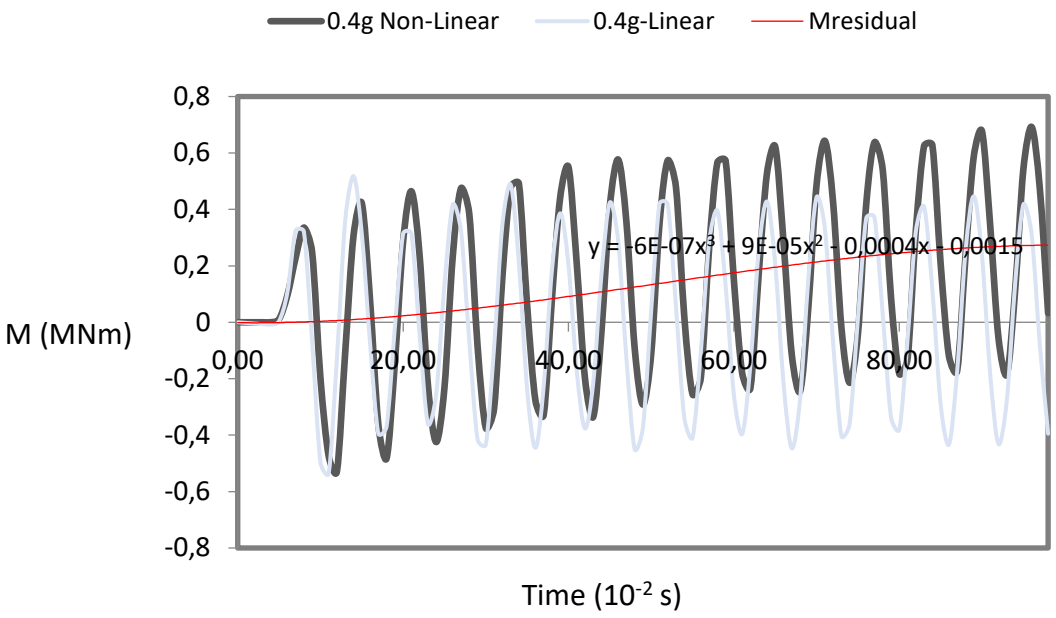

Figure 7.23: Moment- Time graph for the head for case 56-0.4g.

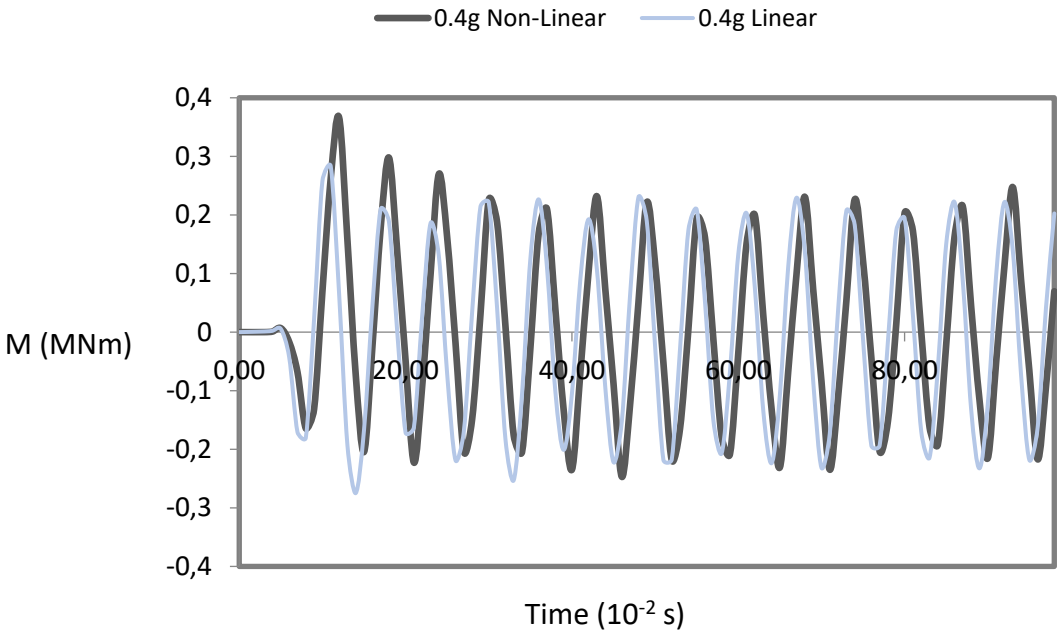

Figure 7.24: Moment – Time graph for the interface for case 56-0.4 g.

7.3.2 Dynamic Analyses

Following are eleven of the sixty analyses, shown in the table 7.1, that were performed. The purpose of them was to derive a close form solution for the bending moments.

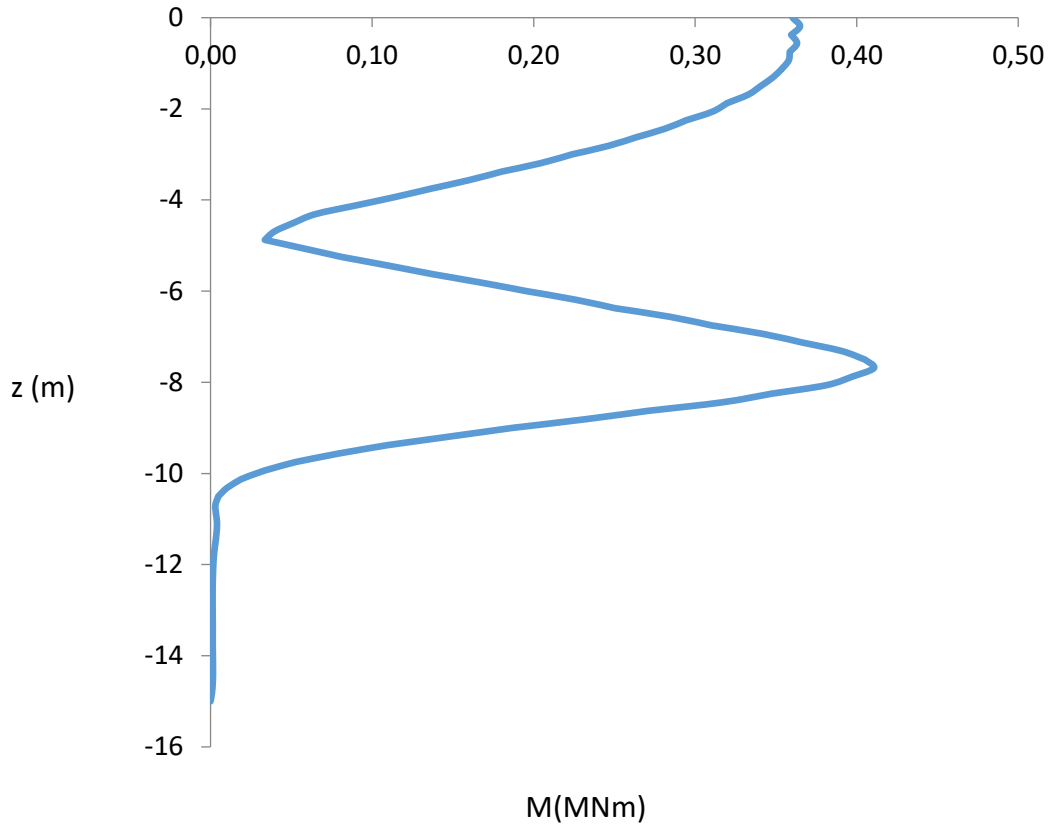

Figure 7.25: Envelope of bending moments for the case 6.

Comments: In this case there is nothing different from the analyses that were shown above. We can see from figure 7.26-27 that even after 11 cycles steady state hasn't been reached especially for the interface. Surprisingly the acceleration at the rock is 0.1g and someone would have thought that the response will be almost linear. But with shear velocities that low for both layers (80 and 400) they enhance the plastic shakedown effect.

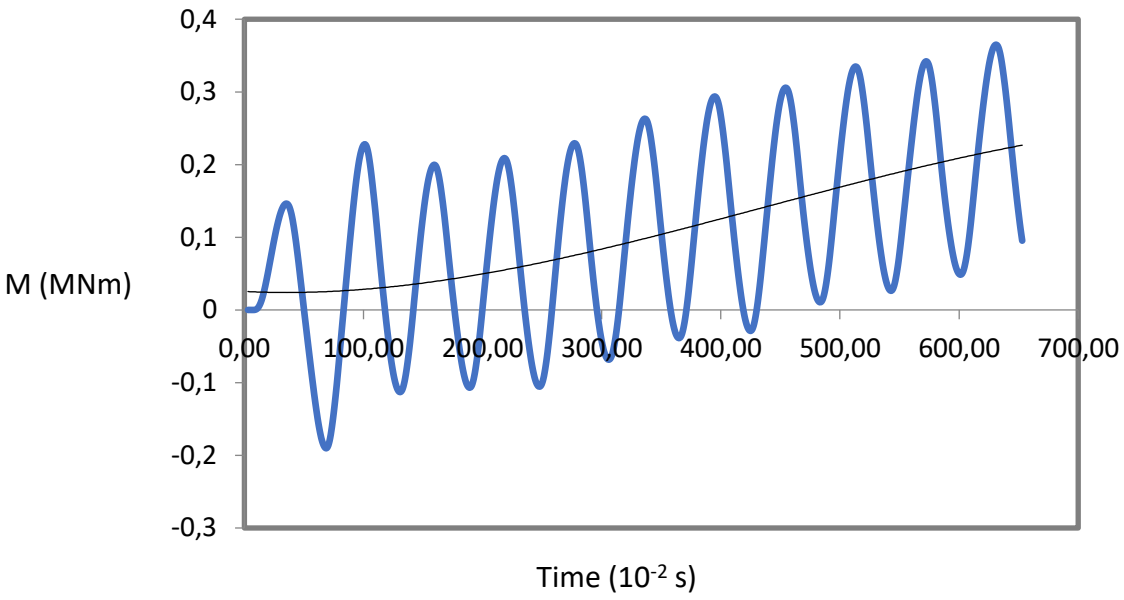

Figure 7.26: Moment - Time graph for the case 6 and the head.

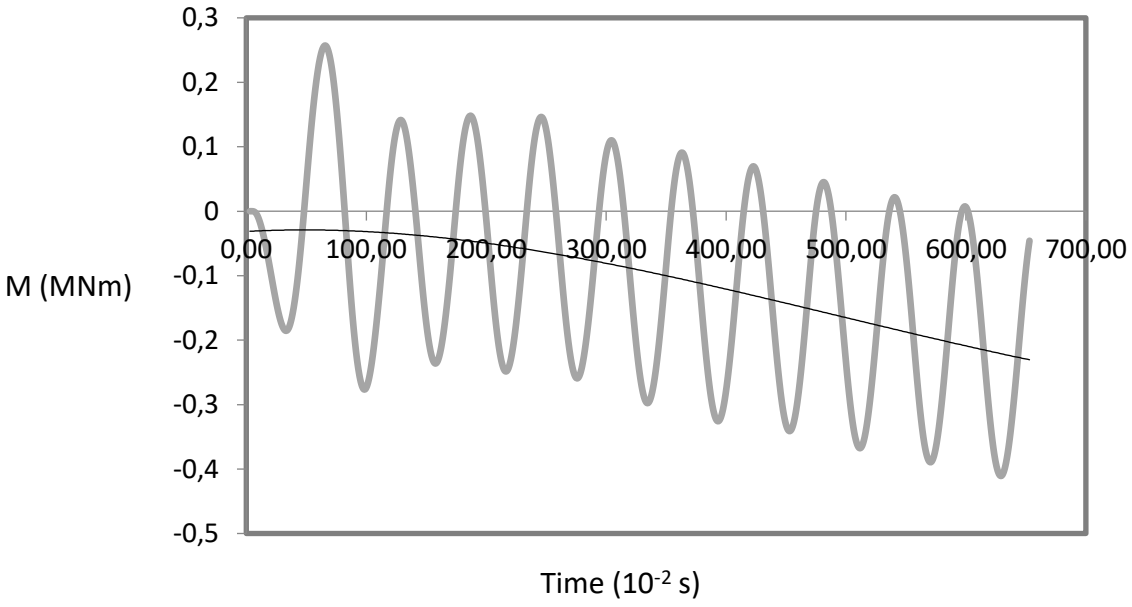

Figure 7.27: Moment- Time graph for the case 6 and the interface.

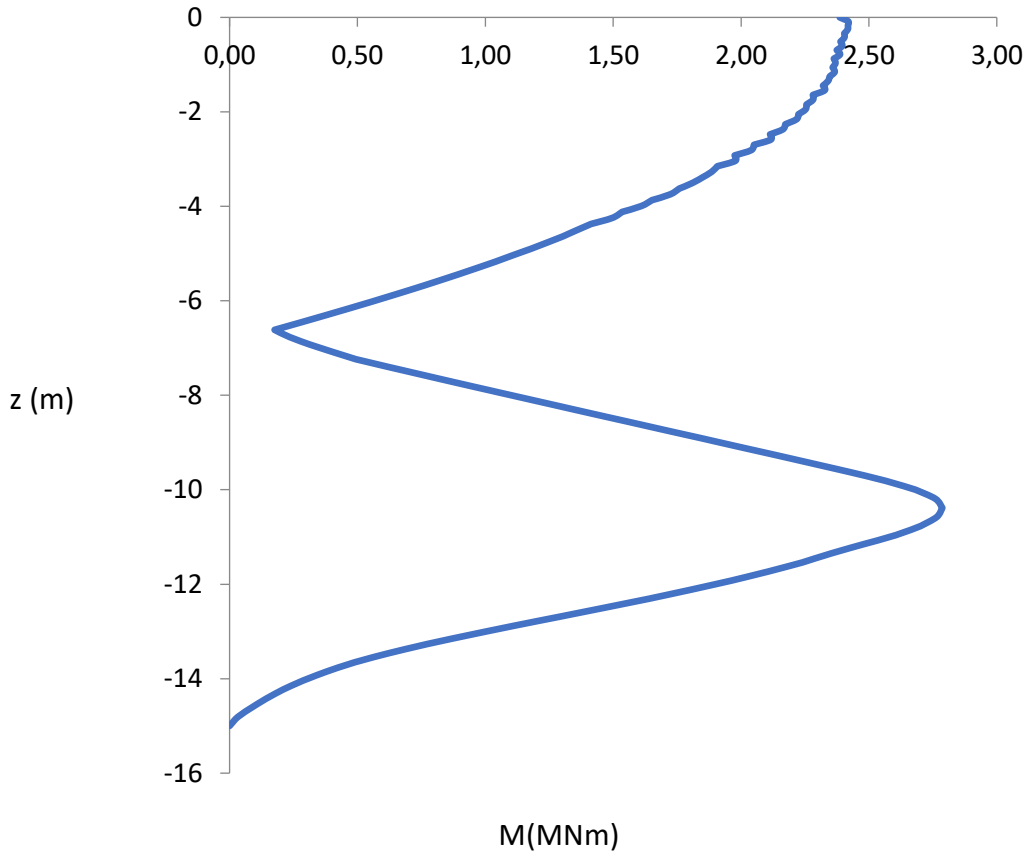

Figure 7.28: Envelope of bending moments for the case 7.

Comments: One thing that we can notice is that the cycles needed in order to reach the steady state part of the analysis are not constant. Number of cycles is a function of the excitation, the shear velocities and geometric parameters of the problem. For example, in this case steady state is reached after 5 cycles.

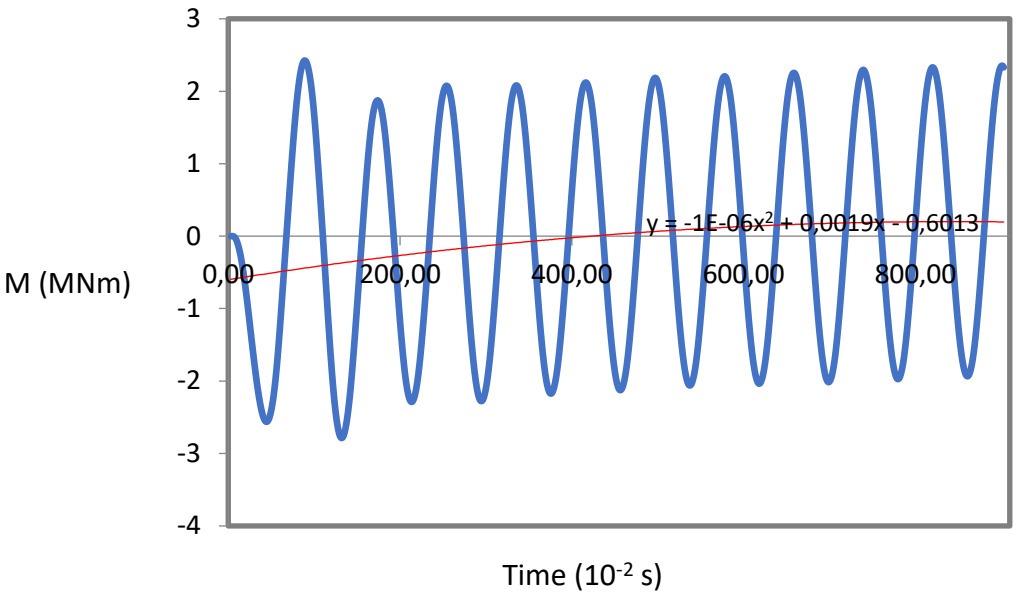

Figure 7.29: Moment - Time graph for the interface and case 7.

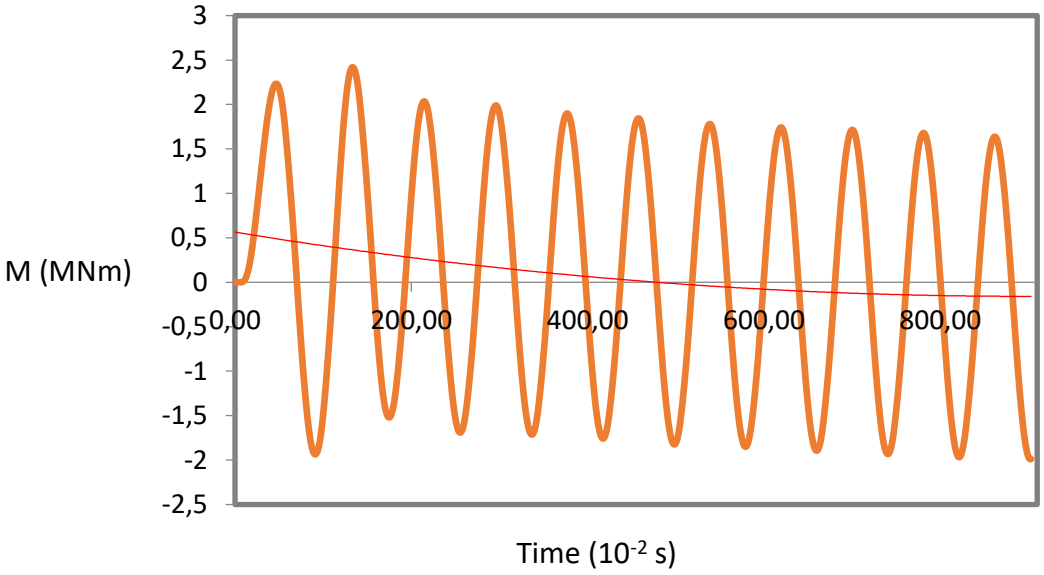

Figure 7.30: Moment - Time graph for the head and case 7.

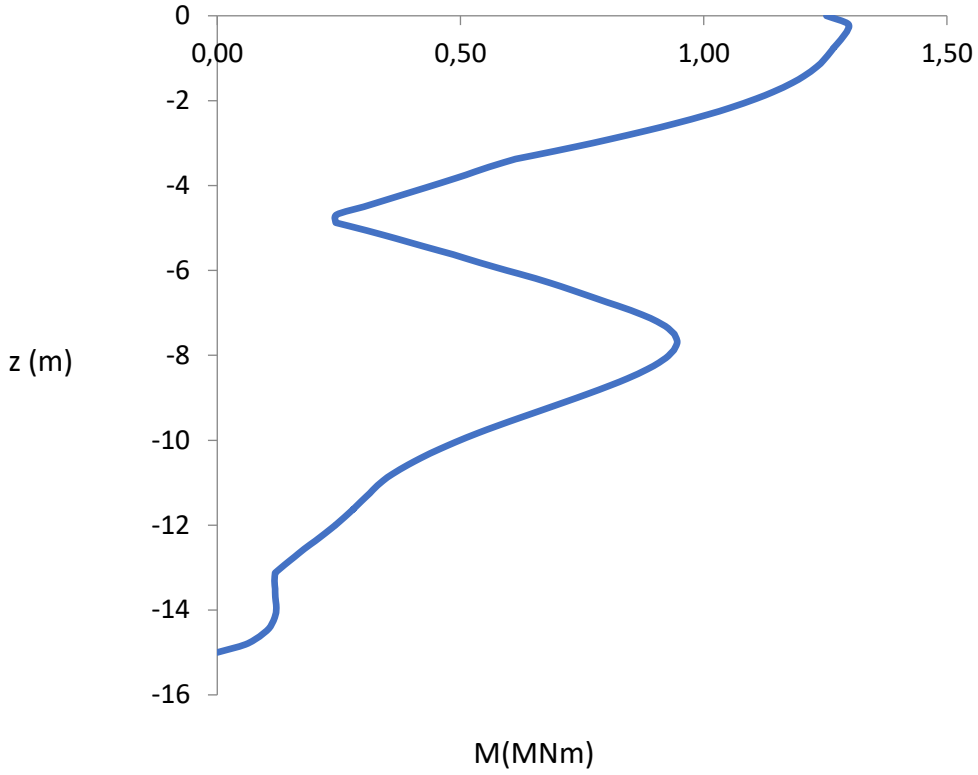

Figure 7.31: Envelope of bending moments for the case 14.

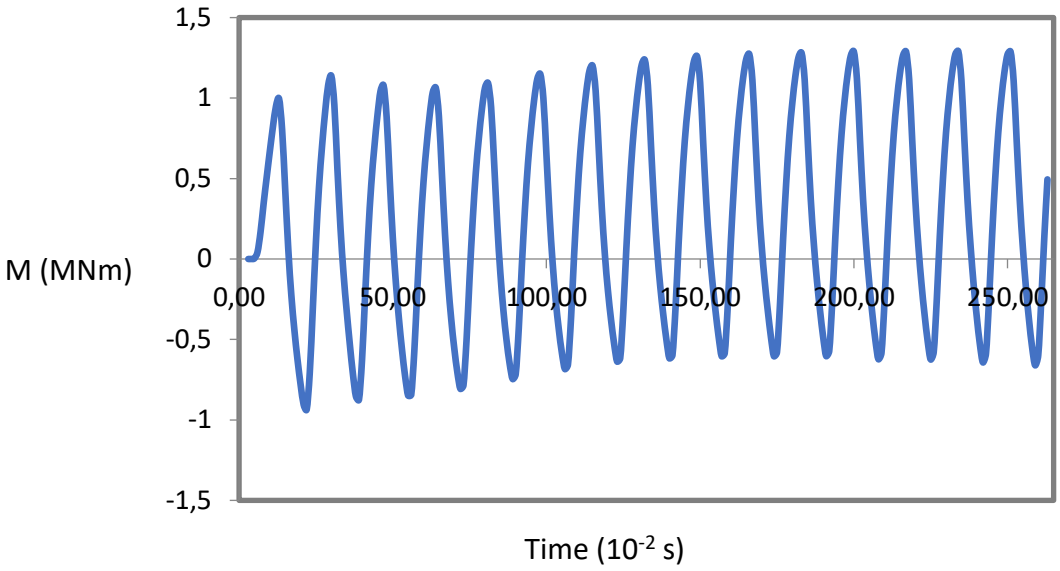

Figure 7.32: Moment –Time graph for the head and case 14.

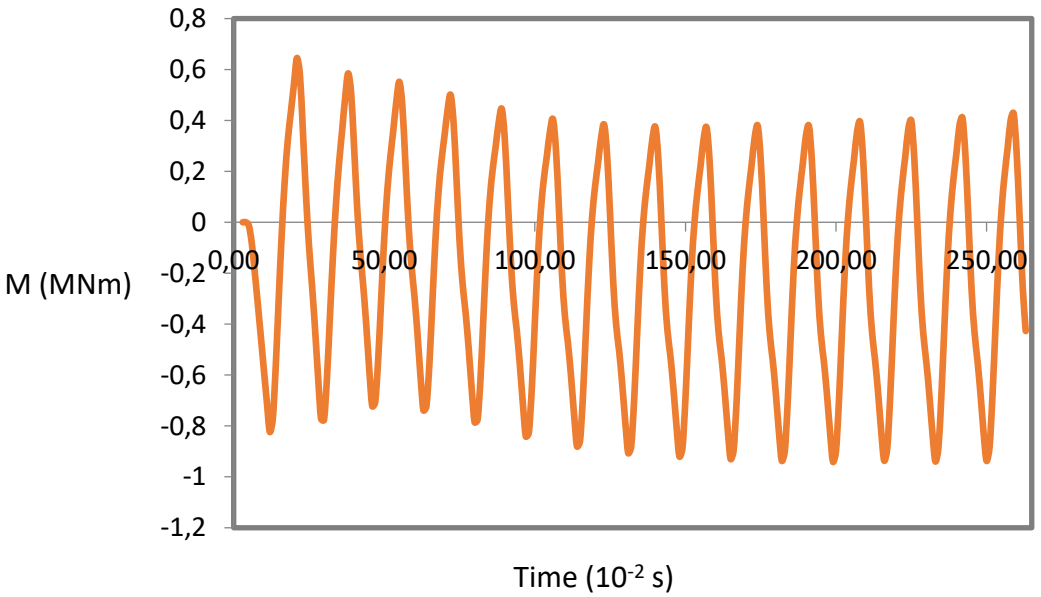

Figure 7.32: Moment – Time graph for the interface and case 14.

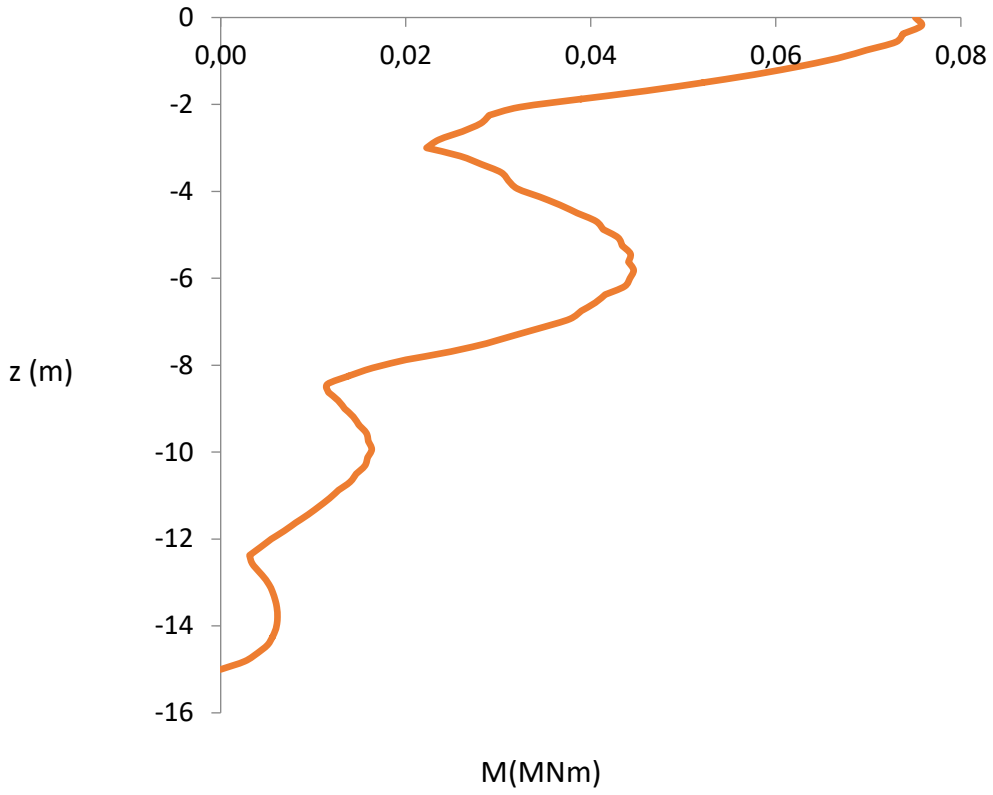

Figure 7.33: Envelope of bending moments for the case 15.

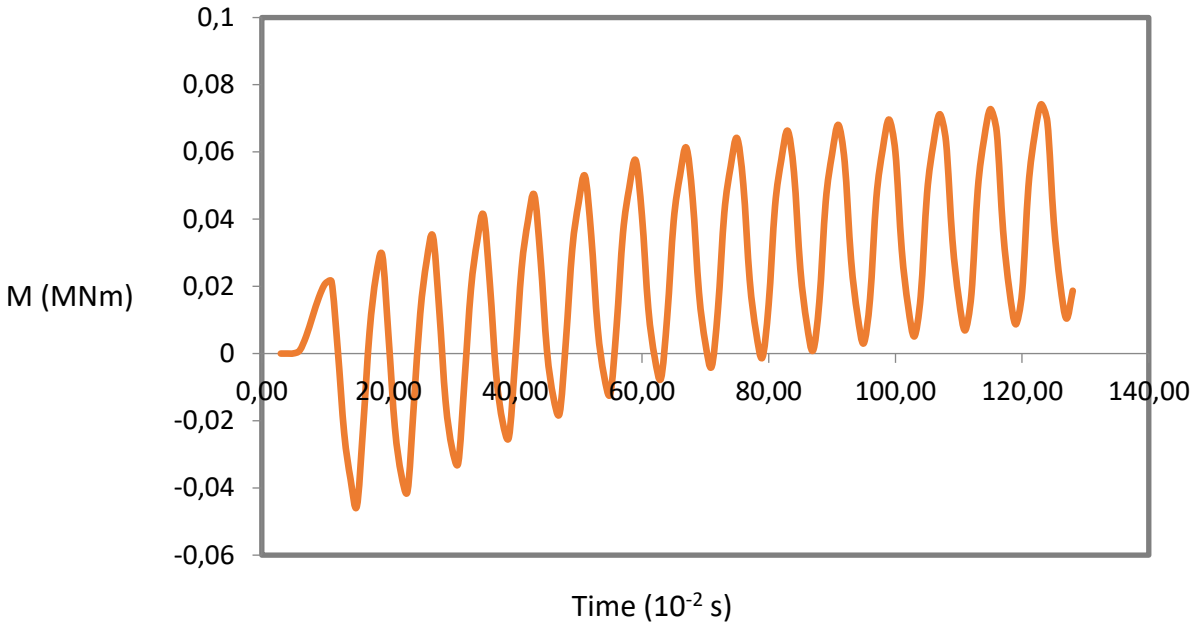

Figure 7.34: Moment - Time graph for head and the case 15.

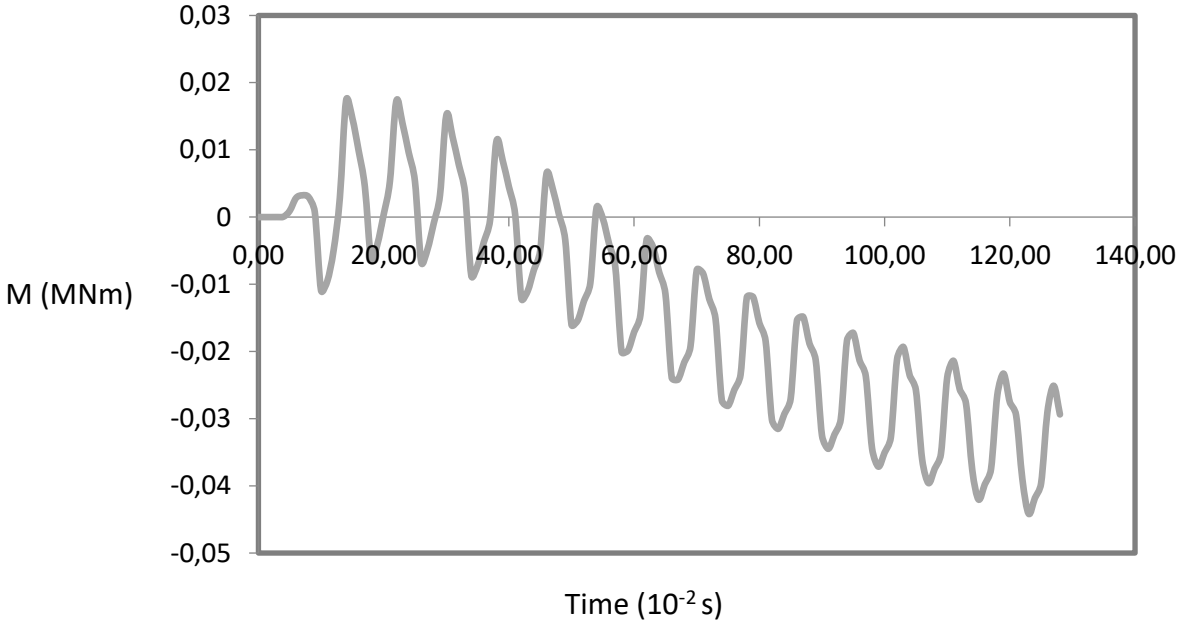

Figure 7.35: Moment- Time graph for the interface and the case 15.

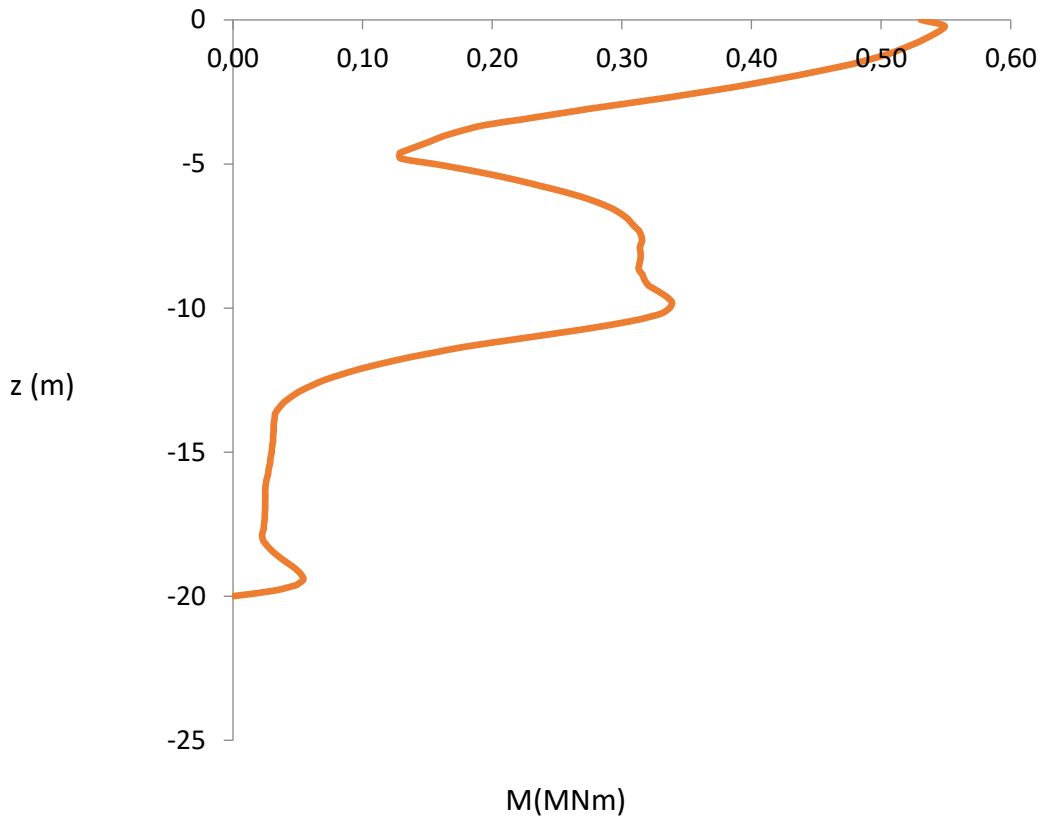

Figure 7.36: Envelope of bending moments for the case 17.

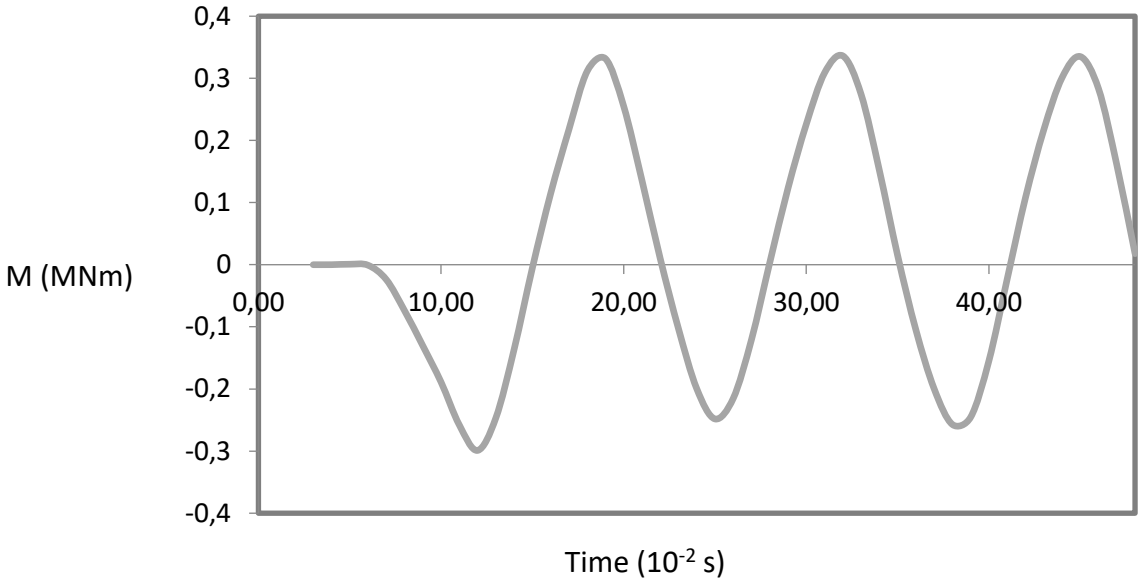

Figure 7.37: Moment - Time graph for the head and case 17.

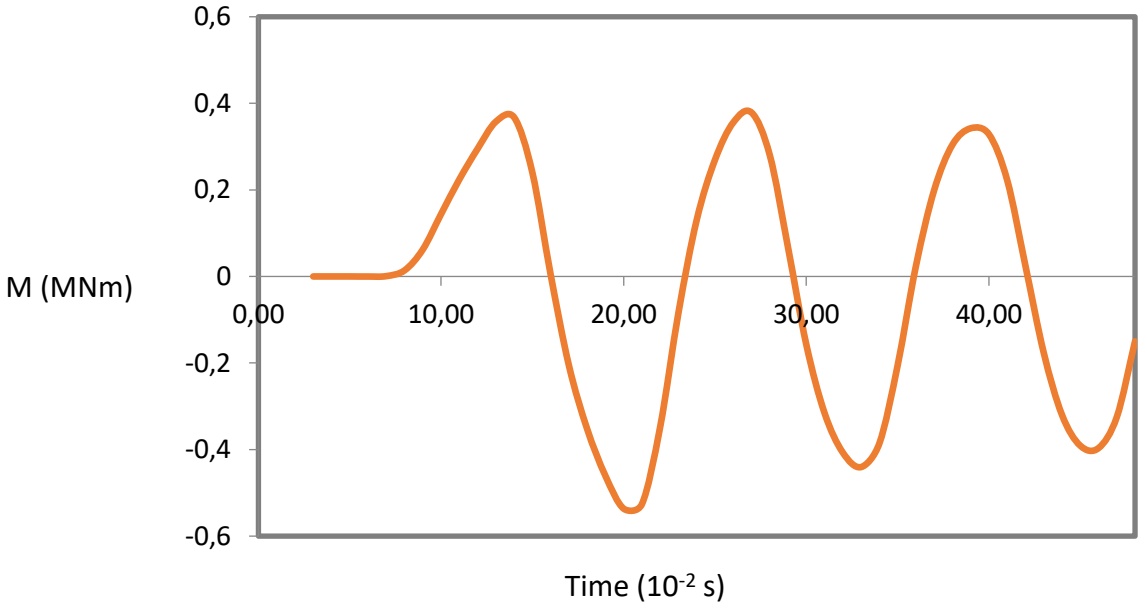

Figure 7.38: Moment - Time graph for the interface and the case 17.

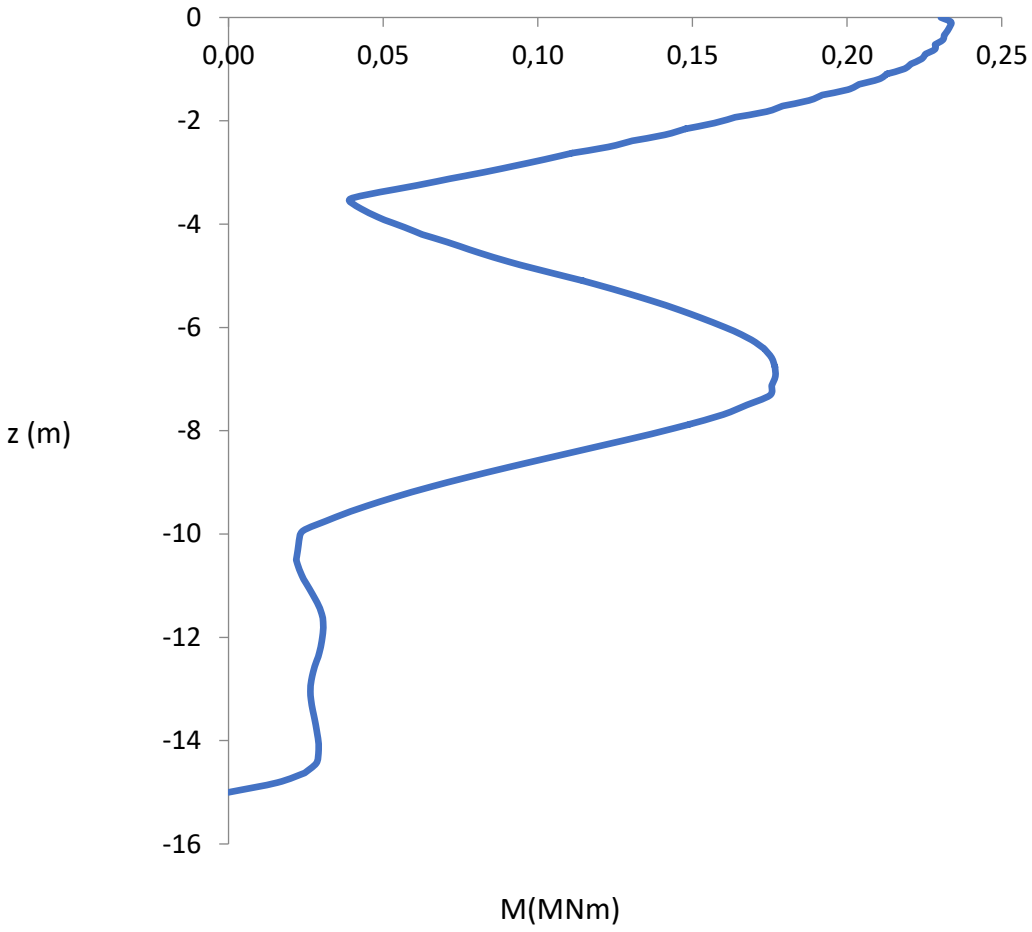

Figure 7.39: Envelope of bending moments for the case 28.

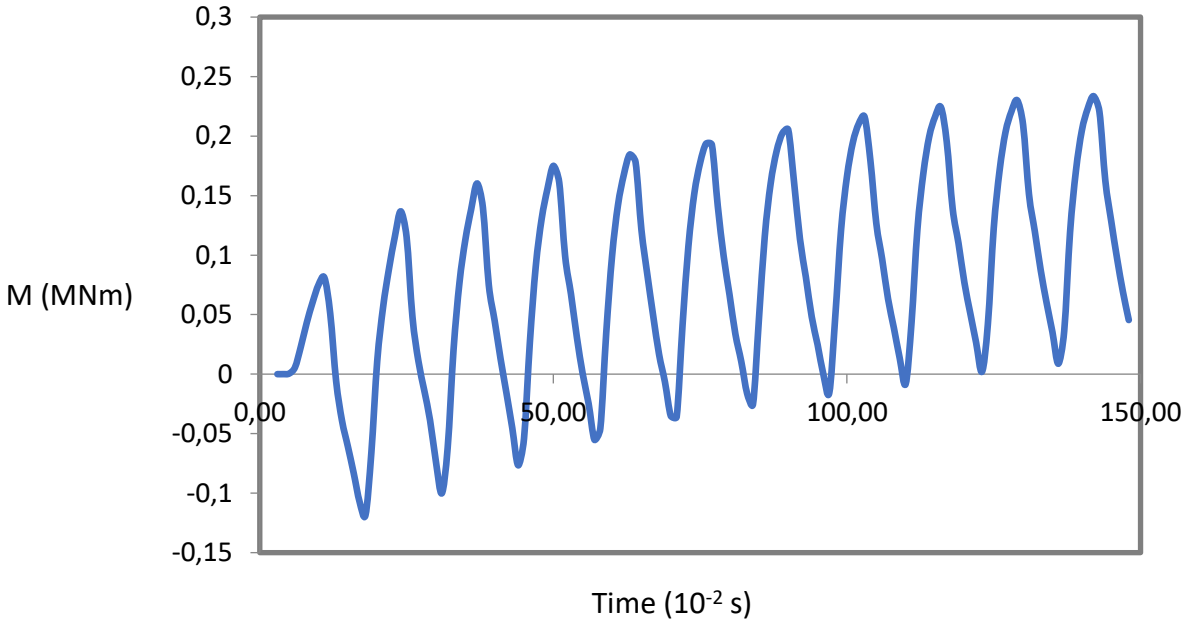

Figure 7.40: Moment – Time graph for the head and the case 28.

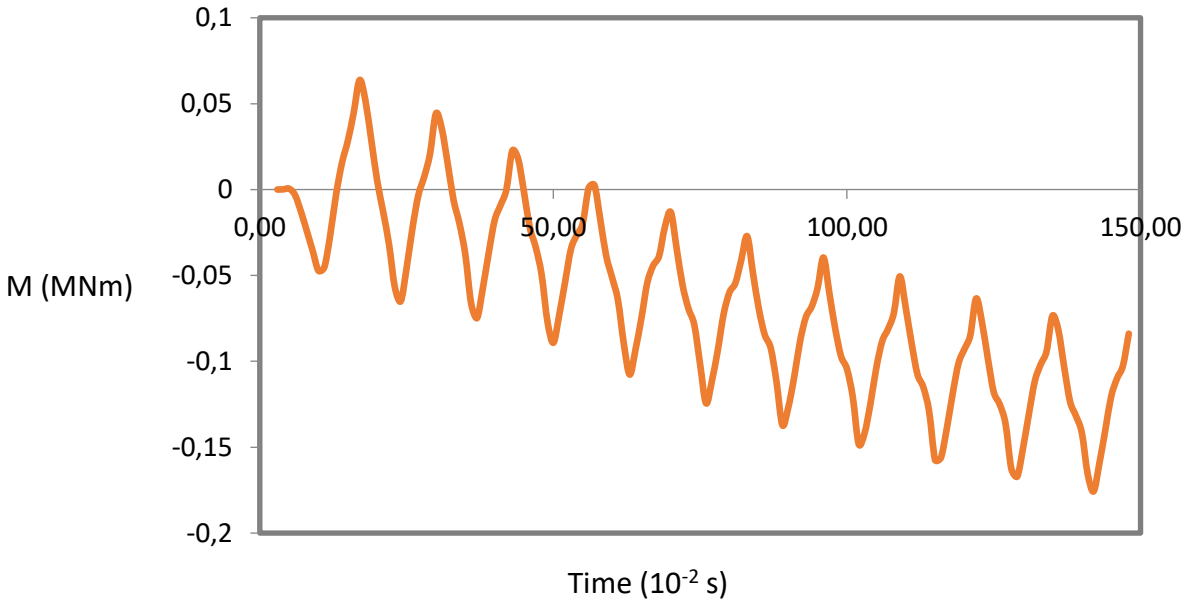

Figure 7.41: Moment - Time graph for the interface and the case 28.

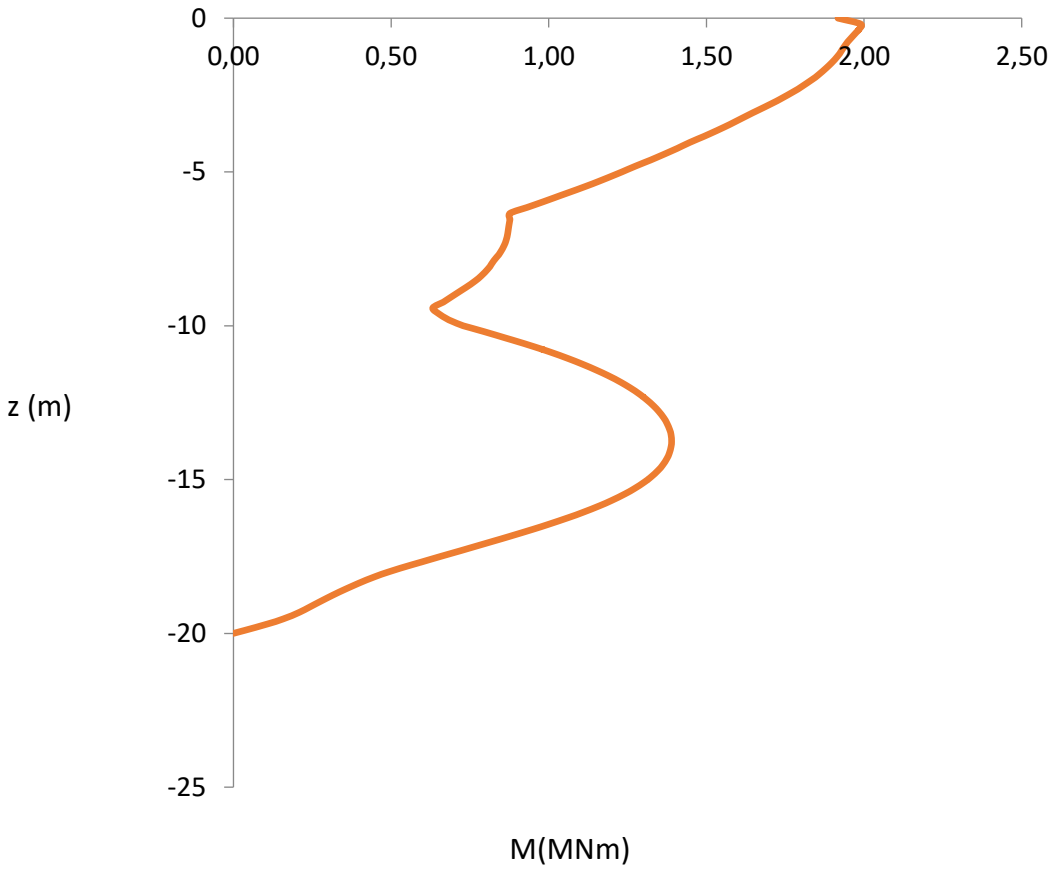

Figure 7.42: Envelope of bending moments for case 29.

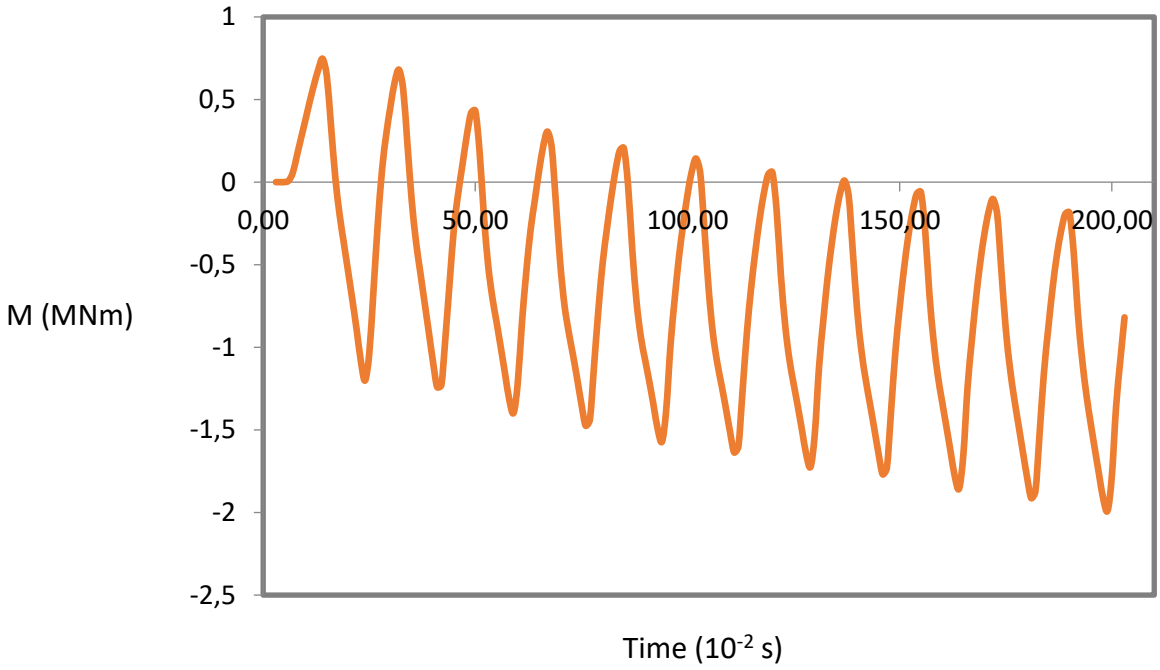

Figure 7.43: Moment – Time graph for the head and case 29.

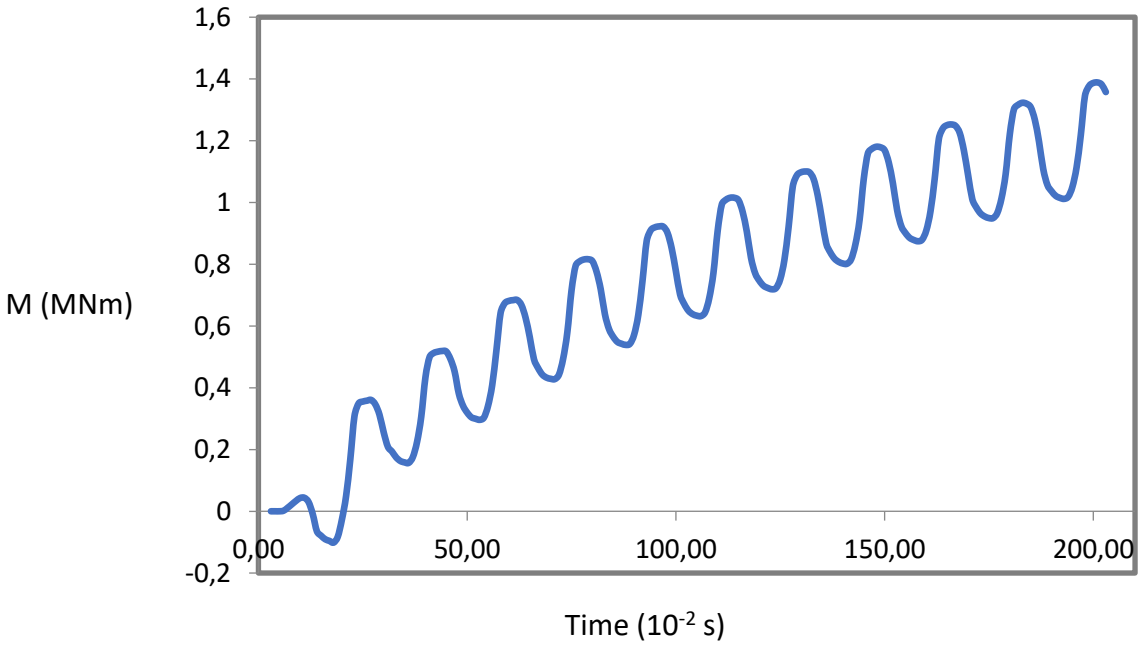

Figure 7.44: Moment - Time graph for the interface and the case 29.

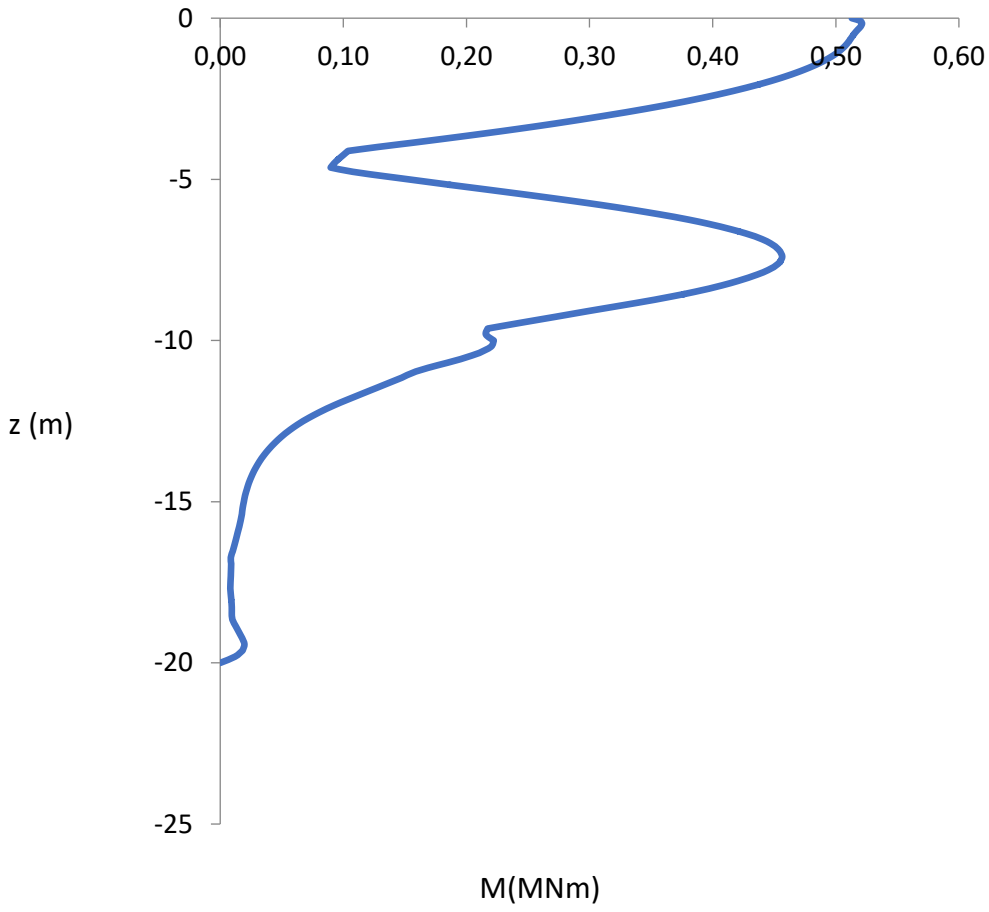

Figure 7.45: Envelope of bending moments for case 37.

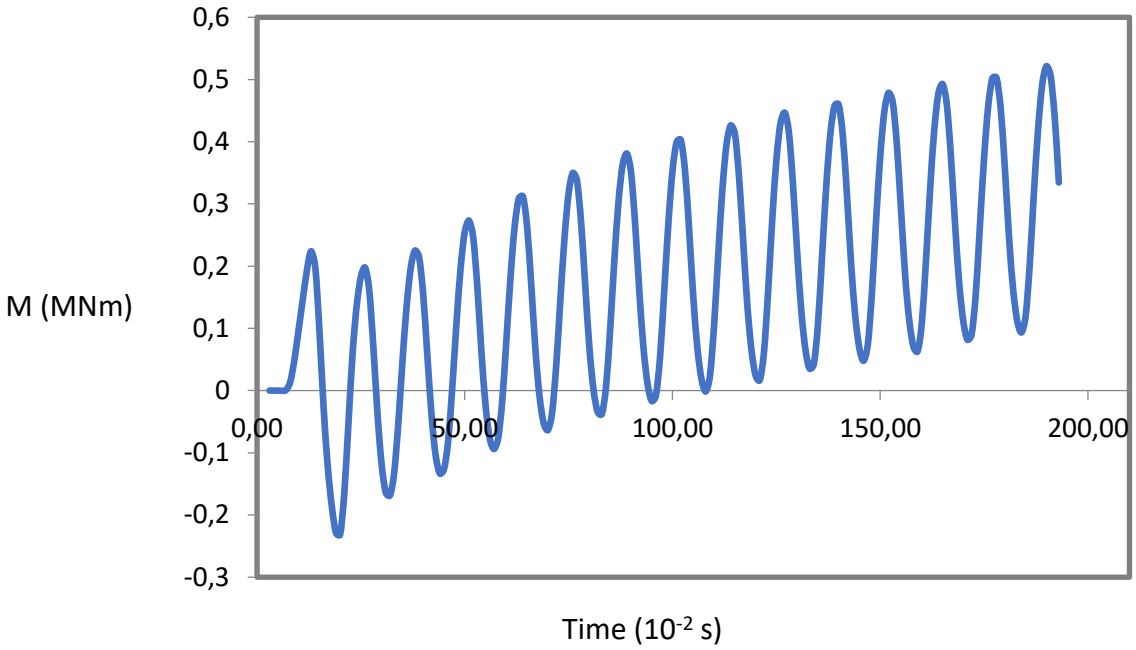

Figure 7.46: Moment - Time graph for the head and the case 37.

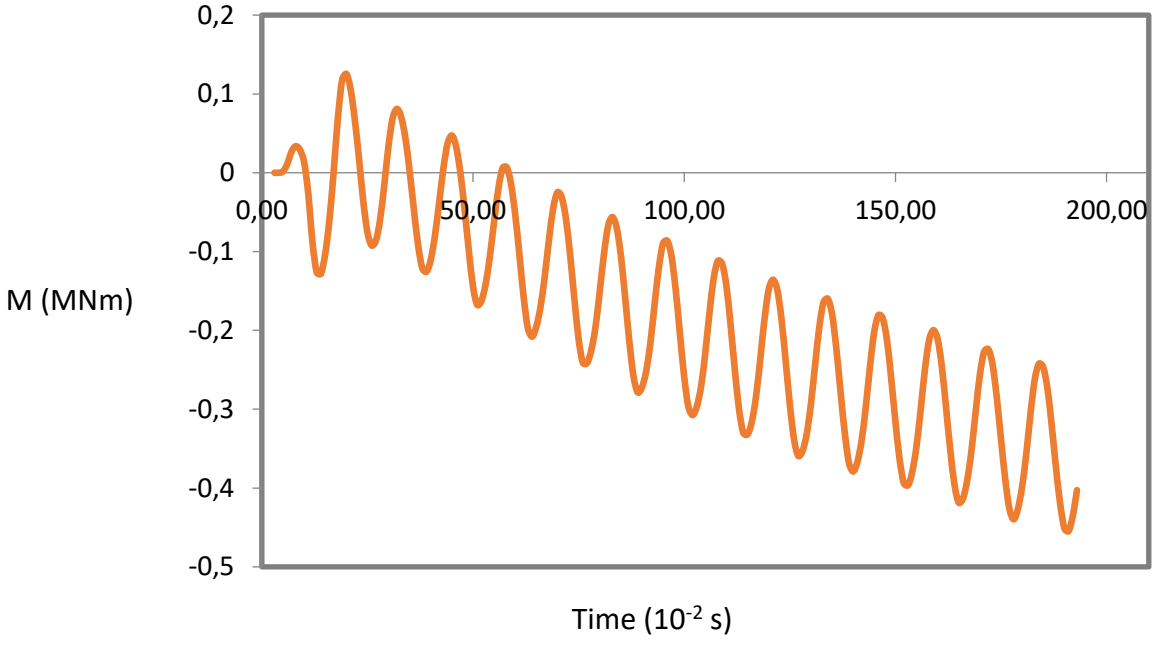

Figure 7.47: Moment – Time graph for the interface and the case 37.

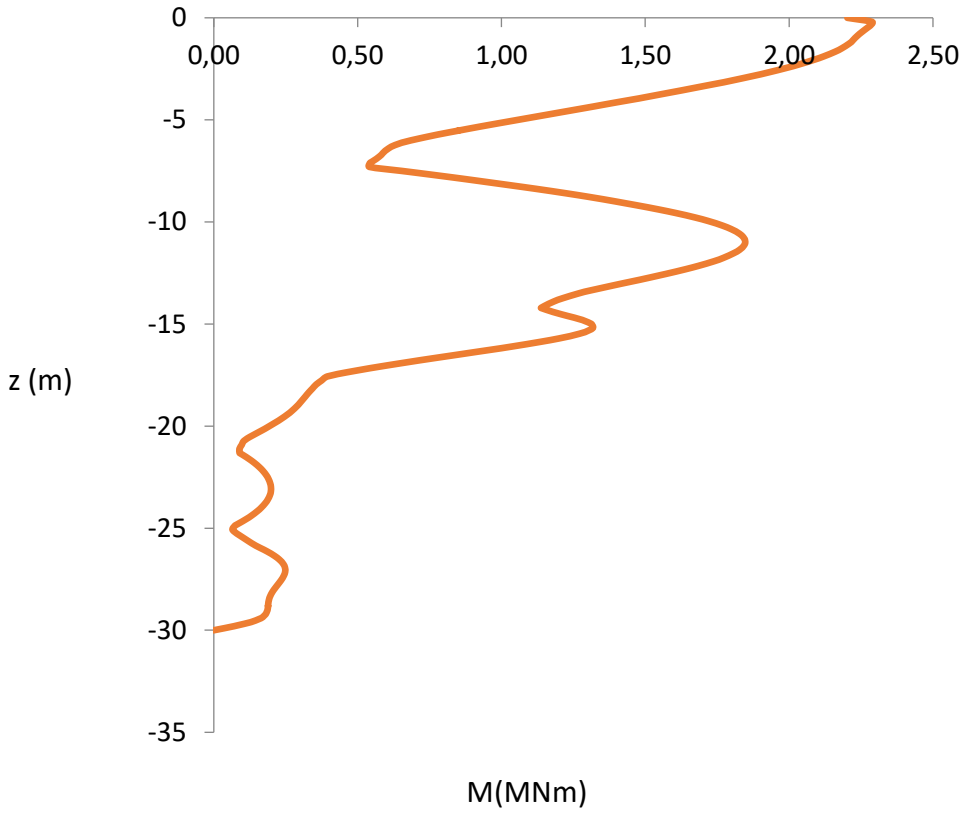

Figure 7.48: Envelope of bending moments for the case 38.

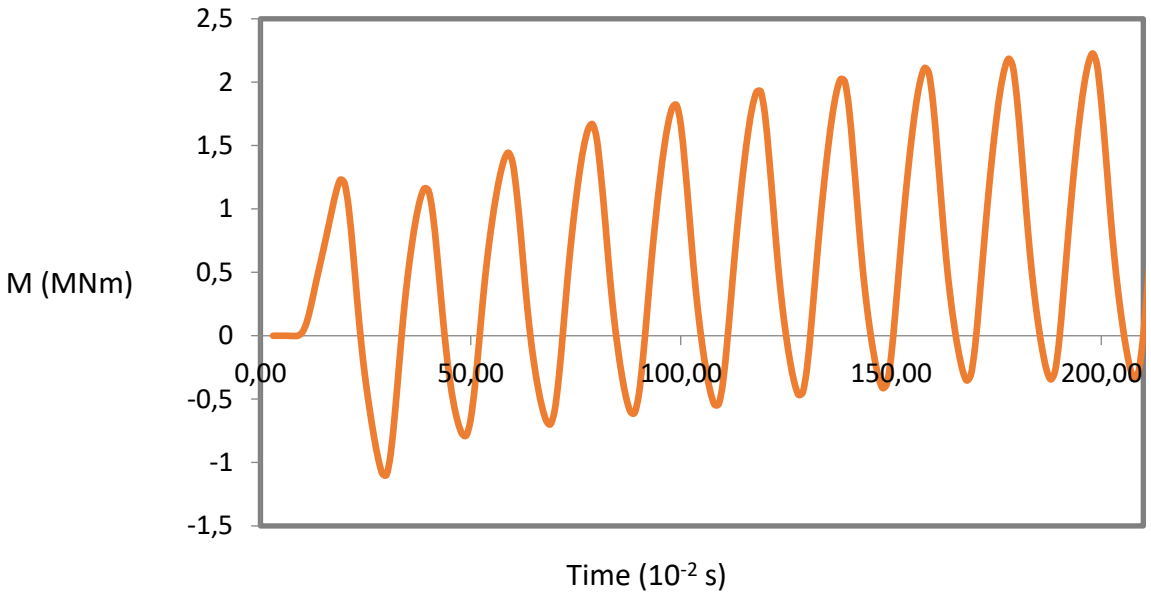

Figure 7.49: Moment - Time graph for the head and case 48.

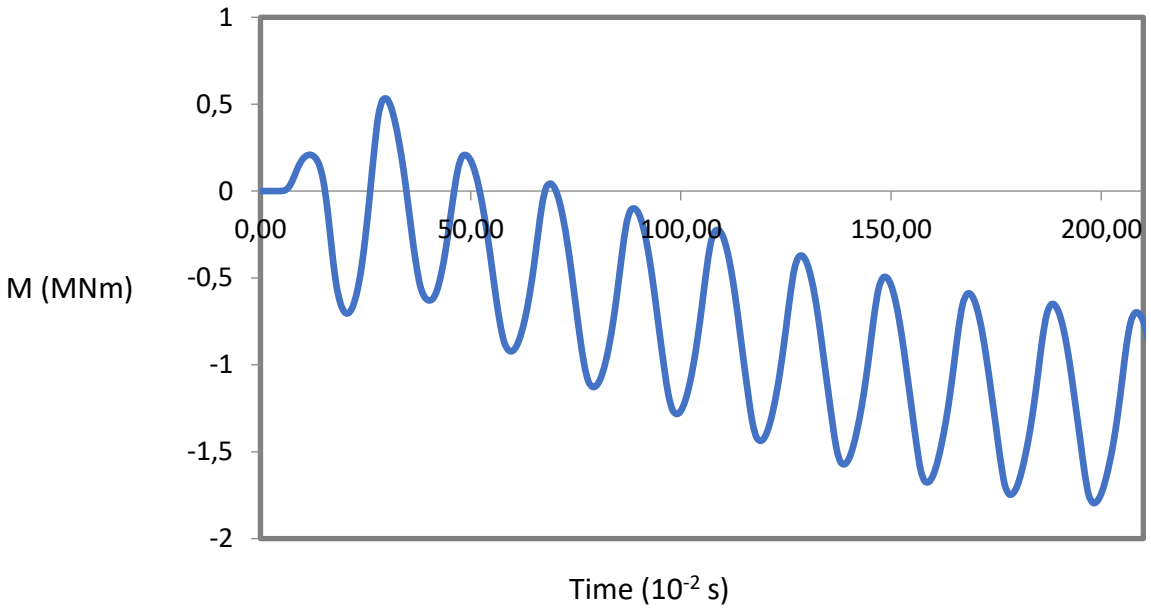

Figure 7.50: Moment - Time graph for the interface and case 48.

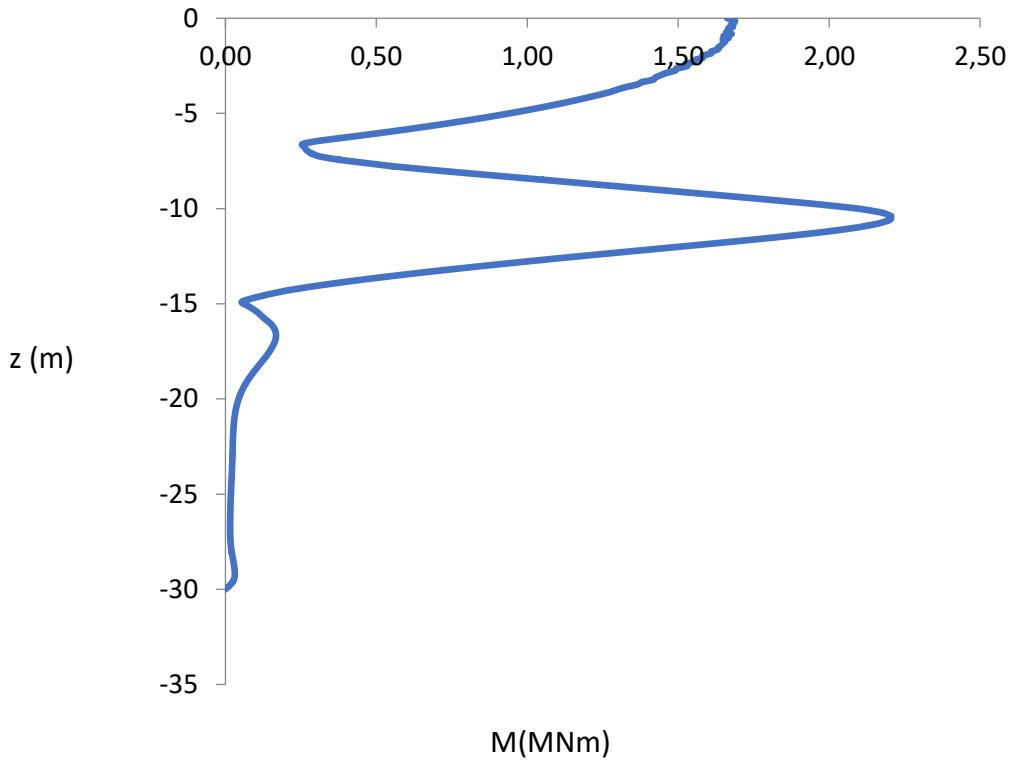

Figure 7.51: Envelope of bending moments for case 46.

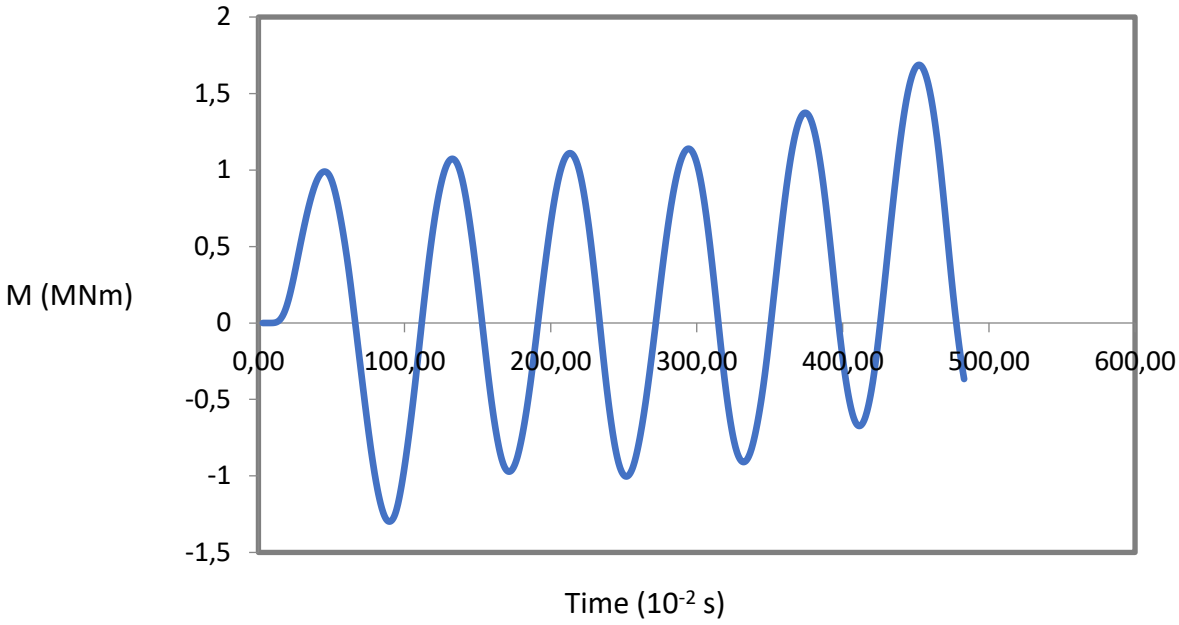

Figure 7.52: Moment - Time graph for the head and case 46.

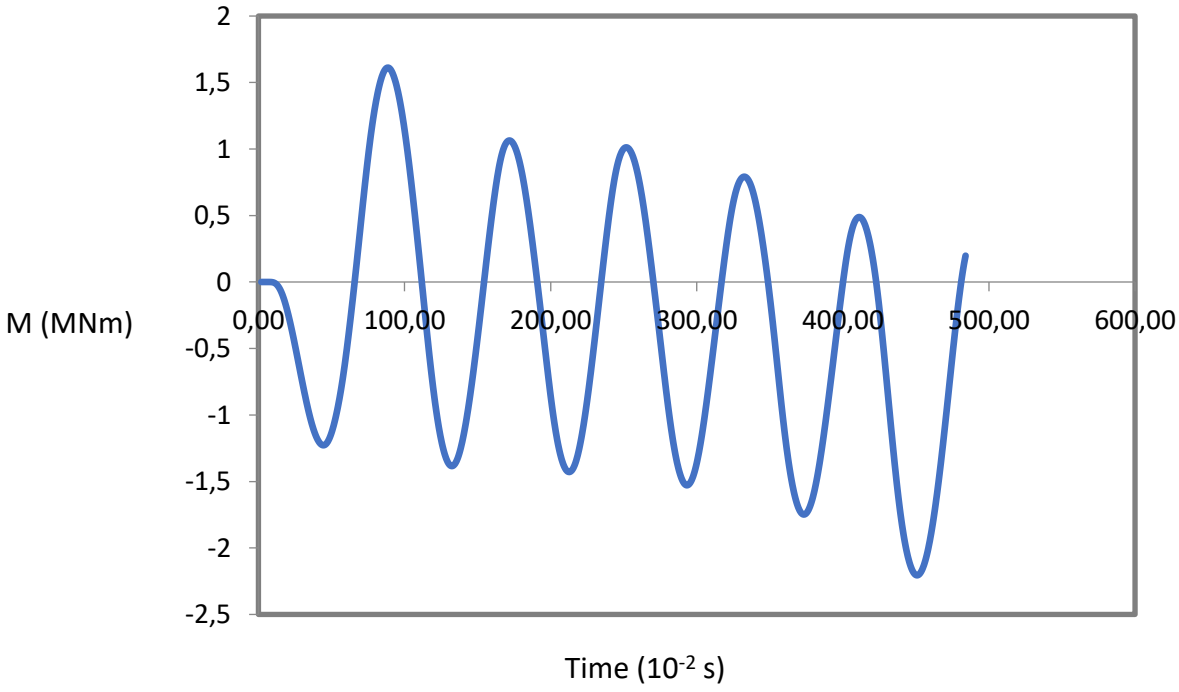

Figure 7.53: Moment – Time graph for the interface and case 46.

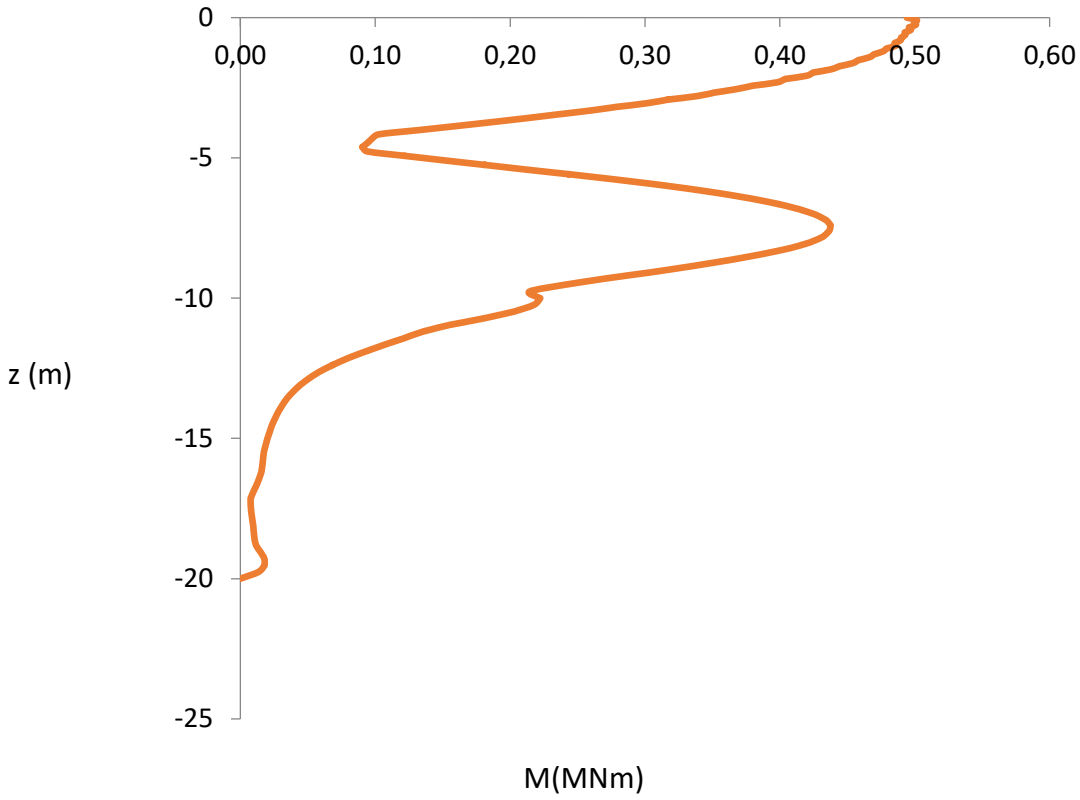

Figure 7.54: Envelope of bending moments for the case 52.

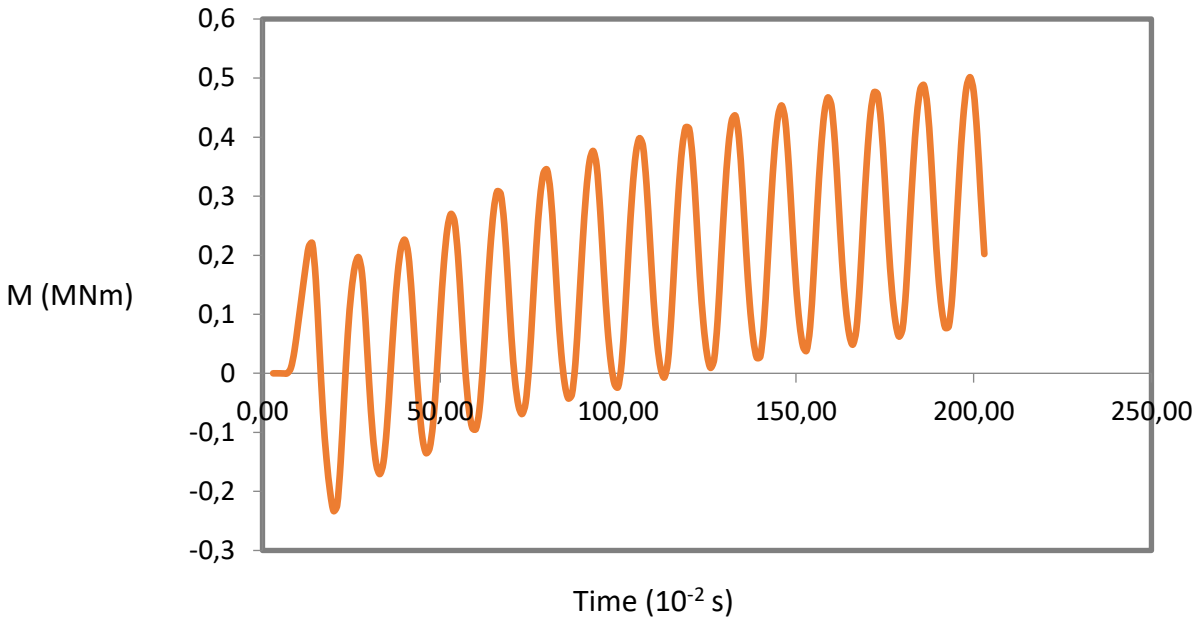

Figure 7.55: Moment - Time graph for the head and case 52.

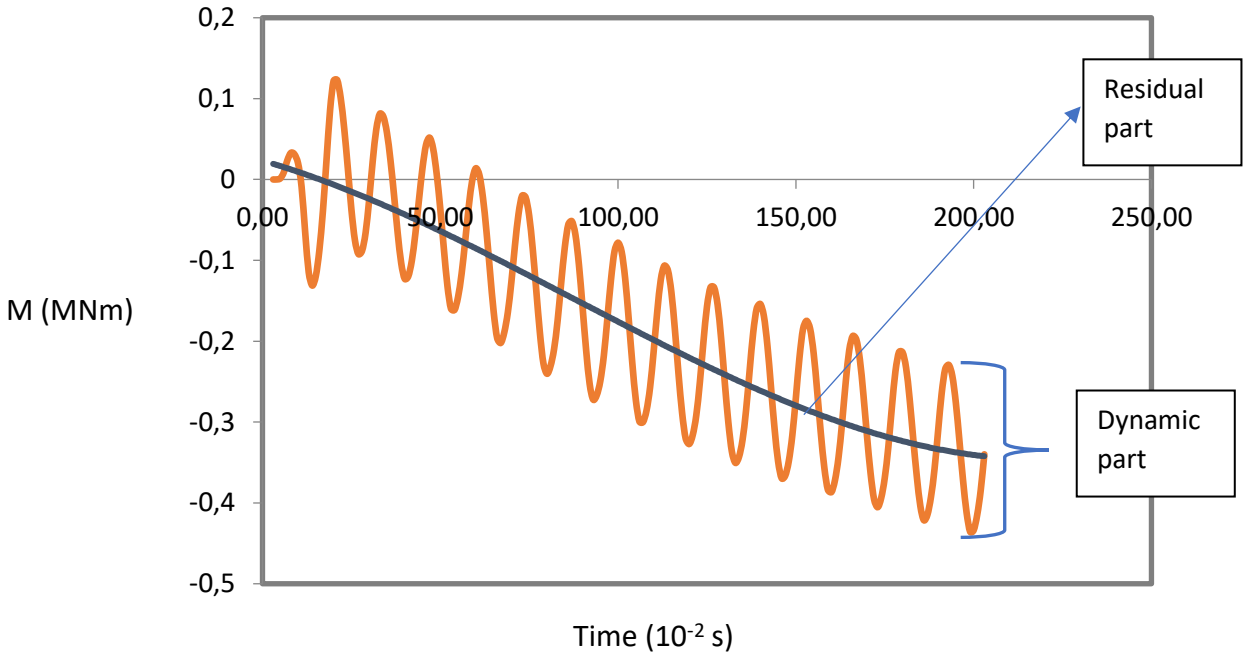

Figure 7.56: Moment - Time graph for the interface and case 52.

7.3.3 Equations for the bending moments in non-Linear soil

From each analysis that was performed three values were derived; dynamic, residual and total part of the bending moments. They were then normalized to fit the following form:

$$\frac{M}{\gamma_1 d^3 H_1} = f\left(\frac{PGA}{g}, \frac{T_{inp}}{Ts1}, N, \frac{E_p}{E_{s1}}, \frac{V_{s2}}{V_{s1}}, \frac{L}{d}, \frac{H_1}{L}\right)$$

To derive an equation linear regression was used using the function LINEST in excel after all the results were logarithmed.

$$f_1 = a * x_1 * x_2 * \dots * x_{n-1} * x_n$$

Using ln in both sides of the above equation:

$$\ln f_1 = \ln a + \ln x_1 + \ln x_2 + \cdots \ln x_{n-1} + \ln x_n$$

Having now a form that can be used for linear regression. The equations that were derived from this are the following:

For the interface:

Residual bending moments:: (Eq. 7.1)

$$\frac{M_{res}^{interf}}{\gamma_1 d^3 H_1} = e^{-11.295}\left(\frac{PGA}{g}\right)^{1.415}\left(\frac{T_{inp}}{T_{s1}}\right)^{1.725} N^{1.184}\left(\frac{E_p}{E_{s1}}\right)^{1.837}\left(\frac{V_{s2}}{V_{s1}}\right)^{-3.278}\left(\frac{L}{d}\right)^{1.28}\left(\frac{H_1}{L}\right)^{0.453}$$

Dynamic bending moments:: (Eq. 7.2)

$$\frac{M_{dyn}^{interf}}{\gamma_1 d^3 H_1} = e^{-3.013}\left(\frac{PGA}{g}\right)^{0.684}\left(\frac{T_{inp}}{T_{s1}}\right)^{0.947} N^{-0.262}\left(\frac{E_p}{E_{s1}}\right)^{0.397}\left(\frac{V_{s2}}{V_{s1}}\right)^{1.834}\left(\frac{L}{d}\right)^{0.082}\left(\frac{H_1}{L}\right)^{-0.61}$$

Total bending moments: (Eq. 7.3)

$$\frac{M_{tot}^{interf}}{\gamma_1 d^3 H_1} = e^{-4.491}\left(\frac{PGA}{g}\right)^{1.022}\left(\frac{T_{inp}}{T_{s1}}\right)^{1.16} N^{0.25}\left(\frac{E_p}{E_{s1}}\right)^{0.939}\left(\frac{V_{s2}}{V_{s1}}\right)^{-0.26481}\left(\frac{L}{d}\right)^{0.461}\left(\frac{H_1}{L}\right)^{0.018}$$

For the head:

Residual bending moments : (Eq. 7.4)

$$\frac{M_{res}^{head}}{\gamma_1 d^3 H_1} = e^{-9.89}\left(\frac{PGA}{g}\right)^{1.444}\left(\frac{T_{inp}}{T_{s1}}\right)^{1.704} N^{0.948}\left(\frac{E_p}{E_{s1}}\right)^{1.963}\left(\frac{V_{s2}}{V_{s1}}\right)^{-3.65}\left(\frac{L}{d}\right)^{0.895}\left(\frac{H_1}{L}\right)^{-0.16}$$

Dynamic bending moments:: (Eq. 7.5)

$$\frac{M_{dyn}^{head}}{\gamma_1 d^3 H_1} = e^{-2.463}\left(\frac{PGA}{g}\right)^{1.125}\left(\frac{T_{inp}}{T_{s1}}\right)^{1.21} N^{-0.142}\left(\frac{E_p}{E_{s1}}\right)^{0.723}\left(\frac{V_{s2}}{V_{s1}}\right)^{0.493}\left(\frac{L}{d}\right)^{-0.09}\left(\frac{H_1}{L}\right)^{-0.785}$$

Total bending moments : (Eq. 7.6)

$$\frac{M_{tot}^{head}}{\gamma_1 \, d^3 H_1} = e^{-4.005} \left(\frac{PGA}{g}\right)^{1.202} \left(\frac{T_{inp}}{T_{s1}}\right)^{1.32} N^{0.22} \left(\frac{E_p}{E_{s1}}\right)^{1.077} \left(\frac{V_{s2}}{V_{s1}}\right)^{-0.864} \left(\frac{L}{d}\right)^{0.298} \left(\frac{H_1}{L}\right)^{-0.435}$$

Following are the graphs representing the validity of the equations. On the x-axis is the normalised bending moment from the analyses and on the y-axis the normalised bending moments using the corresponding equation from the above. The residual expressions for both the head and the interface behave poorly , having R^2=0.26, 0.61 for the interface and the head. The equation for the mean line is far from the derised result y=x. These large deviatons can be explained from the physics of the problem. The residual part of the bending moments is a result from soil hardening occuring at the soil surrounding the pile. In a numerous analyses from the 60 that were performed the soil behaved almost linearly, especially in cases with amplitude equal to 0.1-0.25 g, in which the residual part of the moments was close to zero. Moreover this residual bending moment is a function of soil characteristics, number of cycles, amplitude of excitation (as shown in 7.2) making it really difficult to obtain an accurate equation from the limited number of analyses that were conducted in this thesis.

As far as the dynamic part the results are much better with R^2=0.87, 0.84 for the interface and the head .

The most accurate and practical from the above equaitons is the one of the total bending moments with R^2=0.8, 0.85 and mean lines equations close to the y=x.

7.3.4 Comments on the influence of the parameters on the derived equations:

- PGA/g: A parameter which , in most cases, obtains values lower than 1. This means that the parameter affects more the dynamic moments at the interface as can be seen from the six equations above with a power equal to 0.68.
- T_{inp}/T_{s1}: It is important to notice that for the equation of residual moment at the head and at the interface the exponent attains its maximum value (m=1.4). This can be interpreted , that when the resonance ratio is lower than 1, the residual moments are much less. Instead in the case that the ratio's values are greater than 1, the residual moments are affected negatively by it. An explanation can be given if we consider that the soil's stiffness decays with non-linear soil behaviour. Following this redution the predominant period of the subsoil is increased ($T_{s1} = \frac{4H}{V_s}$) meaning that the resonance ratio will only become smaller while the excitation continues, reaching values closer to 1 and thus resonance. (leading to bigger displacements and therefore more plastic deformations). Where in the case of smaller than unity there is no way of the soil reaching resonance conditions.
- N: As the number of cycles increases the residual and total bending moments increase. Due to the non linear behavior of the soil with each cycle it's deformations increase, leading to larger permanent displacements and therefore to higher bending moments.
- E_p/E_{s1}: Affects more the residual part, plays a dominant role for the pile's motion and bending moments. Comparing the effect of this parameter between the linear and non-linear analyses, it is higher for the latter one. The reason behind this difference is attributed to the plasticization of the soil; the constitutive model of the pile is linear elastic meaning that the elastic modulus of the pile will remain constant during the excitation, on the contrary the plastic deformations that developed at the soil leads to degradation of the soil's stiffness (E_{s1}) and therefore the relative stiffness ratio increases as the excitation continues.
- V_{s2}/V_{s1}: The most critical information that can be derived from these equations in the case of the shear velocities ratio is the following: a) This parameter affects much more the interface than the head for the total bending moments and dynamic bending moments , something that follows the kinematic response for linear soil. Not in all cases does the moment at the interface interfere with the bending moment at the head of the pile. As Mylonakis showed in Mylonakis et al (2013) the length between the soil suface and the interface ,H_1, plays an important role in this problem.b) The negative power at the residual moments both for the head as well as the interface can be justified by the physics of the problem. Increasing the shear velocity ratio means that the deeper soil layer is much stiffer than the upper layer. The deeper layer acts as fixity reducing the part of the pile being on loose soil, meaning active lenth of the pile is also reduced. Lower pile active length means smaller deforamtions leading to smaller permanent displacements and residual mometns.
- H_1/L: For the case of the interface the interface's location plays an insignificant role (m=0.018). On the other hand for the head of the pile as the interface goes deeper the total bending moment at the head increases. This has also been idientified in the

linear case; the closer the interface to the head the bigger the effect to the pile , which tends to reduce pile rotation at the interface thus generating a positive bending moment in that location. A certain percentage (which is dependent on the height of the upper layer h_1) of that moment is transmitted to the head. Furthermore, the reason why the residual moments at the interface have a positive power can be justified with how the pile deforms. Given the fact that the second layer is always stiffer than the first one, the deeper the interface the bigger the length that is embedded in softer soil. This means that as h_1/L increases the displacements will increase leading to bigger residual moments. This dominant effect on the residual part of the moments affects also the total moments, where with increasing shear velocity ratio the total moment is getting lower, attributed in the same phenomenon discussed above.

- L/d: For the slendeness ratio the most important effect of this parameter is the one on the residual moments for both the head and the interface with exponents at 1 and 1.3 respectively. In all the analyses as the length of the pile increased the depth of the interface also increased , given that h_1 is proportional to the total length of the pile. Therefore the reasons behind this differentiation can be seen in the H_1/L comments.

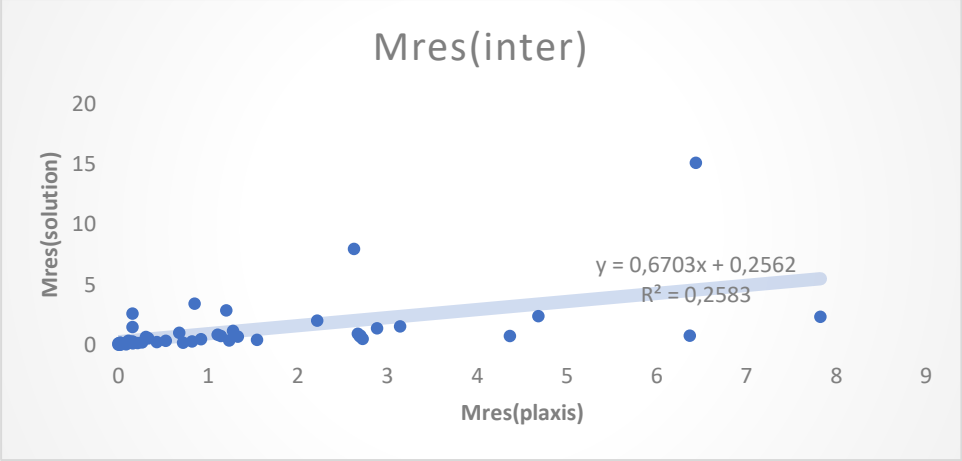

Figure 7.57: Comparison of the equation 7.1, the residual part of the moments for the interface, with the plaxis results.

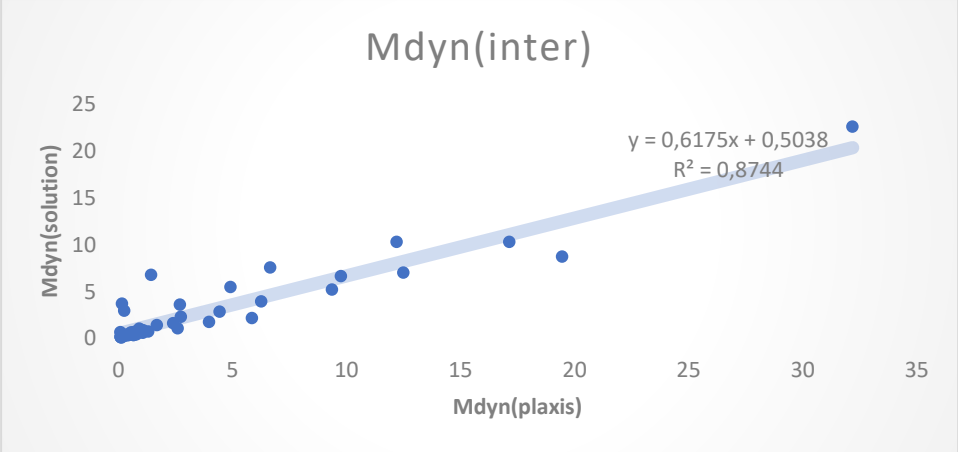

Figure 7.58: Comparison of the equation 7.2, the dynamic part of the moments for the interface, with the plaxis results.

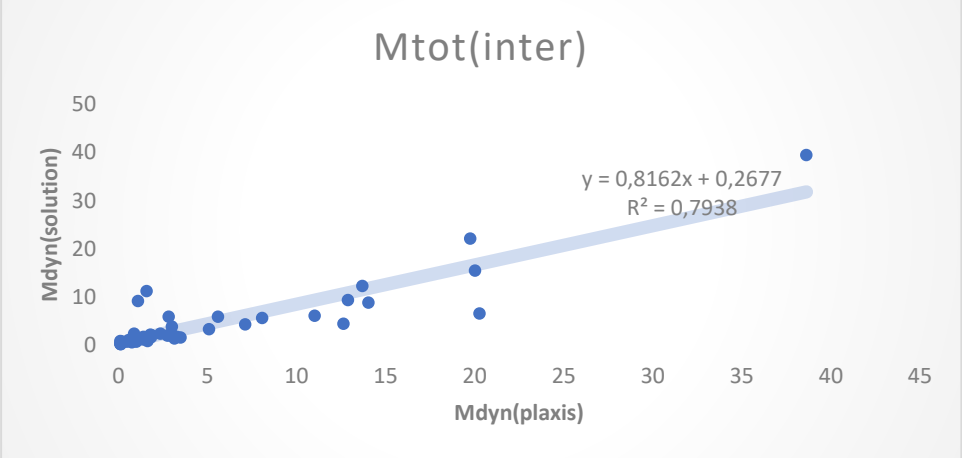

Figure 7.59: Comparison of the equation 7.3, the total bending moments for the interface, with the plaxis results.

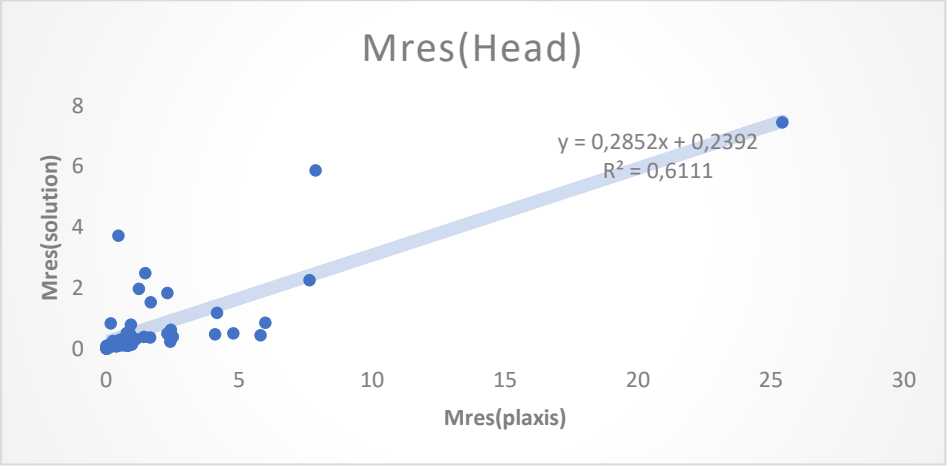

Figure 7.60: Comparison of the equation 7.4, the residual part of the bending moments for the head, with the plaxis results

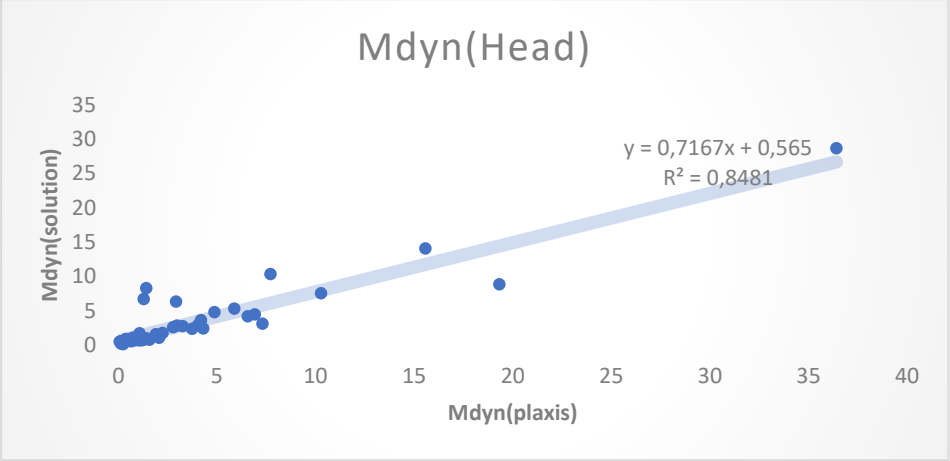

Figure 7.61: Comparison of the equation 7.5, the dynamic part of the bending moments for the head, with the plaxis results.

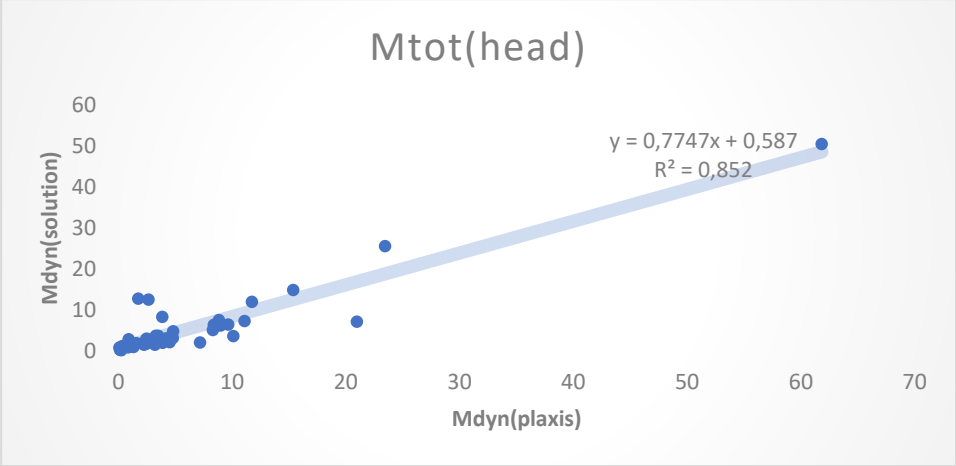

Figure 7.62: Comparison of the equation 7.6, the total bending moments for the head , with the plaxis results.

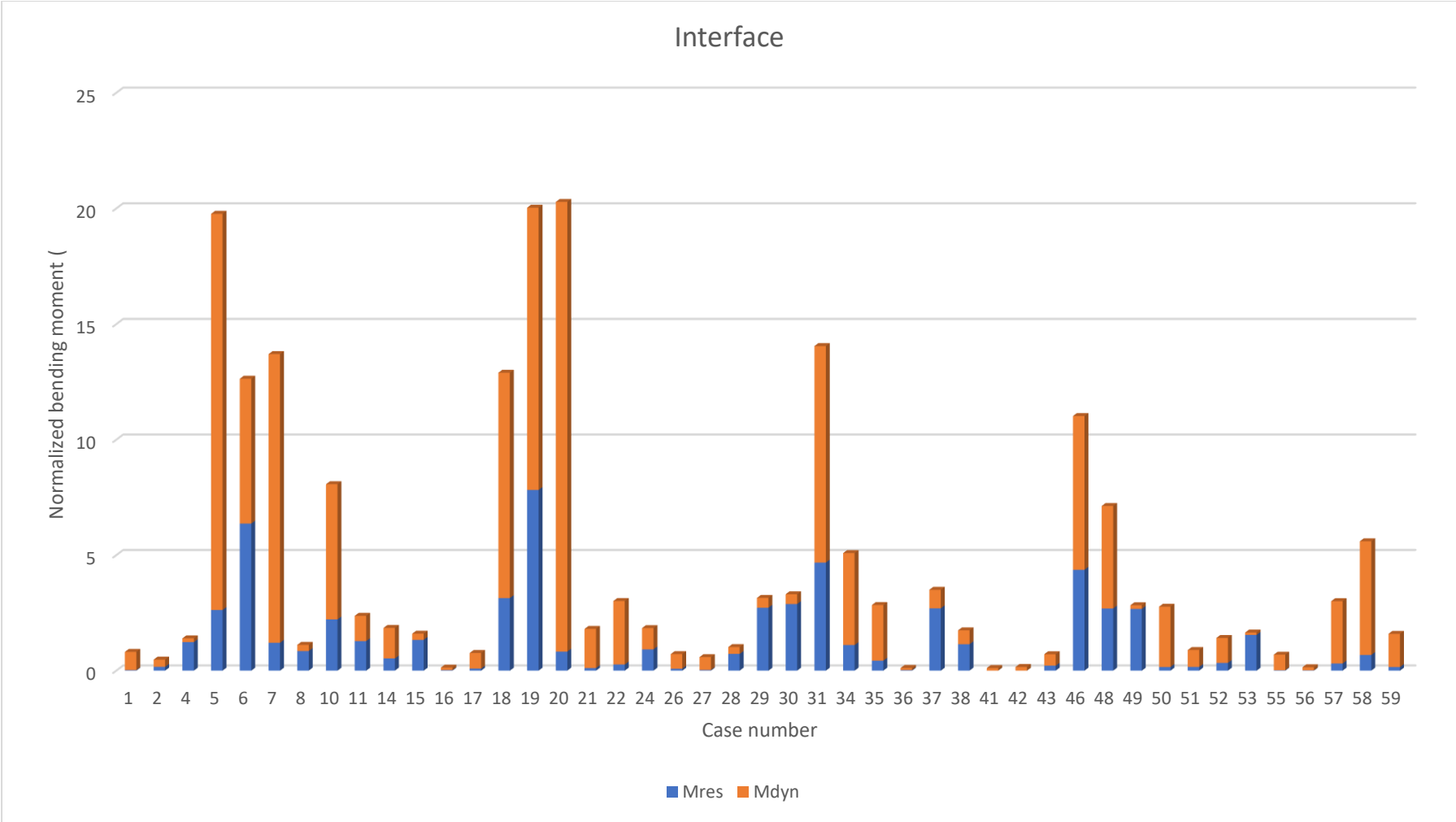

Figure 7.63: Comparison of the dynamic to the residual part for some of the cases that were studied for the interface. The red corresponds to the dynamic part of the moments and the blue to the residual part.

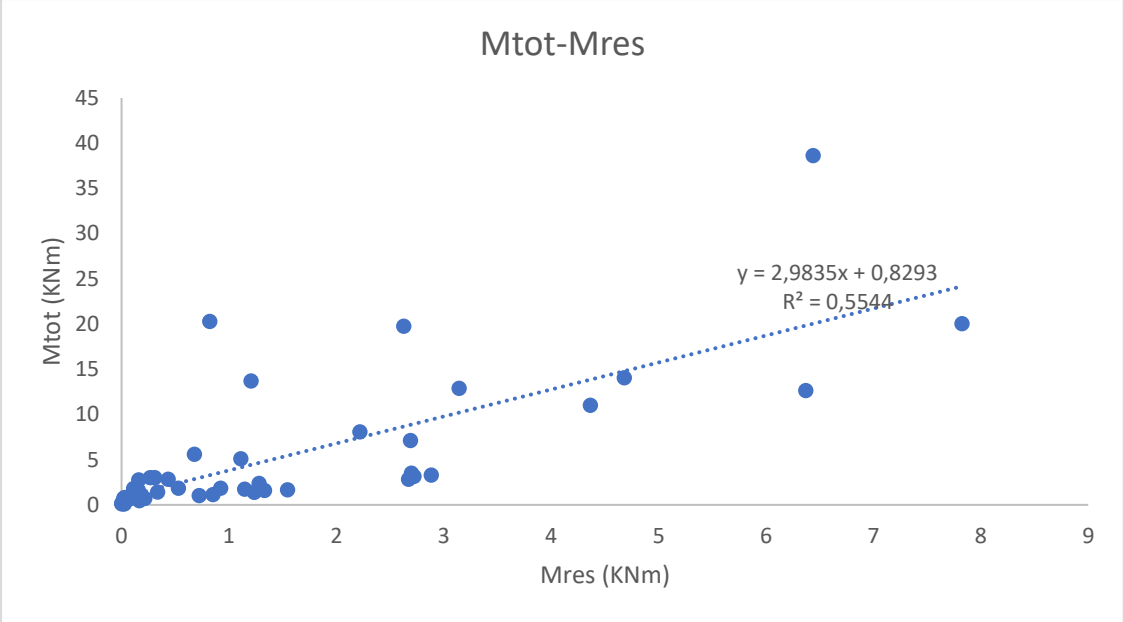

Figure 7.64: The relation between the total bending moment and the residual part for the interface

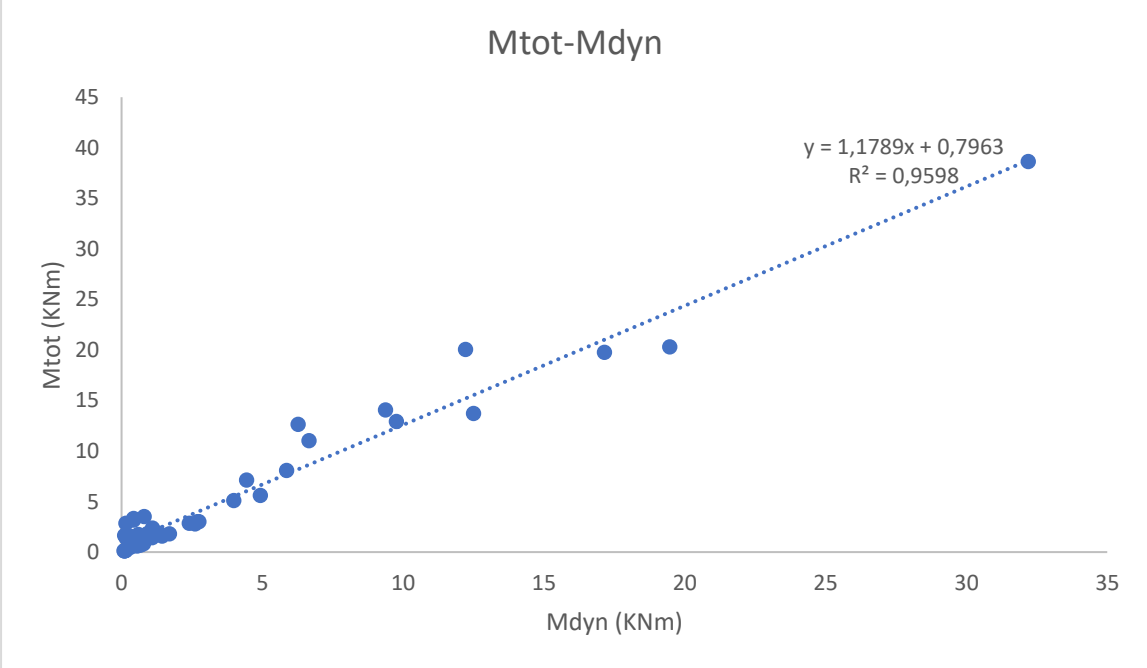

Figure 7.65: The relation between the total bending moment and the dynamic part for the interface.

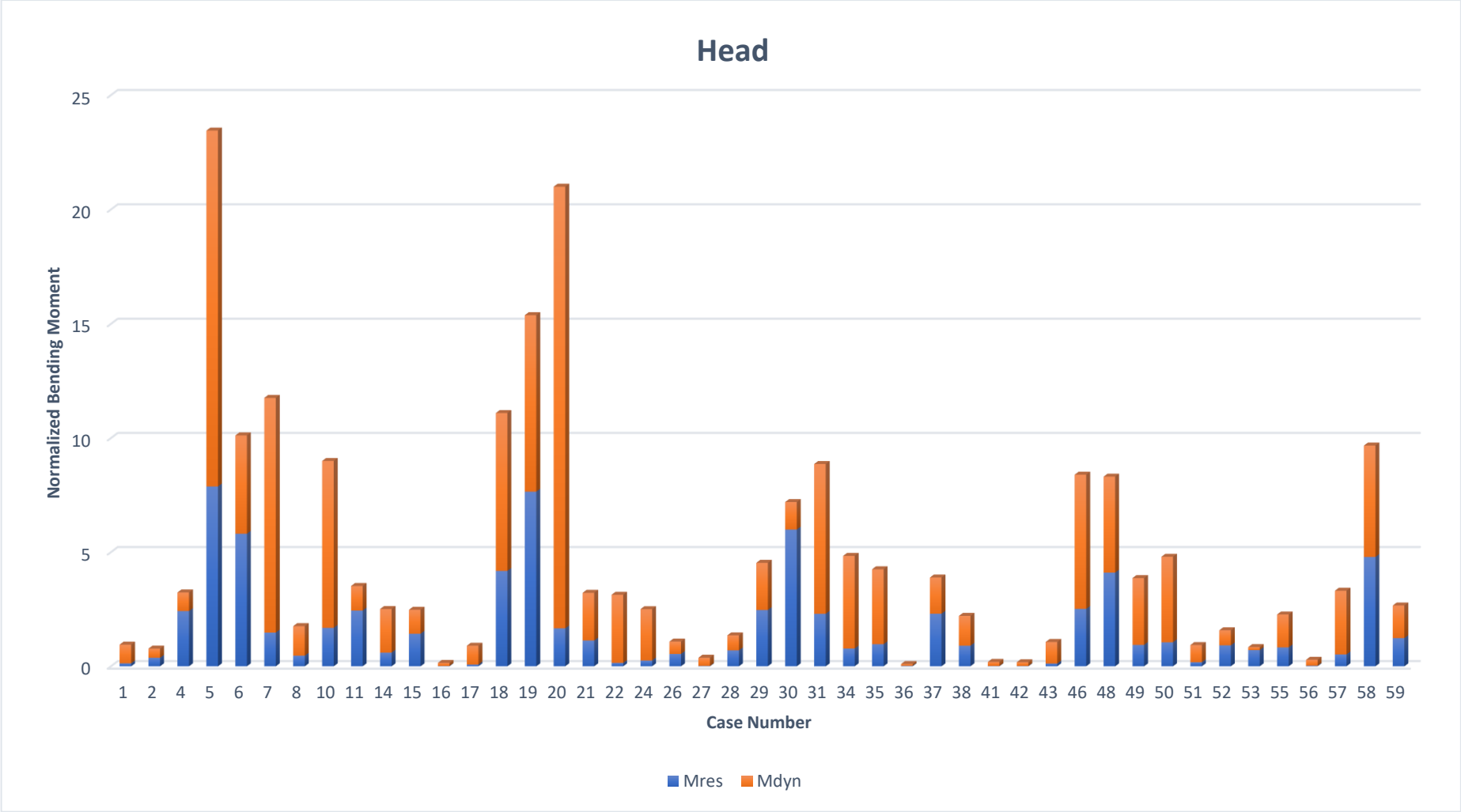

Figure 7.66: Comparison of the dynamic with the residual component of the kinematic bending moment at the head of the pile. The orange colour corresponds to the dynamic component and the blue to the residual component.

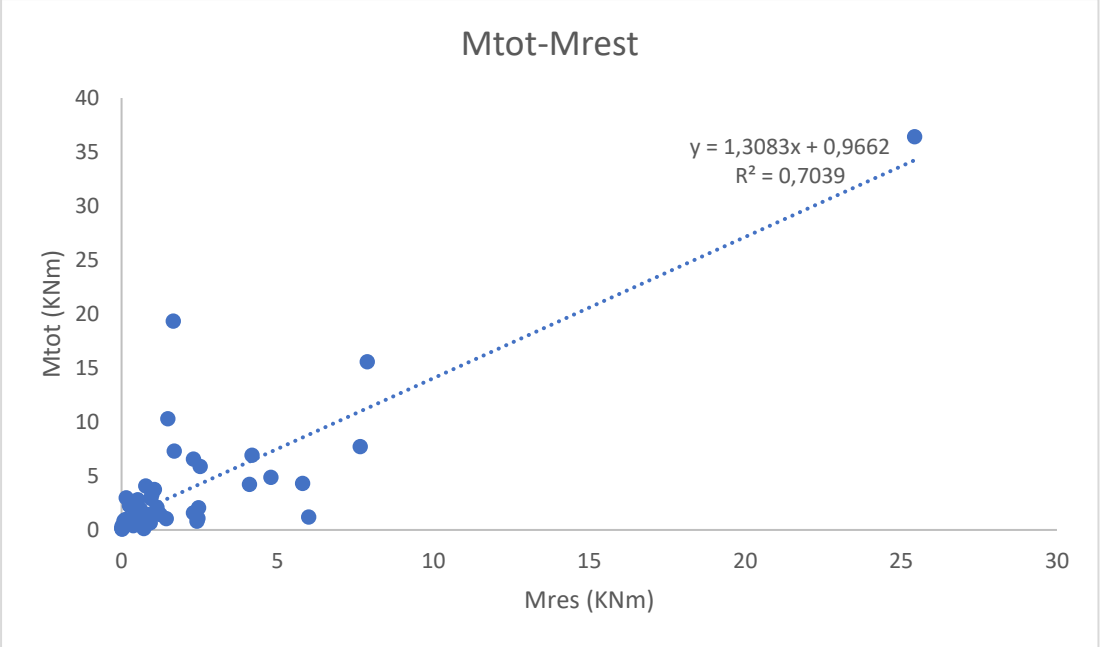

Figure 7.67: The relation between the total bending moment and the residual part for the head of the pile.

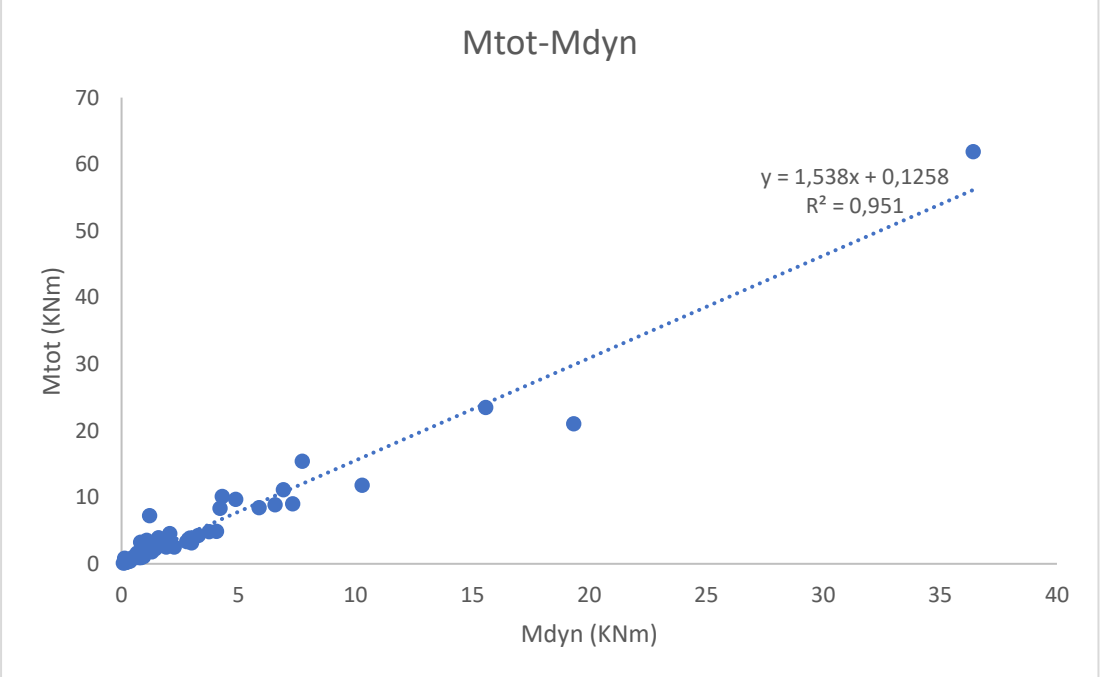

Figure 7.68: The relation between the total bending moment and the residual part for the head of the pile.

From the above figures (7.62-68) a conclusion can be made for the residual and dynamic part. The dynamic part is much bigger than the residual part in the case of interface, instead for the head of the pile the residual part has a greater impact. This difference between the two critical regions of the pile, head and interface, is a result of the displacements of the pile alongside it's length. The bigger deformations occur at the surface of the soil, meaning that the soil plasticizes much more at the region closer to the head, leading to higher residual moments. This can be also seen from the derived equations, where the constant terms (e^m) is significantly larger for the case of the residual moments in head.

7.3.5 Conclusions

- The amplitude of the excitation is of great importance in the case of non-linear analyses. From figure 7.18 it can be easily be distinguished that as the amplitude of the excitation increases, the differences between the linear and the non-linear analysis increase. The soil non-linear response is being enhanced by the two governing parameters of the problem: Shear velocity ratio (V_{s2}/V_{s1}) and relative stiffness ratio (E_p/E_{s1}). Both these parameters are affected by the non-linear soil behavior. As the amplitude of the excitation increases the deformations inflicted on the soil surrounding the pile increase, meaning that the plastic deformations of the soil increase. This accumulation of deformations decreases the soil shear modulus G (G-γ curves), meaning that the E_{s1} in the first parameter will increase also. For the shear velocity ratio, the degradation of the shear modulus for the upper soil layer is higher compared to the deeper one, indicating that the reduction will be higher than that of the V_{s2}, therefore the velocity ratio increases as excitation

- Shear velocity ratio can have a positive aspect in the case of non-linear analyses. The analyses revealed that as V_{s2}/V_{s1} increases the residual part of the moments either decreases or in some cases fades away. This can be explained by thinking about how the motion of the pile changes with increasing shear velocity ratio. The second soil layer acts as a restraining force to the pile which leads to lower displacements at the head and the interface of the pile. This is an important effect of the shear velocity ratio that contradicts with the linear case, where it has only a negative effect in the bending moments especially for the case of the interface.

- Due to Softening of the soil surrounding the pile, the critical area around the interface depth for the bending moments becomes wider. That is a result of the plastic shakedown mechanism, in higher amplitudes of excitation the soil around the pile at the interface depth softens, meaning that for each cycle a bigger volume of soil is needed to counter the forces from the pile to the soil. Another thing to notice is that the forces that the pile inflicts to the soil are the same but the soil around the pile

has lost a part of its strength, meaning that the soil volume energized from the passive forces must be bigger

- In order for the soil pile system to reach its steady state response a number of cycles is needed. This number of cycles is a function of: 1) excitation intensity 2) shear velocity ratio 3) individual maximum shear modulus of each soil layer 4) Interface depth (as the interface depth increases the length of the pile embedded in the soft soil increases benefiting the non-linear soil behavior.

8. Non-Linear analyses in time domain

8.1 Introduction

In this chapter the motion of the pile in the case of time domain analyses will be studied, using accelerograms from past earthquakes that happened in Greece and other parts in the world. The purpose of these analyses is firstly to see the response of the pile and secondly to validate the expressions that were presented in chapter 7.

8.2 Time-domain analyses

The accelerograms that were used can be seen in the figures 8.1-8.4

Kobe-1995 (NorthSouth)

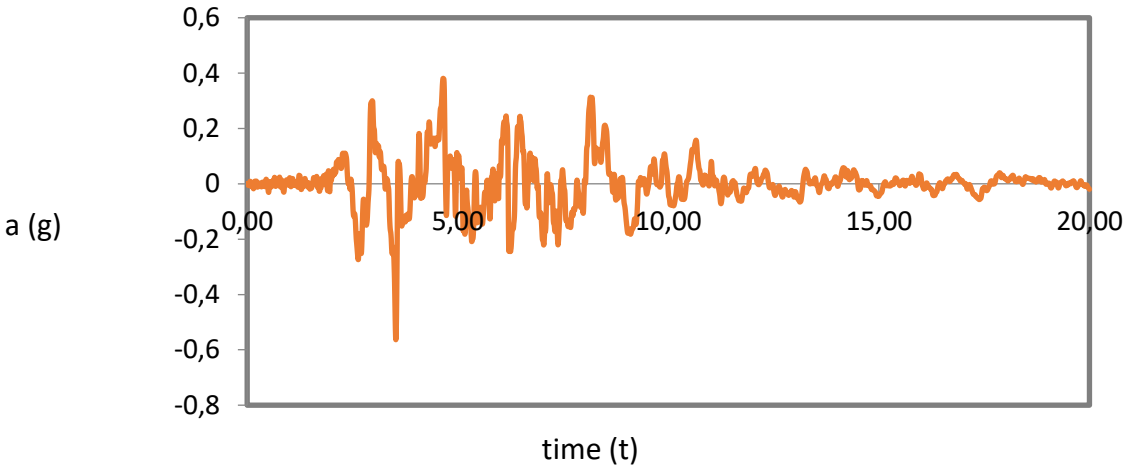

Shakarya-1999

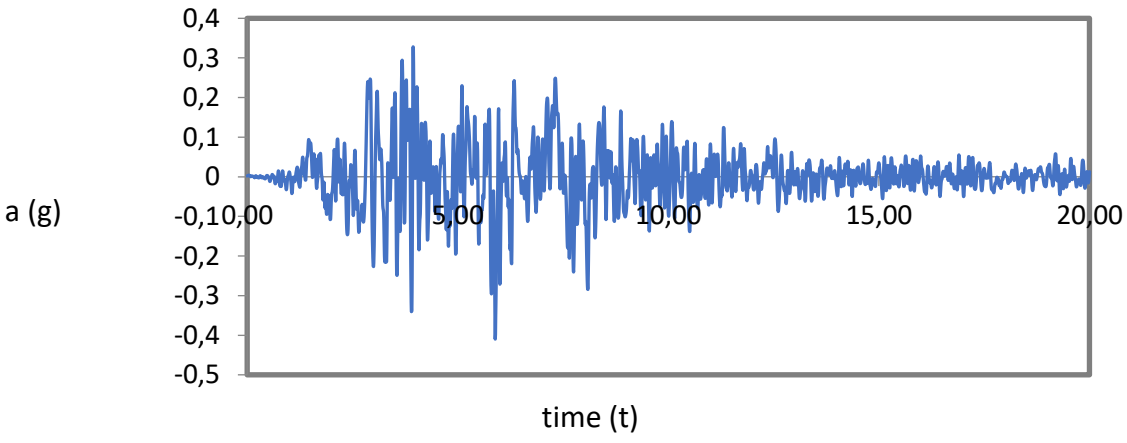

Figure 8.1 Port and Shakarya accelerograms that were used for the analyses

Kalamata-1986 (NorthSouth)

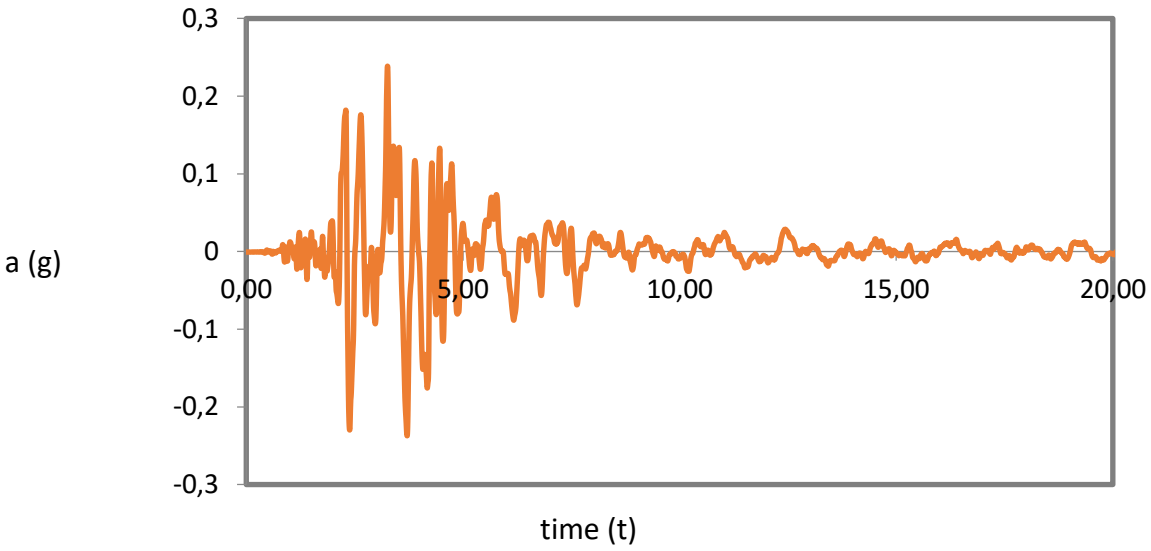

L'Acquila-2009

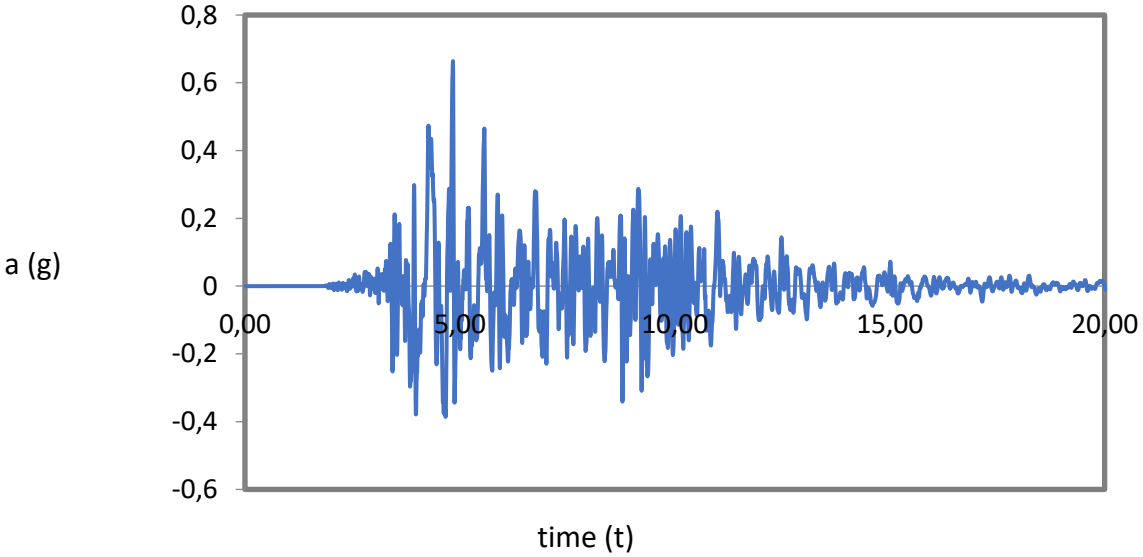

Figure 8.2 Kalamata and L'Acquilla accelerograms that were used for the analyses.

Aigio-1995

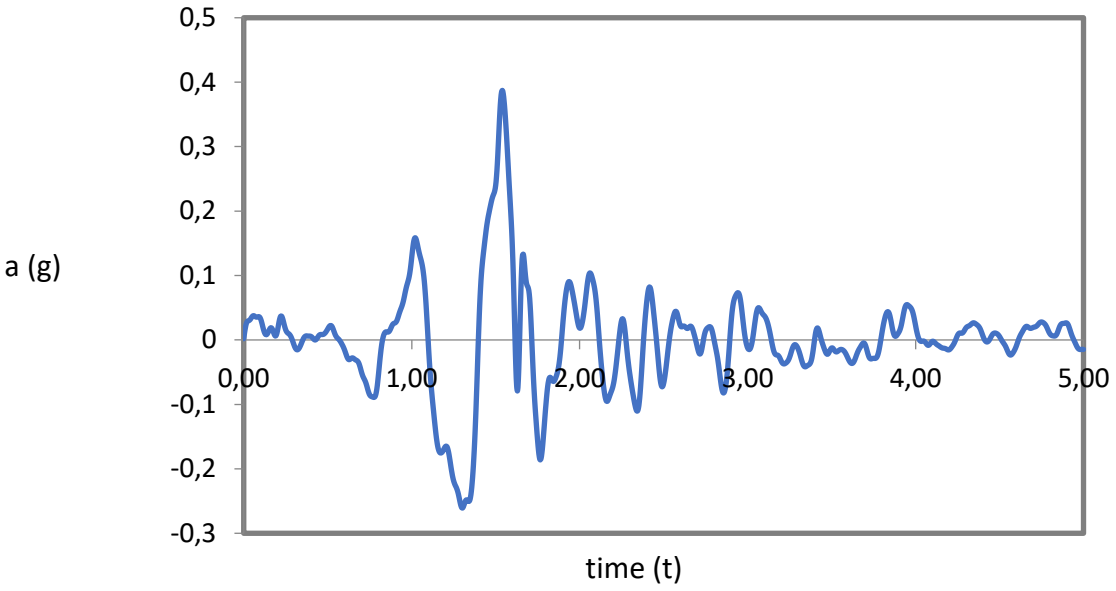

JMA-1995

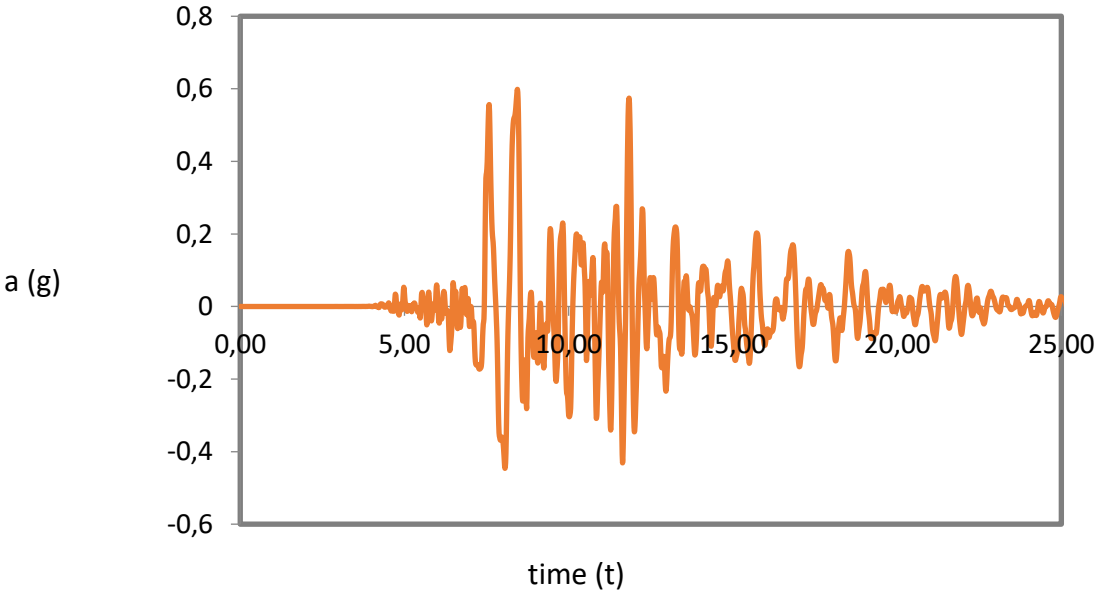

Figure 8.3 Aigio and JMA accelerograms that were used in the analyses.

Corinth-1981

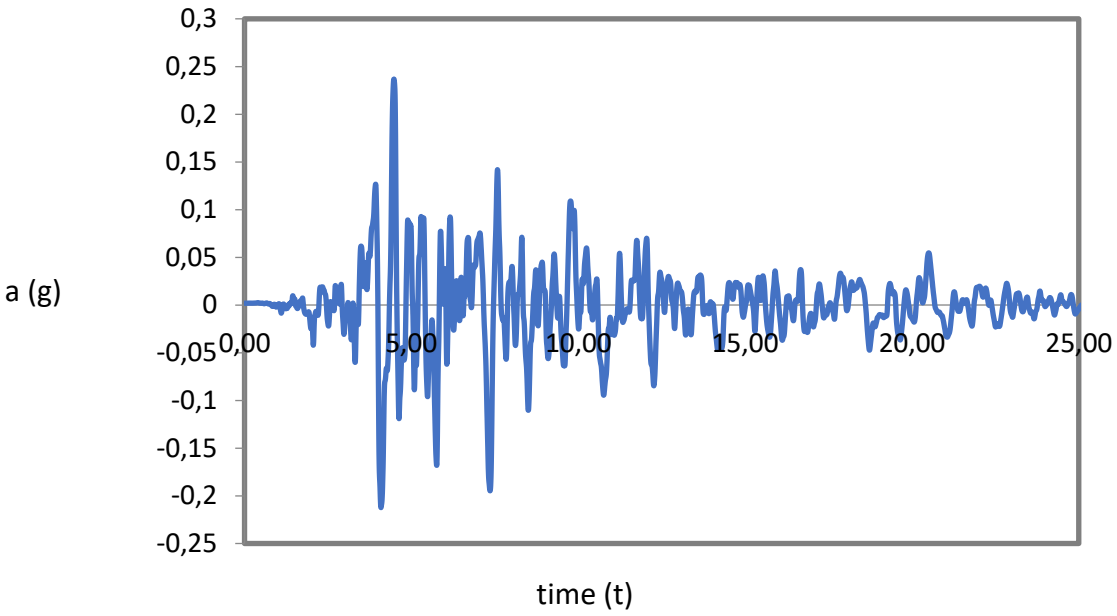

Pyrgos-1993 (Longtidunal)

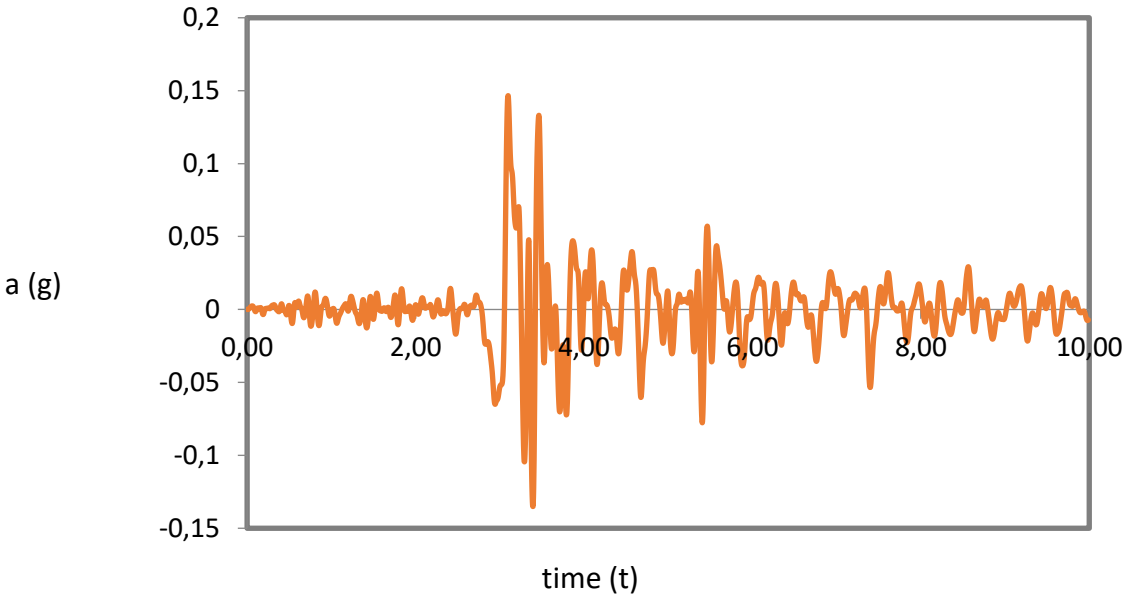

Figure 8.3 Corinth and Pyrgos accelerograms that were used in the analyses.

Ipinia-1980

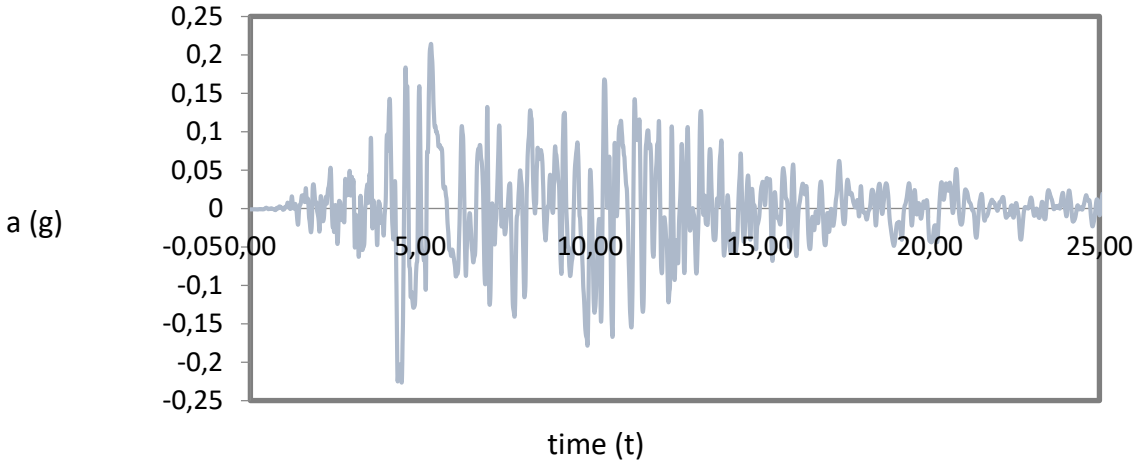

Figure 8.4 Ipinia accelerogram that was used in the analyses.

The specific accelerograms were selected to represent a wide spectra of amplitudes, predominant periods and number of corresponding harmonic cycles. Two questions were raised though, what is the predominant period that must be the input for the equation. There are three different ways to evaluate the predominant period of the accelerogram in question, which are:

1) Equal to the period that coincides with the peak of the Acceleration Spectra
2) Equal to the period that coincides with the peak of the velocity spectra.
3) Equal to the mean period of the accelerogram.

The second question is about the transformation of the accelerogram to corresponding harmonic cycles. An expression of the literature will be used, where:

$$n_{eq} = \frac{\pi^2 \int_0^t |v(t)|\, dt}{a_{ff}\, Tp^2}$$

In which a_{ff}=PGA of the accelerogram and T_p: predominant period of the accelerogram. In this case the three different periods were tested, that led us to pick the 3rd choice, the mean period of the accelerogram. Using the other two periods the number of cycles were too high to even try to continue. (in some cases, more than 20 harmonic cycles).

Following are the characteristics about the accelerograms that were used in the time-domain analyses:

Accelerogram	PGA (g)	Tp (s)	Equivalent harmonic cycles
Kobe	0.56	1.04	4.88
Sakarya	0.41	0.40855	8.36
Kalamata	0.24	0.59	7.71
L'Acquila	0.66	0.333	10.73
Aegion-rock	0.39	0.543	2.16
JMA	0.6	0.65	8.3
Corinth	0.24	0.7	10.32
Purgos	0.15	0.29269	6.66
Ipinia	0.22	0.68	15

Table 8.1: Accelerograms that were used for the analyses with their characteristics

For each accelerogram a case was selected from the 60 that were performed in the last chapter, so that the T_p/T_{s1} is close to the values that have been tested meaning between 0.75-1.5 . In the Table 8.2 are the characteristics of each analysis that was performed:

Accelerogram	γ_1	d	L	H_1	V_2/V_1	N_{eq}	T_p/T_{s1}
Kobe	20	0.6	30	20	5	5	1.25
Sakarya	23	0.6	30	15	3	8	0.76
Kalamata	17	1.5	20	10	5	7.7	1.03
L'Acquila	23	0.6	15	7.5	3	10	1.22
Aigio	23	0.6	30	15	3	2.2	1
JMA	21	1	15	10	5	8.3	1.14
Corinth	13	1.5	30	15	5	10.3	0.86
Purgos	23	0.6	15	7.5	3	6.5	1.08
Ipinia	23	0.6	30	15	3	2	1

Table 8.2: Analyses that were performed with their characteristics.

Results of the analyses in terms of envelope of bending moments and diagrams of Moments to analysis steps. Also the results using the equations 7.3 and 7.6 are shown. For the equation for each analysis the peak aground acceleration was needed, which was measured through the analysis. An example is presented in Figure 8.4

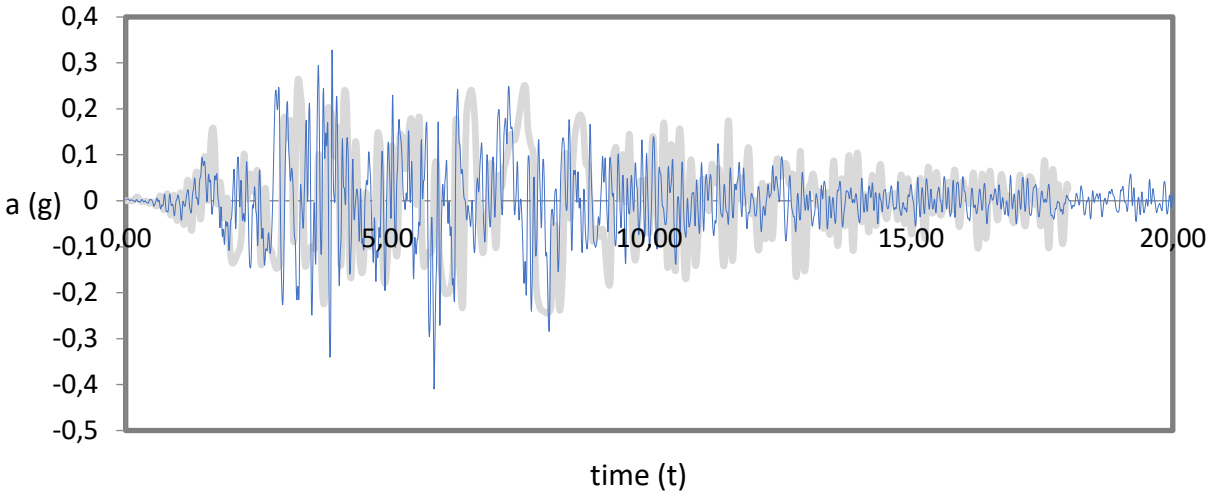

Figure 8.4: Sakarya accelerograms, the blue is the accelerogram that was used at the rock as excitation and the grey one is the one measured at the top of the soil.

Kobe-1995

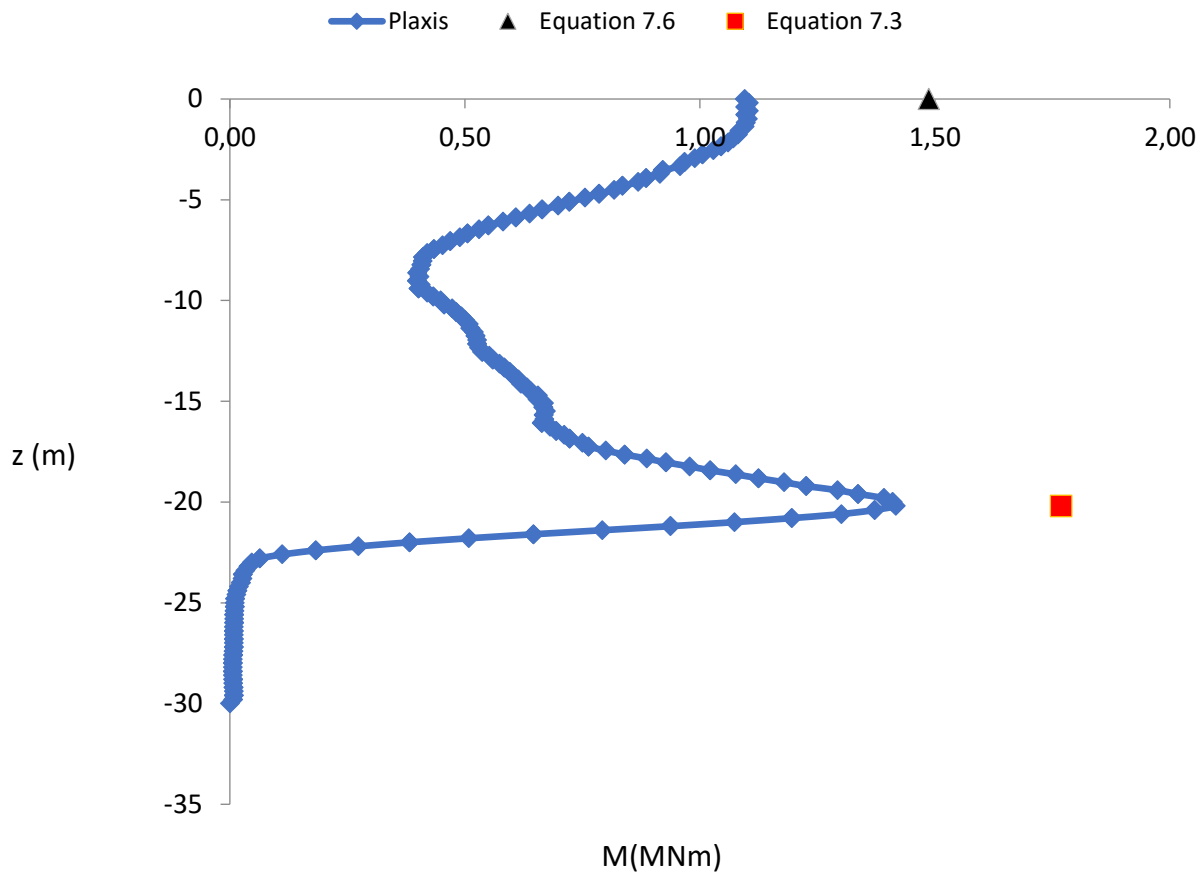

Figure 8.5: Envelope of bending moments for the Kobe excitation, also the results from the equations are shown.

Comments: For this excitation we can see the bending moments in figure 8.5. Due to the high shear velocity ratio equal to 5 the bending moments are higher in the interface than the head, something that coincides with the equations results. The equation over-evaluates the moments both for the head and the interface, with the highest error at the head at 35%. Looking at the Figs 8.6-7, one can point out that there is no residual moment at the case of the interface whereas in the head the residual moment is equal to 400 KNm. This can be justified by the high shear velocity ratio. At the pile's head the soil has much lower strength than the depth of the interface, where the much stiffer 2nd layer acts as a restrain force reducing the permanent displacements. Thus the interface is "saved" by the high velocity difference in the two soil layers. Also the fact that the interface is that deep, leaves the biggest part of the pile in the loose soil, enhancing the phenomenon for the head.

Note: Seeing the velocity difference have a positive effect in the physics of the problem is something that differentiates the linear analyses with the non-linear ones in great extent.

There is also a positive side in the two-layered profiles with significant differences in the soil characteristics .

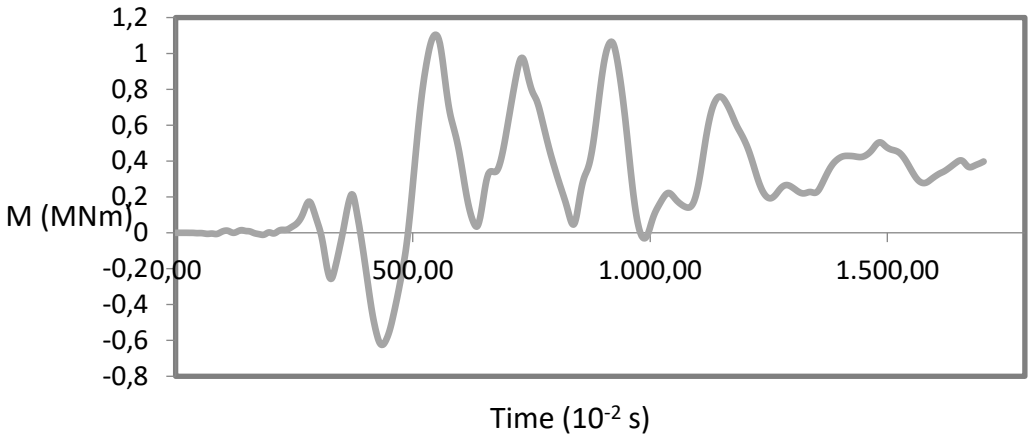

Figure 8.6: Moments-Time diagram for the head of the pile and Kobe excitation.

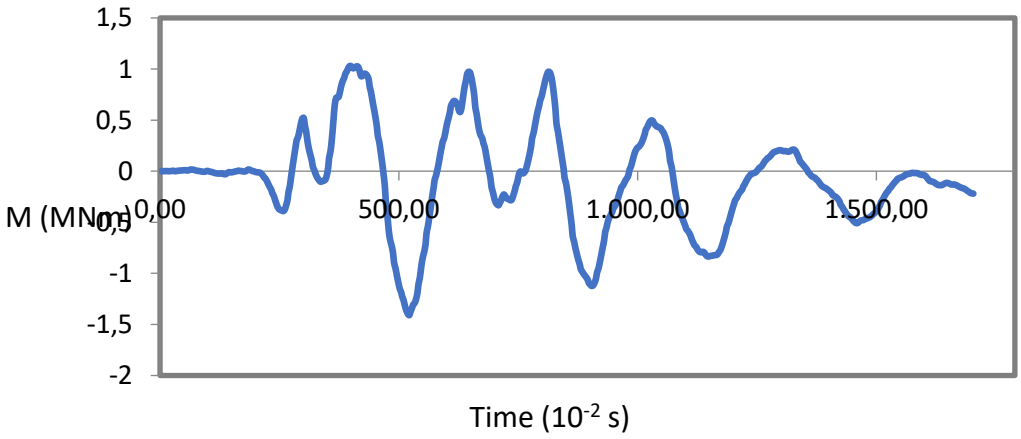

Figure 8.7: Moments-Time diagram for the interface and Kobe excitation.

Sakarya-1999

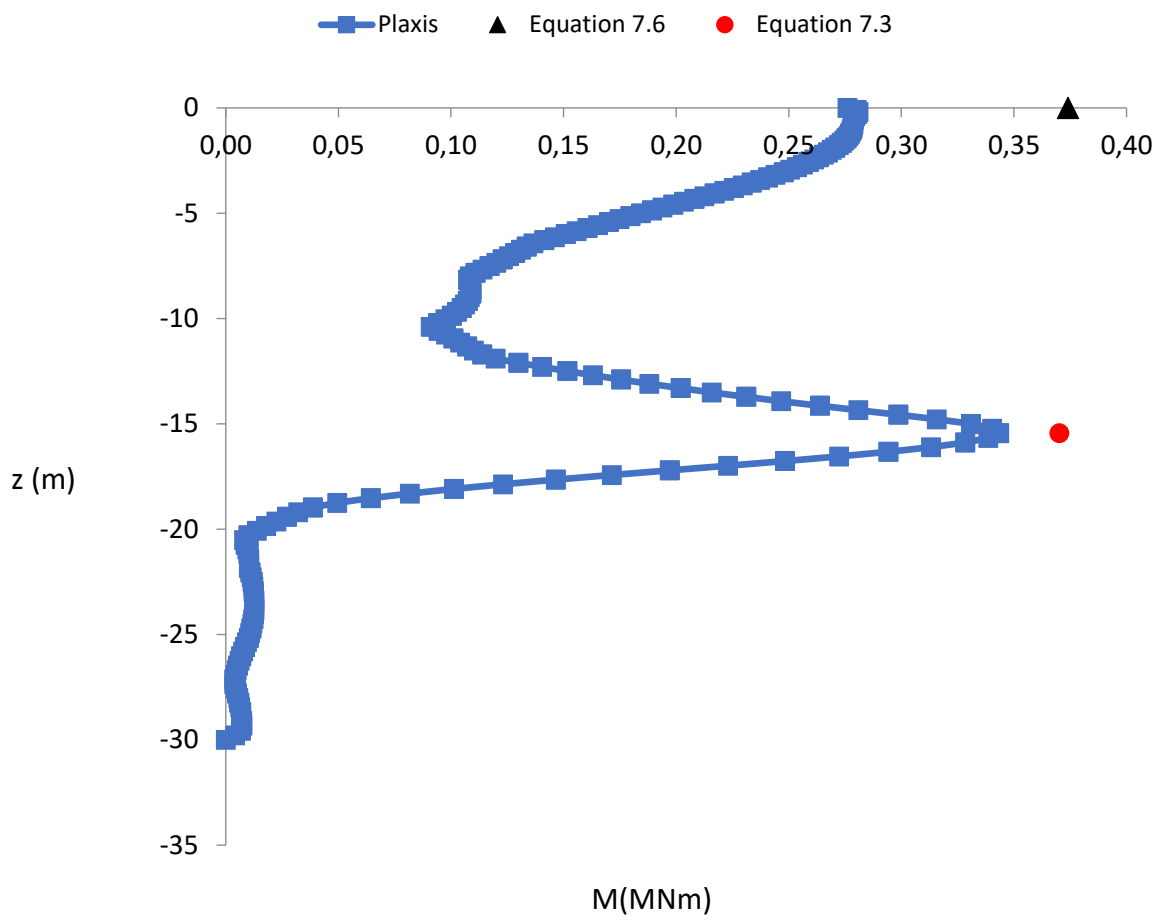

Figure 8.8: Envelope of bending moments for the Sarakya excitation, also the results from the equations are shown.

Comments: In this case too, the maximum moment is placed at the interface due to the difference in shear velocity equal to 3. The equation again over-evaluates the bending moment for the head and the interface with highest deviation at the head equal to 33%. Residual parts for the bending moment occur both at the head and the interface with values 55 and 75 KNm correspondingly. A big difference with the Port analysis, that is a result of two things: a) the smaller discrepancies in the soil characteristics between the two layers and b) the interface is at 15m this time, meaning that the length of the pile in the “softer” soil is smaller, reducing the displacements at the head.

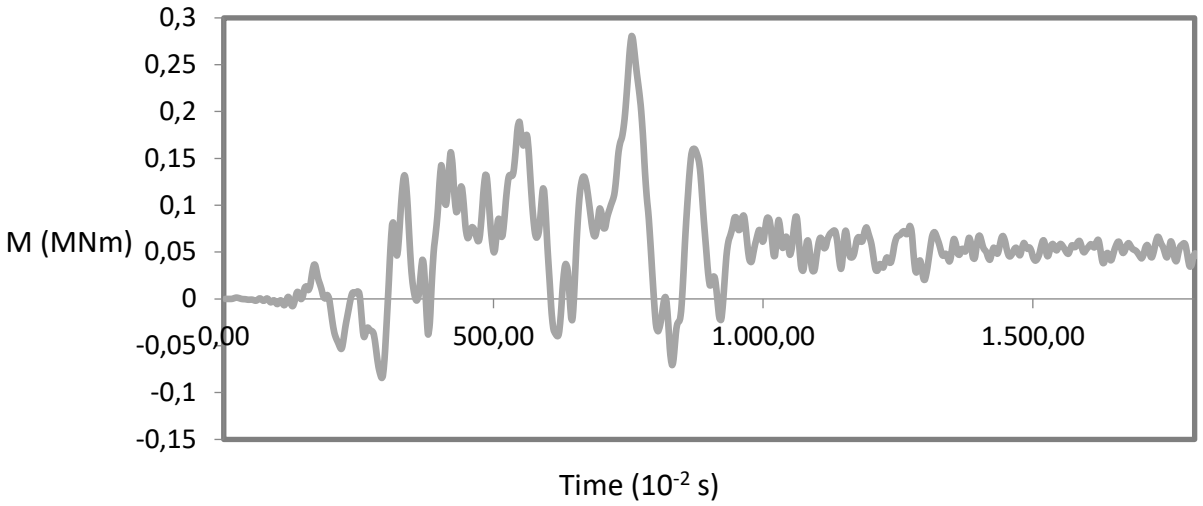

Figure 8.9: Moments-Time diagram for the head of the pile in the Sakarya excitation.

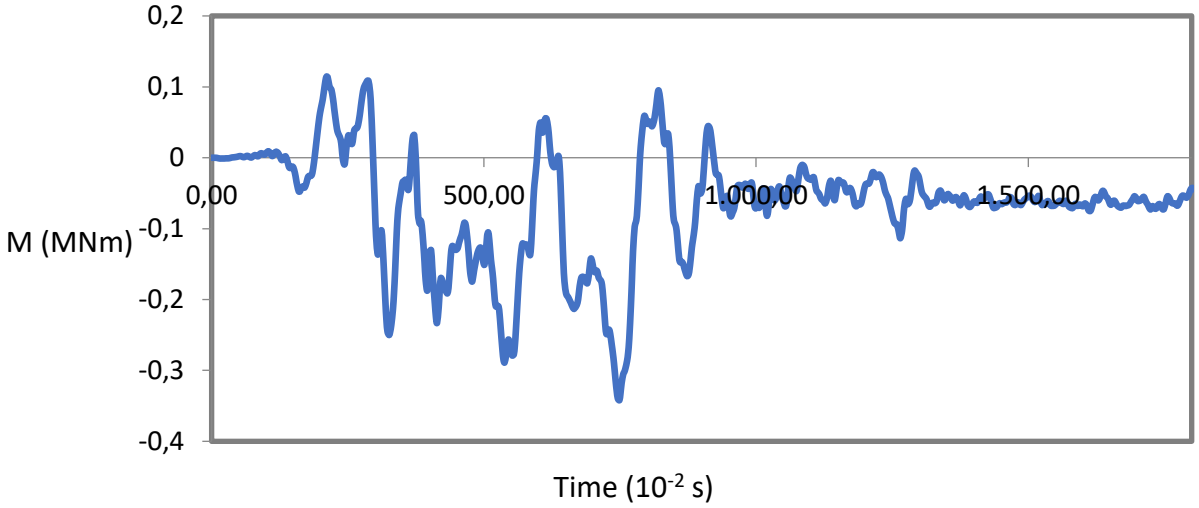

Figure 8.10: Moments-Time diagram for the interface in the Sakarya excitation.

Kalamata-1986

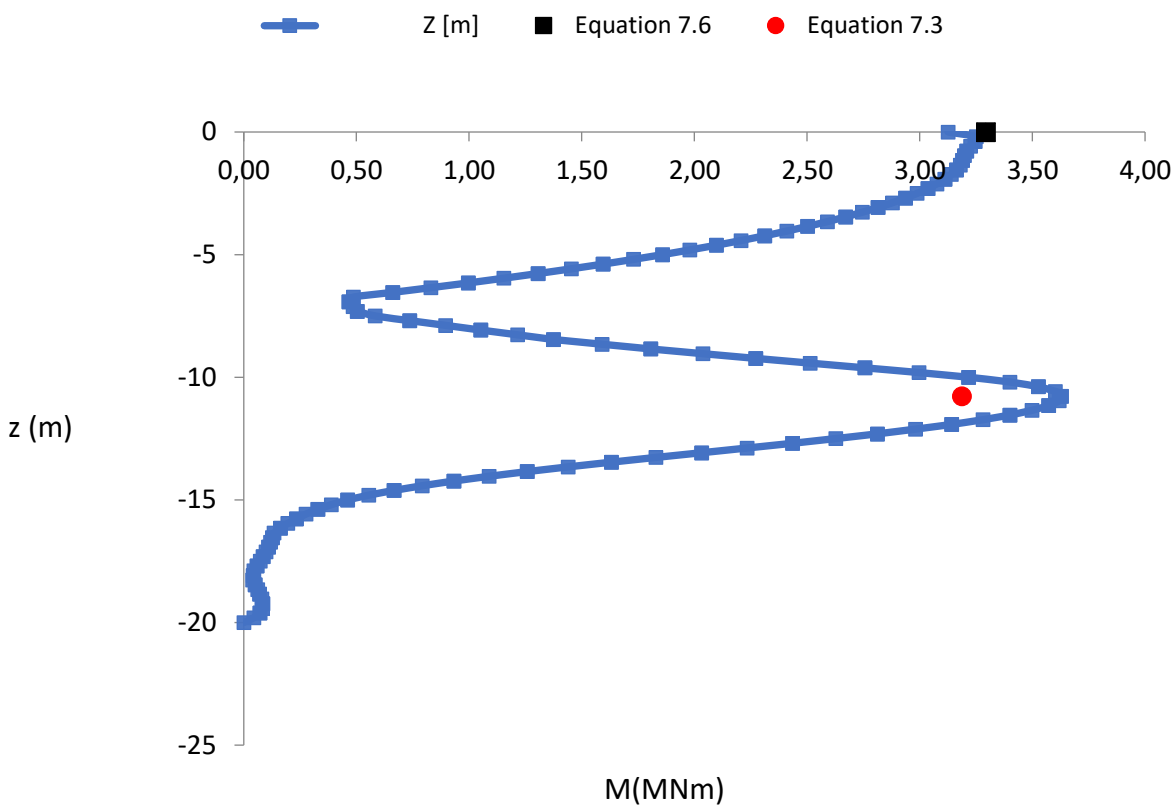

Figure 8.11: Envelope of bending moments for Kalamata excitation, also the results from the equations are shown.

Comments: Kalamata's excitation, not as severe as the ones before with a PGA=0.2 g, which can also be seen from the residual parts of the moments where on both cases the residual part is zero. The discrepancies with the equations 7.3 and 7.6 can bee seen in Fig 8.11, with the highest being in the interface equal to 8 %.

Note: The reason why there is no residual moment in this case is the result from the amplitude of the motion. In the two above cases the exctiations were much more severe 0.5-0.6 g thus by also taking in consideration the analyses that were performed in chapter 7 about how the amplitude of the excitation affects the residual parts of the moments one can say for certain that PGA is the cause.

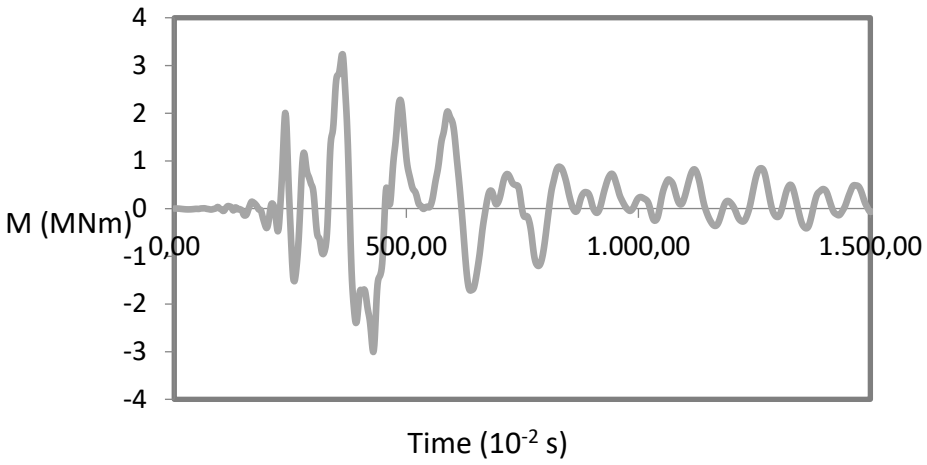

Figure 8.12: Moments-Time diagram for the head in the Kalamata excitation

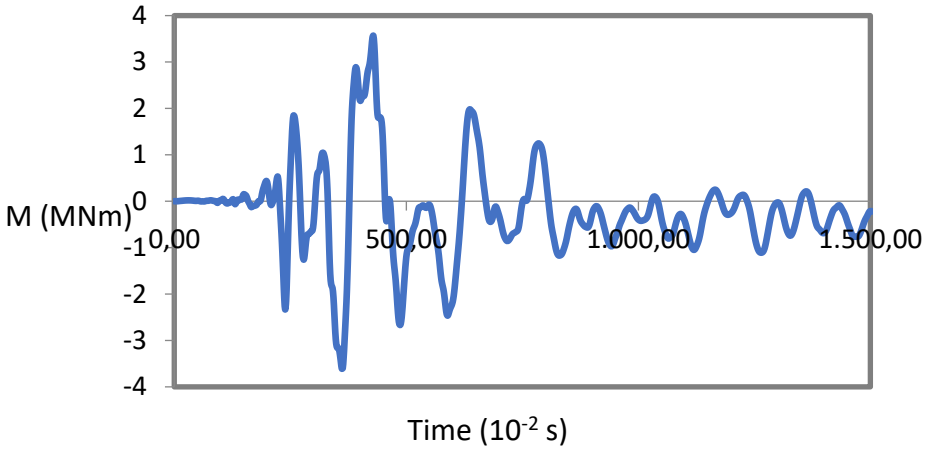

Figure 8.13: Moments-Time diagram for the interface in the Kalamata excitation

L'Aquiila-2009

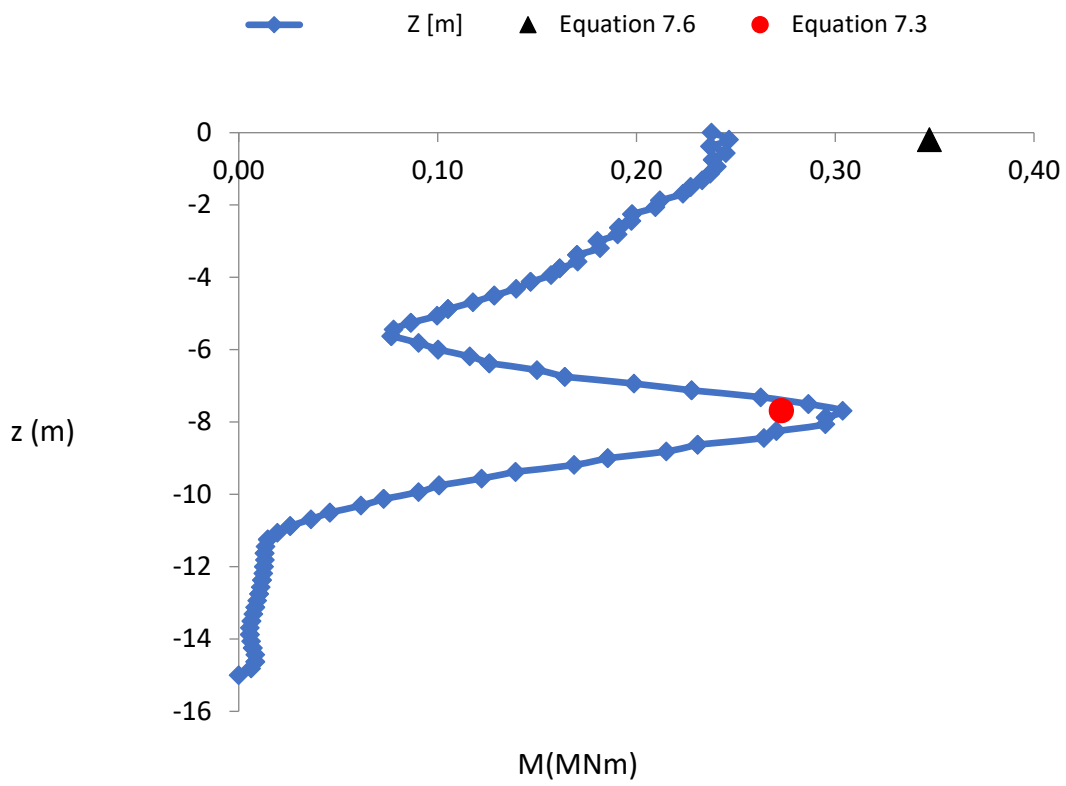

Figure 8.14: Envelope of bending moments for L'Acquila excitation, also the results from the equations are shown.

Comments: The L'Aquila excitation, the most severe excitation from all of the ones that were used for this chapter, with PGA=0.6 g and 11 equivalent harmonic cycles. The proposed equations has failed in identifying that the interface's moment will be larger than the one at the head of the pile. The biggest error is in the head with a 38% while in the interface the equation did quite well. As far as the residual moments, looking at figures 8.15-16 we can see a huge residual moment at head at 125 KNm and a much smaller one at the interface at 35 KNm. This scenario looks exactly like the first excitation; the differences are a result from the much "softer" soil at the head of the pile. The surrounding soil at the pile's head with has two drawbacks with the one at the interface depth: a)much smaller strength (take into account the parabolic curves) b)The displacements inflicted at the head are bigger (no 2nd layer to act as a restraining force and secondly displacements larger at the head). Resulting in the more plasticized reaction at the pile's head.

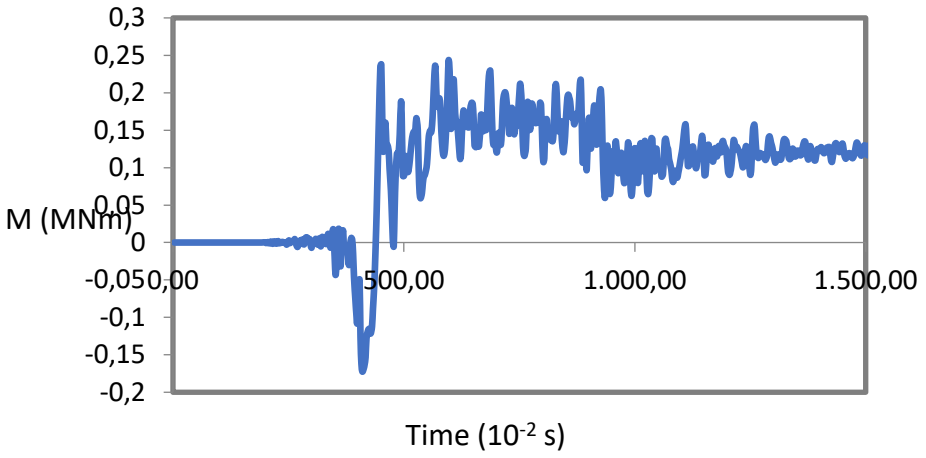

Figure 8.15: Moment-Time diagram for the head in the Kalamata excitation.

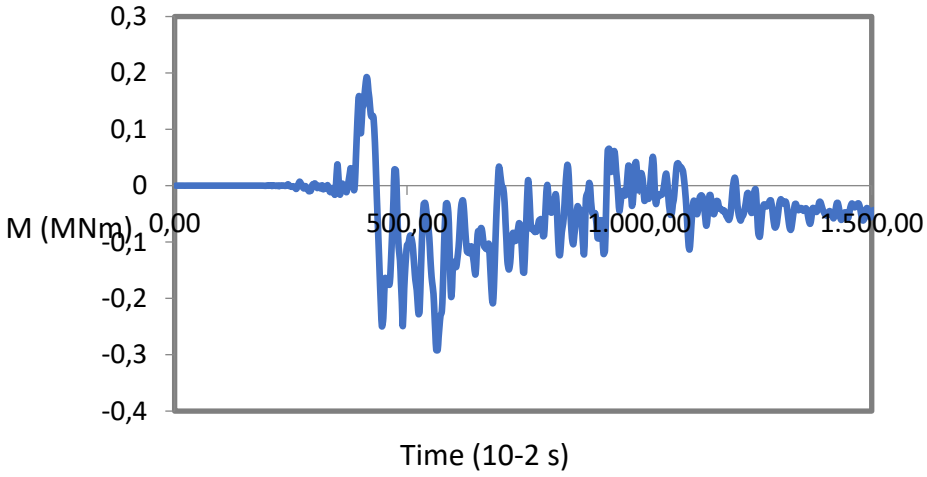

Figure 8.16: Moment-Time diagram for the interface in the Kalamata excitation.

Aigio-1995

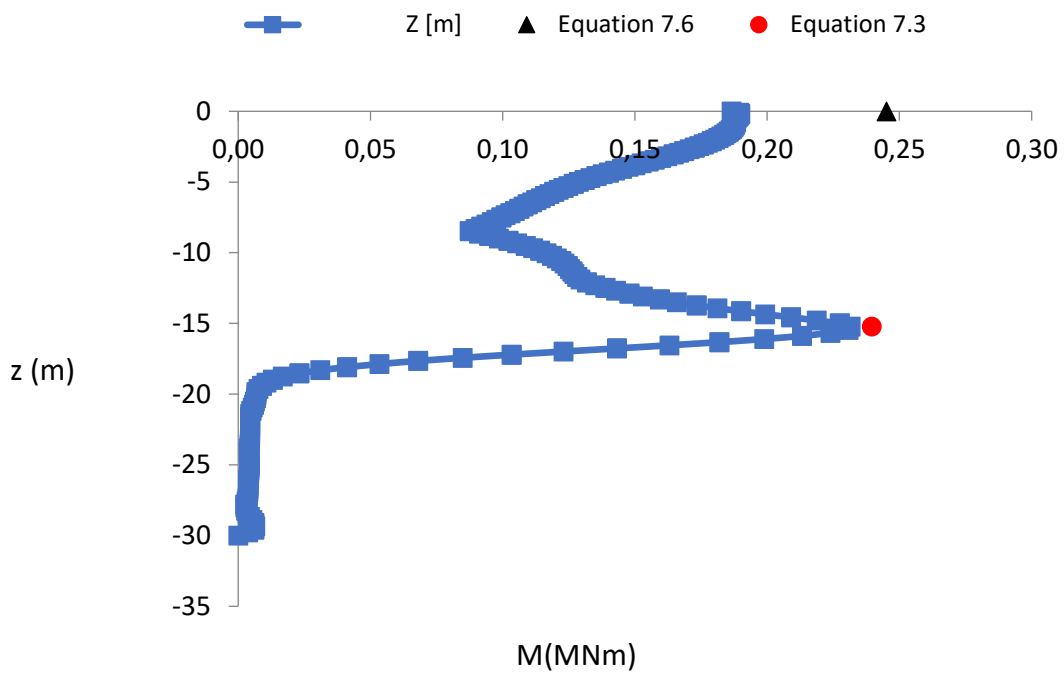

Figure 8.17: Envelope of bending moments for Aigio excitation, also the results from the equations are shown.

Comments: The derived expression overpredicts the moment at the head but at the interface the error is practically zero. The equations failed to understand that the moment at the head will be lower than the interface. Other than that both the head and the interface had a residual moment 100 KNm for the first and 55 KNm for the later. Notice that even for only 2 equivalent harmonic cycles of excitation there is a residual moment. The fact that a higher value of M_{res} is developed at the interface is attributed to the lower shear wave velocity contrast ratio (~ 3) compared to that (~ 5) of the previous cases, implying that the deeper soil layer is less compliant allowing for larger displacements of the pile and therefore for larger permanent deformations of the soil.

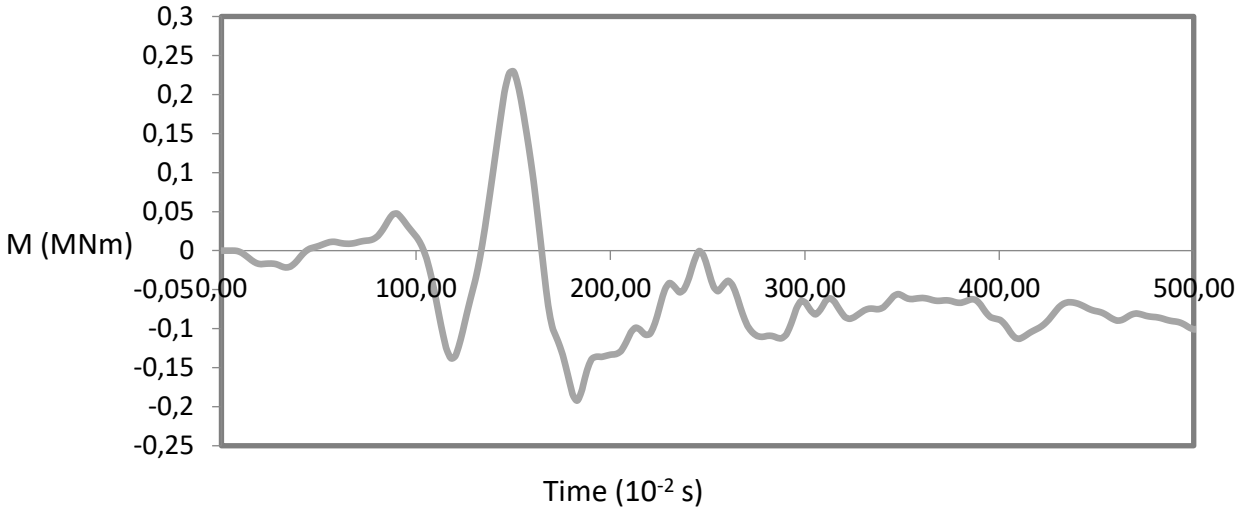

Figure 8.19 Moments-Time diagram for the interface in the Aigio excitation.

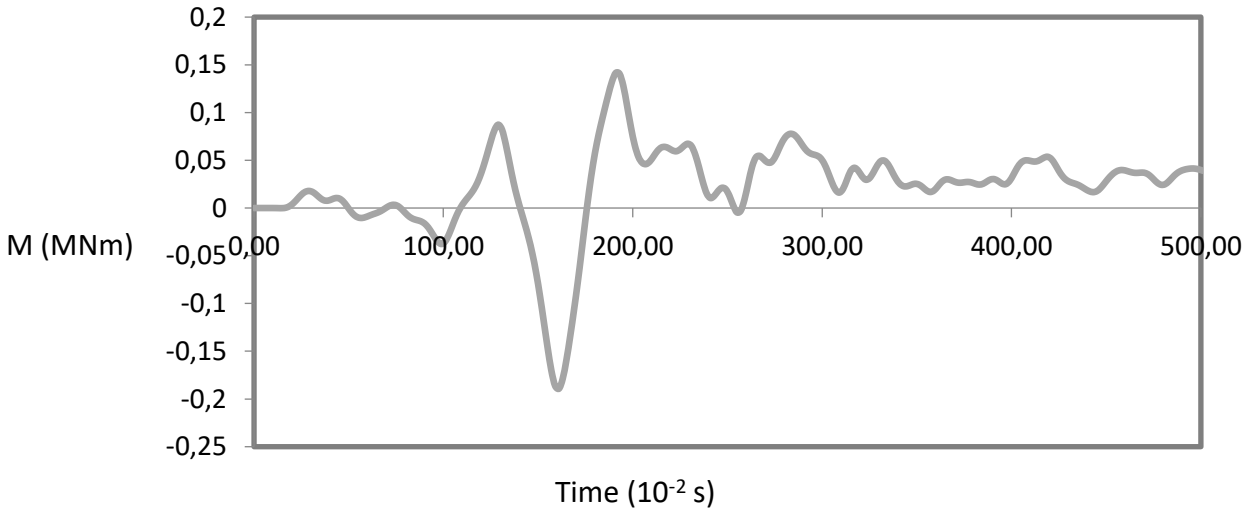

Figure 8.20 Moments-Time diagram for the head in the Aigio excitation.

JMA-1995

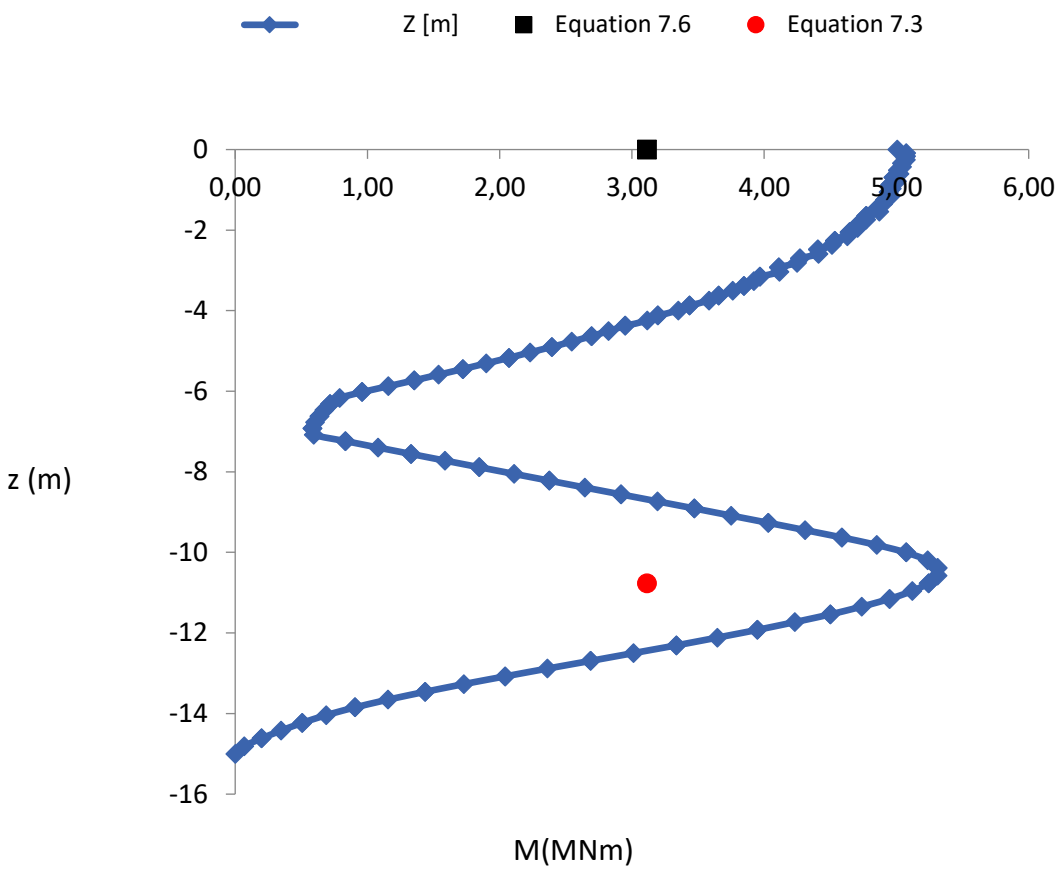

Figure 8.21: Envelope of bending moments for JMA excitation, also the results from the equations are shown.

Comments: The equation significantly underpredicts the response at the head and the interface (almost 45% for the interface). It seems like an intensity miscalculation from the equations part. Residual bending moments are 925 for the head and 800 for the interface, the highest seen till JMA. This excitations intensity is the reason behind this strong total and residual bending moments.

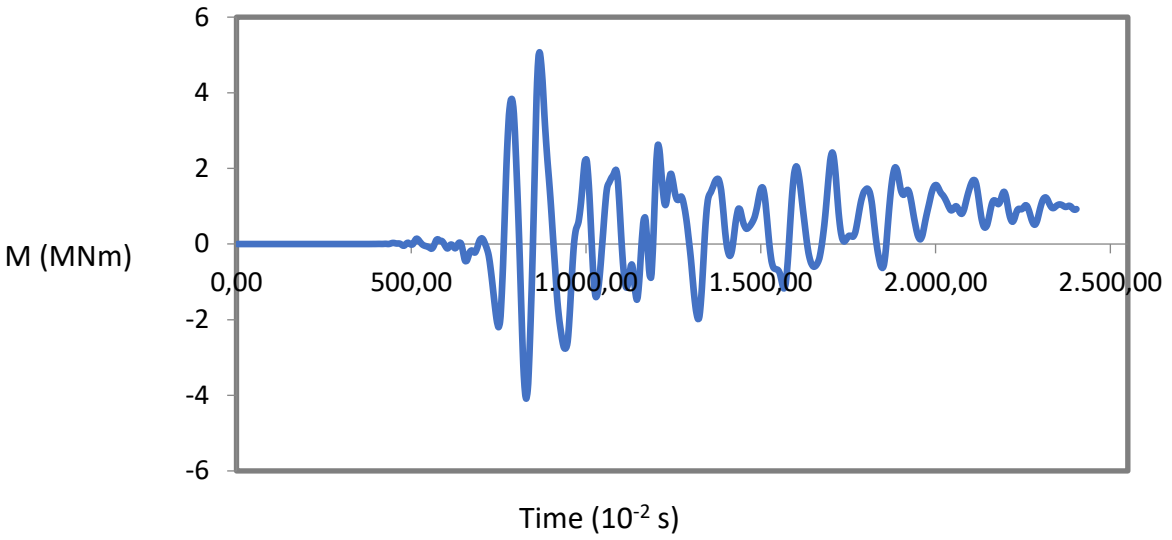

Figure 8.22: Moment-Time diagram for the head in the JMA excitation

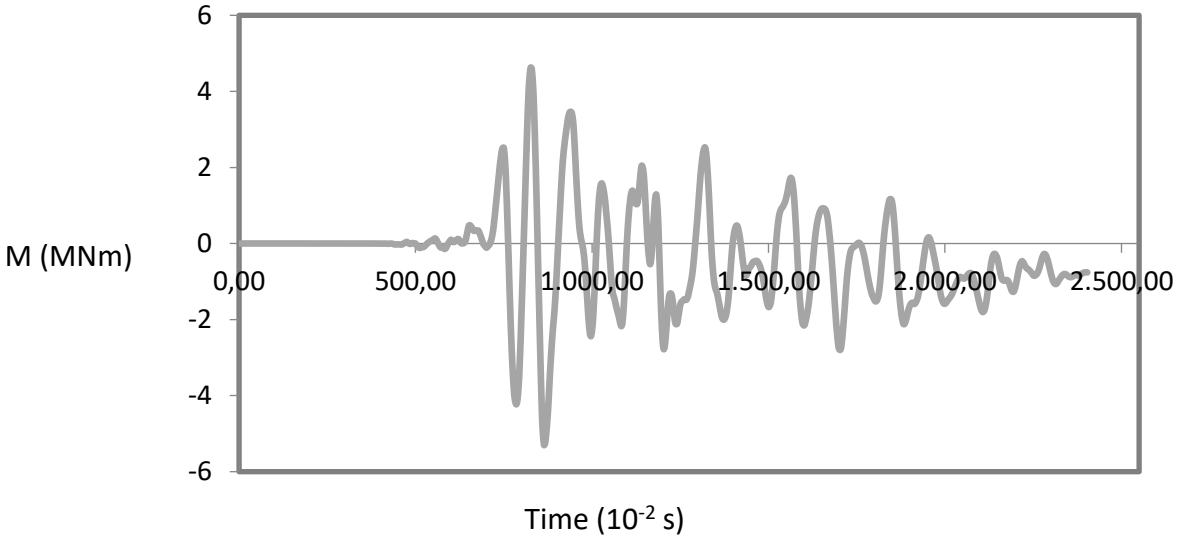

Figure 8.23: Moment-Time diagram for the head in the JMA excitation

Corinth-1981

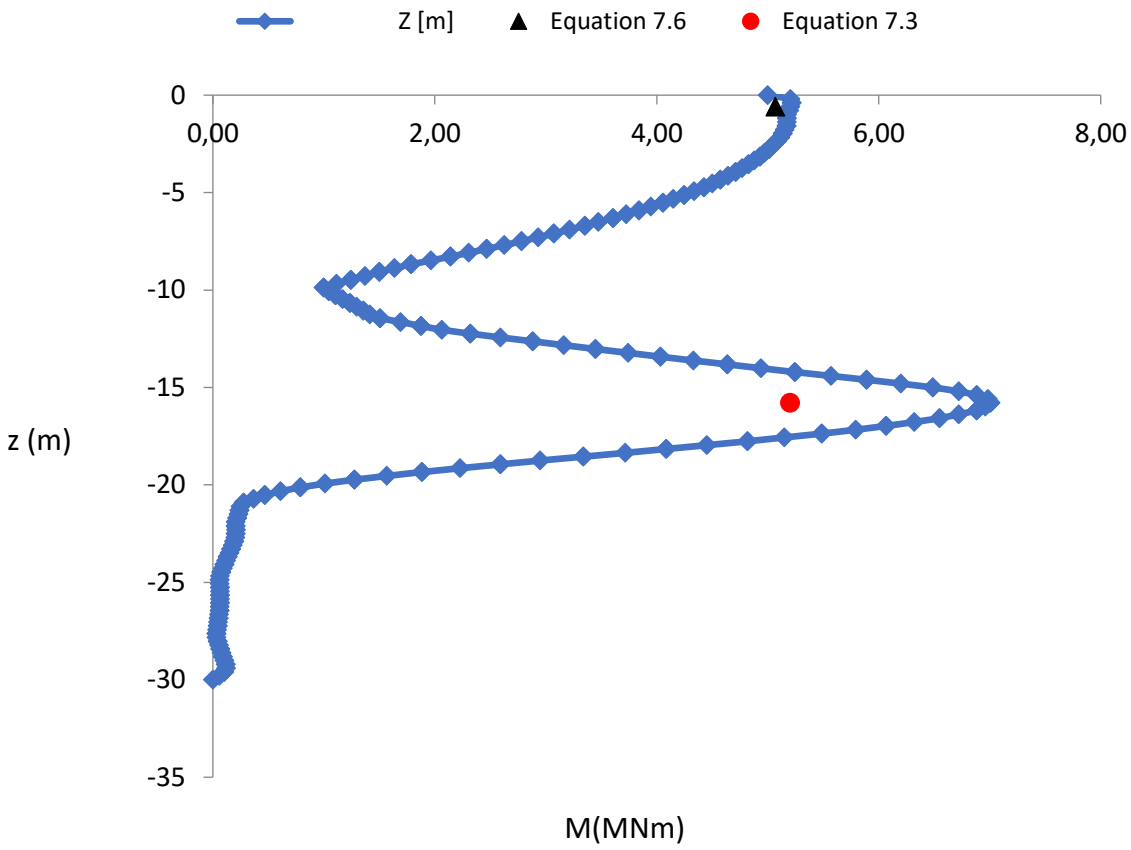

Figure 8.20 Envelope of Bending moments for Corinth excitation, also the results from the equations are shown.

Comments: In the case of the Corinth excitation the moment is again bigger in the interface than the head, coinciding with the equations but the calculated moment at the interface is 25% lower than the moment from the Plaxis. For the residual moments, figure 8.21-22, they appear both at the head and the interface with values equal to 2000 and 2870 respectively.

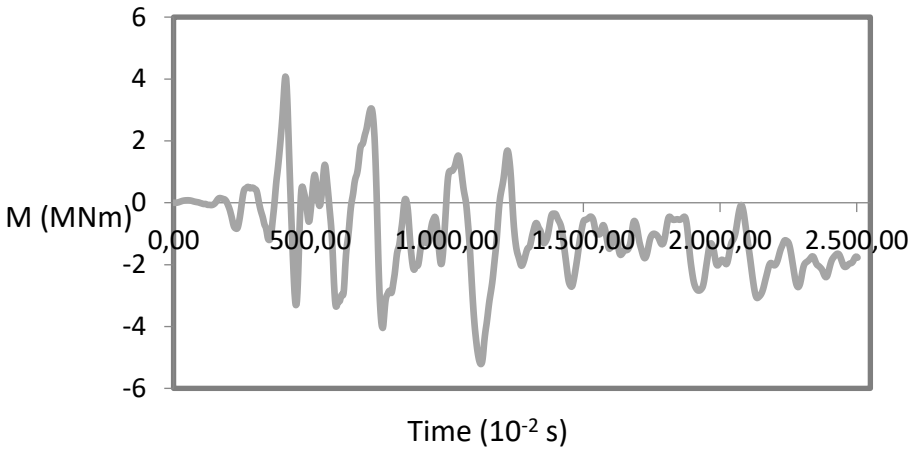

Figure 8.21: Moment-Time diagram for the head in the Corinth excitation.

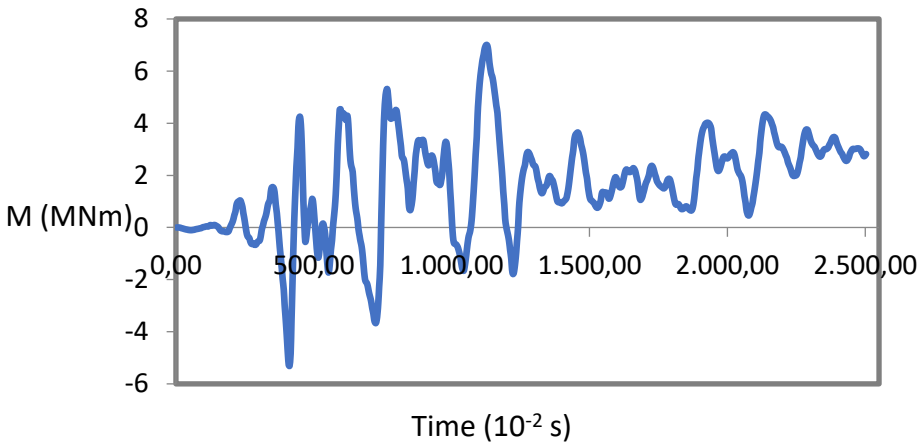

Figure 8.22: Moment-Time diagram for the interface in the Corinth excitation.

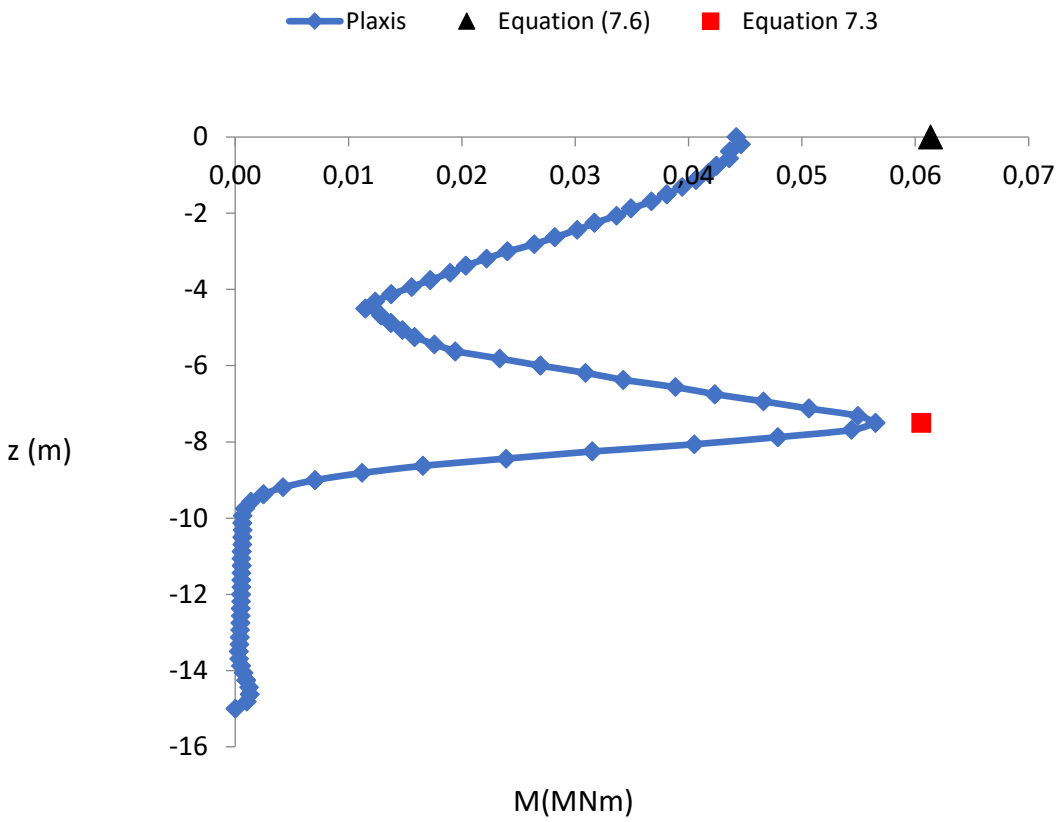

Figure 8.23: Envelope of bending moments for Pyrgos excitation, also the results from the equations are shown.

Comments: Equations overpredicted the moments for both the head and the interface, with highest the error at the head at 24.5%. Also the equations failed at predicting that the moment at the interface will be higher than the one at the head. Other than that for residual moments the pattern is the same as the other analyses. The residual moments are 22 for the head and 18 for the interface.

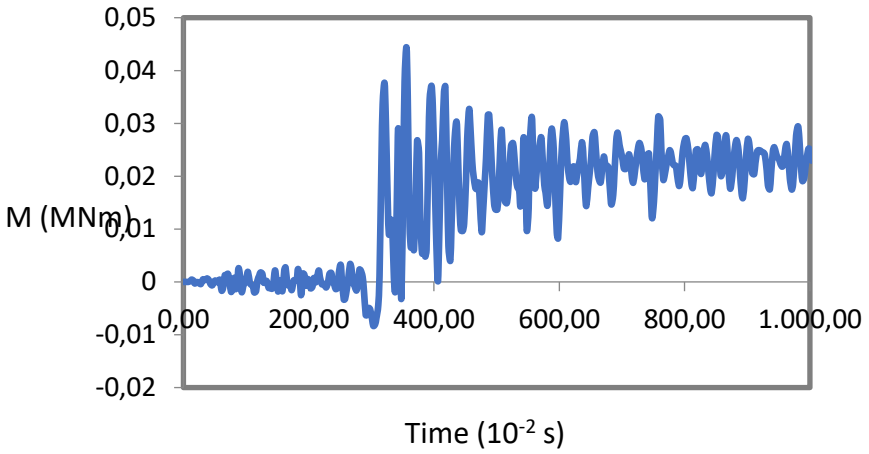

Figure 8.24: Moment-Time diagram for the head in the Pyrgos excitation.

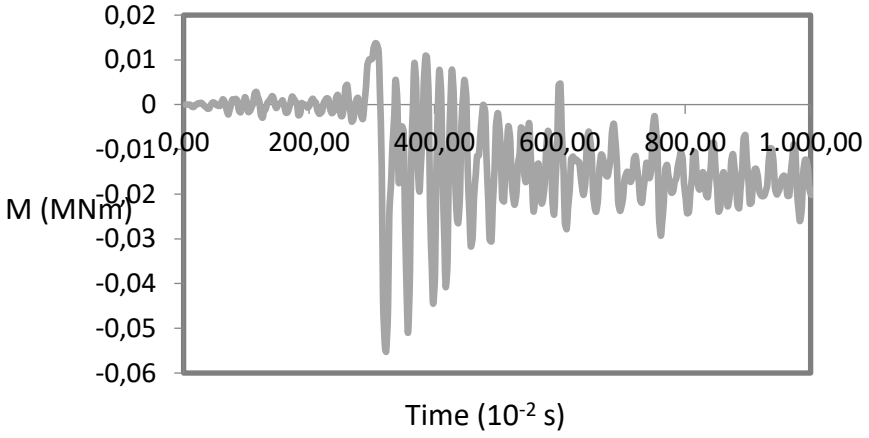

Figure 8.25: Moment-Time diagram for the interface in the Pyrgos excitation.

Ipinia-1980

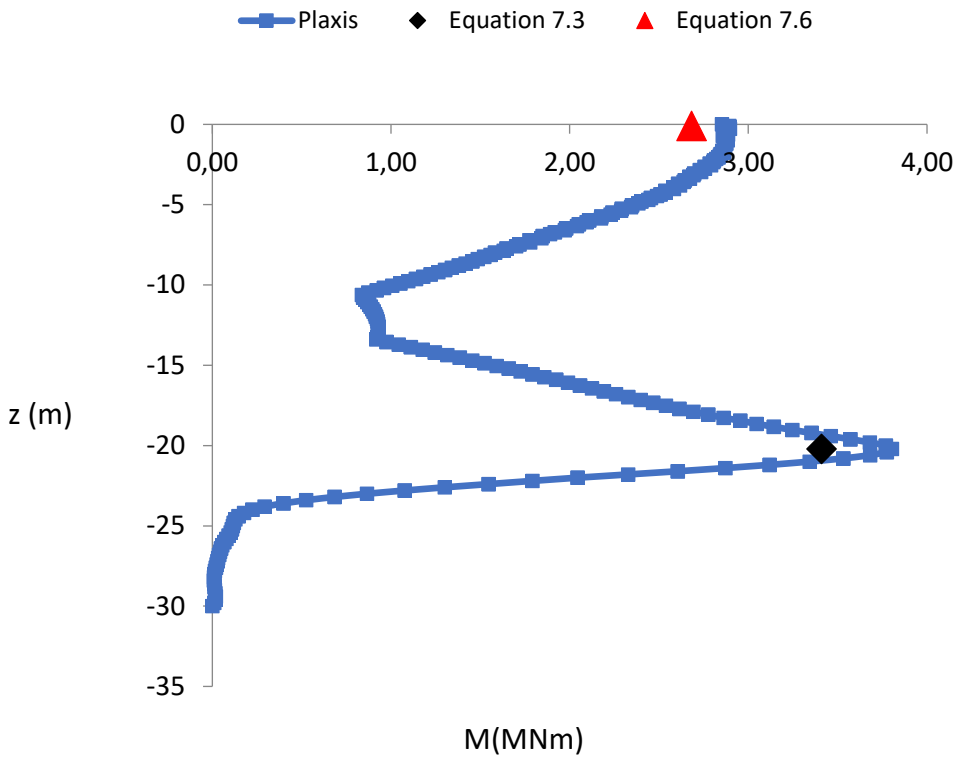

Figure 8.26: Envelope of bending moments for Ipinia excitation, also the results from the equations are shown.

Comments: The equations predicted almost perfectly the maximum bending moments not only in terms of values but also in terms of "pattern". The bending moment at the interface being higher than the head. Other than that zero residual moments for both the head and the interface, which can be explained if we look at the number of cycles which is only 2 , a parameter playing a crucial role for the increase of the "static" part of the moments. Each cycle accumulates deformations around the pile's critical areas increasing the residual moments.

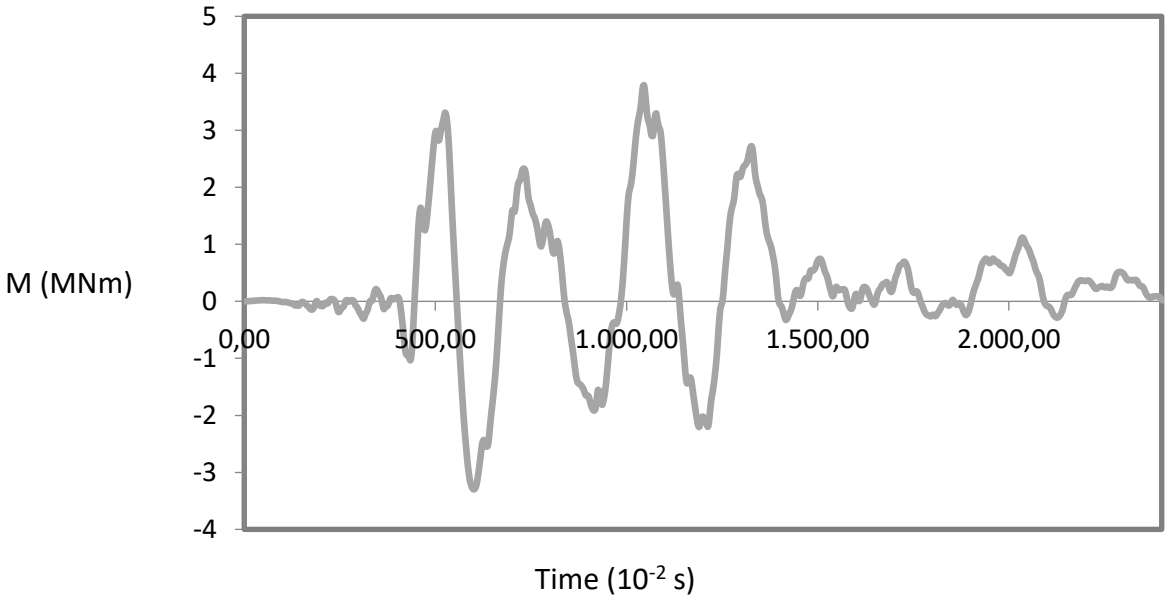

Figure 8.24: Moment-Time diagram for the head in the Ipinia excitation

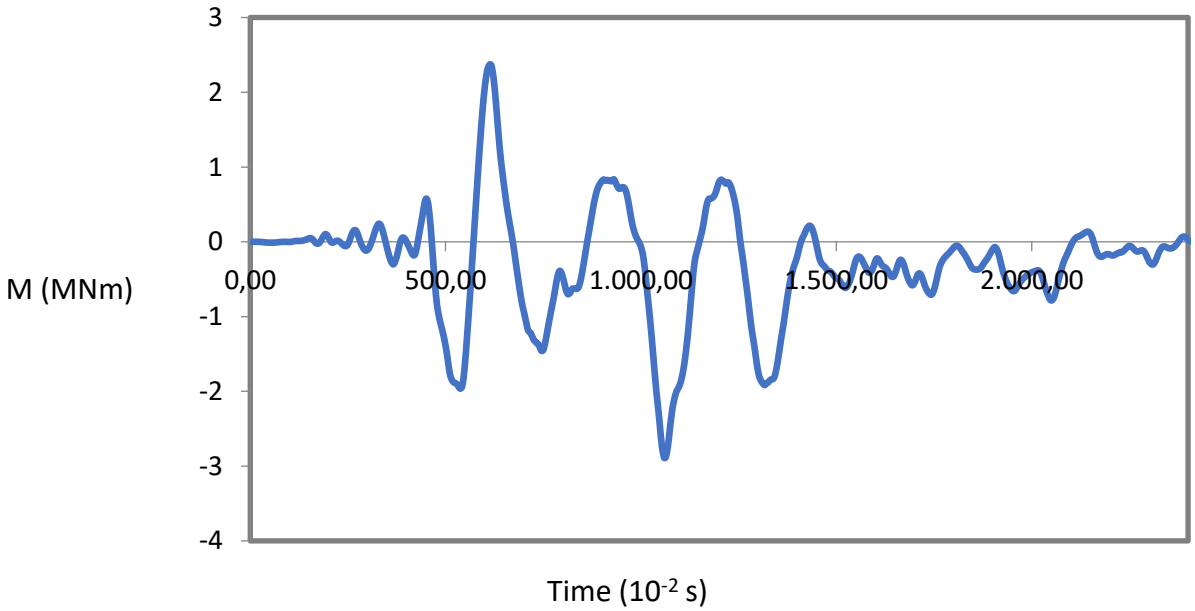

Figure 8.24: Moment-Time diagram for the interface in the Ipinia excitation

Accelerogram	PGA (g)	Plaxis		Equations		Deviations	
		Minter (KNm)	Mhead (KNm)	Minter (KNm)	Mhead (KNm)	Interface (%)	Head (%)
Kobe	0.28	1410,23	1110	1768	1487,3	25,41	34,72
Sakarya	0.3	343	281	370	374	7,94	33,07
Kalamata	0.2	3619	3126	3294	3187	-8,98	1,95
L'Aquila	0.95	295	250	272	347	-7,46	38,94
Aigio	0.2	232	191	239	245	3,02	28,27
JMA	0.55	5312	5006	3753.6	3974	-41.51	-27.6786
Corinth	0.2	6980	5200	5200	5068	-25,49	-2,54
Pyrgos	0.28	56	49	60	61	7,14	24,49
Ipinia	0.2	3798	2890	3409	2681	-11.59	-7.92696
Mean errors						15.39	22.18

Table 8.3: Results from the analyses that were conducted and deviations with the proposed equations.

The above table sums up the results from all the analyses that were performed for this chapter and the deviations with the derived equations.

Time-domain analyses conclusions:

Some of the conclusions from the above analyses are the following:

1) The derived equations proved to work sufficiently in all of the analyses with highest error being at 41 for the interface of the pile in the JMA excitation case and the mean errors for the head is 22.2% and for the interface 15.4 .The problem that was defined from the results is that in many of the analyses the equation failed to evaluate the moments at the interface in comparison with the head. We can see that the analyses shows moments greater at the interface and the equation shows moments greater at the head. Other than that the head in most cases overestimated the bending moments

2) With increasing values of the shear wave velocity ratio, the residual kinematic bending moment at the head and at the interface decreases. The shear velocity ratio plays a beneficial role in the kinematic moments after all, something that differentiates the linear analyses with the non-linear ones in great extent. As It was also explained in chapter 7, the stiffer the deeper soil layer, the smaller the displacement at the head of the pile. Indeed, in the extreme case of a rigid deeper soil layer the pile is fixed at the interface and thus the active pile length is significantly reduced.
3) The depth of the interface, as it can be seen from the comments on the above results acts positively for the moments at the head. The higher the interface the smaller the active pile length that is embedded in the 'softer' soil.
4) The resonance doesn't affect the results, no differences could be identified in the patterns of the moments.

9.General Conclusions and suggestions for further Research

Taking into account what has been shown in the previous chapters, some conclusions can be drawn for the physical phenomena under consideration. However, the complexity of the specific field of study and the limited scope of the investigation research as part of this thesis, leading to the need to pursue the research further. make it necessary to research this subject even further. Therefore, in this chapter an attempt is made to record and sum up the most important of the conclusions emerging from this thesis, as well as to make proposals for further research.

In particular, in chapter 3 a calibration of the HS small method was conducted, for the case of a sand, using of the soil experiment tests of PLAXIS code. The results of the above tests were compared with the Ishibashi G-γ and ξ-γ curves. After a number of soil tests, that were performed for different pairs of values for the main parameters of the model, the best fitting scenario was selected, that was used for the dynamic analyses that were performed in the following chapters of the thesis.

In chapter 4, the definition of the problem was presented. The basic parameters of the problem were identified and the general equation for the normalized bending moments was derived. Using the Haltonset function and proposed values for the 8 different dimensionless ratios, the analyses to be performed later on were determined. In addition, given the fact that there are no analytical solutions for the case of non-linear soil, the double parabolic curves were represented with sublayers of constant G, using the multiple layer amplification function mathematic formulas. Using the Mathcad code, a good estimate for the predominant period of the soil was presented.

In chapter 5, sensitivity analysis was performed to ensure that the boundaries and the mesh discretization were correct and didn't affect the accuracy of the results.

In chapter 6, the model that was created in previous chapter 5 was validated. Linear analyses were performed, and they were compared with the results given by equations from the literature. The deviations between the results and the proposed formulas are insignificant, meaning that the model is valid.

Chapter 7 was divided in two main parts. In the first one, nonlinear analyses were conducted and compared with the respective linear one. The second part was focused in deriving closed form expressions for the kinematic bending moments of the pile's head and interface.

For the 1st part the conclusions are the following:

- The amplitude of the excitation is of great importance in the case of non-linear analyses. As the amplitude increases, the deviations between the non-linear and the corresponding linear analyses also increase. The soil non-linear response is being enhanced by the two governing parameters of the problem: Shear velocity ratio (V_{s2}/V_{s1}) and relative stiffness ratio (E_p/E_{s1}). Both of these two parameters are affected by the non-linear soil behavior. As the excitation continues the pile imposes

displacements at the surrounding soil. The increase of the amplitude excitation leads to higher displacements and therefore bigger reduction of the shear modulus for both soil layers, and knowing that elastic modulus and shear velocities are proportional to shear modulus, means that both shear velocity ratio (V_{s2}/V_{s1}) and relative stiffness ratio (E_p/E_{s1}) increase.

- Shear velocity ratio can have a positive aspect the in the case of non-linear analyses. The analyses have shown that as V_{s2}/V_{s1} increases the residual part of the moments either decreases or in some cases fades away. This can be explained by thinking about how the motion of the pile changes with increasing shear velocity ratio. The second soil layer acts as a restraining force to the pile which leads to lower displacements at the head and the interface of the pile. An important effect of the shear velocity ratio that contradicts with the linear case, where it has only a negative effect in the bending moments especially for the case of the interface.
- Hardening of the soil surrounding the pile leads to : 1) expanding of the interface area due to the plastic shakedown effect (each cycle needs a bigger volume to counterfeit the imposed forces from the pile). 2) Movement of the interface in greater depths
- In order for the soil pile system to reach its steady state response a number of cycles is needed. This number of cycles is a function of: 1) excitation intensity 2) shear velocity ratio 3) individual maximum shear modulus of each soil layer 4) Interface depth (as the interface depth increases the length of the pile embedded in the soft soil increases benefiting the non-linear soil behavior.

For the second part, meaning the bending moment equations that were produced, attention should be applied to the upcoming results:

- PGA/g: As the PGA increases the non-linear behaviour of the soil is enchanced, leading to higher bending moments.
- $\underline{T_{inp}/T_{s1}}$: For values higher than 1 (resonance) the moments are much more affected by this parameter. The hardening of the soil decreases its stifness, leading to higher predominant periods and therefore lower ratios of this parameter as cycles continue.
- N: As the number of cycles increases the residual and total bending moments increase. Due to the non linear behavior of the soil with each cycle the soil deformations increase, leading to larger permanent displacements and therefore to higher bending moments.
- E_p/E_{s1}: Affects more the residual part, plays a dominant role for the pile's motion and bending moments. Comparing the effect of this parameter between the linear and non-linear analysis it is higher for the latter one. The reason behind this difference is attributed to the plastisization of the soil; the constitutive model of the pile is linear elastic meaning that the elastic modulus of the pile will remain constant during the excitation, on the contrary the plastic deformations that developed at the soil leads to degradation of the soil's stiffness (E_{s1}) and therefore the relative stiffness ratio increases as the excitation continues.
- V_{s2}/V_{s1}: This parameter affects much more the interface than the head for the total bending moments and dynamic bending moments, something that follows the kinematic response for linear soil. Not in all cases does the moment at the interface interfere with the bending moment at the head of the pile. The second layer acts as fixity reducing the part of the pile being on loose soil, meaning active lenth of the pile is also reduced. Lower pile active length means smaller deformations leading to smaller permanent displacements and residual moments.

- H_1/L: As the interface goes deeper the total bending moment at the head increases ,the closer the interface to the head the bigger the effect to the pile, which tends to reduce pile rotation at the interface thus generating a positive contribution bending moment in that location. Also, the residual moments at the interface increase with increasing H_1, attributed to the fact that the second layer is always stiffer than the first one, the deeper the interface the bigger the length that is embedded in softer soil.
- L/d: As the length of the pile increases the depth of the interface also increases , given that h_1 is proportional to the total length of the pile. Therefore the effect of the slenderness ratio is much higher for the residual moments case.

Last is chapter 8, the equations were tested using real accelerograms of earthquakes that happened in Greece and other countries. The equations performed adequately with highest value of deviation equal to 45%. The interface estimations were more accurate than the head, where in many cases we had overprediction of the bending moments.

Even though we tried to cover all the parameters of the problem there are still things that need to be researched. First of all the single pile cases in practice are a minority for the structures, therefore pile group analyses should be conducted to identify the kinematic pile interaction in cases of non-linear soil with parameters the number of piles, for different s/d scenarios. Also in this thesis the soil was linked to the pile throughout the dynamic response, an alternative scenario could be to investigate the effect of slide between those two and how the bending moments are affected. Other than that the pile in this thesis was modeled using linear elastic constitutive model, meaning that it behaved linearly.

BIBLIOGRAPHY

Alpan,(1970). Geotechnical properties of soils. Earth Science Review Volume 6, Issue 1, February 1970, Pages 5-49

Agioutantis, Z. (2002). Principles of Soil Mechanics. ION, Athens

Dezi, F., & Poulos, H. (2016, August). Kinematic Bending Moments in Square Pile Groups. *International Journal of Geomechanics*. International Journal of Geomechanics ,Volume 17 Issue 3 - March 2017

Di Laora, R., Mandolini, A., & Mylonakis, G. (2012). Insight on kinematic bending of flexible piles in layered soil. *Elsevier,* Volume42, Issue3,March 2013,Pages 319-337

Di Laora, R., Mandolini, A., & Mylonakis, G. (2013, March). Pile-head kinematic bending in layered soil. *Earthquake Engineering & Structural Dynamics, 42*, 319-337.

Gazetas, G. (2007).Soil Dynamics.

Gazetas G. (1983). "Analysis of Machine Foundation Vibrations State-of-the-Art": International Journal of Soil Dynamics and Earthquake Engineering, Vol. 2

Hardin & Drnevich, (1972). Shear modulus and damping in soil. Proc.ASCE: Journal of the soil mechanics and foundation divisions, pp. 1531-1537.

Kausel, E. & Roesset, J.,(1975). Dynamic stiffness of circular foundations. J Eng Mech

Kramer, S., (1996). Geotechnical Earthquake Engineering.

Lysmer, J. & Kuhlmeyer, R., 1969. Finite dynamic model for infinite media.

Nikolaou, A., & Gazetas, G. (1997). Seismic design procedure for kinematically stressed piles.

Nikolaou, S., Mylonakis, G., Gazetas, G., & Tazoh, T. (2001). Kinematic pile bending during earthquakes: analysis and field measurments. *Geotechnique*. Geotechnique, Vol. 51, pp. 425-440.

PLAXIS3D, (2012). *Material Models.* Delft, The Netherlands: Plaxis b.v..

PLAXIS3D, (2012). *Scientific Manual.* Delft, The Netherlands: Plaxis b.v..

Valalas, D. (1981). Soil Mechanics

C. S. Desai (1979). Elementary Finite Element Method, Prentice Hall.

Spyros Giannakos, Nikos Gerolymos ⇑, George Gazetas (2012). Cyclic lateral response of piles in dry sand: Finite element modeling and validation, Computers and Geotechnics 44 (2012) 116–131

S. Sica, G. Mylonakis, A. L. Simonetti, (2011), Transient kinematic pile bending in two-layer soil, Soil Dynamics and Earthquake Engineering, Volume 31,

Daniel Stutts. (2009), Equivalent Viscous Damping

A.Alipour & E. Zareian. (2008). Rayleigh Damping in Structures; Uncertainties and Treatments

Zheng Lu, Ying Zhou , Xiangdong He. (2017). Studies on damping behavior of vertically mixed structures with upper steel and lower concrete substructures

Gerolymos N., Gazetas G. (2005). Winkler model for lateral response of rigid caisson foundations in linear soil, Soil Dynamics and Earthquake Engineering 26 (2006) 347–361

Tomlinson M. & Woodward J. (2008). Pile Design and Construction Practice, 5th edition

F Dezi, S Carbonari, G Leoni (2009). Kinematic bending moments in pile foundations, October 2009Soil Dynamics and Earthquake Engineering 30(3):119-132

Makris N. & Gazetas G. (1993). “Dynamic Soil Pile Interaction Part II. Lateral and Seismic Response, EARTHQUAKE ENGINEERING AND STRUCTURAL DYNAMICS, VOL. 21, 145-162 (1992)

Kavvadas M. & Gazetas G,(1993). Kinematic Seismic Response and Bending of Free head Piles in Layered Soil, Geotechnique 43, No. 2, 207-222